Revealing, Illuminating, and Modifying Proteins in Human Diseases Using Noncanonical Amino Acids

Thesis by
Ying (Beverly) Y. Lu

In Partial Fulfillment of the Requirements for the degree of
Doctor of Philosophy

California Institute of Technology
Pasadena, California
2014
Defended August 22nd, 2013

I dedicate this thesis to my parents and Sam

for their constant support and unconditional love.

ACKNOWLEDGEMENTS

I am grateful to many people who have provided support and guidance throughout my Ph.D. research dissertation at CalTech. First and foremost I want to thank my adviser, Professor David Tirrell. It has been my honor to be Dave's student, and I appreciate all his time, advice, and funding to make my Ph.D. experience productive and stimulating. Dave has helped me gain tremendous personal growth as an independent scientist. Dave always showed excitement towards promising research results; nevertheless, he also offered guidance and encouragement that motivated me to conquer difficulties. Dave also taught me that the ability to recognize a flawed hypothesis is as important as completing a project in a timely manner. Dave is my role model not only in science but also in life, as he always inspires me with his wisdom, curiosity, and humble personality. I also greatly appreciate the guidance of my committee members, Professor Dennis Dougherty, Professor Robert Grubbs, and Professor Shu-ou Shan.

I would like to thank my parents, William and Jean Lucero, for their unconditional love and support, without which I would not have achieved my accomplishments. My father is a humorous and understanding individual who taught me how to maintain cordial and professional relationships with coworkers. My mother is generous, enthusiastic, and hardworking, and has inspired me in becoming an individual who welcomes challenges and loves to help others. Thanks to their respect and trust, I am able to pursue my dreams with confidence.

I also want to thank Samson Chiu for his consistent support in my life. When I achieved my goals, Sam celebrated with me. When I faced challenges, he cheered me on. When I

encountered difficulties, he stayed with me and provided me with support, care, and love. Sam has shown me how to approach science and life with generosity and patience.

I am fortunate to have many dear friends who have shown continuous support. I thank my close friend, Moon Jean Ho, for accompanying me on fun and memorable vacations away from my busy graduate school life. I am lucky to have Professor Kimberly Beatty as my mentor and friend, as she taught me many things, from research techniques to wine tasting. I am grateful to serve as a mentor and a friend to Katherine Fang. Kat is genuine and kind and has devoted much of her time to editing my thesis. I thank Larry Dooling, Kai Yuet, Dr. Frank Truong, Dr. Marissa Mock, Professor Eileen Fong, Professor Shelly Tzlil, Professor Jeremiah Johnson, Dr. Janek szychowski, Professor Nick Ball, Professor Maren Buck, Professor Cole DeForest, Dr. James Van Deventer, and Dr. Heather Willamson for their encouragement and friendship. I also thank Tirrell lab members Dr. Ayelet Lesman, Professor Wenbin Zhang, Dr. Chethana Kulkarni, Alborz Mahdavi, John Bagert, Brett Babin, Seth Lieblich, Peter Rapp, Shannon Stone, Andy Lim, and Michael Srienc for creating such a pleasant research environment.

In addition to the top-notch scientists, CalTech is a truly amazing place because of its wonderful staff personnel. I thank Anne Hormann, Dave's assistant, for her devotion to her job and her genuine support of me. I thank the associate dean, Felicia Hunt, and the Chemistry graduate program administrator, Agnes Tong, for making great efforts in improving the quality of life for graduate students. Finally, I would like to thank all the wonderful people whom I had the privilege to interact with, learn from, and be friends with for helping me become the curious and enthusiastic individual I am today.

ABSTRACT

The proteome of a cell is highly dynamic, constantly changing in response to environmental stimuli as well as during disease progression. To better understand human diseases, much recent work has focused on proteins to either identify disease targets through proteomics or produce therapeutics via protein engineering. Noncanonical amino acids are tools for altering the chemical and physical properties of proteins, providing a facile strategy not only to label proteins but also to engineer proteins with novel properties. My thesis research has focused on the development and applications of noncanonical amino acids in identifying, imaging, and engineering proteins for studying human diseases.

Noncanonical amino acids have been incorporated to tag and enrich newly synthesized proteins for mass spectrometry through a method termed BONCAT, or bioorthogonal noncanonical amino acid tagging. BONCAT allows time resolution in studies of the proteome, and is ideal for studying proteomic responses within defined windows of time. Chapter 2 describes the investigation of the proteomic response of human breast cancer cells to induced expression of tumor suppressor microRNA miR-126 by combining BONCAT with another proteomic method, SILAC or stable isotope labeling by amino acids in cell culture. This proteomic analysis led to the discovery of a direct target of miR-126, shedding new light on its role in suppressing cancer metastasis.

In addition to mass spectrometry, noncanonical amino acids can also be utilized to fluorescently label proteins. Incorporation of a methionine analogue, azidohomoalanine (Aha), allows subsequent labeling of proteins using copper-catalyzed azide-alkyne cycloaddition. This approach is limited to visualizing snapshots of the proteome in fixed cells

due to the cytotoxicity of copper. Utilizing the recent development of strain-promoted copper-free azide-alkyne cycloaddition, Chapter 3 details the synthesis of a set of cell-permeant cyclooctyne probes and demonstration of selective labeling of newly synthesized proteins in live mammalian cells. Similar to live cell imaging, the ability to selectively label a particular cell type within a mixed cell population is important to interrogating many biological systems. Tumor cells and the surrounding microenvironment are considered a functional whole, and methods for selective labeling of one cell type within such a complex heterogeneous mixture are needed for studying tumor microenvironments *in vitro* and *in vivo*. By taking advantage of the metabolic differences between cancer and normal cells, Chapter 5 discusses efforts to develop selective labeling of cancer cells using a glutamine analogue.

Although many noncanonical amino acids have been incorporated into proteins, there has been no example of global replacement of a polar amino acid. Polar amino acids typically occupy solvent-exposed positions on the protein surface, and incorporation of noncanonical amino acids at these positions should allow easier modification and cause less perturbation compared to replacements at the interior positions of proteins. Chapter 4 describes the first demonstration of global replacement at polar amino acid positions and its application in developing an alternative PEGylation strategy for therapeutic proteins.

Synthetic polymers have also attracted attention in biomedical research. Advances in catalysis and polymer synthesis have enabled the creation of materials with desired function and structural diversity. The appendix includes three studies on synthesis of novel polymeric materials that can either achieve controlled-release of anti-cancer drugs or provide support for cell adhesion or growth.

TABLE OF CONTENTS

LIST OF FIGURES, TABLES, AND SCHEMES

CHAPTER 1

Introduction

Importance of biological polymers in human diseases. Biological polymers make all of the functions of life possible. DNA encodes genetic information within all living organisms and is transcribed into messenger RNA (mRNA), which is then translated to produce the final product, proteins. Proteins are polymers of amino acids, and they perform many cellular functions, such as replicating genetic materials, catalyzing metabolic reactions, and destroying toxins. While genomics has provided valuable information for understanding many diseases, the study of proteins, or proteomics, attracts growing attention because alterations in protein function and regulation are characteristics of many human diseases. For example, accumulation of misfolded proteins that form fibrillar aggregates is central to neurodegenerative diseases, such as Alzheimer's, Parkinson's, and Huntington's disease.[1] Moreover, pro-survival protein Bcl-2 is often upregulated in solid tumor cells and is considered an attractive target for cancer therapy.[2] Such changes in the proteome are important for understanding diseases as well as identifying therapeutic targets; however, the complexity of the proteome makes investigations challenging. While the human genome encodes ~30,000 genes, alternative splicing and posttranslational modifications produce multiple products per gene, making the proteome much more complex. Interrogation of such a complex system is further complicated by the dynamic nature of the proteome; new proteins are made and transported while pre-existing ones are degraded.

Residue-specific incorporation of noncanonical amino acids. To identify a proteomic response to a stimulus such as a disease, proteins made within a time window must be examined. It is difficult to distinguish newly synthesized proteins from the pre-existing ones as all proteins share similar amino acid building blocks. Residue-specific incorporation of reactive amino acids provides a facile strategy to tag newly synthesized proteins (Scheme

1.1).[3] This method takes advantage of the endogenous cellular machinery to allow co-translational incorporation of noncanonical amino acids (ncAAs). The incorporation of ncAAs is operationally similar to conventional protein labeling using ^{35}S-Met, but faster and simpler, as it does not involve handling of radioactive materials. The resulting tagged proteins are chemically and physically distinct from pre-existing proteins. Separation of new and pre-existing proteins allows focused studies, such as identification and visualization, of proteins made in any time window of interest.

Isolating proteomic response using ncAAs. In proteomic studies, mass spectrometry (MS) is routinely used to identify proteins; however, because MS detects the most abundant peptides in a mixture, sample complexity limits depth of peptide and protein identification.[4] To reduce sample complexity prior to MS, it has been demonstrated that newly synthesized proteins can be selectively enriched using a method termed BONCAT, or bioorthognal noncanonical amino acid tagging.[5] This method involves residue-specific incorporation of a reactive methionine analogue, azidohomoalanine (Aha),[6] to tag newly synthesized proteins with azides and subsequent purification of tagged proteins using alkyne-containing affinity probes.[7] In addition to protein identification, quantification of the proteomic changes can be achieved using SILAC, or stable isotope labeling by amino acids in cell culture.[8] Using a combined approach of BONCAT and SILAC,[9] we have investigated the proteomic changes that occur in response to induced expression of a tumor suppressor microRNA (miRNA) in human breast cancer cells. These studies discovered a new direct target of miR-126 (Chapter 2).

Illuminating the proteome using ncAAs. While MS analysis identifies proteins, fluorescence microscopy provides spatial and temporal information about the proteome.

Fluorescent labeling of proteins inside live cells has revolutionized biological studies by allowing researchers to directly monitor dynamic cellular processes. Fluorescent proteins such as GFP are commonly used for live cell imaging.[10] While this method has enabled visualization of many targets, it requires the addition of a 30 kDa tag, which can cause perturbations in the localization and activity of the target proteins. Furthermore, investigating global protein synthesis and transport requires a strategy free of genetic manipulations.

Proteomic imaging can be achieved through metabolic incorporation of small bioorthgonal tags, such as ncAAs. Incorporation of methioine analogues, homopropargylglycine (Hpg) and Aha, tags newly synthesized proteins with alkyne and azide functional groups,[6, 11] allowing for subsequent labeling by copper-catalyzed azide-alkyne cycloaddition.[12] While this approach fluorescently labels newly synthesized proteins, it only provides snapshots of the proteome in fixed cells.[13] To allow labeling of live cells, the strain-promoted azide-alkyne cycloaddition was developed to eliminate the use of the cytotoxic copper catalyst.[14] To provide new tools for live cell imaging, we have synthesized a set of cell-permeant cyclooctyne fluorophores and identified optimum conditions for selective labeling of newly synthesized proteins in living cells (Chapter 3).[15]

Similar to strain-promoted azide-alkyne cycloaddition, hydrazide-ketone chemistry can also proceed under physiological conditions.[16] To expand the chemical toolbox for live cell labeling, we have demonstrated imaging of live bacterial cells through incorporation of the glutamine analogue, L-glutamic acid γ-hydrazide (Gah) (Chapter 4). Moreover, by taking advantage of the differences in glutamine metabolism between cancer and normal cells,[17] we have explored the possibility of using Gah to selectively label cancer cells (Chapter 5).

Replacing polar amino acids with ncAAs for modifying therapeutic proteins. In addition to providing tools for interrogating the proteome to better understand human diseases, residue-incorporation of ncAAs also offers a way to engineer therapeutic proteins. The incorporation of ncAAs has significantly increased the possibility of engineering proteins with novel properties by expanding the building blocks beyond the 20 canonical amino acids.[18] In an effort to further expand the chemical toolbox for protein engineering, we have demonstrated the first example of replacing polar residues (glutamine) with reactive ncAAs (Gah) (Chapter 4). Polar residues are often solvent-exposed,[19] and incorporation of ncAAs at these positions should allow easier access for modifications and cause less structural perturbation than replacement of a nonpolar residue. Furthermore, using the bioorthogonal reactive groups introduced at glutamine positions, we are seeking to develop a strategy for PEGylating therapeutic proteins at multiple sites (Chapter 4).

Synthetic polymers for studying and treating human diseases. In addition to biological polymers, synthetic polymeric materials also play essential roles in advancing knowledge and treatment of human diseases. Synthetic polymers can be fabricated into materials in various shapes with desired pore sizes and different mechanical properties.[20] These versatile materials have extensive applications, such as tissue engineering and drug delivery. To create materials with desired functional and structural diversity, much effort has been made in advancing polymer synthesis. The development of ring-opening metathesis polymerization (ROMP) using fast-initiating ruthenium catalysis has enabled synthesis of diverse side-chain functional polymers with controllable molecular weights and low polydispersities.[21] In collaboration with colleagues in the laboratory of Robert Grubbs, we demonstrated two applications of this polymerization method: synthesis of bivalent-brush polymers capable of

releasing anticancer drugs upon photo activation (Appendix I and II)[22] and generation of thin-film hydrogels for supporting cell adhesion and growth (Appendix III).[23]

Summary. Motivated by developing new tools for interrogating human diseases, my thesis research has focused on the development and applications of noncanonical amino acids. I have demonstrated the powerful use of ncAAs for investigating proteomic response to tumor suppressor microRNA, capturing proteomic dynamics in live cells, and engineering therapeutic proteins. The methods and applications demonstrated in my thesis work should enable many disease studies by providing the scientific community with new tools to identify, illuminate, and modify proteins.

References

1. Chiti, F.; Dobson, C. M., Protein misfolding, functional amyloid, and human disease. *Annu Rev Biochem* **2006,** *75*, 333-66.

2. Kelly, P. N.; Strasser, A., The role of Bcl-2 and its pro-survival relatives in tumourigenesis and cancer therapy. *Cell Death Differ* **2011,** *18* (9), 1414-24.

3. Johnson, J. A.; Lu, Y. Y.; Van Deventer, J. A.; Tirrell, D. A., Residue-specific incorporation of non-canonical amino acids into proteins: recent developments and applications. *Curr Opin Chem Biol* **2010,** *14* (6), 774-80.

4. (a) Elschenbroich, S.; Ignatchenko, V.; Sharma, P.; Schmitt-Ulms, G.; Gramolini, A. O.; Kislinger, T., Peptide separations by on-line MudPIT compared to isoelectric focusing in an off-gel format: application to a membrane-enriched fraction from C2C12 mouse skeletal muscle cells. *J Proteome Res* **2009,** *8* (10), 4860-9; (b) Gilar, M.; Olivova, P.; Chakraborty, A. B.; Jaworski, A.; Geromanos, S. J.; Gebler, J. C., Comparison of 1-D and 2-D LC MS/MS

methods for proteomic analysis of human serum. *Electrophoresis* **2009,** *30* (7), 1157-67; (c) Horvatovich, P.; Hoekman, B.; Govorukhina, N.; Bischoff, R., Multidimensional chromatography coupled to mass spectrometry in analysing complex proteomics samples. *J Sep Sci* **2010,** *33* (10), 1421-37; (d) Schirle, M.; Heurtier, M. A.; Kuster, B., Profiling core proteomes of human cell lines by one-dimensional PAGE and liquid chromatography-tandem mass spectrometry. *Mol Cell Proteomics* **2003,** *2* (12), 1297-305.

5. Dieterich, D. C.; Link, A. J.; Graumann, J.; Tirrell, D. A.; Schuman, E. M., Selective identification of newly synthesized proteins in mammalian cells using bioorthogonal noncanonical amino acid tagging (BONCAT). *Proc Natl Acad Sci U S A* **2006,** *103* (25), 9482-7.

6. Kiick, K. L.; Saxon, E.; Tirrell, D. A.; Bertozzi, C. R., Incorporation of azides into recombinant proteins for chemoselective modification by the Staudinger ligation. *Proc Natl Acad Sci U S A* **2002,** *99* (1), 19-24.

7. (a) Hodas, J. J.; Nehring, A.; Hoche, N.; Sweredoski, M. J.; Pielot, R.; Hess, S.; Tirrell, D. A.; Dieterich, D. C.; Schuman, E. M., Dopaminergic modulation of the hippocampal neuropil proteome identified by bioorthogonal noncanonical amino acid tagging (BONCAT). *Proteomics* **2012,** *12* (15-16), 2464-76; (b) Hinz, F. I.; Dieterich, D. C.; Tirrell, D. A.; Schuman, E. M., Non-canonical amino acid labeling in vivo to visualize and affinity purify newly synthesized proteins in larval zebrafish. *ACS Chem Neurosci* **2012,** *3* (1), 40-49.

8. Ong, S. E.; Mann, M., A practical recipe for stable isotope labeling by amino acids in cell culture (SILAC). *Nat Protoc* **2006,** *1* (6), 2650-60.

9. (a) Howden, A. J.; Geoghegan, V.; Katsch, K.; Efstathiou, G.; Bhushan, B.; Boutureira, O.; Thomas, B.; Trudgian, D. C.; Kessler, B. M.; Dieterich, D. C.; Davis, B. G.;

Acuto, O., QuaNCAT: quantitating proteome dynamics in primary cells. *Nat Methods* **2013,** *10* (4), 343-6; (b) Somasekharan, S. P.; Stoynov, N.; Rotblat, B.; Leprivier, G.; Galpin, J. D.; Ahern, C. A.; Foster, L. J.; Sorensen, P. H., Identification and quantification of newly synthesized proteins translationally regulated by YB-1 using a novel Click-SILAC approach. *J Proteomics* **2012,** *77*, e1-10.

10. (a) Shaner, N. C.; Steinbach, P. A.; Tsien, R. Y., A guide to choosing fluorescent proteins. *Nat Methods* **2005,** *2* (12), 905-9; (b) Tsien, R. Y., The green fluorescent protein. *Annu Rev Biochem* **1998,** *67*, 509-44.

11. van Hest, J. C. M.; Kiick, K. L.; Tirrell, D. A., Efficient Incorporation of Unsaturated Methionine Analogues into Proteins in Vivo. *Journal of the American Chemical Society* **2000,** *122* (7), 1282-1288.

12. Rostovtsev, V. V.; Green, L. G.; Fokin, V. V.; Sharpless, K. B., A stepwise huisgen cycloaddition process: copper(I)-catalyzed regioselective "ligation" of azides and terminal alkynes. *Angew Chem Int Ed Engl* **2002,** *41* (14), 2596-9.

13. (a) Beatty, K. E.; Tirrell, D. A., Two-color labeling of temporally defined protein populations in mammalian cells. *Bioorg Med Chem Lett* **2008,** *18* (22), 5995-9; (b) Beatty, K. E.; Xie, F.; Wang, Q.; Tirrell, D. A., Selective dye-labeling of newly synthesized proteins in bacterial cells. *J Am Chem Soc* **2005,** *127* (41), 14150-1; (c) Beatty, K. E.; Liu, J. C.; Xie, F.; Dieterich, D. C.; Schuman, E. M.; Wang, Q.; Tirrell, D. A., Fluorescence visualization of newly synthesized proteins in mammalian cells. *Angew Chem Int Ed Engl* **2006,** *45* (44), 7364-7.

14. (a) Agard, N. J.; Baskin, J. M.; Prescher, J. A.; Lo, A.; Bertozzi, C. R., A comparative study of bioorthogonal reactions with azides. *ACS Chem Biol* **2006,** *1* (10), 644-8; (b) Agard,

N. J.; Prescher, J. A.; Bertozzi, C. R., A strain-promoted [3 + 2] azide-alkyne cycloaddition for covalent modification of biomolecules in living systems. *J Am Chem Soc* **2004,** *126* (46), 15046-7.

15. Beatty, K. E.; Fisk, J. D.; Smart, B. P.; Lu, Y. Y.; Szychowski, J.; Hangauer, M. J.; Baskin, J. M.; Bertozzi, C. R.; Tirrell, D. A., Live-cell imaging of cellular proteins by a strain-promoted azide-alkyne cycloaddition. *Chembiochem* **2010,** *11* (15), 2092-5.

16. Sletten, E. M.; Bertozzi, C. R., Bioorthogonal chemistry: fishing for selectivity in a sea of functionality. *Angew Chem Int Ed Engl* **2009,** *48* (38), 6974-98.

17. (a) Eagle, H., Nutrition needs of mammalian cells in tissue culture. *Science* **1955,** *122* (3168), 501-14; (b) Neu, J.; Shenoy, V.; Chakrabarti, R., Glutamine nutrition and metabolism: where do we go from here ? *FASEB J* **1996,** *10* (8), 829-37; (c) Reitzer, L. J.; Wice, B. M.; Kennell, D., Evidence that glutamine, not sugar, is the major energy source for cultured HeLa cells. *J Biol Chem* **1979,** *254* (8), 2669-76; (d) Suzannec Klimberg, V.; McClellan, J. L., Glutamine, cancer, and its therapy. *The American Journal of Surgery* **1996,** *172* (5), 418-424; (e) Thompson, C. B.; Bauer, D. E.; Lum, J. J.; Hatzivassiliou, G.; Zong, W. X.; Zhao, F.; Ditsworth, D.; Buzzai, M.; Lindsten, T., How do cancer cells acquire the fuel needed to support cell growth? *Cold Spring Harb Symp Quant Biol* **2005,** *70*, 357-62.

18. Link, A. J.; Mock, M. L.; Tirrell, D. A., Non-canonical amino acids in protein engineering. *Curr Opin Biotechnol* **2003,** *14* (6), 603-9.

19. Lesser, G. J.; Rose, G. D., Hydrophobicity of amino acid subgroups in proteins. *Proteins* **1990,** *8* (1), 6-13.

20. Gunatillake, P. A.; Adhikari, R., Biodegradable synthetic polymers for tissue engineering. *Eur Cell Mater* **2003,** *5*, 1-16; discussion 16.

21. (a) Conrad, R. M.; Grubbs, R. H., Tunable, temperature-responsive polynorbornenes with side chains based on an elastin peptide sequence. *Angew Chem Int Ed Engl* **2009,** *48* (44), 8328-30; (b) Kolonko, E. M.; Pontrello, J. K.; Mangold, S. L.; Kiessling, L. L., General synthetic route to cell-permeable block copolymers via ROMP. *J Am Chem Soc* **2009,** *131* (21), 7327-33.

22. (a) Johnson, J. A.; Lu, Y. Y.; Burts, A. O.; Xia, Y.; Durrell, A. C.; Tirrell, D. A.; Grubbs, R. H., Drug-loaded, bivalent-bottle-brush polymers by graft-through ROMP. *Macromolecules* **2010,** *43* (24), 10326-10335; (b) Johnson, J. A.; Lu, Y. Y.; Burts, A. O.; Lim, Y. H.; Finn, M. G.; Koberstein, J. T.; Turro, N. J.; Tirrell, D. A.; Grubbs, R. H., Core-clickable PEG-branch-azide bivalent-bottle-brush polymers by ROMP: grafting-through and clicking-to. *J Am Chem Soc* **2011,** *133* (3), 559-66.

23. Patel, P. R.; Kiser, R. C.; Lu, Y. Y.; Fong, E.; Ho, W. C.; Tirrell, D. A.; Grubbs, R. H., Synthesis and cell adhesive properties of linear and cyclic RGD functionalized polynorbornene thin films. *Biomacromolecules* **2012,** *13* (8), 2546-53.

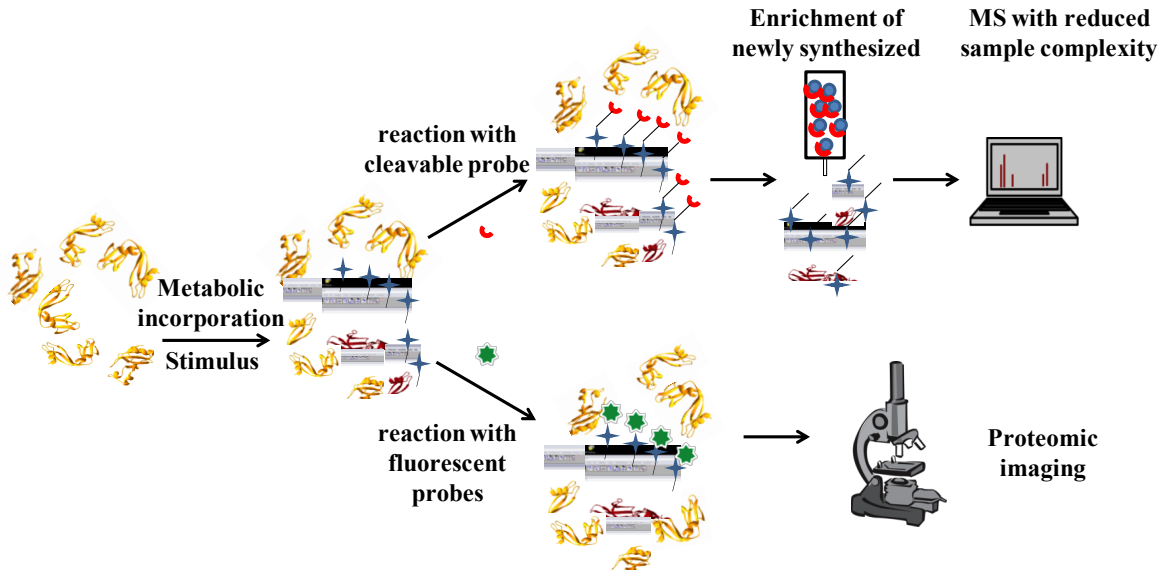

Scheme 1.1. Residue-specific incorporation of ncAAs for tagging of newly synthesized proteins and its applications.

CHAPTER 2

Pro-metastatic GPCR CD97 is a Direct Target of Tumor Suppressor miR-126

Abstract

Many studies have shown that expression of microRNA-126 (miR-126) is downregulated in cancer cells. Overexpression of miR-126 is found to inhibit cancer metastasis, consistent with its identity as a tumor suppressor. To better understand the regulatory effects of miR-126, we combined BONCAT and SILAC to analyze the proteomic response to miR-126 overexpression in the human metastatic breast cancer cell line MDA-MB-231. Among the list of responsive proteins, we discovered a direct target of miR-126, CD97. CD97 is a member of the epidermal growth factor seven-span transmembrane (EGF-TM7) family of adhesion G-protein-coupled receptors (GPCRs) and plays an important role in mediating cell-cell interaction. Expression of CD97 is upregulated in various cancers, and its overexpression has been shown to promote cancer metastasis by stimulating tumor cell migration and invasion. Furthermore, CD97 plays a non-cell-autonomous role in activating endothelial cell migration to promote angiogenesis, an essential process in cancer metastasis. The discovery that tumor suppressor miR-126 directly targets the metastasis promoter CD97 provides new mechanistic insights into roles of miR-126 in inhibiting both cell-autonomous and non-cell-autonomous cancer progression.

Introduction

microRNAs (miRNAs) are a family of small noncoding RNAs that regulate gene expression posttranscriptionally and have been predicted to control more than 60% of all protein-coding genes in mammals.[1] miRNAs play essential roles in many biological processes, including angiogenesis and tumorigenesis.[2] Unsurprisingly, dysregulation of certain miRNAs has been

observed in various human cancers.[3] For instance, miR-126, a microRNA involved in angiogenesis,[4] has been reported to exhibit reduced expression in many types of human cancers including breast, lung, gastric, and prostate.[5] miR-126 has been defined as a metastasis suppressor because its overexpression was found to suppress the *in vivo* metastasis of breast cancer cells to lung and bone.[5d] Much effort has since been made to understand the roles of miR-126 in metastatic progression; however, the underlying mechanism of regulation remains incompletely understood.

In this study, we investigated the regulatory effects of miR-126 in human breast cancer cells by combining SILAC and BONCAT to determine the influence of miR-126 overexpression on protein synthesis. BONCAT (bioorthogonal noncanonical amino acid tagging) is used to isolate proteins synthesized within specified time intervals, and provides the temporal resolution needed to study proteomic responses to various stimuli.[6] Moreover, BONCAT reduces sample complexity, a major limitation in protein identification using mass spectrometry, by removing the pre-existing proteome.[7] To quantify proteomic changes, SILAC was used in conjunction with BONCAT.[8] SILAC (stable isotope labeling by amino acids in cell culture) is a widely used method for mass spectrometry (MS)-based quantitative proteomics.[9] Using this combined approach, we have discovered that a metastasis-promoting adhesion G-protein coupled receptor (GPCR), CD97, is a direct target of miR-126, shedding new light on its role in tumor suppression.

Results

Inducible expression of miR-126 in human breast cancer cells. In order to assess the proteomic response to miR-126 overexpression, we modified the metastatic human breast cancer cell line MDA-MB-231 by lentiviral transduction with the SparQ^{TM} Cumate Switch system. The resulting cell line (designated MDA-CuO-miR) is characterized by constitutive expression of GFP as a selection marker and by cumate-inducible expression[10] of a miR-126 precursor (Figure 2.2a). Because endogenous miR-126 is encoded by intron 7 of the epidermal growth-factor-like domain 7 (*EGFL7*) gene,[11] we designed the precursor sequence to include the pre-miR-126 and flanking regions from the intron of *EGFL7* to ensure proper transcription and processing of miR-126. Cells were separated on the basis of GFP fluorescence to obtain cell populations with similar numbers of transgene integrations (Figure 2.1).

Next, we assessed the induced expression of miR-126 in these cells by using the reverse transcriptase polymerase chain reaction (RT-PCR) (Figure 2.2b). At 2, 8, 24, and 72 h after induction with various concentrations of cumate, cells were harvested and total RNA was isolated. The abundance of mature miR-126 was measured and relative expression was calculated by using commercially available probes designed to bind mature miR-126.[12] Expression of miR-126 increased with induction time, and overexpression became significant 8 h after induction. miRNA expression was about 8-fold higher compared to cells without cumate at 24 h and more than 10-fold higher 72 h post-induction. While induction time is the most important determinant of miR-126 expression, increasing cumate concentration above 150 μg/mL had a small additional effect. To achieve an expression level that is both significant and physiologically relevant for proteomic studies, we chose to induce with 300

μg/mL cumate for 24 h. It has been reported that expression of miR-126 can be reduced by ~6-fold in some cancers.[13]

Assessing regulatory effects of miR-126 using proteomics. To quantify proteomic changes in response to miR-126 overexpression, cells were first adapted in SILAC medium containing either light lysine (Lys) or heavy lysine with an 8-Da mass shift (Lys8) for five doubling times to ensure near quantitative incorporation of Lys+8 in the heavy culture. Expression of miR-126 was induced in the heavy culture by addition of cumate. A label-swap experiment was performed to control for changes in protein expression caused by the isotopes, where cumate was added to the light culture instead. At 24 h post induction, both cultures were treated with azidohomoalanine (Aha), a methionine analogue that can be subsequently conjugated with affinity probes via copper-catalyzed azide-alkyne cycloaddition.[14] Cells were incubated with Aha for 4 h before they were harvested and lysed; lysates were then mixed at equal protein concentrations. This mixture was subjected to reaction with an acid-cleavable biotin tag[15] to allow for isolation of newly synthesized proteins for MS analysis.

MS data analysis revealed many proteins that exhibit significant changes of at least 20% in expression. To address the possible effects of the inducer, control experiments were performed in which cumate was added both to MDA-CuO-miR cells and to a control cell line (MDA-CuO) transduced with empty vector. A set of 33 responsive proteins was identified by applying two criteria: the protein must 1) be quantified on the basis of six or more peptide ratio measurements, and 2) exhibit at least a 20% change in expression with consistent direction of regulation in both sets of experiments described above (Table 2.1). We imagined that this set of proteins would include some that are directly regulated by miR-126, and

others that are affected indirectly. The most prevalent mechanism of regulation by human miRNAs involves translational repression as a consequence of miRNA binding in the 3'-untranslated region (UTR) of the target transcript.[16] To identify potential direct targets, we cross-referenced the down-regulated proteins with the lists of predicted targets of miR-126 obtained from the following resources: MicroCosm[17] using the miRanda algorithm (v3.0),[18] Target Scan (v6.2),[1b, 19] and microRNA.org[20] using mirSVR algorithm,[21] and identified one predicted target, *CD97*. The fact that Cd97 is an established promoter of tumor metastasis[22] made this observation especially intriguing.

miR-126 regulates *CD97* expression via direct binding to its 3' UTR. To determine whether *CD97* is a direct target of miR-126, a widely used luciferase reporter assay was employed. First, the miR-126 precursor sequence used for MS studies was cloned downstream of the CMV promoter in an expression vector pcDNA^{TM}3.1(+) to generate pcDNA3.1(+)-miR126. Next, the entire 3'-UTR of *CD97* was cloned downstream of a firefly luciferase reporter construct pMIR-REPORT^{TM} and cotransfected with either pcDNA3.1(+)-miR126 or pcDNA3.1(+) empty vector into human embryonic kidney (HEK293) cells. To validate this assay, several controls were also included (Figure 2.3a). pMIR does not contain any 3'-UTR downstream of luciferase so the reporter signal from this construct should not be affected by miR-126. As a positive control for repressed luciferase expression, two miR-126 binding sites were introduced to create 2miR. Further, the 3'-UTR of insulin receptor substrate-1 (IRS1), a known direct target of miR-126,[23] was cloned downstream of the luciferase reporter to provide a reference for efficient knockdown. As expected, luciferase expression from reporter constructs containing 2miR and IRS1 was decreased in cells expressing miR-126. In the presence of miR-126, cells expressing reporter construct

containing *CD97* 3'-UTR exhibited a ~40% decrease in luciferase activity, an even more significant knockdown than the decrease of ~20% observed for known target IRS1 (Figure 2.3b). These results provide the first evidence that *CD97* is a direct target of miR-126.

In order to identify possible miR-126 binding sites, we aligned the 3'-UTR of CD97 with the mature miR-126 sequence using the microRNA target prediction algorithm RNAhybrid[24] and found extensive sequence complementarity, including a 5-nucleotide seed-matched site (Figure 2.4a). We created several luciferase reporter constructs containing *CD97* 3'-UTR mutants and evaluated the effects of miR-126 on expression (Figure 2.4a). Guided by the predicted binding site, we made *CD97*-ex by removing all 11 interacting nucleotides and *CD97*-M3-126 by introducing three point mutations in the predicted binding region. A control construct, CD97-R1, has three point mutations at a random site that is not predicted to bind miR-126. To address the possibility that the flanking sequences may produce false-positive results, we did not use empty vector as the control for miR-126 expression. Instead, we constructed pcDNA3.1^{+}-miR-ex, which lacks the pre-miR-126 sequence and leaves the flanking regions intact. Compared to cells expressing miR-ex, cells cotransfected with miR-126 and the luciferase construct containing *CD97* 3'-UTR exhibited a significant knockdown of ~40% in luciferase activity. Expression can be rescued either by removing the predicted binding site or by introducing three point mutations in the binding site (Figure 2.4b). In contrast, mutating three nucleotides at an arbitrary site within the *CD97* 3'-UTR had little effect on luciferase activity. From these results, we have determined the binding site for miR-126 in the 3'-UTR of CD97.

In addition to miR-126, pre-miR-126 contains another known microRNA, miR-126*. Since it has been shown that miR-126 and miR-126* can repress expression of the same target by

binding to different sites in the 3' UTR,[25] we assessed whether miR-126* also targets *CD97*. In contrast to miR-126, the predicted binding site in the *CD97* 3' UTR does not share strong sequence complementarity with the seed region of miR-126* (Figure 2.5a). We constructed three luciferase reporter constructs: *CD97*-M3-126* contains three mutations in the predicted binding site for miR-126*, *CD97*-M3-126+126* has mutations in both of the binding regions predicted for miR-126 and for miR-126*, and *CD97*-M3-R1+R2 is a control construct with mutations at two random sites. Similar to previous experiments, mutations at random sites within the 3'UTR of CD97 did not affect the robust suppression of luciferase activity by miR-126 (Figure 2.5b). While mutations in the predicted binding site for miR-126* also had little effect on the luciferase signal, the additional mutation in the miR-126 binding site abolished the suppression of luciferase activity. These results indicate that miR-126, not miR-126*, controls expression of *CD97*.

Discussion

Reduced expression of miR-126 is observed in many cancers, identifying it as a putative tumor suppressor. To better understand its role in cancer metastasis, we investigated the regulatory effects of miR-126 on protein synthesis in human breast cancer cells and identified 29 responsive proteins that exhibit miR-126-dependent expression. Further, we discovered that miR-126 represses expression of *CD97* by binding directly to its 3' UTR. This discovery establishes a link between two well-documented observations in cancer biology: the downregulation of tumor suppressor miR-126[5d, 23, 26] and the overexpression of *CD97*.[27]

CD97 is an adhesion G-protein coupled receptor (GPCR) involved in cell adhesion and migration.[28] Expression levels of CD97 were found to correlate with the *in vitro* migration and invasion capacity of many colorectal tumor cell lines.[27d] Tumor cells at the invasion front of colorectal and gastric carcinomas are found to exhibit stronger CD97 expression than other cells within the same tumor.[27d, 29] Further, overexpression of CD97 has been shown to stimulate single cell motility *in vitro* and increase invasiveness of the fibrosarcoma cell line HT-1080 in *scid* mice.[30] Similarly, CD97 has been shown to promote tumor invasion in thyroid cancer as well as glioblastoma.[31] All of these observations suggest that CD97 plays a role in promoting tumor invasion by stimulating tumor cell migration. Similar functions have also been reported for a known target of miR-126, CRK.[5a, 32] CRK is a component of the focal adhesion network, and decreased CRK expression has been shown to suppress tumor cell migration.[32] Furthermore, it has been shown that miR-126 inhibited gastric cancer metastasis, partially through the downregulation of CRK.[26b] Our discovery that miR-126 targets CD97, a key prometastasis factor in gastric cancer, suggests that perhaps miR-126 suppresses metastasis through downregulation of both CRK and CD97.

In addition to promoting tumor progression in a cell-autonomous manner, CD97 has also been shown to function non-cell-autonomously. CD97 can stimulate the motility and invasion of endothelial cells by binding to cell surface integrins to promote angiogenesis,[33] an essential process in cancer metastasis. Previous reports have indicated that miR-126 represses angiogenesis by restricting VEGF-induced signals through direct targeting of Sprout-related EVH1 domain-containing protein 1 (*SPRED1*), vascular endothelial growth factor A (*VEGFA*), and phosphatidylinositol 3-kinase regulatory beta subunit (*PI3KR2*).[26c, 34] Since endothelial cell migration is essential to angiogenesis, it is reasonable to hypothesize

that downregulation of CD97, a proangiogenic factor that stimulates endothelial cell migration and invasion, also contributes to suppression of angiogenesis by miR-126. Similar to CD97, three recently revealed miR-126 targets also regulate endothelial recruitment. Knockdown of genes coding insulin-like growth factor binding protein 2 (*IGFBP2*), c-Mer tyrosin kinase (*MERTK*), and phosphatidylinositol transfer protein (*PITPNC1*) significantly suppressed the ability of metastatic breast cancer cells to recruit endothelial cells, leading to inhibition of metastatic colonization *in vivo*.[35] This suppressive role of miR-126 in non-cell-autonomous cancer progression is further illustrated by the discovery that miR-126 also inhibits recruitment of mesenchymal stem cells and inflammatory monocytes by targeting stromal cell-derived factor-1 alpha (SDF-1α).[25]

miR-126 has been shown to regulate genes involved in both cell-autonomous and non-cell-autonomous cancer progression (Figure 2.6). miR-126 can suppress cell-autonomous cancer progression by targeting *IRS1* and *CRK* to inhibit tumor cell proliferation, migration, and invasion. miR-126 also inhibits metastasis in a non-cell autonomous manner by down-regulating IGFBP2, MERTK, PITPNC1, and SDF-1α to limit cell recruitment. In addition, we now know that miR-126 targets CD97, a molecule that has been shown to promote metastasis both by stimulating tumor cell invasion and by inducing angiogenesis through recruitment of endothelial cells. This discovery provides new insight into the mechanism of tumor-suppression by miR-126 and identifies a potential therapeutic target for controlling both cell-autonomous and non-cell autonomous cancer progression.

Materials and Methods

Cell culture

Lentivectors and plasmids. SparQ™ cumate switch inducible expression constructs, pCDH-EF1-CymR-T2A-Puro (QM200PA-2) and pCDH-CuO-MCS-EF1-GFP dual promoter lentivector (QM511B-1) were purchased from System Biosciences (SBI). pMIR-REPORT™ miRNA expression reporter (AM5795) and pcDNA™3.1(+) vector (V790-20) were from Invitrogen. *Cd97* 3'-UTR was amplified from human genomic DNA using the following primers: AAT TAA CTA GTA GGC GCA TGG TTC TGG ACG GCC CAG (forward) and ATT TTT CAG TGT TGA CAC TTA AAA TTA AAC ACA TGC ATA CAG AAG AAA GCT TTA TA (reverse).

Lentiviral transduction. MDA-CymR cells stably expressing pCDH-EF1-CymR-T2A-Puro were generated by transducing MDA-MB-231 breast cancer cells (ATCC) with pCDH-EF1-CymR-T2A-Puro virus (SBI, QM200VA-2) followed by a 14-day selection with 10 μg/mL puromycin. To produce lentivirus containing inducible miR-126 constructs, HEK293 cells at 80% confluency were transiently transfected using Lipofectamine 2000 (Invitrogen) according to the manufacturer's instructions. The cells were transfected with either pCDH-CuO-miR126-EF1-GFP or pCDH-CuO-MCS-EF1-GFP, along with two packaging plasmids and a fourth plasmid used to produce VSV-G pseudotyped lentivirus. The cell culture medium was collected 24, 48 and 72 h post transfection, filtered through an 0.8 μm filter, concentrated using a 30,000 MW cutoff spin column (Millipore), and stored at -80 °C. The MDA-CymR cells were infected with a 1:10 dilution of the concentrated lentiviral stocks

before further passaging and subdivision by FACS analysis based on the intensity of GFP fluorescence in order to obtain populations with similar numbers of transgene integrations.

Fluorescence activated cell sorting. Cells were detached and pelleted by centrifugation (200 *g*, 3 min) and washed once with 1 mL Hank's balanced salt solution (0.2% BSA, 10 mM HEPES), and once with a cushion of FBS added to the bottom of the tube. Finally, cells were resuspended in 400 μL Hank's buffer before filtering through a 50 μm Nytex nylon mesh screen (Sefar). Cells were stored on ice until flow cytometry analysis on a FACSAria flow cytometer (BD Biosciences Immunocytometry Systems) at the Flow Cytometry Facility of the Beckman Institute at Caltech.

RT-PCR. Cumate solution (SBI) was added to cells carrying inducible miR-126 constructs at final concentrations of 0, 30, 150, 300, or 600 μg/mL. At 2, 8, 24, and 72 h post induction, cells were washed with PBS, trypsinized, and harvested. Total RNA from these cells was isolated with mirVana miRNA isolation kits (Invitrogen, AM1560). Reverse transcriptase (RT)-PCR was performed according to manufacturer's protocols (TaqMan® microRNA Assays, Invitrogen, 4427975). Briefly, RNA concentrations were measured and 10 ng of RNA was used as template for reverse transcription using TaqMan® microRNA reverse transcription kit (Invitrogen, 4366596). Products from the RT reaction served as templates for quantitative PCR (qPCR) using a Model 7300 real-time PCR system (Applied Biosystems). Reagents used for qPCR include, TaqMan® Universal PCR master mix without AmpErase® UNG (Invitrogen, 4324018) and primers from TaqMan® microRNA assays (Invitrogen, has-miR-126, ID000450; U6 snRNA control, ID001973). Relative miR-126 expression was calculated using the ΔΔCt method as previously described.[36]

Cell culture and amino acid incorporation. Cells were maintained in a 37 °C, 5% CO_2 humidified incubator chamber in customized Dulbecco's modified Eagle's medium (DMEM) (Invitrogen) supplemented with 10% dialyzed fetal bovine serum (Invitrogen), 50 U/mL penicillin, 50 μg/mL streptomycin, 0.2 mM methionine, 0.398 mM arginine, and 0.798 mM lysine or lys+8 (Cambridge Isotopes) [9]. One day prior to cumate addition, cells were passaged and seeded at a density of 3×10^6 in 150 cm^2 tissue culture flasks. Cumate was added to cells at a final concentration of 300 μg/mL. At 24 h post induction, cells were washed with PBS and fresh medium containing 1 mM Aha was added.

Enrichment of newly synthesized proteins. After incubation with Aha for 4 h, cells were washed, detached, and lysed using cold 4% SDS/PBS solution containing protease inhibitors (Roche). Lysates were clarified by centrifugation at 14,000 g for 5 min. Supernatant was collected and diluted to a final SDS concentration of 0.1%. Total protein concentration in each lysate sample was quantified using a BCA protein assay according to the manufacturer's protocol (Pierce). Lysates from light and heavy cultures were mixed at equal protein concentration. Affinity probes were attached using published click chemistry conditions [37]. Excess probes were removed by precipitating proteins with cold acetone at -20 °C.

To enrich for newly synthesized proteins, pelleted protein was dissolved in 0.1% SDS/PBS solution and allowed to bind Streptavidin Plus UltraLink resin (Pierce) for 1 h at RT. Samples were washed thoroughly with 1% SDS/PBS and 0.1% SDS/PBS and bound proteins were cleaved by incubation with 5% formic acid for 4 h. Newly synthesized proteins were then eluted with 0.1% SDS/PBS and concentrated for further preparation for MS.

Sample preparation for MS. Enriched proteins were separated by SDS-PAGE gel electrophoresis and each lane was cut into eight equal gel slices. Gel slices containing proteins were subjected to reduction with 7 mM DTT solution for 30 min at 50 °C before alkylation with 37 mM chloroacetamide for 30 min in the dark. In-gel digestion was carried out in 3 ng/μL lysC (Promega) solution at 37 °C overnight. Peptides were extracted from gel slices and desalted on C-18 columns prior to MS analysis.

Mass spectrometry. Mass spectrometry experiments were performed on an EASY-nLC (Thermo Scientific) connected to a hybrid LTQ-Orbitrap Classic with a nanoelectrospray ion source (Thermo Scientific). Binding and separation of the peptides took place on a 15cm silica analytical column (75 μm ID) packed in-house with reversed phase ReproSil-Pur C_{18AQ} 3 μm resin (Dr Maisch GmbH, Ammerbuch-Entringen, Germany). Samples were run for 60 min on a 2% to 30% acetonitrile gradient in 0.2% formic acid at a flow rate of 350 nL per minute. The mass spectrometer was programmed to acquire data in a data-dependent mode, automatically switching between full-scan MS and tandem MS acquisition. Survey full scan MS spectra (from m/z 300 to 1,700) were acquired in the Orbitrap after the accumulation of 500,000 ions, with a resolution of 60,000 at 400 m/z. The ten most intense ions were sequentially isolated, and after the accumulation of 5,000 ions, fragmented in the linear ion trap by CID (collisional energy 35% and isolation width 2 Da). Precursor ion charge state screening was enabled and singly charged and unassigned charge states were rejected. The dynamic exclusion list was set for a 90s maximum retention time, a relative mass window of 10 ppm, and early expiration was enabled.

MS data analysis. Thermo raw data files were analyzed by MaxQuant (v 1.2.2.5)[38] and were searched against the IPI human database (75,710 sequences) and an in-house contaminant database (259 sequences) including human keratins and proteases. All default options were used except as follows: match between runs was enabled (2 min maximum), variable modifications on methionine of Aha (-4.9863), AlST (+835.4300), AlST-X (+93.0868), Oxidation (+15.9949), and protein N-terminal acetylation (+42.0106), fixed modification on cysteine of Carbamidomethyl (+57.0215) and multiplicity of 2 with heavy label Lys8 (+8.014199). LysC digest was specified with up to two missed cleavages. Initial precursor mass tolerance was 7 ppm; however, MaxQuant calculates tighter individual precursor tolerances after recalibration. Fragment ion tolerance was 0.5 Daltons. Peptide, protein, and site false discovery rates were fixed at 1% using the target-decoy approach with a reversed database.[38] The minimum number of peptides for quantification was 1. Further data processing was performed to calculate ratios and standard errors of the ratios using in-house scripts described previously.[39] Briefly, hierarchical models are constructed of the data, where the overall ratio for each protein is the geometric mean of the biological replicates and the biological replicate ratio is the median of all of the peptide ratios in the replicate. The standard error of the overall protein ratio is calculated by estimating the global peptide ratio standard error using pooled variance (calculated separately for peptide ratios based on requantified isotopic patterns) and using a bootstrapping procedure to resample at each level in the hierarchical model. In cases where the protein replicate ratios are inconsistent (i.e. upregulated in one sample and downregulated in another), the standard error would be very large and the protein would not be considered significantly changed from 1:1.

Luciferase reporter assays. HEK293 cells (20,000 per well) were seeded in a 96-well plate and grown for 24 h. Cells were transfected with a plasmid cocktail containing 50 ng pRL-CMV (renilla luciferase control), 50 ng firefly luciferase construct outfitted with the 3' UTR of interest, and either pcDNA3.1+-miR126 or pcDNA3.1+-miRex, using lipofectamine LTX (Invitrogen). At 48 h post transfection, the Dual-Glo luciferase assay was performed according to the manufacturer's instructions (Promega). Luminescence was measured on a microplate reader (Tecan).

Oligonucleotides used in this study.

CD97 3'UTR PCR primer fwd: 5'-AATTA**ACTAGT**AGGCGCATGGTTCTGGACGGCCCAG-3' (restriction sites underlined)

CD97 3' UTR PCR primer rev: 5'-TATA**AAGCTT**TCTTCTGTATGCATGTGTTTAATTTTAAGTGTCAACACTGAAAAAT-3'

CD97-ex PCR1 fwd: 5'- GTGTTTGTGGACGAAGTACCGAAAGGTC-3'

CD97-ex PCR1 rev: 5'- ***GCAGGCCTCTCTCAGGCAGT***GGCCCCAAGG-3' (overlapping region in bold italics)

CD97-ex PCR2 fwd: 5'- ACTGCCTG***AGAGAGGCCTGCCCTGCCTG***-3'

CD97-ex PCR2 rev: 5'- GCAAGGCGATTAAGTTGGGTAACGCC-3'

CD97-ex PCR3 fwd: 5'-AATTA**ACTAGT**AGGCGCATGGTTCTGGACGGCCCAG-3'

CD97-ex PCR3 rev: 5’-

TATA**AAGCTT**TCTTCTGTATGCATGTGTTTAATTTTAAGTGTCAACACTGAAAAA

T-3’

CD97-M3-126: 5’-

TGGGGCCACTGCCTGAGGCTC***TGC***GTACAGAGGCCTGCCCTGCCT-3’ (mutations in bolded italics)

CD97-M3-126*: 5’-

TCCCTCCACCCTCCCTCCCTGATCCCGT***CAT***CCACCAGGAGGGAGTGGCAGCTAT

AGTCT-3’

CD97-M3-R1: 5’-

GGAGCCACTGGTCCTGCTGCTGGCTGCC***AGA***CTGCTCCACCTTGTGACCCAGGGT

GGGGA-3’

CD97-M3-R2: 5’-

TGGGGCTCAGCTTCCCTCTTAAGCTAAG***TGA***GATGTCAGAGGCCCCATGGCGAG

GCCCCT-3’

miR-126 with flanking region sequence: pre-miR-126 sequence in bolded italics

5’-

GCTAGCGAATTCGCCCTTGTGGACATTGCCGTGTGGCTGTTAGGCATGGTGGGGG

GCACTGGAATCTGGGCGGAAGGCGGTGGGGACTCCCTCTCCAGGGAGGGAGGAT

GGGGAGGGAGGATAGGTGGGTTCCCGAGAACTGGGGGCAGGTTGCCCGGAGCC

TCATATCAGCCAAGAAGGCAGAAGTGCCCCGTCCCGGGGTCCTGTCTGCATCCA

GCGCAGCATTCTGGAAGACGCCACGCCTC***CGCTGGCGACGGGACATTATTACTTT TGGTACGCGCTGTGACACTTCAAACTCGTACCGTGAGTAATAATGCGCCGTCCACG GCACCGCATCGAAAACGCCGCTGAGACCTCAGCCTTGACCTCCCTCAGCGTGGCC GGGA***CCCTGAGCCTCTGCGCAGAGCCACCCGCCCCGACGTACTTAGGCGGCATA GCCCTGAGACCTCTGGCCAGCGCCAGGCAGGCAGCGGGGGCGGCAGAGGCCTG GGCCTGAGTCTTCTGGCTCTGCCTCGCGGCCGC -3'

Acknowledgments

We thank Sonja Hess, Michael Sweredoski, Bobby Graham, Annie Moradian, and Geoffrey Smith at the Proteomic Exploration Laboratory (PEL) of the Beckman Institute at Caltech for assistance with proteomic studies. We thank Katharine Fang, Kai Yuet, and Larry Dooling for cloning advice, and Shelley Diamond for assistance with flow cytometry.

References

1. (a) Ambros, V., MicroRNA pathways in flies and worms: growth, death, fat, stress, and timing. *Cell* **2003,** *113* (6), 673-6; (b) Friedman, R. C.; Farh, K. K.; Burge, C. B.; Bartel, D. P., Most mammalian mRNAs are conserved targets of microRNAs. *Genome Res* **2009,** *19* (1), 92-105.

2. (a) Bartel, D. P., MicroRNAs: genomics, biogenesis, mechanism, and function. *Cell* **2004,** *116* (2), 281-97; (b) Lagos-Quintana, M.; Rauhut, R.; Lendeckel, W.; Tuschl, T., Identification of novel genes coding for small expressed RNAs. *Science* **2001,** *294* (5543),

853-8; (c) Garzon, R.; Calin, G. A.; Croce, C. M., MicroRNAs in Cancer. *Annu Rev Med* **2009,** *60*, 167-79.

3. Croce, C. M., Causes and consequences of microRNA dysregulation in cancer. *Nat Rev Genet* **2009,** *10* (10), 704-14.

4. Parker, L. H.; Schmidt, M.; Jin, S. W.; Gray, A. M.; Beis, D.; Pham, T.; Frantz, G.; Palmieri, S.; Hillan, K.; Stainier, D. Y.; De Sauvage, F. J.; Ye, W., The endothelial-cell-derived secreted factor Egfl7 regulates vascular tube formation. *Nature* **2004,** *428* (6984), 754-8.

5. (a) Crawford, M.; Brawner, E.; Batte, K.; Yu, L.; Hunter, M. G.; Otterson, G. A.; Nuovo, G.; Marsh, C. B.; Nana-Sinkam, S. P., MicroRNA-126 inhibits invasion in non-small cell lung carcinoma cell lines. *Biochem Biophys Res Commun* **2008,** *373* (4), 607-12; (b) Meister, J.; Schmidt, M. H., miR-126 and miR-126*: new players in cancer. *ScientificWorldJournal* **2010,** *10*, 2090-100; (c) Musiyenko, A.; Bitko, V.; Barik, S., Ectopic expression of miR-126*, an intronic product of the vascular endothelial EGF-like 7 gene, regulates prostein translation and invasiveness of prostate cancer LNCaP cells. *J Mol Med (Berl)* **2008,** *86* (3), 313-22; (d) Tavazoie, S. F.; Alarcon, C.; Oskarsson, T.; Padua, D.; Wang, Q.; Bos, P. D.; Gerald, W. L.; Massague, J., Endogenous human microRNAs that suppress breast cancer metastasis. *Nature* **2008,** *451* (7175), 147-52; (e) Yang, J.; Lan, H.; Huang, X.; Liu, B.; Tong, Y., MicroRNA-126 inhibits tumor cell growth and its expression level correlates with poor survival in non-small cell lung cancer patients. *PLoS One* **2012,** *7* (8), e42978.

6. Dieterich, D. C.; Link, A. J.; Graumann, J.; Tirrell, D. A.; Schuman, E. M., Selective identification of newly synthesized proteins in mammalian cells using bioorthogonal

noncanonical amino acid tagging (BONCAT). *Proc Natl Acad Sci U S A* **2006,** *103* (25), 9482-7.

7. (a) Elschenbroich, S.; Ignatchenko, V.; Sharma, P.; Schmitt-Ulms, G.; Gramolini, A. O.; Kislinger, T., Peptide separations by on-line MudPIT compared to isoelectric focusing in an off-gel format: application to a membrane-enriched fraction from C2C12 mouse skeletal muscle cells. *J Proteome Res* **2009,** *8* (10), 4860-9; (b) Gilar, M.; Olivova, P.; Chakraborty, A. B.; Jaworski, A.; Geromanos, S. J.; Gebler, J. C., Comparison of 1-D and 2-D LC MS/MS methods for proteomic analysis of human serum. *Electrophoresis* **2009,** *30* (7), 1157-67; (c) Horvatovich, P.; Hoekman, B.; Govorukhina, N.; Bischoff, R., Multidimensional chromatography coupled to mass spectrometry in analysing complex proteomics samples. *J Sep Sci* **2010,** *33* (10), 1421-37; (d) Schirle, M.; Heurtier, M. A.; Kuster, B., Profiling core proteomes of human cell lines by one-dimensional PAGE and liquid chromatography-tandem mass spectrometry. *Mol Cell Proteomics* **2003,** *2* (12), 1297-305.

8. (a) Howden, A. J.; Geoghegan, V.; Katsch, K.; Efstathiou, G.; Bhushan, B.; Boutureira, O.; Thomas, B.; Trudgian, D. C.; Kessler, B. M.; Dieterich, D. C.; Davis, B. G.; Acuto, O., QuaNCAT: quantitating proteome dynamics in primary cells. *Nat Methods* **2013,** *10* (4), 343-6; (b) Somasekharan, S. P.; Stoynov, N.; Rotblat, B.; Leprivier, G.; Galpin, J. D.; Ahern, C. A.; Foster, L. J.; Sorensen, P. H., Identification and quantification of newly synthesized proteins translationally regulated by YB-1 using a novel Click-SILAC approach. *J Proteomics* **2012,** *77*, e1-10.

9. Ong, S. E.; Mann, M., A practical recipe for stable isotope labeling by amino acids in cell culture (SILAC). *Nat Protoc* **2006,** *1* (6), 2650-60.

10. Mullick, A.; Xu, Y.; Warren, R.; Koutroumanis, M.; Guilbault, C.; Broussau, S.; Malenfant, F.; Bourget, L.; Lamoureux, L.; Lo, R.; Caron, A. W.; Pilotte, A.; Massie, B., The cumate gene-switch: a system for regulated expression in mammalian cells. *BMC Biotechnol* **2006,** *6*, 43.

11. Ren, G.; Kang, Y., A one-two punch of miR-126/126* against metastasis. *Nat Cell Biol* **2013,** *15* (3), 231-3.

12. Jusufovic, E.; Rijavec, M.; Keser, D.; Korosec, P.; Sodja, E.; Iljazovic, E.; Radojevic, Z.; Kosnik, M., let-7b and miR-126 are down-regulated in tumor tissue and correlate with microvessel density and survival outcomes in non--small--cell lung cancer. *PLoS One* **2012,** *7* (9), e45577.

13. Li, Z.; Li, N.; Wu, M.; Li, X.; Luo, Z.; Wang, X., Expression of miR-126 suppresses migration and invasion of colon cancer cells by targeting CXCR4. *Mol Cell Biochem* **2013,** *381* (1-2), 233-42.

14. (a) Kolb, H. C.; Finn, M. G.; Sharpless, K. B., Click Chemistry: Diverse Chemical Function from a Few Good Reactions. *Angew Chem Int Ed Engl* **2001,** *40* (11), 2004-2021; (b) Rostovtsev, V. V.; Green, L. G.; Fokin, V. V.; Sharpless, K. B., A stepwise huisgen cycloaddition process: copper(I)-catalyzed regioselective "ligation" of azides and terminal alkynes. *Angew Chem Int Ed Engl* **2002,** *41* (14), 2596-9; (c) Tornoe, C. W.; Christensen, C.; Meldal, M., Peptidotriazoles on solid phase: [1,2,3]-triazoles by regiospecific copper(i)-catalyzed 1,3-dipolar cycloadditions of terminal alkynes to azides. *J Org Chem* **2002,** *67* (9), 3057-64; (d) Wang, Q.; Chan, T. R.; Hilgraf, R.; Fokin, V. V.; Sharpless, K. B.; Finn, M. G., Bioconjugation by copper(I)-catalyzed azide-alkyne [3 + 2] cycloaddition. *J Am Chem Soc* **2003,** *125* (11), 3192-3.

15. Szychowski, J.; Mahdavi, A.; Hodas, J. J.; Bagert, J. D.; Ngo, J. T.; Landgraf, P.; Dieterich, D. C.; Schuman, E. M.; Tirrell, D. A., Cleavable biotin probes for labeling of biomolecules via azide-alkyne cycloaddition. *J Am Chem Soc* **2010,** *132* (51), 18351-60.

16. Huntzinger, E.; Izaurralde, E., Gene silencing by microRNAs: contributions of translational repression and mRNA decay. *Nat Rev Genet* **2011,** *12* (2), 99-110.

17. Griffiths-Jones, S.; Saini, H. K.; van Dongen, S.; Enright, A. J., miRBase: tools for microRNA genomics. *Nucleic Acids Res* **2008,** *36* (Database issue), D154-8.

18. Enright, A. J.; John, B.; Gaul, U.; Tuschl, T.; Sander, C.; Marks, D. S., MicroRNA targets in Drosophila. *Genome Biol* **2003,** *5* (1), R1.

19. (a) Lewis, B. P.; Burge, C. B.; Bartel, D. P., Conserved seed pairing, often flanked by adenosines, indicates that thousands of human genes are microRNA targets. *Cell* **2005,** *120* (1), 15-20; (b) Grimson, A.; Farh, K. K.; Johnston, W. K.; Garrett-Engele, P.; Lim, L. P.; Bartel, D. P., MicroRNA targeting specificity in mammals: determinants beyond seed pairing. *Mol Cell* **2007,** *27* (1), 91-105; (c) Garcia, D. M.; Baek, D.; Shin, C.; Bell, G. W.; Grimson, A.; Bartel, D. P., Weak seed-pairing stability and high target-site abundance decrease the proficiency of lsy-6 and other microRNAs. *Nat Struct Mol Biol* **2011,** *18* (10), 1139-46.

20. Betel, D.; Wilson, M.; Gabow, A.; Marks, D. S.; Sander, C., The microRNA.org resource: targets and expression. *Nucleic Acids Res* **2008,** *36* (Database issue), D149-53.

21. Betel, D.; Koppal, A.; Agius, P.; Sander, C.; Leslie, C., Comprehensive modeling of microRNA targets predicts functional non-conserved and non-canonical sites. *Genome Biol* **2010,** *11* (8), R90.

22. Liu, D.; Trojanowicz, B.; Ye, L.; Li, C.; Zhang, L.; Li, X.; Li, G.; Zheng, Y.; Chen, L., The invasion and metastasis promotion role of CD97 small isoform in gastric carcinoma. *PLoS One* **2012,** *7* (6), e39989.

23. Zhang, J.; Du, Y. Y.; Lin, Y. F.; Chen, Y. T.; Yang, L.; Wang, H. J.; Ma, D., The cell growth suppressor, mir-126, targets IRS-1. *Biochem Biophys Res Commun* **2008,** *377* (1), 136-40.

24. Kruger, J.; Rehmsmeier, M., RNAhybrid: microRNA target prediction easy, fast and flexible. *Nucleic Acids Res* **2006,** *34* (Web Server issue), W451-4.

25. Zhang, Y.; Yang, P.; Sun, T.; Li, D.; Xu, X.; Rui, Y.; Li, C.; Chong, M.; Ibrahim, T.; Mercatali, L.; Amadori, D.; Lu, X.; Xie, D.; Li, Q. J.; Wang, X. F., miR-126 and miR-126* repress recruitment of mesenchymal stem cells and inflammatory monocytes to inhibit breast cancer metastasis. *Nat Cell Biol* **2013,** *15* (3), 284-94.

26. (a) Li, X. M.; Wang, A. M.; Zhang, J.; Yi, H., Down-regulation of miR-126 expression in colorectal cancer and its clinical significance. *Med Oncol* **2011,** *28* (4), 1054-7; (b) Feng, R.; Chen, X.; Yu, Y.; Su, L.; Yu, B.; Li, J.; Cai, Q.; Yan, M.; Liu, B.; Zhu, Z., miR-126 functions as a tumour suppressor in human gastric cancer. *Cancer Lett* **2010,** *298* (1), 50-63; (c) Liu, B.; Peng, X. C.; Zheng, X. L.; Wang, J.; Qin, Y. W., MiR-126 restoration down-regulate VEGF and inhibit the growth of lung cancer cell lines in vitro and in vivo. *Lung Cancer* **2009,** *66* (2), 169-75; (d) Saito, Y.; Friedman, J. M.; Chihara, Y.; Egger, G.; Chuang, J. C.; Liang, G., Epigenetic therapy upregulates the tumor suppressor microRNA-126 and its host gene EGFL7 in human cancer cells. *Biochem Biophys Res Commun* **2009,** *379* (3), 726-31.

27. (a) Aust, G.; Steinert, M.; Schutz, A.; Boltze, C.; Wahlbuhl, M.; Hamann, J.; Wobus, M., CD97, but not its closely related EGF-TM7 family member EMR2, is expressed on gastric, pancreatic, and esophageal carcinomas. *Am J Clin Pathol* **2002,** *118* (5), 699-707; (b) Liu, Y.; Chen, L.; Peng, S.; Chen, Z.; Gimm, O.; Finke, R.; Hoang-Vu, C., The expression of CD97EGF and its ligand CD55 on marginal epithelium is related to higher stage and depth of tumor invasion of gastric carcinomas. *Oncol Rep* **2005,** *14* (6), 1413-20; (c) Aust, G.; Eichler, W.; Laue, S.; Lehmann, I.; Heldin, N. E.; Lotz, O.; Scherbaum, W. A.; Dralle, H.; Hoang-Vu, C., CD97: a dedifferentiation marker in human thyroid carcinomas. *Cancer Res* **1997,** *57* (9), 1798-806; (d) Steinert, M.; Wobus, M.; Boltze, C.; Schutz, A.; Wahlbuhl, M.; Hamann, J.; Aust, G., Expression and regulation of CD97 in colorectal carcinoma cell lines and tumor tissues. *Am J Pathol* **2002,** *161* (5), 1657-67; (e) ACS Chem BiolHoang-Vu, C.; Bull, K.; Schwarz, I.; Krause, G.; Schmutzler, C.; Aust, G.; Kohrle, J.; Dralle, H., Regulation of CD97 protein in thyroid carcinoma. *J Clin Endocrinol Metab* **1999,** *84* (3), 1104-9.

28. Kwakkenbos, M. J.; Kop, E. N.; Stacey, M.; Matmati, M.; Gordon, S.; Lin, H. H.; Hamann, J., The EGF-TM7 family: a postgenomic view. *Immunogenetics* **2004,** *55* (10), 655-66.

29. Wobus, M.; Huber, O.; Hamann, J.; Aust, G., CD97 overexpression in tumor cells at the invasion front in colorectal cancer (CC) is independently regulated of the canonical Wnt pathway. *Mol Carcinog* **2006,** *45* (11), 881-6.

30. Galle, J.; Sittig, D.; Hanisch, I.; Wobus, M.; Wandel, E.; Loeffler, M.; Aust, G., Individual cell-based models of tumor-environment interactions: Multiple effects of CD97 on tumor invasion. *Am J Pathol* **2006,** *169* (5), 1802-11.

31. (a) Safaee, M.; Clark, A. J.; Oh, M. C.; Ivan, M. E.; Bloch, O.; Kaur, G.; Sun, M. Z.; Kim, J. M.; Oh, T.; Berger, M. S.; Parsa, A. T., Overexpression of CD97 confers an invasive phenotype in glioblastoma cells and is associated with decreased survival of glioblastoma patients. *PLoS One* **2013,** *8* (4), e62765; (b) Ward, Y.; Lake, R.; Martin, P. L.; Killian, K.; Salerno, P.; Wang, T.; Meltzer, P.; Merino, M.; Cheng, S. Y.; Santoro, M.; Garcia-Rostan, G.; Kelly, K., CD97 amplifies LPA receptor signaling and promotes thyroid cancer progression in a mouse model. *Oncogene* **2013,** *32* (22), 2726-38.

32. Li, X.; Shen, Y.; Ichikawa, H.; Antes, T.; Goldberg, G. S., Regulation of miRNA expression by Src and contact normalization: effects on nonanchored cell growth and migration. *Oncogene* **2009,** *28* (48), 4272-83.

33. Wang, T.; Ward, Y.; Tian, L.; Lake, R.; Guedez, L.; Stetler-Stevenson, W. G.; Kelly, K., CD97, an adhesion receptor on inflammatory cells, stimulates angiogenesis through binding integrin counterreceptors on endothelial cells. *Blood* **2005,** *105* (7), 2836-44.

34. (a) Guo, C.; Sah, J. F.; Beard, L.; Willson, J. K.; Markowitz, S. D.; Guda, K., The noncoding RNA, miR-126, suppresses the growth of neoplastic cells by targeting phosphatidylinositol 3-kinase signaling and is frequently lost in colon cancers. *Genes Chromosomes Cancer* **2008,** *47* (11), 939-46; (b) Wang, S.; Aurora, A. B.; Johnson, B. A.; Qi, X.; McAnally, J.; Hill, J. A.; Richardson, J. A.; Bassel-Duby, R.; Olson, E. N., The endothelial-specific microRNA miR-126 governs vascular integrity and angiogenesis. *Dev Cell* **2008,** *15* (2), 261-71.

35. Png, K. J.; Halberg, N.; Yoshida, M.; Tavazoie, S. F., A microRNA regulon that mediates endothelial recruitment and metastasis by cancer cells. *Nature* **2012,** *481* (7380), 190-4.

36. Livak, K. J.; Schmittgen, T. D., Analysis of relative gene expression data using real-time quantitative PCR and the 2(-Delta Delta C(T)) Method. *Methods* **2001,** *25* (4), 402-8.

37. Hong, V.; Presolski, S. I.; Ma, C.; Finn, M. G., Analysis and optimization of copper-catalyzed azide-alkyne cycloaddition for bioconjugation. *Angew Chem Int Ed Engl* **2009,** *48* (52), 9879-83.

38. Cox, J.; Mann, M., MaxQuant enables high peptide identification rates, individualized p.p.b.-range mass accuracies and proteome-wide protein quantification. *Nat Biotechnol* **2008,** *26* (12), 1367-72.

39. Pierce, N. W.; Lee, J. E.; Liu, X.; Sweredoski, M. J.; Graham, R. L.; Larimore, E. A.; Rome, M.; Zheng, N.; Clurman, B. E.; Hess, S.; Shan, S. O.; Deshaies, R. J., Cand1 promotes assembly of new SCF complexes through dynamic exchange of F box proteins. *Cell* **2013,** *153* (1), 206-15.

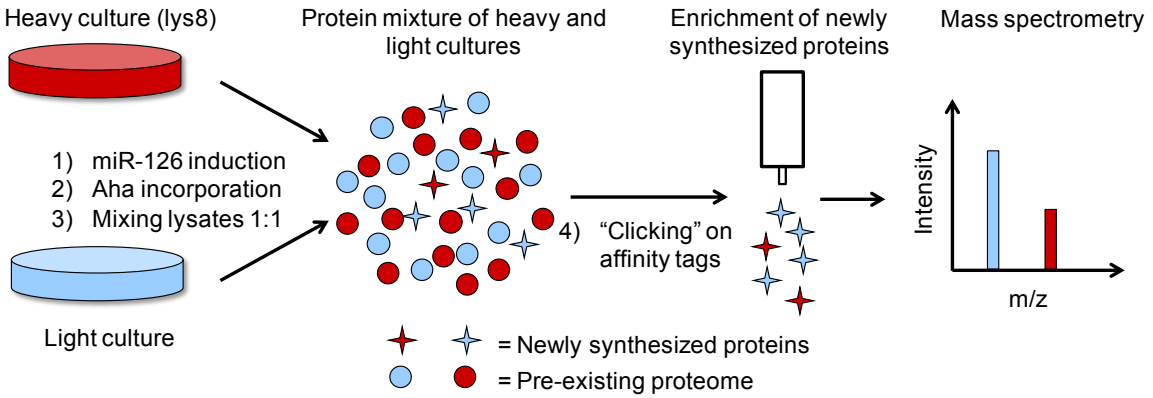

Scheme 2.1. A combined proteomic approach of BONCAT and SILAC.

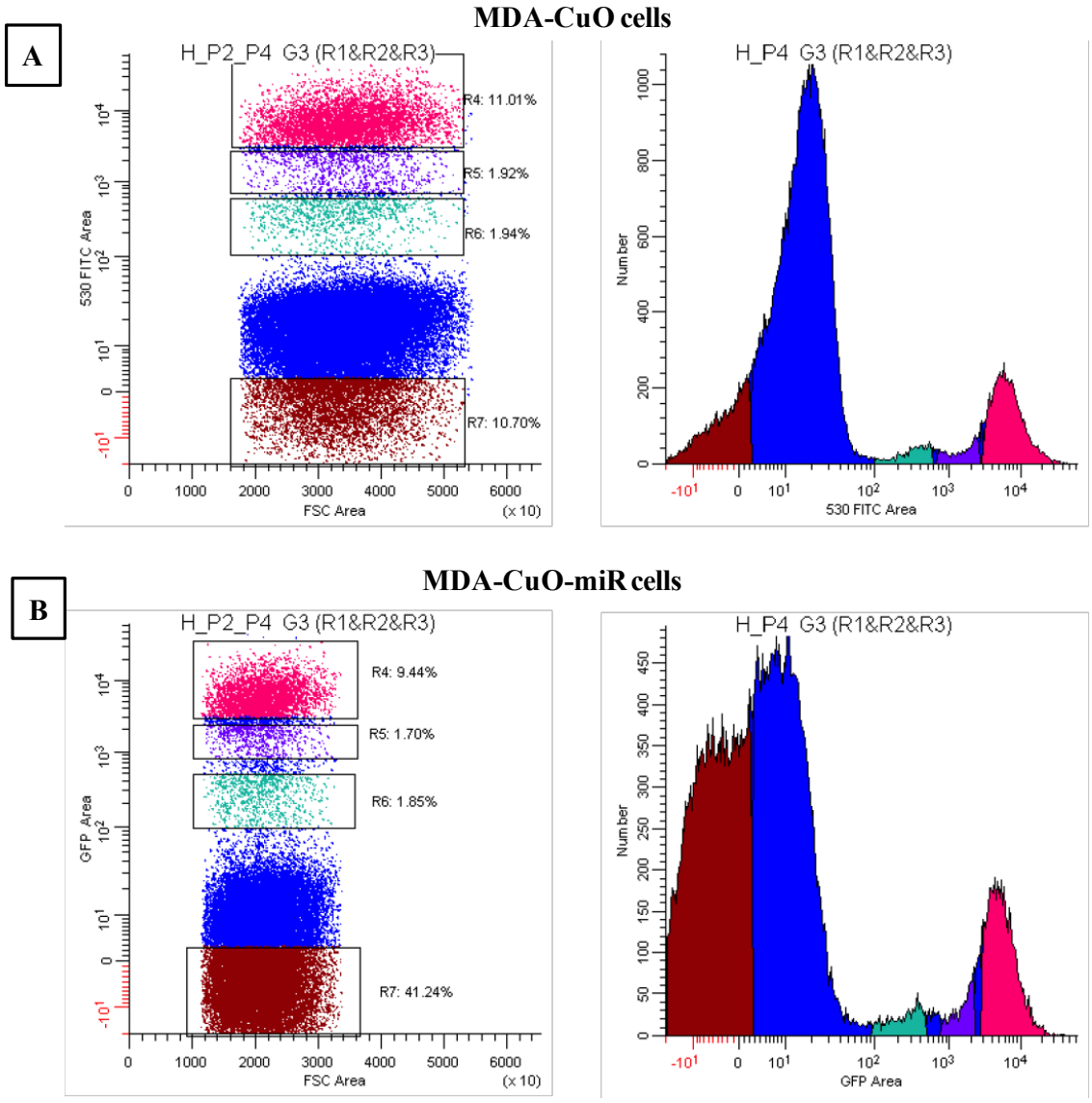

Figure 2.1. Fluorescence activated cell sorting (FACS) analysis of transduced MDA-MB-231 breast cancer cells. MDA-CuO cells (A) containing CymR repressor vector and empty SparQ cumate inducible vector and MDA-CuO-miR cells (B) capable of inducible expression of miR-126 precursor sequence were sorted according to GFP fluorescence to obtain cell populations with similar numbers of transgene integrations. Three cell populations with low (turquoise), medium (purple) and high (pink) fluorescence were collected, and cells with low fluorescence were used in subsequent studies.

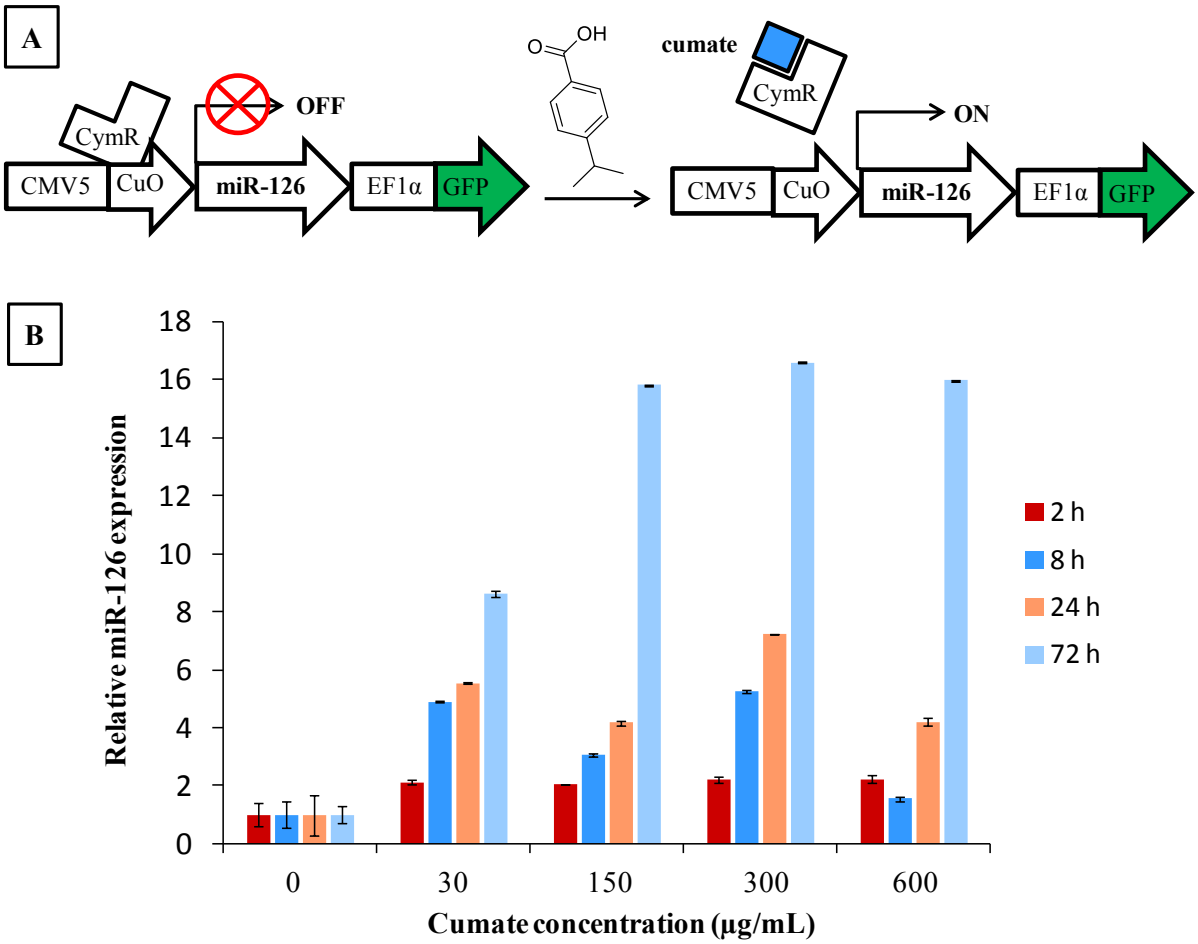

Figure 2.2. Cumate-inducible expression of miR-126 in MDA-MB-231 cells. (A) Cumate binds to repressor CymR and allows expression of miR-126. (B) RT-PCR analysis of relative miR-126 expression at various time points after induction with concentrations of cumate ranging from 0 to 600 µg/mL.

Protein	Fold change (log_2)
SDPR	-0.68
KIF4	-0.45
HSP27	-0.45
CNN3	-0.43
CD97	-0.40
EIF4F	-0.34
EGFR	0.31
COX6C	0.33
ASPH	0.39
NT5	0.39
PPIL3	0.39
LTB4DH	0.41
ACS3	0.41
CARS	0.43
DIA4	0.43
AARS	0.45
MSN	0.46
ETFA	0.46
CTSL	0.47
LAMB2	0.47
NDUFA4	0.48
ANTXR2	0.49
MMP14	0.52
ASNS	0.55
ETFB	0.56
ORCA	0.57
UGDH	0.63
PSA	0.71
ECH1	0.72
CD49B	0.82
TSC22D1	0.86
HMOX1	1.13
PGDH3	1.16

Table 2.1. Proteins responsive to miR-126 overexpression identified by a combined BONCAT-SILAC approach. Listed are proteins quantified using at least 6 independent measurements that exhibit consistent regulation of more than 20% in both initial experiments and cumate control experiments.

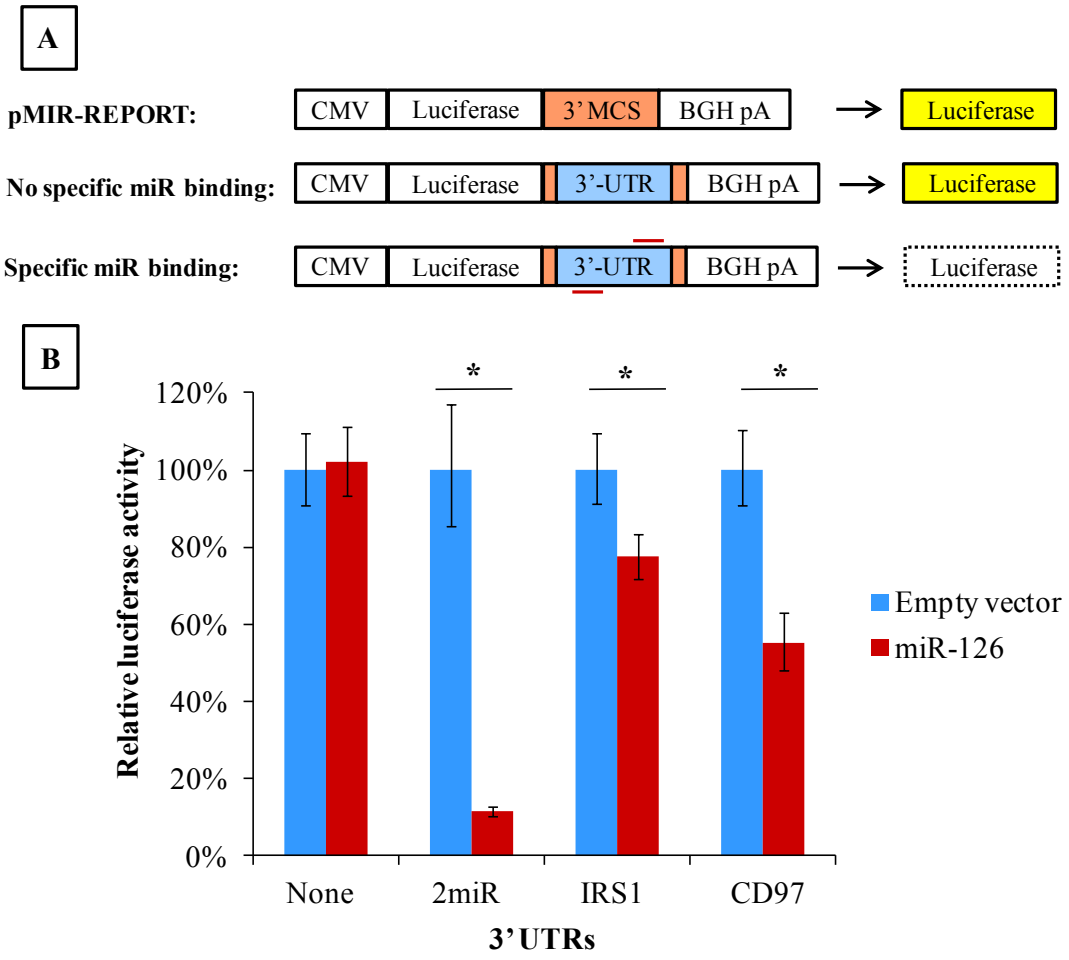

Figure 2.3. *CD97* is a direct target of miR-126. (A) pMIR-REPORT construct was used for luciferase assay, and specific miRNA binding in the 3'-UTR regulates reporter expression. (B) Human embryonic kidney (HEK) cells were cotransfected with pMIR-REPORT containing the indicated 3'-UTRs and pcDNA3.1^{+}-miR126 or pcDNA3.1^{+} empty vector control. Relative luciferase activity was measured 48 h later. 2miR contains two miR-126 binding sites and IRS1 is a known target of miR-126. Vector control was taken as 100%. *P* values were obtained using one-sided unpaired Student's t-tests. *$P < 0.01$.

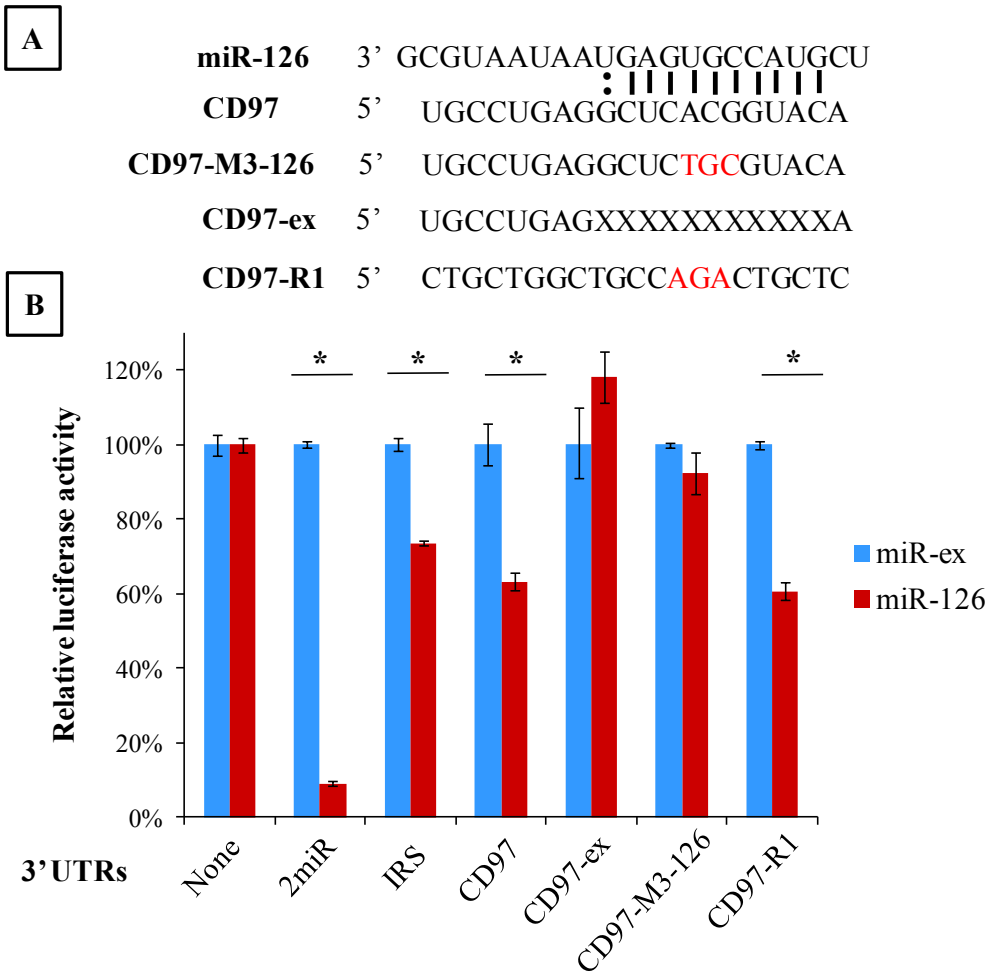

Figure 2.4. Identification of the binding site of miR-126 in *CD97* 3'UTR. (A) A computationally predicted miR-126 interaction site in *CD97* 3'UTR and *CD97* 3'UTR mutants used for luciferase assay. (B) Either removing the predicted binding site or mutating three nucleotides within the binding site abolished miR-126-dependent suppression of the luciferase activity of the *CD97* 3'UTR construct. Mutations at a random site within the *CD97* 3'UTR had no effect on suppression of luciferase activity. miR-ex control was taken as 100%. *P* values were obtained using one-sided unpaired Student's t-tests. *$P < 0.01$.

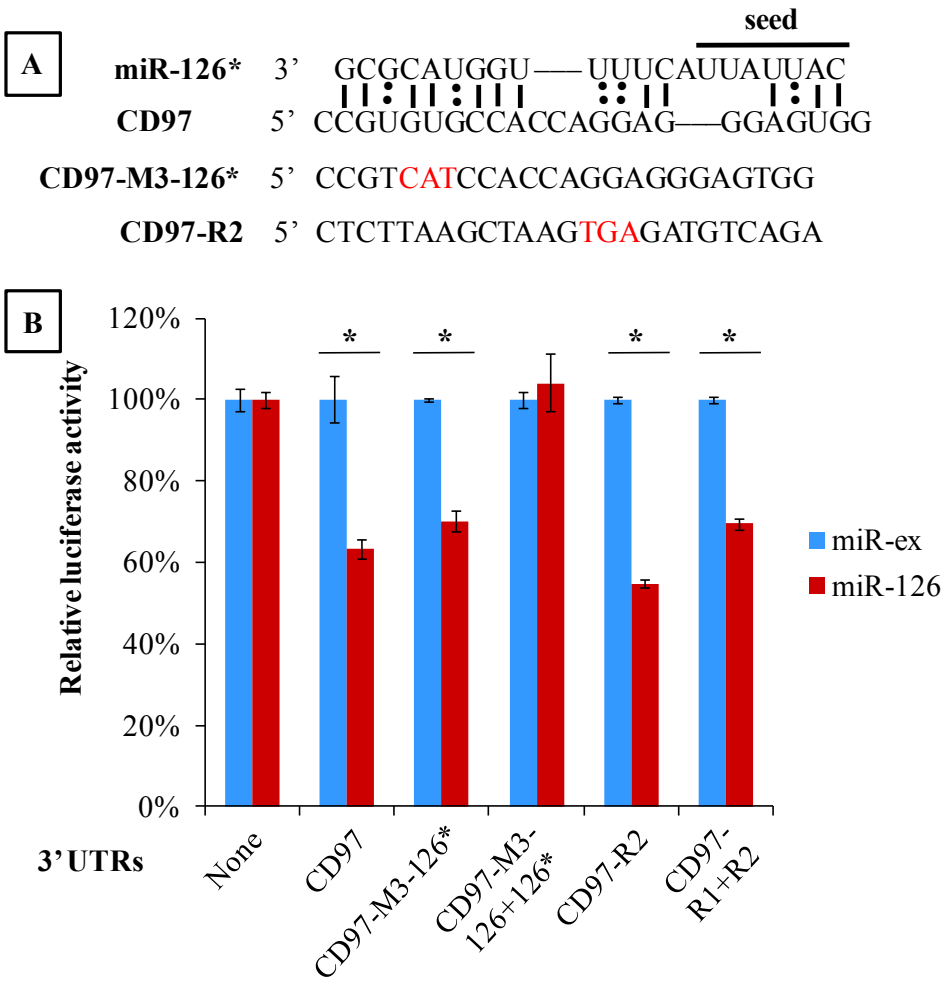

Figure 2.5. *CD97* is a direct target of miR-126, not miR-126*. (A) The most favorable miR-126* interaction site in *CD97* 3'UTR predicted by RNAhybrid algorithm and *CD97* 3'UTR mutants used for luciferase assay. (B) Neither mutations at the predicted binding site for miR-126* nor at any other random position within *CD97* 3'UTR rescued suppression of luciferase activity. miR-ex control was taken as 100%. *P* values were obtained using one-sided unpaired Student's t-tests. *$P < 0.01$.

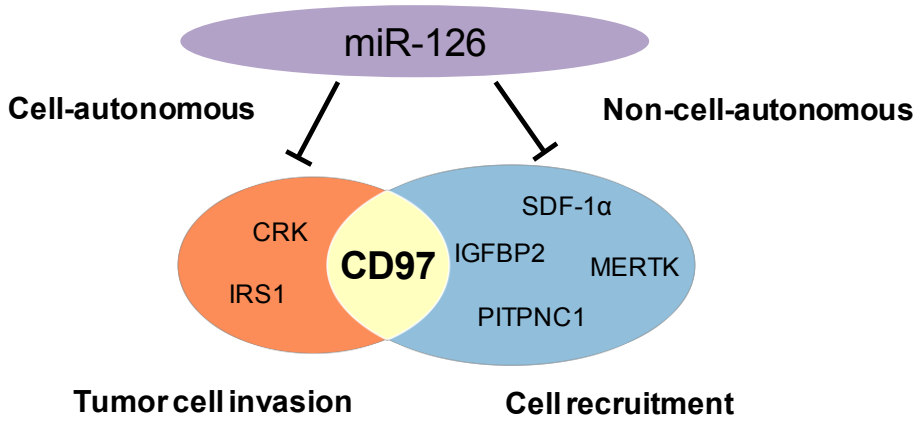

Figure 2.6. Direct targets of miR-126 in cancer. CD97, a pro-metastatic GPCR, has been reported to promote tumor cell invasion cell-autonomously by increasing tumor cell mobility and to induce angiogenesis non-cell-autonomously by recruiting endothelial cells. The identification of CD97 as a direct target of miR-126 sheds new light on the tumor suppressive roles of miR-126 in both cell-autonomous and non-cell-autonomous cancer progression.

CHAPTER 3

Developing Cyclooctyne Fluorophores for Imaging Living Cells using Noncanonical Amino Acids

This chapter was adapted with permission from: Beatty, KE; Fisk, JD; Smart, BP; Lu, YY; Szychowski, J; Hangeuer, MJ; Baskin, JM; Bertozzi, CR; Tirrell, DA. *Live-cell imaging of cellular proteins by a strain-promoted azide-alkyne cycloaddition*. ChemBioChem, 2010. **11** (15): 2092-2095.

Abstract

Circumventing the need for genetic manipulation, residue-specific incorporation of reactive amino acids allows labeling of newly synthesized proteins for visualization of cellular events. Copper-catalyzed azide-alkyne ligation is highly selective and has been previously used to label proteins within cells; however, the toxicity of copper limits its use to imaging fixed specimens. Here we report the synthesis of a set of membrane-permeant cyclooctyne coumarin dyes and demonstrate labeling of azide-containing proteins in live cells using copper-free strain-promoted azide-alkyne cycloaddition. Confocal fluorescence micrographs showed specific fluorescence in Rat-1 fibroblasts pre-treated with azidohomoalanine (Aha), an azide-containing methionine analogue. Counterstaining using MitoTracker Red showed healthy mitochondrial morphology of cells after Aha pulse and dye labeling. Further, we identified optimum labeling conditions for the cyclooctynes, providing powerful new tools for visualizing dynamic cellular processes in living cells.

Introduction

Protein synthesis, degradation, and trafficking contribute to the highly dynamic and complex nature of many cellular processes. Imaging studies of fixed cells can only provide snapshots of these processes. Live cell imaging has allowed scientists to observe internal structures and cellular processes in real time, providing invaluable insights to understanding biology. The most widely used protein-labeling strategy for live cell imaging is to create a fusion between the target protein and a fluorescent protein.[1] While this strategy allows tracking of

preselected proteins, it requires genetic manipulation and is not suitable for studying global protein synthesis and transport in living cells.

Circumventing the need for genetic manipulation, residue-specific incorporation of reactive amino acids allows tagging of newly synthesized proteins for subsequent selective modifications.[2] Azidohomoalanine (Aha) and homopropargylglycine (Hpg) are reactive methionine (Met) analogues that can be incorporated into proteins.[3] Proteins containing Aha or Hpg can be labeled with fluorophores by highly selective copper-catalyzed azide-alkyne ligations.[4] This approach has allowed selective labeling of newly synthesized proteins, but the toxicity of copper has limited its use in imaging fixed cells.[5]

The development of the strain-promoted, copper-free azide-alkyne cycloaddition provides excellent chemistry for labeling live cells.[6] Further, the reactivity of the cyclooctyne can be increased by elevated ring strain or by fluorination adjacent to the alkyne.[6b, 6c, 7] Using this efficient chemical reaction, glycan trafficking has been monitored in live cells and zebrafish embryos using membrane impermeable fluorophores.[6c, 7d] In order to explore beyond cell-surface labeling, we need new generations of fluorophores that will enable us to monitor dynamic cellular events inside living cells. In this study, we describe the design of a set of cell-permeable cyclooctyne coumarin dyes for labeling newly synthesized proteins inside living cells.

Results and Discussion

Designing cell-permeable cyclooctyne fluorophores. In order to create cell-permeant fluorophores for rapid labeling of live cells, we focused on two components: the fluorophore

and the cycloocytne. We chose coumarin as the fluorophore for its small size, membrane-permeant property, and two-photon excitation. Two-photon excitation fluorescence imaging is particularly advantageous for imaging living cells because it provides deeper penetration into the specimen with higher spatial resolution and less photodamage than single-photo confocal microscopy.[8] For cyclooctyne design, we chose to test several cyclooctyne acids with varying degree of fluorination. Commercially available dimethylaminocoumarin (DMAC) was conjugated to various differentially-activated cyclooctyne acids via a short linker to yield the coumarin-cyclooctyne conjugates **1-3** (Scheme 3.1). The linker was designed to improve the solubility of the molecules and to increase the distance between the dye and its protein target, which could potentially enhance the fluorescence signal.[9] The membrane permeability of these probes was assessed by Caco-2 permeability analysis,[10] and the results confirm their membrane permeability.

Determination of optimal conditions for labeling live cells. We used flow cytometry to optimize labeling conditions as a function of dye concentration, Aha pulse duration, and dye-labeling time. Rat-1 fibroblasts were pulsed with either Aha or Met for 4 h before reaction with each dye at concentrations between 0.5 to 50 μM for 10 min. The mean fluorescence increased with increasing dye concentration for all three probes (Figure 3.1a). The fluorescence enhancement is the ratio between the mean fluorescence for Aha-treated cells and that for Met-treated cells. With increasing concentrations of **1** and **2**, fluorescence enhancement increased with increasing dye concentrations. However, the fluorescence enhancement peaked at 10 μM for **3**, and increasing the dye concentration further did not improve fluorescence enhancement. This property of **3** was hypothesized to be due to

significant side reactions with cellular nucleophiles. Further investigations confirmed that **3** can react with cysteines *in vitro*.[11]

Cells pulsed for 0.5-4 h and dye-labeled for 6- 60 min at the optimum concentration of each dye were also analyzed using flow cytometry. Longer Aha-pulse duration led to increased fluorescence enhancement (Figure 3.1b). A 6 min dye-labeling yielded significant fluorescence enhancement for all three dyes and the fluorescence enhancement increased with dye-labeling time for probes **1** and **2** (Figure 3.1c). The more reactive **3** exhibited different optimum reaction conditions, including a shorter labeling time of 10 min at a lower dye concentration of 10 μM.

Labeling live mammalian cells. To assess the ability of these coumarin-cyclooctyne conjugates to label azide-containing proteins inside living cells, Rat-1 fibroblast cells were labeled and examined using confocal fluorescence microscopy. Near-confluent fibroblast cells were pulsed with 1 mM Aha or Met. Cells that had been pretreated with the protein synthesis inhibitor anisomycin were also pulsed with 1 mM Aha as a control for assessing the contribution of free Aha to the fluorescence signal. After a 4 h pulse, cells were washed and subjected to reaction with each of the coumarin conjugates for 10 min at 37 °C using optimized probe concentrations, 50 μM for **1** and **2**, and 10 μM for **3**. We used MitoTracker Red, a fluorescent dye that localizes to functional mitochondria, as a counterstain to assess mitochondrial morphology as a measure of cell viability. Following the reaction, cells were washed and examined by confocal microscopy (Figure 3.2). For all three dyes, bright fluorescence was observed in cells treated with Aha alone, while cells treated with Met or Aha plus anisomycin showed a lack of fluorescence. Further, the mitochondrial morphology observed by staining with MitoTracker Red suggested that cells were alive and healthy after

dye-labeling. Together, these images demonstrate the selective labeling of Aha-containing proteins in live cells.

Labeling patterns of these probes appears to vary depending on the type of cyclooctyne attached to DMAC. Fluorescence in Aha-treated cells was brighter in the cytoplasm and dim in the nucleus for **1** and **2**, while the fluorescence of cells labeled with **3,** a difluorinated cyclooctyne, appears to be more uniform. This observation could potentially be due to differences in reactivity and hydrophobicity attributed to the additional fluorination in **3.**

Evaluating the extent of labeling in cellular compartments. To confirm that labeling by these coumarin-cycooctynes is not confined to the cell membrane, we evaluated the extent of labeling in different cellular compartments. Rat-1 fibroblasts cells were pulsed with either 1 mM Aha, Met, or Aha plus anisomycin for 4 h. Cells were then washed and treated with 10 μM of each probe for 30 min. After dye-labeling, cells were detached, washed, counted, and collected by centrifugation. Cells were then lysed and four fractions containing cytoplasmic, membrane, nuclear, and cytoskeletal proteins were collected. To confirm efficient fractionation, fractionated protein samples were subjected to western blotting analysis using antibodies for compartment-specific protein markers, including the cytosolic protein β-tubulin, the endoplasmic reticulum (ER)-resident glucose-regulated protein (GRP78), and the nucleolar protein fibrillarin (Figure 3.3). Each protein marker was specifically detected in the expected fractions, indicating efficient separation of cellular compartments.

Protein concentrations in the fractionated protein samples were determined and fluorescence from each fraction was measured using a microplate reader. Raw fluorescence data were normalized by either cell number or protein concentration to yield the fluorescence

percentage for each fraction (Figure 3.4). Fluorescence was detected in all four cellular compartments for all three probes, confirming labeling within cells. Furthermore, although cells treated with probes **1** and **2** exhibit little fluorescence in the nucleus by fluorescence imaging, this study confirms labeling of nuclear proteins.

Conclusions

We synthesized a set of coumarin-cyclooctynes for labeling newly synthesized proteins in living cells. Brief exposure of these dyes to Aha-treated cells resulted in specific fluorescence in cells pulsed with Aha by both fluorescence microscopy and flow cytometry. Optimal labeling conditions were identified for each probe. Further, fluorescence was observed in different cellular compartments, confirming that labeling using these probes occurs throughout the cell, and is not confined to the cell membrane. The synthesis and characterization of these cell-permeant cyclooctyne fluorophores provide researchers with new tools to visualize dynamic cellular events by labeling azide-containing proteins in living cells.

Material and Methods

Cell Maintenance. Rat-1 fibroblasts cells were grown in Dulbecco's modified Eagle's medium (DMEM) (Invitrogen) supplemented with 10% (v/v) fetal bovine serum, 50 U/mL penicillin, and 50 μg/mL streptomycin. Cells were maintained in a 37 °C, 5% CO2 humidified incubator chamber. Near confluent cells were passaged with 0.05% trypsin in 0.52 mM EDTA.

Preparation of Cells for Fluorescence Microscopy. Lab-Tek chambered coverglass slides (8-well, Nalge Nunc International) were prepared by treatment with fibronectin solution (10 μg/mL). The wells were rinsed twice with PBS, blocked with a 2 mg/mL solution of heat inactivated BSA at room temperature, and rinsed with PBS.

Near-confluent cells in 100 mm Petri dishes were rinsed twice with warm phosphate-buffered saline (PBS). Cells were detached with trypsin in EDTA and added to the appropriate media. The cells were pelleted via centrifugation (200 *g*, 3 min) and counted. Cells were added at a density of 1 x 10^4 cells per well to prepared slides. Cells were grown in media overnight. After growth overnight in DMEM++, each well was washed twice (200 μL) with warm PBS. Cells were incubated for 5 min in serum-free medium lacking Met [SFM: DMEM, with 1 mg/mL bovine serum albumin (BSA, fraction V, Sigma-Aldrich), with 2 mM Glutamax I (Invitrogen), without Met], followed by 30 min in fresh SFM to deplete intracellular Met stores. Anisomycin (40 μM, Sigma-Aldrich) was added to cells during this time to inhibit protein synthesis. After incubation,

either 1 mM Met or 1 mM Aha was added to the medium. After 4 h, wells were rinsed twice with DMEM++ before adding the dye-labeling mixture.

Cells were exposed to coumarin-cyclooctyne in the labeling medium DMEM-Imaging [DMEM lacking phenol red, with HEPES (Invitrogen), supplemented with 10% FBS and 1 mg/mL BSA]. Each coumarin-cyclooctyne was added to the labeling medium as a dilution from a 10 mM stock solution in DMSO. Labeling was allowed to proceed for 10 min at 37 °C in the incubator chamber. After labeling, cells were washed twice before counterstaining. Cells were counterstained for 10 min with 300 nM MitoTracker Red CMXRos (Invitrogen).

After treatment, cells were washed thrice with DMEM-Imaging and then imaged in DMEM-Imaging. Cells were kept in an incubator until they could be imaged (up to 3 h).

For counterstaining with propidium iodide, cells were washed twice with DMEM++ before addition of a 1:1000 dilution of propidium iodide (1.0 mg/mL; Invitrogen) in DMEM-Imaging for 10 min. Cells were washed thrice before imaging. Fixed (3.7% paraformaldehyde, 10 min) and permeabilized (0.1% Triton X-100 in PBS, 3 min) cells were also imaged as a control. Fixed cells stained with propidium iodide were not treated with coumarin-cyclooctyne.

Live cells were imaged on a confocal microscope (Zeiss LSM 510 Meta NLO) at the Biological Imaging Center of the Beckman Institute at Caltech. A heated chamber was placed around the microscope to image the cells at ~37 °C. MitoTracker Red or propidium iodide fluorescence was obtained by excitation at 543 nm with emission collected between 565 and 615 nm. Transmitted light images were also collected to differentiate individual cells. Coumarin fluorescence was obtained by two-photon excitation at 800 nm (Ti:sapphire laser) with emission collected between 376 and 494 nm. The set of images for each dye was obtained with identical conditions to capture coumarin fluorescence. Individual optical slices of coumarin fluorescence were collected at 0.5 μm intervals in order to create an extended focus image (i.e., projection). Images were acquired with a Plan-Apochromat 63x/1.4 oil objective (Zeiss) and analyzed with Zeiss LSM and ImageJ1 software.

Preparation of Cells for Flow Cytometry. Pulse-labeling was performed directly in the 6-well tissue culture dishes in which cells were grown. Each well was washed twice with warm PBS, followed by a 30 min incubation in SFM to deplete intracellular Met stores. Cells were

then exposed to 1 mM Aha or 1 mM Met for 4 h. In addition to examining a 4 h pulse length, we also examined 0.8, 0.25, 0.5, and 1 h pulses. Then, cells were washed twice with PBS. Coumarin-cyclooctyne dye in DMEM-Imaging was added to each well for coumarin-labeling. Dye concentrations of 0.5 μM to 50 μM were examined. To examine alternative dye-labeling times, 10 μM dye was added for 6-60 min in DMEM-Imaging. After labeling, cells were washed twice with warm PBS and detached using 250 μL of 0.05% trypsin in EDTA. Cells were added to 750 μL DMEM++, and 100 μL FBS was added to the bottom of the Eppendorf tube to improve cell pelleting. Cells were pelleted by centrifugation (200 *g*, 3 min) and washed once with 1 mL DMEM-Imaging, once with a cushion of FBS added to the bottom of the tube. Finally, cells were resuspended in 400 μL DMEM-Imaging before filtering through a 50 μm Nytex nylon mesh screen (Sefar). Cells were stored on ice until analysis.

Flow Cytometry. Cells were analyzed on a FACSAria flow cytometer (BD Biosciences Immunocytometry Systems) at Caltech's Flow Cytometry Facility. Coumarin fluorescence was excited by a 407 nm laser and detected after passage through a 450/40 bandpass filter. Forward- and side-scatter properties were used to exclude doublets, dead cells, and debris from analysis. 7-

aminoactinomycin D (7-AAD; Beckman Coulter) was used to exclude dead cells from analysis. 7-AAD was excited by a 488 nm laser and detected after passage through a 695/40 filter. Unlabeled cells, 7-AAD labeled cells, and coumarin-labeled cells were analyzed to ensure minimal cross-over fluorescence in each channel. When necessary, compensation was applied to

reduce cross-over fluorescence. Data was analyzed using FloJo7 software (Tree Star).

Preparation of Live Cells for Fractionation. Pulse-labeling was performed directly in the 10 cm tissue culture dishes in which cells were grown. Each plate was washed twice with warm PBS and incubated 30 min in SFM to deplete intracellular Met. Anisomycin, a protein synthesis inhibitor, was added at this time. Cells were exposed to 1 mM Aha, 1 mM Aha with anisomycin, or 1 mM Met for pulse-labeling (4 h). Then plates were washed twice with warm PBS. Coumarin-cyclooctyne dyes (10 μM) in DMEM++ were added to each plate for fluorophore labeling. After labeling for 30 min, cells were washed twice with warm PBS and detached using 1 mL of 0.05% trypsin in EDTA. Plates were scraped using a cell scraper and cells were collected and added to 4 mL DMEM++. Cells were pelleted by centrifugation (500*g*, 10 min) and washed once with 2 mL ice-cold PBS. Cells were transferred to a clean eppendorf tube. Cells were then fractionated using the QProteome cell compartment kit (Qiagen). Briefly, each cell pellet was gently resuspended in 1 mL ice-cold extraction buffer CE1 and incubated at 4°C in a lab rotator for 10 min. The lysates were centrifuged at 1000 g for 10 min at 4°C. The supernatants (fraction 1) were carefully collected and saved on ice; this fraction should contain primarily cytoplasmic proteins. The pellets were then resuspended in ice-cold 1 mL extraction buffer CE2 and incubated at 4°C in a lab rotator for 30 min. The suspensions were then centrifuged at 6000 g for 10 min at 4°C. The supernatants (fraction 2) were carefully collected and put on ice; this fraction should contain primarily membrane proteins and proteins from the lumen of organelles. The pellets were then treated with Benzonase nuclease for 15 min at room temperature. Then 500 μL of ice-cold extraction buffer CE3 was added to each tube. The tubes were incubated at 4°C in a lab rotator for 10 min. The suspensions were then pelleted by centrifugation (6800 g, 4°C, 10 min). The

supernatants were carefully collected (fraction 3); this fraction should primarily contain nuclear proteins. The pelleted material was resuspended in 100 μL of room temperature buffer CE4 (fraction 4); this final fraction contains the remaining proteins, most of which should be cytoskeletal.

Western Blotting. Fractionated protein samples were separated on a 12% SDS-polyacrylamide gel and transferred to a nitrocellulose membrane (hybond ECL, GE Healthcare) using a semidry transfer system (Amersham Biosciences). After being blocked in 5% non-fat milk at room temperature for 1 h, the blots were incubated with primary antibodies (anti-GRP78, 1:250 and anti-fibrillarin, 1:1000, Abcam) for 2 h at room temperature. For β-tubulin detection, the blot was incubated with anti-β-tubulin-HRP conjugated antibodies (1:1000, Abcam) for 1 h at room temperature. After incubation in secondary HRP-conjugated anti-mouse IgG (1:10000) for 1 h at room temperature, the blots were washed with PBST three times prior to signal detection using ECL+ kit (GE Healthcare). The blots were imaged using a Typhoon molecular imager (GE Healthcare).

Preparation for fluorescence measurement. Fractionated protein samples were isolated using acetone precipitation and resuspended in RIPA buffer (Sigma). Protein concentrations were then determined by BCA assay. Fluorescence from each fraction was measured using a Safire II (Tecan) plate reader. Raw fluorescence data were normalized using either cell number or protein concentration and analyzed to yield fluorescence percentage in each fraction.

Synthesis of Coumarin-Cyclooctyne Dyes. All chemicals were purchased from Aldrich and used as received unless otherwise noted. Dry solvents were obtained from commercial

suppliers and used as received. Silica chromatography was performed using 230-400 mesh silica gel 60 (EMD). TLC was performed using Baker-flex silica gel IB-F plates; Rf values are reported under the same solvent conditions as those used for chromatography unless otherwise noted. TLC plates were examined under UV light for fluorescent compounds or alternatively stained with $KMnO_4$, ceric ammonium molybdenate, or *p*-anisaldehyde. NMR spectra were recorded on Varian spectrometers (300 MHz for ^1H) and processed with NUTS NMR software. NMR spectra were referenced to internal standards; proton and carbon spectra were referenced to tetramethylsilane. Fluorine spectra were referenced to hexafluorobenzene. All coupling constants are reported in hertz. FAB mass spectrometry was performed at the California Institute of Technology Mass Spectrometry Facility.

1-Boc-amino-13-amino-4,7,10-trioxotridecane, ***8*** (Scheme 3.2). A solution of ditert-butyldicarbonate (5.0 g, 23 mmol) in 100 mL of CH_2Cl_2 was added via a dropping funnel to a rapidly stirred solution of 1,13-diamino-4,7,10-trioxotridecane (10.1 g, 46 mmol) in 200 mL CH_2Cl_2 over a period of ~1 h. The resulting clear solution was stirred 16 h then transferred to a separatory funnel and washed twice with 100 mL of 0.1 M HCl and the aqueous layer was back-extracted 5 times with 50 mL of CH_2Cl_2. The combined organics were dried over $NaSO_4$ and evaporated to give 6.6 g (90%) of an opaque viscous oil, which was used without further purification. ^1H NMR (300 MHz, $CDCl_3$) δ 1.44 (s, 9 H), 1.55 (br s,2H), 1.68-1.84 (m, 4H), 2.81 (t, 2H, J = 6.8), 3.23 (br q, 2H, J = 6.2), 3.51-3.72 (m, 12H), 5.02-5.29 (2x br t, rotomers, 1H); ^{13}C NMR (75 MHz, $CDCl_3$) δ 28.46, 29.61, 33.26, 38.48, 39.62, 69.47, 69.56, 70.18, 70.22, 70.58, 70.60, 78.80, 156.05, 156.10; FAB MS calc for $C_{15}H_{33}N_2O_5$ $(M+H)^+$ 321.2389, observed 321.2386.

Boc-Linker-Coumarin ***9*** (Scheme 3.2). To a solution of 1-Boc-amino-13-amino-4,7,10-trioxotridecane, **8**, (0.027g, 80 μmol) and triethylamine (0.015 g, 140 μmol) in 2 mL of CH_2Cl_2 in a foil-wrapped flask was added 7-dimethylaminocoumarin-4-acetic acid succinimidyl ester (0.025 g, 73 μmol, Anaspec) in 1 mL of CH_2Cl_2. The reaction was stirred for 12 h and then the solvent was removed and the product purified by silica chromatography (1:19 ethanol:ethyl acetate, Rf = 0.25) yielding 40 mg ~100%. ^{1}H NMR (300 MHz, CDCl3) δ 1.43 (s, 9 H), 1.73 (app quintet, 4 H, *J* = 6.2), 3.06 (s, 6 H), 3.19 (br q, 2 H, *J* = 6.3), 3.36 (q, 2 H, *J* = 6.0), 3.45-3.65 (m, 14 H), 5.01 (br, t, 1 H), 6.07 (s, 1 H), 6.50 (d, 1 H, *J* = 2.8), 6.62 (dd, 1 H, *J* = 2.5, 9.0), 6.75 (br t, 1 H), 7.53 (d 1 H, *J* = 9.0); ^{13}C NMR (75 MHz, CDCl3) δ 28.44, 28.61, 29.66, 38.52, 40.12, 40.62, 69.42, 70.02, 70.08, 70.14, 70.24, 70.39, 78.89, 98.14, 108.50, 109.13, 110.24, 125.84, 150.18, 153.04, 155.98, 161.86, 168.01; FAB MS calc for $C_{28}H_{43}N_3O_8$ $(M+H)^+$ 549.3050, observed 549.3027.

1. Cyclooctyne acid **5** (Scheme 3.2) (0.0245 g, 0.095 mmol) was dissolved in 2 mL of DMF in a foil wrapped flask and placed under argon. Pyridine (18 μL, 0.11 mmol) was added, and the solution was cooled in an ice bath. Pentafluorophenyl trifluoroacetate (18 μl, 0.11 mmol) was added, and the solution was stirred for 2 h. The solvent was diluted with ethyl acetate (20 mL), extracted twice with 1 M HCl, extracted once with saturated $NaHCO_3$, dried over Na_2SO_4, and evaporated to give a clear oil that was resuspended in 2 ml of CH_2Cl_2. This solution was added to a solution of **9** (0.043 g, 0.072 mmol) that had been deprotected by treatment with 1:1 TFA:CH_2Cl_2 for 2 h, followed by solvent removal and resuspension in 2 mL CH_2Cl_2 and 22 μL (0.160 mmol) triethylamine. The combined solution was stirred under argon and monitored by TLC. After 6 h, the reaction mixture was applied directly to a silica column and eluted with 2:9:9 ethanol:CH_2Cl_2:ethyl acetate (Rf = 0.24 in 1:19

ethanol:CH2Cl2) to give 0.044 g (0.064 mmol, 88%) of a yellow-white solid. ^{1}H NMR (300 MHz, CDCl3) δ 1.46 (m, 1 H), 1.59-1.76 (m, 4 H),

1.79-1.93 (m, 5 H), 1.93-2.39 (m, 4 H), 3.04 (s, 6 H), 3.27 (app q, 2 H, *J* = 5.9), 3.41-3.47 (m, 4 H), 3.51-3.66 (m, 12 H), 4.22 (m, 1 H), 4.16 (d, 1 H, *J* = 12.5), 4.69 (d, 1 H, *J* = 12.5), 6.06 (s, 1 H), 6.46 (d, 1 H, *J* = 2.4), 6.59 (dd, 1 H, *J* = 9.1, 2.5), 6.79 (br t, 1 H), 7.27 (br t, 1 H), 7.38 (d, 2 H, *J* = 8.1), 7.49 (d, 1 H, *J* = 9.1), 7.77 (d, 2 H, *J* = 8.1);13C NMR (75 MHz, CDCl3) δ 20.70, 26.37, 28.53, 28.85, 29.72, 34.30, 38.63, 38.89, 40.09, 40.49, 42.32, 53.46, 69.92, 70.06, 70.17, 70.28, 70.42, 70.46, 72.04, 92.50, 98.04, 100.66, 108.38, 109.20, 110.06, 125.76, 127.11, 127.70, 133.53, 141.81, 150.19, 153.07, 155.94, 162.12, 167.58, 168.39; FAB MS calculated for $C_{39}H_{51}N_3O_8$ $(M+H)^+$ 690.3754, observed 690.3720.

2. Cyclooctyne acid **6** (Scheme 3.2) (0.005 g, 0.019 mmol) was dissolved in 0.2 mL of DMF in a foil wrapped flask and placed under argon. Pyridine (6 μL, 0.08 mmol) was added, and the solution was cooled in an ice bath. Pentafluorophenyl trifluoroacetate (4 μL, 0.02 mmol) was added, and the solution was stirred for 3 h. The solvent was diluted with ethyl acetate (20 mL), extracted twice with 1 M HCl, extracted once with saturated $NaHCO_3$, dried over Na_2SO_4, and evaporated to give a clear oil that was resuspended in 2 mL of CH_2Cl_2. This solution was added to a solution of **9** (0.020 g, 0.04 mmol) that had been deprotected by treatment with 2 mL of 1:1 TFA:CH_2Cl_2 for 2 h, followed by solvent removal and resuspension in 2 mL CH_2Cl_2 and 22 μL (0.160 mmol) triethylamine. The combined solution was stirred under argon and monitored by TLC. After 8 h the reaction mixture was applied directly to a silica column and eluted with 1:19 ethanol:CH_2Cl_2 (Rf = 0.24) to give 0.006 g (0.009 mmol, 45%) of oily yellow product. ^{1}H NMR (300 MHz, $CDCl_3$) δ 1.29-1.45 (m, 1H), 1.60-1.76 (m, 4 H), 1.77-2.10 (m, 6 H), 2.13-2.36 (m, 3 H), 3.03 (s, 1 H), 3.04 (s, 6H) 3.07

(d, 1H), 3.25, 3.37 (app q, 2 H), 3.38-3.46 (m, 4 H), 3.52-3.68 (m, 12 H), 6.06 (s, 1 H), 6.49 (d, 1 H, *J* = 2.5), 6.60 (dd, 1 H, *J* = 2.5, 9.0), 6.64 (br t, 1 H), 7.16 (br t, 1H), 7.34 (d, 2 H, *J* = 7.9), 7.51 (d, 1H, *J* = 9.0), 7.74 (d, 2 H, *J* = 8.4); FAB MS calculated for $C_{39}H_{51}N_3O_7F$ $(M+H)^+$ 692.3711, observed 692.3726.

3. Cyclooctyne acid **7** (Scheme 3.2) (0.0028 g, 0.014 mmol) was dissolved in 200 mL of CH_2Cl_2 in a foil-wrapped flask and placed under argon. Triethylamine (8 μL, 0.06 mmol) was added, and the solution was cooled in an ice bath. Pentafluorophenyl trifluoroacetate (3 μL, 0.02 mmol) was added, and the solution was stirred for 1 h. The solvent was removed under reduced pressure, and the resulting oil was resuspended in 3 mL of 1:1 ethyl acetate:hexane and passed through a short plug of silica (in a pasteur pipette). The solvent was removed under reduced pressure, and the material was resuspended in 1 mL of CH_2Cl_2. This solution was added to a solution of **9** (0.0125 g, 0.023 mmol) that had been deprotected by treatment with 1.5 mL of 1:1 TFA:CH_2Cl_2 for 2 h, followed by solvent removal, azeotropic removal of TFA with toluene and resuspension in 0.2 mL CH_2Cl_2 and 30 μL (0.21 mmol) triethylamine. The combined solution was stirred under argon and monitored by TLC. After 3 h the reaction mixture was applied directly to a silica column and eluted with 1:19 ethanol:CH_2Cl_2 (Rf = 0.22) to give 5.3 mg (0.0082 mmol, 64%) of a yellow glassy solid. ^{1}H NMR (300 MHz, CDCl3) δ 1.68-1.87 (m, 4H), 1.98-2.08 (m, 2H), 2.13-2.31 (m, 3H), 2.39-2.63 (m, 3H), 3.06 (s, 6H), 3.31-3.45 (m, 4H), 3.45-3.69 (m, 15H), 3.92 (s, 2H), 6.07 (s, 1H), 6.48 (d, 1H, *J* = 2.6), 6.61 (dd, 1H, *J* = 2.9, 8.8), 6.79 (br t, 1H), 6.98 (br t, 1H), 7.51 (d, 2H, *J* = 9.3); FAB MS calculated for $C_{33}H_{46}N_3O_8F_2$ $(M+H)^+$ 650.3253, observed 650.3233.

Caco-2 Permeability Analysis. Each of the three coumarin cyclooctynes **1-3** was submitted to Apredica (Watertown, MA) for Caco-2 (human colon carcinoma cell) permeability

analysis. Briefly, each probe was supplied as a 10 mM stock solution in DMSO. A test concentration of 10 μM probe was applied to the apical side of a monolayer of differentiated Caco-2 cells. Each probe was applied in transport buffer (1.98 g/L glucose in 10 mM HEPES, 1x Hank's Balanced Salt Solution, pH 6.5) supplemented with 100 μM of the impermeable dye Lucifer Yellow. For comparison, low permeability controls (Ranitidine, Vinblastine), Quinidine, and a high permeability control (Warfarin) were also applied to the cells.

After 2 h, the amount of permeation for each probe was determined by LC/MS/MS analysis of the transport buffer removed from the basolateral side of the monolayer. The value obtained is the permeability of each compound (P_{app}), which is defined as:

$$Papp = \frac{\frac{dQ}{dt}}{CoA}$$

where dQ/dt is the rate of permeation, C_0 is the initial concentration of the test agent, and A is the area of the monolayer. The P_{app} value for **1-3** and the standards are given in Table 1. From the P_{app} values, we conclude that each of the probes is membrane permeable and able to pass through the Caco-2 monolayer, although the assay also predicts that the bioavailability would be low.

References

1. (a) Shaner, N. C.; Steinbach, P. A.; Tsien, R. Y., A guide to choosing fluorescent proteins. *Nat Methods* **2005,** *2* (12), 905-9; (b) Tsien, R. Y., The green fluorescent protein. *Annu Rev Biochem* **1998,** *67*, 509-44.

2. Johnson, J. A.; Lu, Y. Y.; Van Deventer, J. A.; Tirrell, D. A., Residue-specific incorporation of non-canonical amino acids into proteins: recent developments and applications. *Curr Opin Chem Biol* **2010,** *14* (6), 774-80.

3. (a) Kiick, K. L.; Saxon, E.; Tirrell, D. A.; Bertozzi, C. R., Incorporation of azides into recombinant proteins for chemoselective modification by the Staudinger ligation. *Proc Natl Acad Sci U S A* **2002,** *99* (1), 19-24; (b) Kiick, K. L.; Weberskirch, R.; Tirrell, D. A., Identification of an expanded set of translationally active methionine analogues in Escherichia coli. *FEBS Lett* **2001,** *502* (1-2), 25-30.

4. (a) Rostovtsev, V. V.; Green, L. G.; Fokin, V. V.; Sharpless, K. B., A stepwise huisgen cycloaddition process: copper(I)-catalyzed regioselective "ligation" of azides and terminal alkynes. *Angew Chem Int Ed Engl* **2002,** *41* (14), 2596-9; (b) Tornoe, C. W.; Christensen, C.; Meldal, M., Peptidotriazoles on solid phase: [1,2,3]-triazoles by regiospecific copper(i)-catalyzed 1,3-dipolar cycloadditions of terminal alkynes to azides. *J Org Chem* **2002,** *67* (9), 3057-64.

5. (a) Beatty, K. E.; Liu, J. C.; Xie, F.; Dieterich, D. C.; Schuman, E. M.; Wang, Q.; Tirrell, D. A., Fluorescence visualization of newly synthesized proteins in mammalian cells. *Angew Chem Int Ed Engl* **2006,** *45* (44), 7364-7; (b) Beatty, K. E.; Tirrell, D. A., Two-color labeling of temporally defined protein populations in mammalian cells. *Bioorg Med Chem Lett* **2008,** *18* (22), 5995-9; (c) Dieterich, D. C.; Link, A. J.; Graumann, J.; Tirrell, D. A.; Schuman, E. M., Selective identification of newly synthesized proteins in mammalian cells using bioorthogonal noncanonical amino acid tagging (BONCAT). *Proc Natl Acad Sci U S A* **2006,** *103* (25), 9482-7; (d) Link, A. J.; Tirrell, D. A., Cell surface labeling of Escherichia coli via copper(I)-catalyzed [3+2] cycloaddition. *J Am Chem Soc* **2003,** *125* (37), 11164-5.

6. (a) Agard, N. J.; Prescher, J. A.; Bertozzi, C. R., A strain-promoted [3 + 2] azide-alkyne cycloaddition for covalent modification of biomolecules in living systems. *J Am Chem Soc* **2004,** *126* (46), 15046-7; (b) Agard, N. J.; Baskin, J. M.; Prescher, J. A.; Lo, A.; Bertozzi, C. R., A comparative study of bioorthogonal reactions with azides. *ACS Chem Biol* **2006,** *1* (10), 644-8; (c) Baskin, J. M.; Prescher, J. A.; Laughlin, S. T.; Agard, N. J.; Chang, P. V.; Miller, I. A.; Lo, A.; Codelli, J. A.; Bertozzi, C. R., Copper-free click chemistry for dynamic in vivo imaging. *Proc Natl Acad Sci U S A* **2007,** *104* (43), 16793-7.

7. (a) Ning, X.; Guo, J.; Wolfert, M. A.; Boons, G. J., Visualizing metabolically labeled glycoconjugates of living cells by copper-free and fast huisgen cycloadditions. *Angew Chem Int Ed Engl* **2008,** *47* (12), 2253-5; (b) Debets, M. F.; van Berkel, S. S.; Schoffelen, S.; Rutjes, F. P.; van Hest, J. C.; van Delft, F. L., Aza-dibenzocyclooctynes for fast and efficient enzyme PEGylation via copper-free (3+2) cycloaddition. *Chem Commun (Camb)* **2010,** *46* (1), 97-9; (c) Jewett, J. C.; Sletten, E. M.; Bertozzi, C. R., Rapid Cu-free click chemistry with readily synthesized biarylazacyclooctynones. *J Am Chem Soc* **2010,** *132* (11), 3688-90; (d) Codelli, J. A.; Baskin, J. M.; Agard, N. J.; Bertozzi, C. R., Second-generation difluorinated cyclooctynes for copper-free click chemistry. *J Am Chem Soc* **2008,** *130* (34), 11486-93.

8. Piston, D. W., Imaging living cells and tissues by two-photon excitation microscopy. *Trends Cell Biol* **1999,** *9* (2), 66-9.

9. Hermanson, G. T., *Bioconjugate techniques*. Academic Press: 1996.

10. Stenberg, P.; Norinder, U.; Luthman, K.; Artursson, P., Experimental and computational screening models for the prediction of intestinal drug absorption. *J Med Chem* **2001,** *44* (12), 1927-37.

11. Beatty, K. E.; Fisk, J. D.; Smart, B. P.; Lu, Y. Y.; Szychowski, J.; Hangauer, M. J.; Baskin, J. M.; Bertozzi, C. R.; Tirrell, D. A., Live-cell imaging of cellular proteins by a strain-promoted azide-alkyne cycloaddition. *Chembiochem* **2010,** *11* (15), 2092-5.

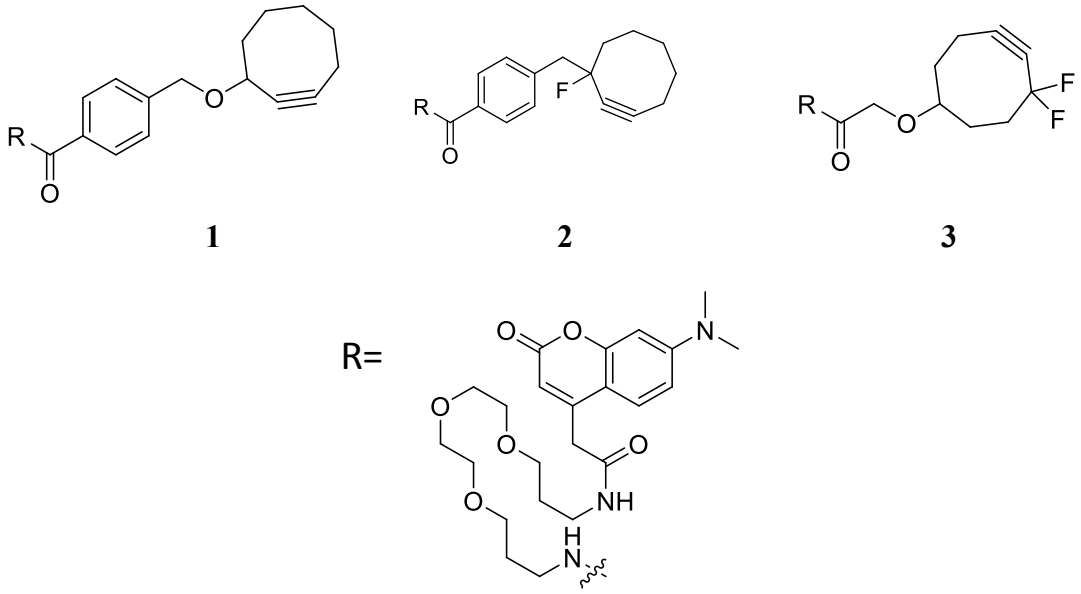

Scheme 3.1. Chemical structures of coumarin-cyclooctynes.

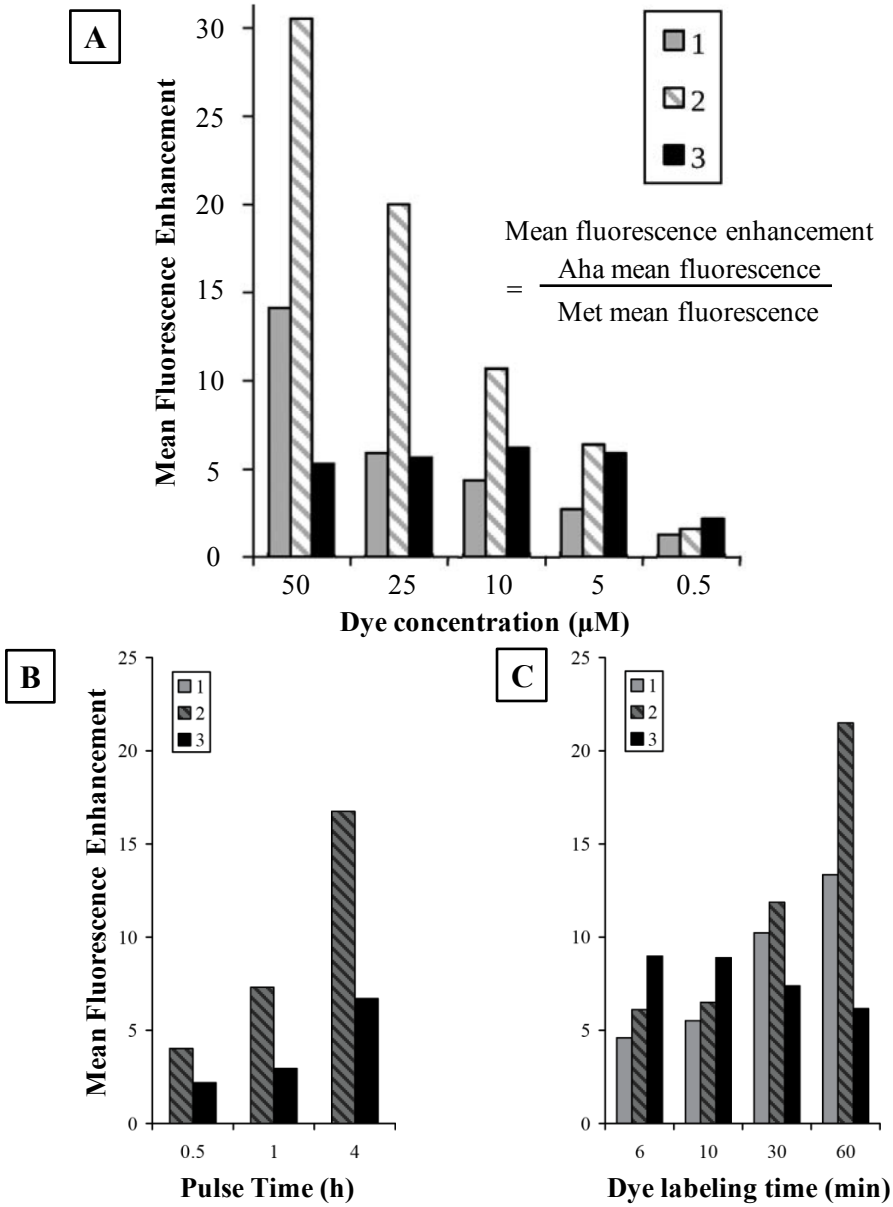

Figure 3.1. Identifying optimum labeling conditions by flow cytometry. (A) Mean fluorescence enhancement as a function of dye concentration for cells pulsed for 4 h and dye-labeled for 10 min; (B) Fluorescence enhancement as a function of pulse duration for cells dye-labeled with 10 μM **3** or 50 μM **2** for 10 min; (C) Fluorescence enhancement as a function of dye-labeling duration for cells labeled with 10 μM **1**, **2**, or **3** after a 4 h pulse.

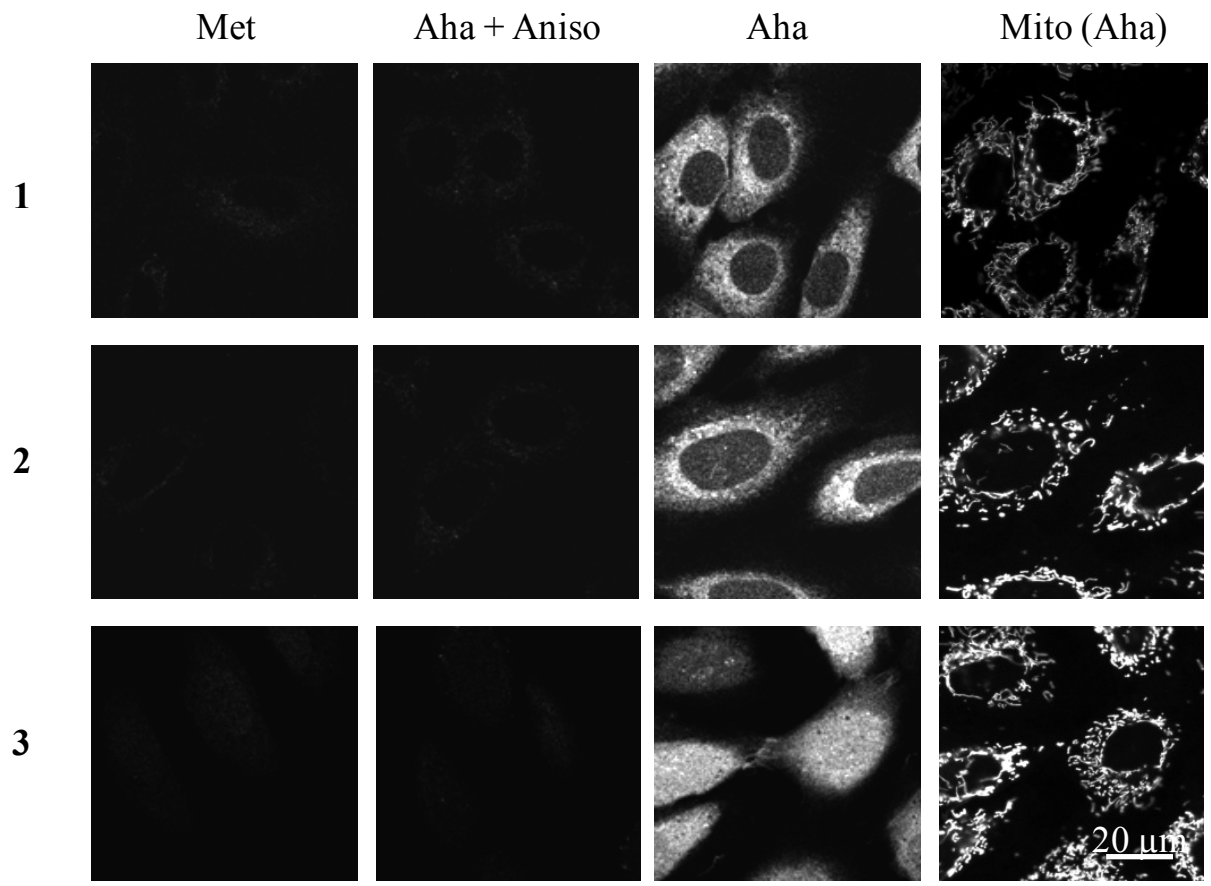

Figure 3.2. Labeling live cells using coumarin-cyclooctynes. Confocal fluorescence imaging of Rat-1 firbroblasts pulsed for 4 h with 1 mM Met, 1 mM Aha pre-treated with the protein synthesis inhibitor anisomycin, or 1 mM Aha with or without counterstaining with MitoTracker Red. Cells were dye-labeled for 10 min with 50 μM **1**, 50 μM **2**, or 10 μM **3** before imaging.

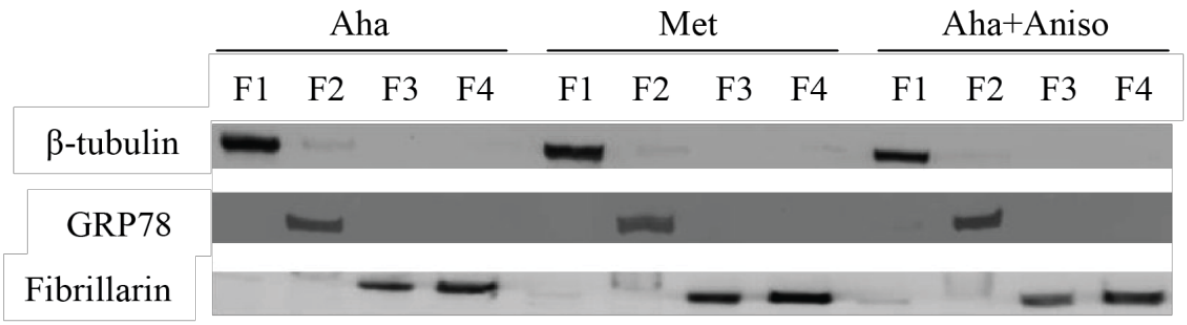

Figure 3.3. Western blot analysis of cellular fractions. Cells were fractionated into four portions containing cytoplasmic (F1), membrane (F2), nuclear (F3), and cytoskeletal (F4) proteins. An sample of 5 μg total protein was loaded from each fraction, separated by gel electrophoresis, and subjected to western blotting using antibodies for cytosolic protein β-tubulin, membrane-bound protein GRP78, and nucleolar protein fibrillarin.

A

	Cytosol	Membrane	Nucleus	Cytoskeleton
	F1	**F2**	**F3**	**F4**
1	13.7± 0.8%	55.8± 2.7%	11.3± 2.9%	19.2± 0.7%
2	15.1± 1.1%	58.1± 3.0%	9.6± 4.3%	17.2± 0.2%
3	21.4± 1.4%	36.5± 0.5%	19.0± 1.6%	23.1± 0.7%

B

	F1	F2	F3	F4
1	25.5± 0.8%	61.0± 2.7%	6.7± 1.7%	6.8± 0.1%
2	25.4± 2.4%	63.6± 1.1%	5.4± 2.3%	5.6± 0.9%
3	40.0± 3.4%	38.5± 2.6%	11.7± 1.3%	10.0± 0.5%

Figure 3.4. Fluorescence labeling in different cellular compartments. Fibroblasts cells were pulsed with either Aha or Met for 4 h, dye-labeled for 10 min with 50 μM **1**, 50 μM **2**, or 10 μM **3** before fractionation to separate proteins from different cellular compartments. Fluorescence was measured on a microplate reader and percent fluorescence was calculated by either normalizing for protein concentration (A) or cell number (B).

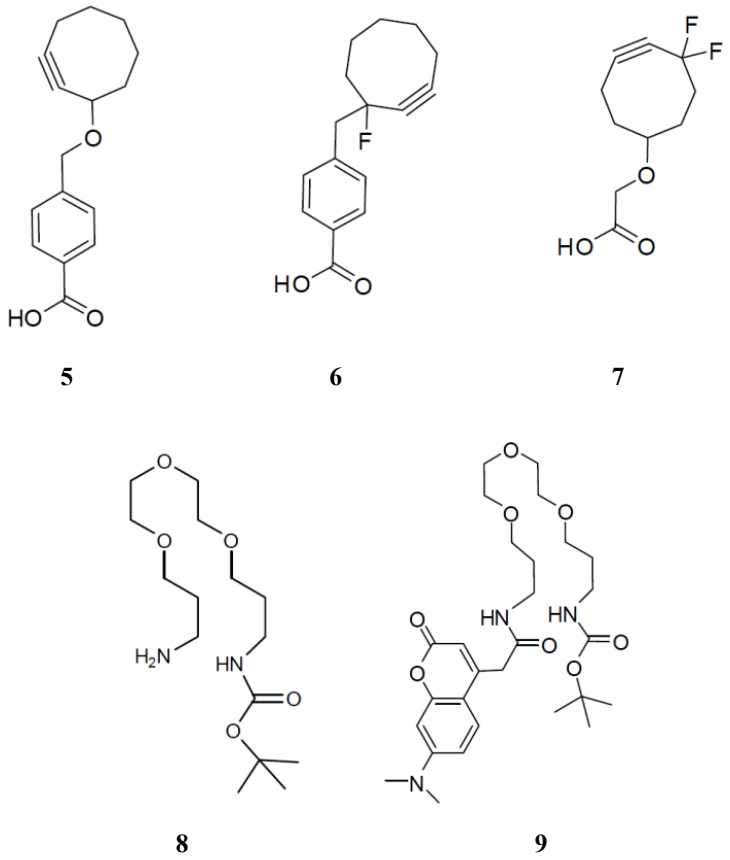

Scheme 3.2. Chemical structures of intermediates for coumarin-cyclooctyne synthesis.

CHAPTER 4

An Approach to Multisite PEGylation of Proteins at Glutamine Positions

Abstract

Residue-specific incorporation of noncanonical amino acids (ncAAs) has greatly expanded the toolbox for engineering proteins with novel chemical and physical properties. To further expand this chemical toolbox, here we report the first demonstration of global replacement of a polar amino acid, glutamine, by its reactive noncanonical analogue, L-glutamic acid γ-hydrazide (Gah). Using an *E. coli* strain that is deficient in glutamine synthesis (a glutamine auxotroph), we achieved near-quantitative incorporation of Gah at glutamine sites of a reporter protein, dihydrofolate reductase (mDHFR). Incorporation of Gah decorates proteins with bioorthogonal hydrazide groups that can undergo selective reaction with ketones under physiological conditions. To demonstrate the novel reactivity of Gah-containing proteins, we synthesized a ketone tag for western blot analysis and showed specific detection of Gah-containing mDHFR. We also designed a ketone-modified fluorophore and demonstrated selective labeling of live bacterial cells. In addition, using the surface accessibility of glutamine residues, we are exploring an alternative strategy for PEGylating therapeutic proteins at multiple sites using Gah.

Introduction

Protein engineering has relied on mutagenesis to produce proteins with new sequences. While changing the primary sequence can create proteins with desired properties, the diversity of engineered proteins is limited by the intrinsic properties of the 20 canonical amino acids. Residue-specific incorporation of noncanonical amino acids (ncAA) has expanded the possibilities of modifying protein structures and functions. For example, global

replacement of leucine by trifluoroleucine has created a more thermally stable variant of leucine zipper structure.[1] Proteins can also be evolved to tolerate ncAAs and recover wild-type properties.[2] Aside from physical properties, incorporation of ncAAs can also create proteins with novel chemical reactivity by introducing various functional groups, such as azides, alkynes, alkenes, and ketones.[3] So far, many nonpolar residues have been replaced with ncAAs; however, incorporation of ncAAs at polar amino acid positions has been investigated to a lesser extent. Replacing polar amino acids with ncAAs is attractive for several reasons. Polar residues typically occupy solvent exposed positions on protein surfaces,[4] and incorporation of ncAAs at these positions should cause less structural and functional perturbation. Further, reactive ncAAs at surface positions will allow chemical modifications under native conditions.

L-glutamic acid-γ-hydrazide (Gah) (Scheme 4.1), an analogue of the polar amino acid glutamine, is known to support protein synthesis *in vivo*[5] and has also been shown to be tolerated by the *Escherichia coli* (*E. coli*) glutaminyl-tRNA synthetase (GlnRS) using *in vitro* assays.[6] Furthermore, hydrazides react with ketones selectively under physiological conditions (Scheme 4.1),[7] making the incorporation of Gah particularly attractive for protein modification. In this work, we demonstrate the residue-specific incorporation of Gah into newly synthesized proteins in *E. coli* and its applications in protein labeling, live-cell imaging, and modifying therapeutic proteins.

Results and Discussion

Residue-specific incorporation of Gah. We first assessed the ability of Gah to support protein synthesis using bacterial cells harboring an inducible expression vector. The expression vector pQE-80L encodes a common reporter protein, mouse dihydrofolate reductase (mDHFR), under control of a bacteriophage T5 promoter, and an N-terminal hexahistidine sequence for purification. Glutamine auxotrophic *E. coli* strain M5004, obtained from the Coli Genetic Stock Center at Yale University, was transformed with the pQE-80L construct and grown to an OD_{600} of 1 before a medium shift was performed. Cells were pelleted from complete medium, washed with cold saline solution, and resuspended in medium supplemented with 19 amino acids (lacking Gln), 19 amino acids plus 4 mM Gah, or 19 amino acids plus 4 mM Gln. DHFR expression was induced by addition of isopropyl-β-D-thiogalactopyranoside (IPTG) at a concentration of 1 mM. After 4 h, cells were harvested by centrifugation, washed twice, and subjected to lysis. Cell lysates were analyzed using polyacrylamide gel electrophoresis (Figure 4.1). A band at the expected molecular weight of DHFR (24 kDa) is present in samples prepared from cultures supplemented with either Gln or Gah after IPTG induction. In contrast, the DHFR band is absent in samples containing only 19 amino acids because these auxotrophic cells cannot support protein synthesis without Gln or its analogues. Taken together, these data suggest that Gah exhibits sufficient translational activity to support protein synthesis in the absence of Gln.

Incorporation of Gah into mDHFR was confirmed by matrix-assisted laser desorption ionization mass spectrometry (MALDI-MS) and liquid chromatography mass spectrometry (LC-MS). mDHFR was purified using immobilized chelate affinity chromatography. Tryptic peptides of mDHFR from the Gah-treated culture were analyzed by MALDI-MS. The peak

of a Gln-containing peptide with sequence LLPEYPGVLSEVQEEK (amino acid position 173-188) is absent at its expected mass of 1830 Da, while a new peptide peak emerged at 1845 Da, consistent with the 15 Da mass difference between Gah and L-glutamine (Figure 4.2). These MALDI data suggests near-quantitative incorporation of Gah at Gln positions. By comparing the integrated areas of the corresponding signals in the chromatogram from LC-MS, the extent of replacement was determined to be ~93%, and the identity of each peptide was confirmed by tandem mass spectrometry (Figure 4.3).

Selective detection of Gah-containing proteins. Next, we investigated the chemical properties of Gah-containing proteins. To selectively label proteins containing Gah, a biotin tag with a ketone moiety was designed and synthesized (scheme 4.2). mDHFR was purified from cultures grown in the presence of Gln or Gah. These mDHFR samples (40 μM) were treated with 400 μM ketone biotin tag in aqueous solution, pH 6.5, at RT, for 12 h. Proteins were separated using gel electrophoresis, transferred to a nitrocellulose membrane, and detected using a fluorescent streptavidin conjugate. Strong fluorescence signal was observed for the sample prepared from the Gah-treated culture; minimal signal was present in the sample prepared from the culture supplemented with Gln, suggesting selective biotinylation of Gah-labeled mDHFR. Positive anti-His signals, providing a loading control, indicate similar amounts of protein were present in both lanes.

Using the western blotting analysis, we investigated the timing of Gah incorporation into proteins. After the medium shift, aliquots of Gah and Gln cultures were collected every 10 min over a total of 2 h. Cultures were lysed, normalized by OD_{600}, treated with ketone biotin tag, and analyzed by western blotting (Figure 4.4a). In the sample prepared from the Gah-treated culture, a significant biotin signal was observed just 5 min post medium shift; the

signal accumulated with increasing expression time. In the Gln-treated culture, no significant biotin signal was observed. These observations suggest Gah is rapidly taken up by bacterial cells and incorporated into newly synthesized proteins.

Imaging live cells in Gah-treated cultures. Gah is particularly attractive as a Gln analogue because it provides a biocompatible labeling strategy via hydrazide ketone reaction. Here we demonstrate selective fluorescence labeling of live bacterial cells by metabolically incorporating Gah and subsequent reaction with a ketone coumarin dye (Scheme 4.2). After 4 h expression in the presence of Gah or Gln, cells were washed to remove excess free amino acids before dye-labeling in M9 medium, pH 6.5, for 3 h at 4 °C. Post dye reaction, cells were washed, stained by cell viability markers, and imaged using fluorescence microscopy (Figure 4.4b). Gah-treated cells showed strong coumarin fluorescence while cells grown in Gln culture exhibited little fluorescence. In addition, only very few cells were dead as shown by propidium iodide staining. Taken together, these results demonstrate selective fluorescence labeling of live Gah-treated cells using hydrazide ketone chemistry.

Multisite PEGylation using Gahs at Gln sites. By populating Gln sites with its reactive analog, we can develop a new approach to modifying therapeutic proteins at multiple sites. The covalent attachment of polyethylene glycol (PEG) to proteins, PEGylation, is a well-established and widely employed method to improve properties of therapeutic proteins.[8] Its main advantages include improved solubility, increased stability and *in vivo* circulation time, and decreased immunogenicity.[9] Many FDA-approved therapeutic proteins are PEGylated randomly at lysine residues using amine chemistry. Such a method, even at defined stoichiometric ratios, will result in complex mixtures of mono-, di-, tri-, and numerous higher-PEGylated species, requiring stringent downstream purification.[8] Furthermore,

because multiple lysines can participate in reactions, even mono-PEGylation leads to positional isomers that can differ substantially in biological and biomedical properties.[8] As a result, a major drawback of the classical PEGylation approach is significantly reduced biological activity.[10]

L-Asparaginase II (ASNase) is currently used to treat acute lymphoblastic leukemia because it kills leukemic cells by depriving them of their essential growth factor, asparagine.[11] The native *E. coli* ASNase has shown limited effects in delaying intensification phases of leukemia due to the development of neutralizing antibodies in patients and often requires high dosage due to a short *in vivo* circulation period.[12] A 5 kDa PEG chain was coupled using random PEGylation at lysine residues to improve immune tolerance and circulation duration; however, the modified enzyme retains only 8% of its original *in vitro* biological activity.[13] ASNase contains a lysine residue at its catalytic site,[14] and undesired PEGylation at this lysine could account for the loss in catalytic activity. Herein we explore multisite PEGylation of *E. coli* ASNase using hydrazide-ketone chemistry provided by incorporation of Gah at Gln sites.

To express the Gah-containing enzyme, *E. coli* ASNase with a C-terminal His tag was cloned into the multiple cloning site (MCS) of the pQE-80L vector for inducible expression by IPTG. Gln-auxotrophic *E. coli* cells harboring this construct were grown and subjected to a medium shift. ASNase expression was induced in the presence of 4 mM Gah and allowed to proceed for 2 h. Because previous reports have shown expression and transport of *E. coli* ASNase to the periplasmic region,[15] we obtained three lysis fractions, periplasmic, cytoplasmic, and inclusion bodies, and analyzed them using gel electrophoresis and western blotting (Figure 4.5). The expression of ASNase is evident by the appearance of a band at the

expected molecular weight of 38 kDa in anti-His as well as anti-ASNase western blots. The majority of the protein is present in the periplasmic fraction as expected in both Gah and Gln-treated samples, whereas no protein is detected in the culture supplemented with 19 amino acids, consistent with Gah incorporation into ASNase, which was further confirmed by MALDI-MS.

ASNase was purified by metal chelate chromatography followed by size exclusion chromatography (SEC). SEC fractions were analyzed using a colorimetric activity assay (Figure 4.6). As a negative control, ASNase with a single threonine to alanine mutation (T12A) showed little activity as previously published.[16] Canonical ASNase exhibited 0.9 U/mg activity, which was improved by SEC isolation of the active tetrameric form of the enzyme. Although Gah-containing ASNase showed significant activity, it is 10-fold lower than that of wt ASNase.

Ongoing Work

Several studies are currently underway to improve the catalytic activity of Gah-containing ASNase. Global replacement of Gln by Gah would likely cause structural and functional perturbation. Initial calculations for solvent accessibility of all Gln residues suggest that some may be buried.[17] Moreover, these calculations correspond to the crystal structure, which also shows several Gln residues solvent inaccessible and near the inter-subunit interface of the tetramer.[14] These Gln residues could be important for proper folding and formation of the catalytically active tetramer and will be mutated to other canonical amino acids. Asparagine is a good candidate since it may be able to form the same hydrogen bond

interactions as Gln. Histidine and glutamic acid have been shown to be structural homologs of Gln with the ability to mimic secondary structural motifs.[18] Finally, comparative studies on the sequence homology within the ASNase family have yielded several additional candidates such as alanine, methionine, and glutamic acid. After recovering the enzymatic activity of Gah-containing ASNase, we will subject the enzyme to reaction with ketone modified PEGs of various sizes. The PEGylated ASNase will be purified and assayed for *in vitro* biological activity prior to efficacy assessment *in vivo.*

Conclusions

In this work, we have demonstrated the first example of global replacement of a polar amino acid by its noncanonical analogue. Using a Gln-auxotrophic *E. coli* strain, we have shown near-quantitative incorporation of Gah at Gln positions. To demonstrate the novel chemical property of Gah-containing proteins, we designed ketone-containing probes for protein modifications using hydrazide-ketone chemistry. We synthesized a ketone biotin tag and showed selective labeling of Gah-containing mDHFR using western blotting. We dye-labeled live bacterial cells using ketone-modified coumarin and observed highly specific fluorescence in cells cultured with Gah. Residue-specific incorporation of Gah introduces novel reactivity to cellular proteins and can be applied to monitor cellular events via live-cell imaging and to produce novel engineered proteins. As an example, we are currently using this method to explore PEGylating therapeutic proteins at multiple sites.

Materials and Methods

Materials. All 20 natural amino acids and L-glutamic acid γ-hydrazide (Gah) were obtained from Sigma and Santa Cruz Biotechnology. Gln-auxotrophic *E. coli* strain M5004 was obtained from the Yale *E. coli* Genetic Stock Center.

***In vivo* incorporation assays**. Glutamine auxotrophic strain M5004 was grown in M9 minimal medium supplemented with 0.8% D-glucose, 35 mg/L thiamin, 1 mM $MgSO_4$, 0.1 mM $CaCl_2$, 20 amino acids (4 mM L-glutamine and 40 mg/L for other amino acids), and 200 mg/L ampcillin. The overnight culture was diluted 50-fold in fresh M9 minimal medium. The cells were grown to an OD_{600} between 0.8 and 1.0, sedimented by centrifugation, and washed twice with ice-cold 0.9% NaCl. The cell pellet was resuspended in fresh M9 minimal medium containing either 19 amino acids (40 mg/L), 19 amino acids plus 4 mM L-glutamine, or 19 amino acids plus 4 mM Gah. After 10 min, 1 mM isopropyl β-D-thiogalactopyranoside (IPTG) was added to induce mDHFR expression. After 4 h, cells were pelleted and kept at -80 °C. Whole cell lysates were analyzed by SDS-PAGE.

Quantification of incorporation using mass spectrometry. mDHFR was purified on a Ni-NTA column under denaturing conditions according to the supplier's instructions (Qiagen). After purification, mDHFR concentration was determined by UV absorbance at 280 nm using a calculated extinction coefficient of 30,940 $M^{-1}cm^{-1}$.[19] After concentration of the protein by ultrafiltration (Millipore), 10 µL of protein solution was diluted into 90 µL of 75 mM $(NH_4)_2CO_3$ for trypsin digestion. Modified trypsin (2 µL, Promega, 0.2 µg/µL) was added, and the mixture was incubated for 4 h at 37°C. The reaction was quenched by addition of 20 µL of 5% trifluoroacetic acid (TFA) solution and the mixture was subjected to LC-MS.

LC-MS analysis of protease-digested peptides was performed using a Premier XE LC-MS coupled with an Acquity UPLC chromotography system (Waters Co.). Peptides were separated on an Acquity UPLC^{TM} BEH C18 column (1.7 μm, 300 Å, 2.1 × 100 mm) and eluted at a flow rate of 0.3 mL/min using a gradient of 0-50% of solvent B (89% acetonitrile/10% H2O/0.02% TFA/1% formic acid) and solvent A (2% acetonitrile/97% H_2O/0.02% TFA/1% formic acid) in 55 min.

Live cell fluorescence microscopy. After expressing mDHFR in the presence of either L-glutamine or Gah for 1-4 h, bacterial cells were collected by centrifugation at 6000 g for 5 min at 4 °C. For dye labeling, 2.5 mL of bacterial culture with OD_{600} of 1 was used per reaction. Cells were washed twice using 19 aa M9 to remove excess Gah in the medium before treatment with 500 μM coumarin ketone dye in 20aa M9, pH 6.5 for 3 h at 4 °C. After coumarin labeling, cells were washed three times with 19 aa M9 to remove excess dye. Viability of the cells was assessed using a Live/dead BacLight Bacterial viability Kit (Molecular Probes, L13152). Briefly, dry powder of live stain SYTO 9 and dead stain propidium iodide was dissolved in 5 mL ddH_2O to make 2 × solution. Equal volumes of the 2 × solution and coumarin-labeled culture were mixed at RT and kept in the dark for 45 min. Cells were washed once and resuspended in imaging solution (20% glycerol in 20 aa M9, pH 7). Live cells were imaged on a confocal microscope (Zeiss LSM 510 upr) at the Biological Imaging Center of the Beckman Institute at Caltech. Propidium iodide fluorescence was obtained by excitation at 543 nm with emission collected between 565 and 615 nm. SYTO 9 fluorescence was obtained by excitation at 488 nm with emission collected between 500 and 530 nm. Transmitted light images were also collected to differentiate individual cells. Coumarin fluorescence was obtained by two-photon excitation at 800 nm (Ti: sapphire laser)

with emission collected between 376 and 494 nm. Cells treated with Gln or Gah were imaged using identical parameters in order to compare coumarin fluorescence. Images were acquired with a Plan-Apochromat 100 ×/1.4 oil DIC objective (Zeiss) and analyzed with Zeiss LSM and ImageJ software.

Biotinylation and western blot detection. After expressing mDHFR in the presence of Gln or Gah, cells were collected and resuspended in lysis buffer (8 M urea, 10 mM Na_2PO_4, 300 mM NaCl, pH 6.5). Cell suspension was subjected to a freeze-thaw cycle to achieve sufficient lysis. Cell lysate was biotinylated using 400 μM biotin ketone in urea solution, pH 6.5, for 12 h at RT. For western blot analysis, equal amounts of protein samples were separated on a 12% SDS-PAGE. The gel was transferred to a nitrocellulose membrane (Hybond ECL, GE Healthcare) using a semi-dry transfer system (Amersham Biosciences). The membrane was blocked with 5% milk at RT for 1 h. The membrane was washed three times using 0.1% tween/PBS before incubation with antibodies for 1 h at RT [streptavidin TexasRed-conjugated (Abcam), 1:5000 and anti-pentahis Alexa488-conjugated (Invitrogen), 1:5000]. Washed membrane was imaged on a Typhoon molecular imager (GE Healthcare).

ASNase expression, purification, and detection. The gene encoding for *E. coli* ASNase was amplified from *E. coli* genomic DNA using forward and reverse primers to include a C-terminal histidine tag for ease of purification and two restriction sites flanking the ends (*Eco*R1, *Sal1)* through PCR amplification (Stratagene, Agilent Technologies). Standard cloning protocols were used to construct the pQE80L-msig-ansB-his expression plasmid through restriction enzyme digestion and ligation of the digested PCR product and pQE80L plasmid backbone at *EcoR*1 and *Sal*1 sites. Mutant ASNase (T12A) was constructed using Quikchange mutagenesis of the pQE80L-msig-ansB-his plasmid (Stratagene, Agilent

Technologies). Incorporation of Gah into ASNase was done as previously described for mDHFR. After expression for 3 h at 37°C, cells were pelleted (15 min at 5000 *g*, 4°C) and gently resuspended in 20 mL per liter culture volume x cell OD_{600} of ice-cold 0.75 M sucrose, 0.1M Tris (Tris/sucrose buffer). The periplasmic fraction was extracted as previously described[20] and dialyzed for 36 h against a solution of Ni-NTA binding buffer (0.3M NaCl, 0.05M NaH_2PO_4, pH 8.0) using 6-8 kilodalton molecular weight cutoff (MWCO) dialysis tubing (Spectrum Labs). ASNase was purified on a Ni-NTA column under native conditions according to the supplier's instructions (Qiagen) with one change, the addition of 10% glycerol to all Ni-NTA purification buffers, which has been used as a protein stabilizer to prevent aggregation.[21] Ni-NTA fractions containing ASNase was then further purified using size-exclusion chromatography (SEC) on an AktaPrime FPLC (GE Healthcare). All purification steps were assessed by SDS-PAGE analysis and identity of ASNase was confirmed via western blotting with asparaginase- and histidine-tag specific antibodies. Further, SEC fractions containing ASNase were then assayed for activity using an asparaginase activity assay kit (Sigma MAK007), which colorimetrically detects the appearance of aspartic acid using a microplate reader (Tecan).

Synthesis of ketone probes. Coumarin ketone. 1-Amino-2-propanol (12 μL, 0.155 mmol) was added to a solution of coumarin NHS ester (50 mg, 0.145 mmol) in anhydrous CH_2Cl_2 (5 mL). The resulting solution was stirred overnight at RT to generate the coumarin alcohol intermediate. Dess-Martin periodinane (86 mg, 0.202 mmol) was added, and the suspension was stirred for 18 h. Isopropanol (100 μL) was added, and the mixture was stirred for 1 h, transferred to a separatory funnel, and washed 3 times with 1M HCl, 3 times with saturated $NaHCO_3$, and once with brine. The organic layer was dried over sodium sulfate, filtered, and

concentrated on a rotary evaporator. Purification by column chromatography (MeOH/CH_2Cl_2) gave ketone **1c** (29 mg, 66%). ^{1}H NMR (600 MHz, methanol-d_4) δ 7.59 (d, J = 9.0 Hz, 1H), 6.75 (dd, J = 9.0, 2.6 Hz, 1H), 6.54 (d, J = 2.6 Hz, 1H), 6.09 (s, 1H), 4.09 – 4.04 (m, 2H), 3.78 – 3.74 (m, 2H), 3.05 (s, 6H), 2.12 (s, 3H). ^{13}C NMR (151 MHz, methanol-d_4) δ 202.38, 167.60, 161.19, 156.00, 153.11, 149.33, 125.50, 110.28, 108.88, 104.99, 97.96, 49.80, 45.00, 39.90, 27.02.

Biotin ketone. 1-Amino-2-propanol (6.3 μL, 81.6 μmol) was added to a solution of biotin NHS ester (**1a**, 50 mg, 77.7 μmol) in anhydrous CH_2Cl_2 (5 mL). The resulting solution was stirred overnight at RT to generate the biotin alcohol intermediate. Dess-Martin periodinane (46 mg, 0.11 mmol) was added, and the suspension was stirred for 18 h. Isopropanol (100 μL) was added, and the mixture was stirred for 1 h, transferred to a separatory funnel, and washed 3 times with 1M HCl, 3 times with saturated $NaHCO_3$, and once with brine. The organic layer was dried over sodium sulfate, filtered, and concentrated on a rotary evaporator. Purification by preparatory-HPLC (H_2O/MeCN) gave ketone **2c** (15 mg, 32%). ^{1}H NMR (600 MHz, Methanol-d_4) δ 4.51 (dd, J = 7.8, 5.0 Hz, 1H), 4.32 (dd, J = 7.8, 4.4 Hz, 1H), 4.04 (s, 2H), 3.67 – 3.64 (m, 4H), 3.61 (dt, J = 5.9, 2.8 Hz, 4H), 3.54 (td, J = 6.2, 3.5 Hz, 4H), 3.28 (td, J = 6.6, 3.3 Hz, 4H), 3.26 – 3.20 (m, 1H), 2.95 (dd, J = 12.8, 5.0 Hz, 1H), 2.76 – 2.68 (m, 1H), 2.58 (t, J = 7.5 Hz, 2H), 2.50 (t, J = 6.9 Hz, 2H), 2.22 (t, J = 7.5 Hz, 2H), 2.16 (s, 3H), 1.77 (td, J = 6.5, 4.2 Hz, 4H), 1.73 – 1.58 (m, 4H), 1.50 – 1.43 (m, 2H). ^{13}C NMR (151 MHz, Methanol-d_4) δ 204.48, 174.51, 173.53, 173.00, 70.11, 69.81, 69.79, 68.51, 68.45, 61.95, 60.19, 55.57, 48.94, 45.01, 39.60, 36.45, 36.40, 35.42, 30.80, 30.55, 28.99, 28.95, 28.37, 28.08, 25.54, 25.45.

Primers used:

For PCR ampfilication of ASNase:

FWD: 5'-AATAGAATTCATTAAAGAGGAGAAATTAACTATGGAGTTTTTCAAAAA-3'

REV: 5'-TAATTGTCGACTTAACCATGATGATGATGATGATGACCGTACTGATTGAAGATC-3'

For T12A Mutant:

Fwd: 5'-CCATTTTAGCAACCGGCGGGGCCATTGCCGGTGGTGGTGAC-3'

Rev: 5'-GTCACCACCACCGGCAATGGCCCCGCCGGTTGCTAAAATGG-3'

Acknowledgements

We thank Katharine Fang for collaboration on the development of multisite PEGylation using Gah. We thank Professor Jeremiah Johnson for assistance in synthesizing ketone probes used in this work.

References

1. Tang, Y.; Ghirlanda, G.; Vaidehi, N.; Kua, J.; Mainz, D. T.; Goddard, I. W.; DeGrado, W. F.; Tirrell, D. A., Stabilization of coiled-coil peptide domains by introduction of trifluoroleucine. *Biochemistry* **2001,** *40* (9), 2790-6.

2. (a) Montclare, J. K.; Tirrell, D. A., Evolving proteins of novel composition. *Angew Chem Int Ed Engl* **2006,** *45* (27), 4518-21; (b) Yoo, T. H.; Link, A. J.; Tirrell, D. A., Evolution of a fluorinated green fluorescent protein. *Proc Natl Acad Sci U S A* **2007,** *104* (35), 13887-90.

3. (a) Kiick, K. L.; Saxon, E.; Tirrell, D. A.; Bertozzi, C. R., Incorporation of azides into recombinant proteins for chemoselective modification by the Staudinger ligation. *Proc Natl Acad Sci U S A* **2002,** *99* (1), 19-24; (b) Kiick, K. L.; Weberskirch, R.; Tirrell, D. A., Identification of an expanded set of translationally active methionine analogues in Escherichia coli. *FEBS Lett* **2001,** *502* (1-2), 25-30; (c) Tang, Y.; Wang, P.; Van Deventer, J. A.; Link, A. J.; Tirrell, D. A., Introduction of an aliphatic ketone into recombinant proteins in a bacterial strain that overexpresses an editing-impaired leucyl-tRNA synthetase. *Chembiochem* **2009,** *10* (13), 2188-90; (d) van Hest, J. C.; Tirrell, D. A., Efficient introduction of alkene functionality into proteins in vivo. *FEBS Lett* **1998,** *428* (1-2), 68-70; (e) van Hest, J. C. M.; Kiick, K. L.; Tirrell, D. A., Efficient Incorporation of Unsaturated Methionine Analogues into Proteins in Vivo. *Journal of the American Chemical Society* **2000,** *122* (7), 1282-1288.

4. (a) Lesser, G. J.; Rose, G. D., Hydrophobicity of amino acid subgroups in proteins. *Proteins* **1990,** *8* (1), 6-13; (b) Lins, L.; Thomas, A.; Brasseur, R., Analysis of accessible surface of residues in proteins. *Protein Sci* **2003,** *12* (7), 1406-17; (c) Miller, S.; Janin, J.; Lesk, A. M.; Chothia, C., Interior and surface of monomeric proteins. *J Mol Biol* **1987,** *196* (3), 641-56; (d) Rose, G. D.; Geselowitz, A. R.; Lesser, G. J.; Lee, R. H.; Zehfus, M. H., Hydrophobicity of amino acid residues in globular proteins. *Science* **1985,** *229* (4716), 834-8.

5. Neal, A. L.; Libman, L.; Smulson, M. E., Influence of gamma-glutamylhydrazide on protein synthesis of Pseudomonas aeruginosa. *Arch Biochem Biophys* **1968,** *127* (1), 426-8.

6. Hartman, M. C.; Josephson, K.; Lin, C. W.; Szostak, J. W., An expanded set of amino acid analogs for the ribosomal translation of unnatural peptides. *PLoS One* **2007,** *2* (10), e972.

7. Chang, P. V.; Prescher, J. A.; Hangauer, M. J.; Bertozzi, C. R., Imaging cell surface glycans with bioorthogonal chemical reporters. *J Am Chem Soc* **2007,** *129* (27), 8400-1.

8. Jevsevar, S.; Kunstelj, M.; Porekar, V. G., PEGylation of therapeutic proteins. *Biotechnol J* **2010,** *5* (1), 113-28.

9. Veronese, F. M.; Pasut, G., PEGylation, successful approach to drug delivery. *Drug Discov Today* **2005,** *10* (21), 1451-8.

10. Fishburn, C. S., The pharmacology of PEGylation: balancing PD with PK to generate novel therapeutics. *J Pharm Sci* **2008,** *97* (10), 4167-83.

11. Verma, N.; Kumar, K.; Kaur, G.; Anand, S., L-asparaginase: a promising chemotherapeutic agent. *Crit Rev Biotechnol* **2007,** *27* (1), 45-62.

12. Avramis, V. I.; Sencer, S.; Periclou, A. P.; Sather, H.; Bostrom, B. C.; Cohen, L. J.; Ettinger, A. G.; Ettinger, L. J.; Franklin, J.; Gaynon, P. S.; Hilden, J. M.; Lange, B.; Majlessipour, F.; Mathew, P.; Needle, M.; Neglia, J.; Reaman, G.; Holcenberg, J. S.; Stork, L., A randomized comparison of native Escherichia coli asparaginase and polyethylene glycol conjugated asparaginase for treatment of children with newly diagnosed standard-risk acute lymphoblastic leukemia: a Children's Cancer Group study. *Blood* **2002,** *99* (6), 1986-94.

13. Kamisaki, Y.; Wada, H.; Yagura, T.; Matsushima, A.; Inada, Y., Reduction in immunogenicity and clearance rate of Escherichia coli L-asparaginase by modification with monomethoxypolyethylene glycol. *J Pharmacol Exp Ther* **1981,** *216* (2), 410-4.

14. Swain, A. L.; Jaskolski, M.; Housset, D.; Rao, J. K.; Wlodawer, A., Crystal structure of Escherichia coli L-asparaginase, an enzyme used in cancer therapy. *Proc Natl Acad Sci U S A* **1993,** *90* (4), 1474-8.

15. Harms, E.; Wehner, A.; Jennings, M. P.; Pugh, K. J.; Beacham, I. R.; Rohm, K. H., Construction of expression systems for Escherichia coli asparaginase II and two-step purification of the recombinant enzyme from periplasmic extracts. *Protein Expr Purif* **1991,** *2* (2-3), 144-50.

16. Derst, C.; Henseling, J.; Rohm, K. H., Probing the role of threonine and serine residues of E. coli asparaginase II by site-specific mutagenesis. *Protein Eng* **1992,** *5* (8), 785-9.

17. Fraczkiewicz, R.; Braun, W., Exact and efficient analytical calculation of the accessible surface areas and their gradients for macromolecules. *Journal of Computational Chemistry* **1998,** *19* (3), 319-333.

18. Fasman, G. D., *Prediction of protein structure and the principles of protein conformation*. Springer: 1989.

19. Touchette, N. A.; Perry, K. M.; Matthews, C. R., Folding of dihydrofolate reductase from Escherichia coli. *Biochemistry* **1986,** *25* (19), 5445-52.

20. Van Deventer, J. A. Biophysics and protein engineering with noncanonical amino acids. California Institute of Technology, 2010.

21. Vagenende, V.; Yap, M. G.; Trout, B. L., Mechanisms of protein stabilization and prevention of protein aggregation by glycerol. *Biochemistry* **2009,** *48* (46), 11084-96.

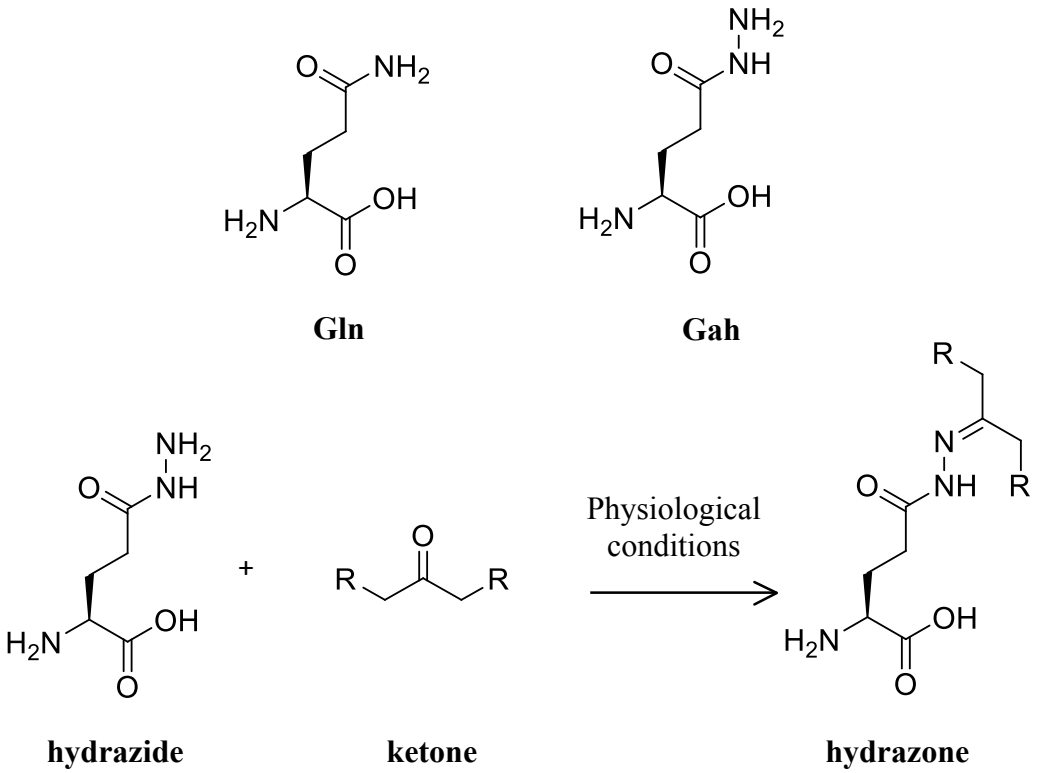

Scheme 4.1. Chemical structures of Gln and Gah. The hydrazide group on Gah reacts with ketones under physiological conditions to form a stable hydrazone linkage.

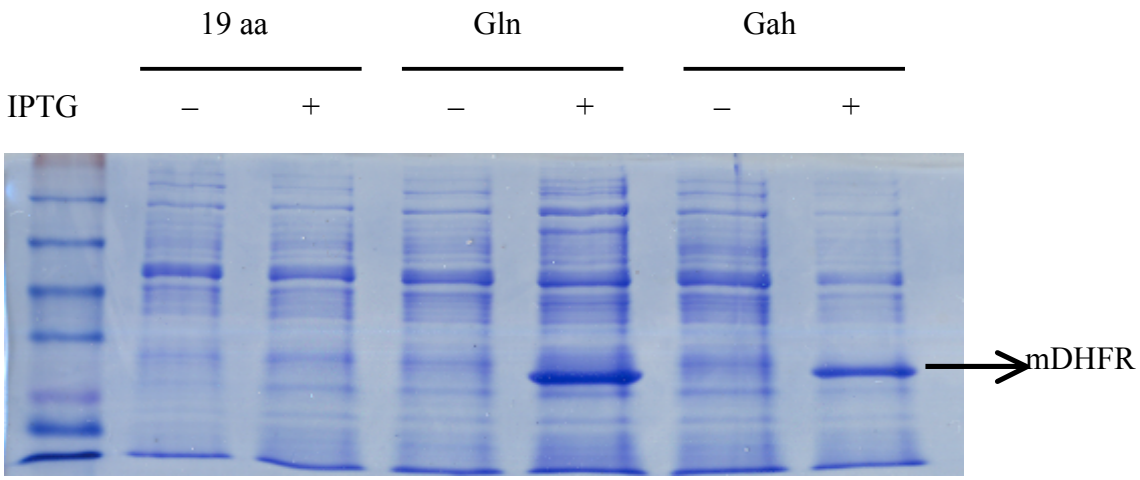

Figure 4.1. Gel electrophoresis analysis of mDHFR expression. Protein expression was induced in cultures containing 19 amino acids, 19 amino acids plus 4 mM Gln, or 19 amino acids plus 4 mM Gah. mDHFR expression is evident by the appearance of a band at the expected molecular weight of 24 kDa in cultures containing Gln or Gah.

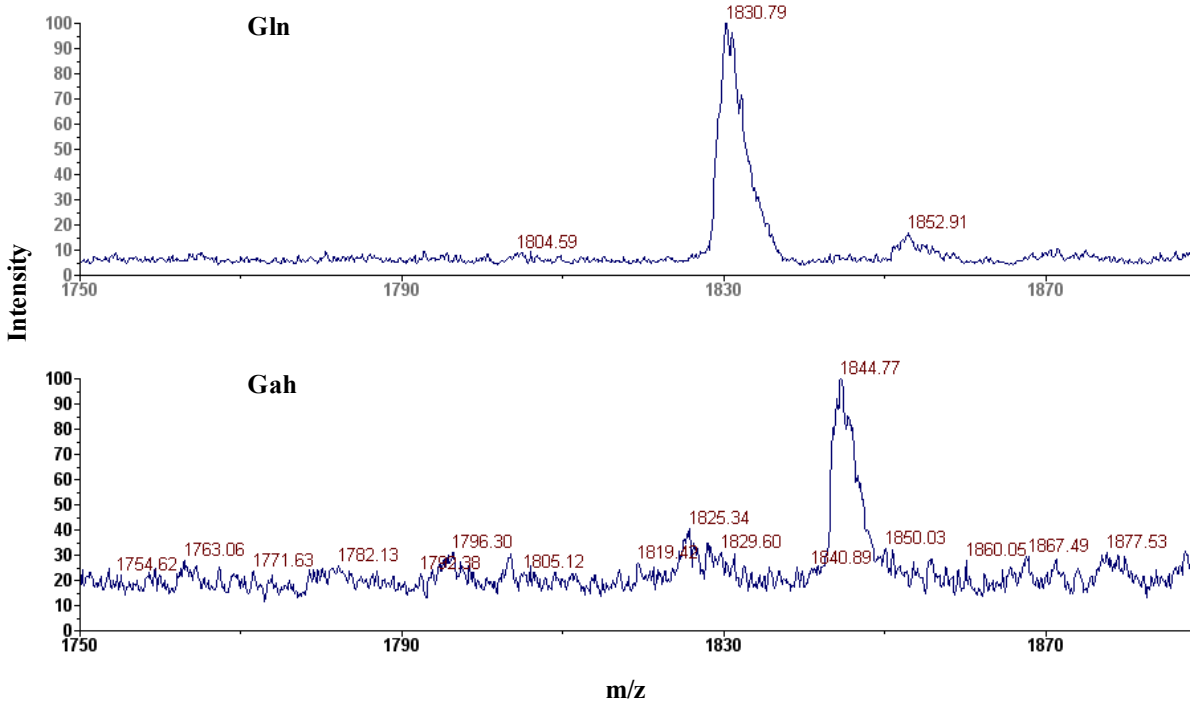

Figure 4.2. MALDI-MS analysis of tryptic digested peptides of mDHFR. The protein was expressed in medium containing 19 amino acids plus either Gln or Gah, purified, and subjected to trypsin digestion. A peptide fragment of sequence LLPEYPGVLSEVQEEK (amino acids 173-188, expected mass 1830.79 Da) yields the spectra shown. Replacement of Gln by Gah results in a 15 Da mass increase. The disappearance of the original peptide signal and the emergence of a new signal in the Gah sample suggest near-quantitative replacement of Gln by Gah.

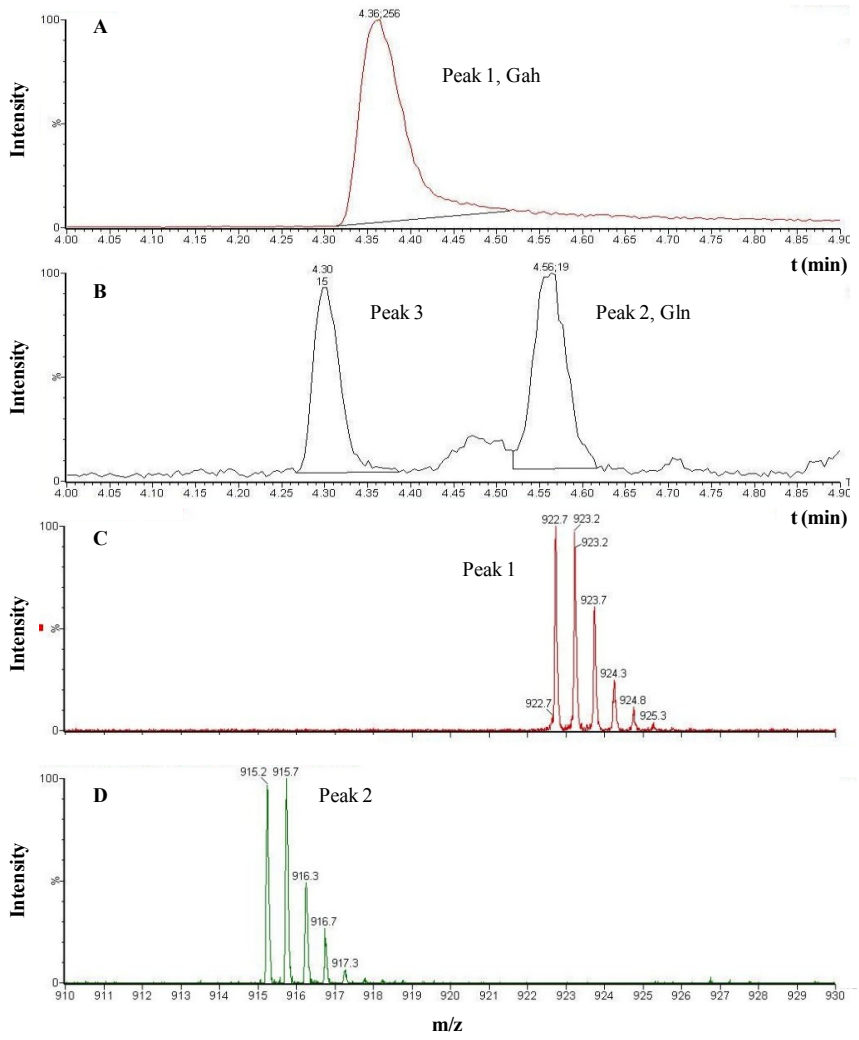

Figure 4.3. Quantitative analysis of Gah incorporation by LC-MS. (A) Chromatography peak 1 corresponds to peptide LLPEYPGVLSEVZEEK (amino acids 173-188) with Gah at the Z position. Its relative integrated area is 267. (B) Chromatograph peak 2 corresponds to the peptide with natural amino acids; its relative integrated area is 19. (C) Mass spectrum of peak 1, shown as doubly-charged ions for the peptide with calculated mass of 1845 Da. A mass shift of 15 Da, corresponding to the mass difference between Gah and Gln, confirms incorporation of Gah. (D) Mass spectrum of peak 2, doubly-charged ions for peptide with calculated mass of 1830 Da. Peak 3 corresponds to an irrelevant peak that has an isotope mass at 915 Da.

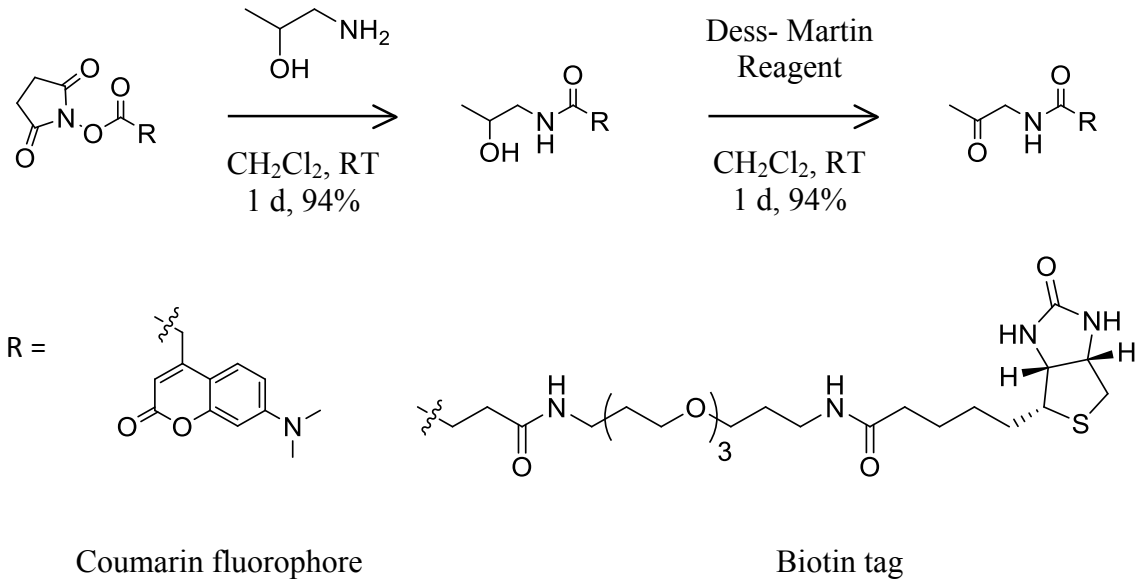

Scheme 4.2. Synthetic scheme for preparation of ketone probes.

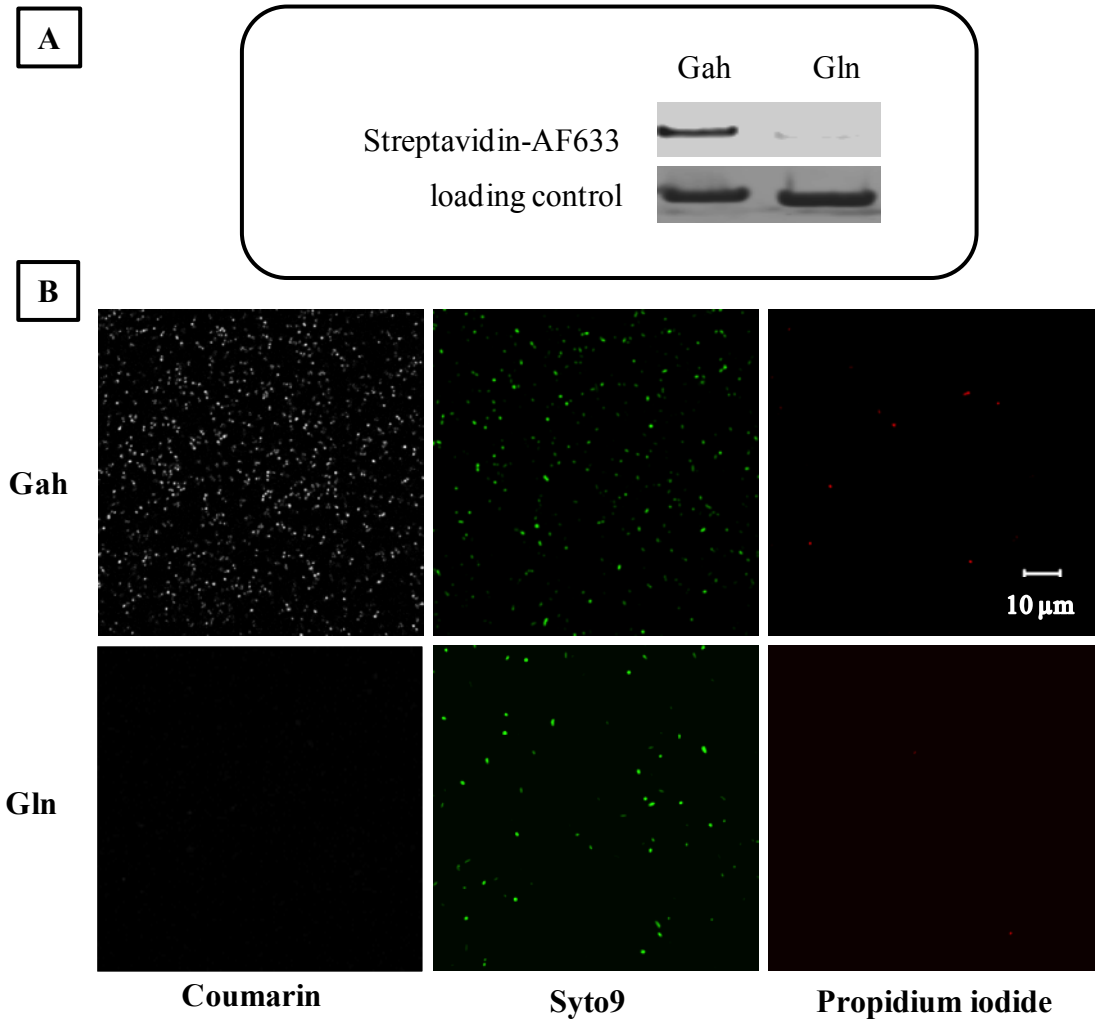

Figure 4.4. Selective labeling of Gah-containing proteins using ketone probes. (A) Gah and Gln-containing mDHFR was subjected to reaction with biotin ketone in PBS, pH 6.5, at RT, for 12 h. Specific biotin signal in Gah sample was detected using a fluorescent streptavidin conjugate. (B) Bacterial cells grown in the presence of either Gah or Gln were treated with coumarin ketone in minimal medium containing 20 amino acids, pH 6.5, at 4 °C for 3 h prior to cell viability staining. Syto9 (green) is a cell-permeant dye and stains all cells while propidium iodide (red) only stains dead cells. Gah-treated cells exhibit strong fluorescence while cells cultured in 20 aa are not fluorescent.

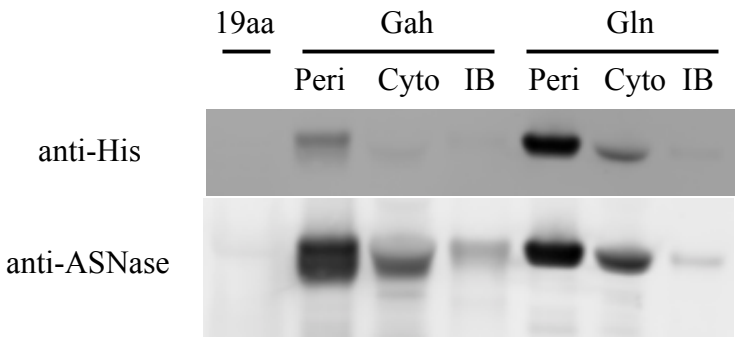

Figure 4.5. Western blotting analysis of asparaginase expression. Using both anti-His and anti-ASNase antibodies, expression of asparaginase was confirmed in cultures supplemented either with Gah or with Gln. Peri = periplasmic space; cyto = cytosolic soluble fraction; IB = inclusion bodies.

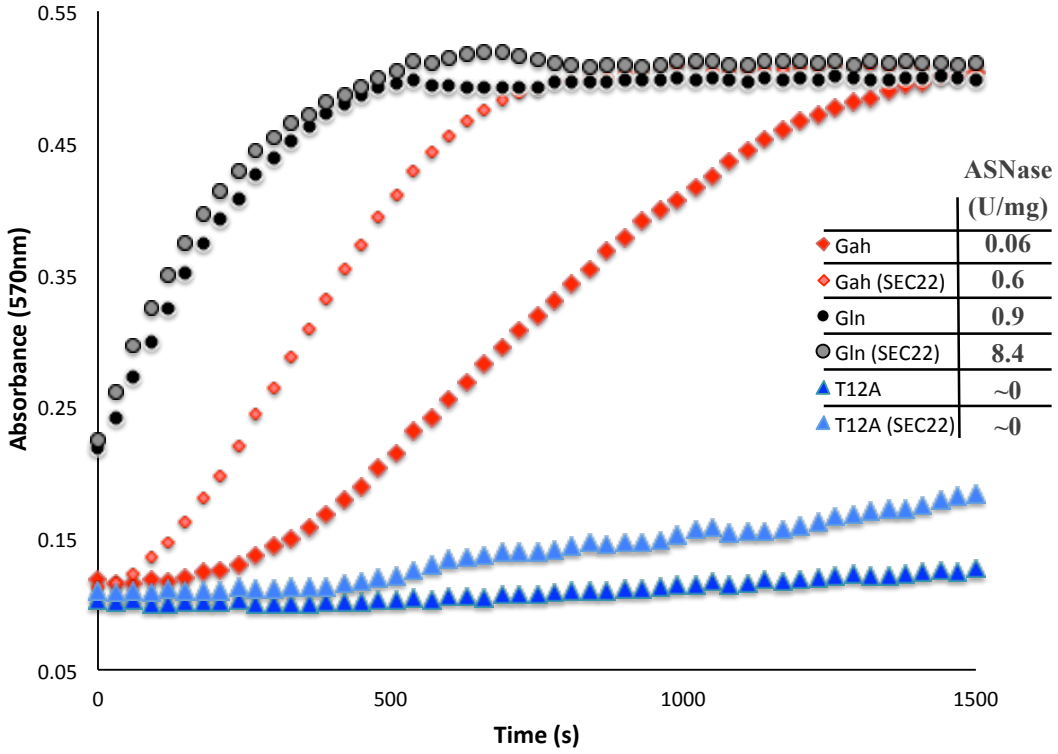

Figure 4.6. ASNase activity assay. Absorbance at 570 nm was measured at 30 second intervals for 25 min for protein samples before (Gah, Gln, T12A) and after SEC-FPLC (SEC22). Asparaginase activity values for Gah sample were found to be 15-fold less than Gln. The T12A mutant was found to have no activity, indicating that there was minimal noise.

CHAPTER 5

Selective Metabolic Labeling of Cancer Cells by the Glutamine Analogue L-Glutamic Acid-γ-Hydrazide

Abstract

Our understanding of cancer has been shifted dramatically by the discovery that the tumor microenvironment plays an important role in tumorigenesis. As a result, there has been a growing interest in interrogation of tumors and their microenvironments using both *in vitro* and *in vivo* models; however, the selective labeling of a particular cell type in the complex microenvironment of many cell types presents a technological challenge. In this study, we explore the possibility of using a reactive glutamine analogue L-glutamic γ-hydrazide (Gah) for selective labeling of tumor cells by taking advantage of the difference in glutamine metabolism between cancer and normal cells. We treated cervical cancer HeLa cells and normal human dermal fibroblasts (NHDF) with Gah and found that Gah exhibited specific toxicity towards HeLa cells (IC50 = 80 μM) and had little effect on NHDF (IC50 > 2 mM), indicating a preferential uptake of Gah by HeLa cells. Further, we demonstrated selective fluorescent labeling of Gah-treated tumor cells using an aldehyde-containing fluorophore.

Introduction

In the course of tumor progression, the tumor microenvironment emerges as a result of interactions between tumor cells and tumor stroma, blood vessels, infiltrating inflammatory cells, and associated tissue cells.[1] The microenvironment has been considered the "soil" for carcinogenesis, and studying the immediate microenvironment within a developing tumor has become as important as studying the dysfunctional cells within that tumor.[2] Recently, much effort has been focused on interrogating both *in vitro* and *in vivo* models of tumor microenvironments; however, selective monitoring of one cell type in such a complex

mixture of many cell types is challenging. Fluorescent proteins are commonly used for cell tracking; however, this approach requires genetic manipulation of tumor cells prior to formation of the microenvironment, which limits its use to *in vitro* studies. Since *in vitro* models of tumor microenvironment do not replicate the original structural milieu such as relative cell populations, and do not reflect the heterogeneity that is characteristic of solid tumors,[3] there is a growing interest in *ex vivo* culture models that incorporate human tumor tissue in its native 3D state and enable dynamic manipulation of the system.[4] A simple approach that circumvents the requirement for genetic manipulation is needed to selectively label tumor cells for investigations of these tumor microenvironment models.

Metabolic differences between cancer cells and normal cells have been established since the 1920s when it was observed that tumor cells predominantly produce energy by an unexpectedly high rate of glycolysis in the presence of oxygen (the Warburg effect).[5] Cancer cells have had major modifications in their metabolic pathways in order to provide energy and macromolecules to sustain their increased proliferation.[6] Recent studies have suggested that activating mutations in phosphoinositol 3-kinase (PI3K) and its downstream effectors induce the conversion of mitochondria within the transformed cells into synthetic organelles that support glucose-dependent lipid synthesis and non-essential amino acid production.[7] This metabolic phenotype is also the basis for tumor imaging using ^{18}F-labeled glucose analogues for positron emission tomography (PET) and has become an important diagnostic tool for cancer detection and management.[8]

In addition to glucose, glutamine (Gln) is another essential nutrient for cell growth and viability.[9] Glutamine is the major source of nitrogen for nucleotide and amino acid synthesis.[10] Further, Gln can replenish intermediates of the citric acid (TCA) cycle to

generate energy for maintaining cellular homeostasis through the process of glutaminolysis, whereby glutamine is converted to glutamate.[11] In cancer cells, fewer glucose-derived metabolites feed into the TCA cycle as a result of the Warburg effect, and cancer cells typically have an increased reliance on alternative metabolites such as glutamine.[12] Gln metabolism in cancer cells has been reported to far exceed the use of any other amino acid.[9b, 13] In cancer patients, some tumors have been reported to consume such an abundance of glutamine that they depress plasma glutamine levels.[14] Although glutamine is considered a non-essential amino acid in normal cells, certain cancer cells cannot survive without exogenous glutamine, exhibiting a glutamine addiction phenotype.[9b, 15] Taking advantage of this difference in glutamine metabolism, in this work, we demonstrate the selective labeling of tumor cells using a reactive glutamine analogue, L-glutamic acid-γ-hydrazide (Gah) (Scheme 5.1).

Results and Discussion

Incorporation of Gah into auxotrophic bacterial cells. Gah has been shown to exhibit translational activity 70% of that of Gln in an *in vitro* assay using reconstituted *E. coli* translational components.[16] The *in vivo* incorporation of Gah using a glutamine auxotrophic *E. coli* strain and a medium shift procedure was demonstrated and discussed in Chapter 4. We also attempted to incorporate Gah without performing a medium shift to remove residual glutamine, and found no evidence of incorporation by matrix-assisted laser desorption ionization mass spectrometry (MALDI-MS) (Figure 1). These observations suggest that Gah does not compete successfully with endogenous levels of glutamine. Thus, Gah is not

expected to be incorporated into mammalian cells, which can typically synthesize glutamine; however, we hypothesized that Gah might be selectively incorporated into tumor cells that rely on exogenous supplies of glutamine.

Preferential uptake of Gah by tumor cells. To test our hypothesis, we first compared the *in vitro* cytotoxicity of Gah in normal and tumor cells. The human cervical cancer cell line (HeLa) and normal human dermal fibroblasts (NHDF) were chosen for this study for two reasons: 1) HeLa cells have been shown to exhibit the glutamine addiction phenotype;[15] 2) HeLa and fibroblasts cells are widely used model cell lines for studying interactions between tumor and stroma.[17] Cells were seeded at a density of 10,000 cells per well in 96-well plates and grown for 24 h. The culture medium was replaced with serum-free medium (SFM) lacking Gln. Gah was then added to final concentrations ranging from 0 to 4 mM. After a 96-h incubation, cells were washed with phosphate buffered saline (PBS) prior to cell viability evaluation by the MTT assay (Figure 2).[18] The viability of HeLa cells was dramatically reduced at low concentrations of Gah (IC50 = 80 ± 8.6 μM); whereas NHDF cells were affected by Gah only at high concentrations (IC50 > 2 mM). This specific cytotoxicity of Gah towards HeLa cells, evident by the 25-fold difference in IC50 values, could be a result of inhibition of macromolecular synthesis by Gah.

Selective labeling of tumor cells. After demonstrating the specific cytotoxicity of Gah, we evaluated the possibility of selectively labeling tumor cells using Gah and subsequent reaction with a fluorescent dye (**1**, Scheme 5.1). The Gah side chain provides hydrazide groups that selectively react with ketones or aldehydes in aqueous solution.[19] Proteins and live bacterial cells containing Gah have been selectively modified using ketone probes as

discussed in Chapter 4. Herein, we describe dye-labeling of mammalian cells using Gah and an aldehyde derivative of fluorescein, **1**.

To identify optimum conditions for selective labeling of cancer cells, we screened various pulse durations and concentrations of Gah. HeLa and NHDF cells were grown for 24 h on 8-well chamber slides pretreated with fibronectin to promote cell adhesion and growth. Cells were washed with PBS and the culture medium was replaced with SFM lacking Gln. Gah was added to each well to a final concentration of 0, 1, 5, or 10 mM. After an incubation period of either 2 or 6 h, cells were washed with PBS to remove free Gah, fixed with paraformaldehyde, blocked with bovine serum albumin (BSA) before reaction with 10 μM of **1** in PBS, pH 6.5, for 2 h at room temperature.

Cells were washed with PBS after dye labeling and examined by fluorescence microscopy. Fluorescence images were acquired with identical acquisition settings for all samples, and mean fluorescence intensities were compared (Figure 3). At 2 h, HeLa and NHDF cells exhibited similar levels of fluorescence that were close to the background fluorescence observed for samples without Gah, indicating that little Gah was incorporated by either cell type. However, at 6 h, HeLa cells exhibited an elevated mean fluorescence signal, compared to that of NHDF at Gah concentrations of 1 and 5 mM; in contrast, fluorescence from NHDF cells showed no dependence on either pulse length or Gah concentration. Although the fluorescence enhancement was moderate, the selectivity of dye-labeling is evident in images acquired with identical instrument settings (Figure 4). The fluorescence images show bright fluorescence in HeLa cells and a lack of fluorescence from NHDF cells after 6-h pulses with either 1 mM or 5 mM Gah. At 10 mM, Gah did not enhance the fluorescence of HeLa cells;

this result could be caused by the inhibitory effects of Gah on protein synthesis and cell growth at high concentrations.

Conclusions

The differences between cancer and normal cells in metabolism of basic nutrients have been known for several decades.[20] Based on the difference in glutamine metabolism, we hypothesized that a reactive glutamine analogue, Gah, might be preferentially incorporated into tumor cells. Gah exhibits highly specific cytotoxicity toward HeLa cells compared to NHDF cells, suggesting a difference in its rate of consumption by the two cell types. We utilized this difference in uptake and demonstrated selective labeling of HeLa cells using an aldehyde-fluorescein dye. By taking advantage of the distinct metabolic differences between cancer and normal cells, this approach circumvents the need for genetic manipulation and provides a facile strategy to selectively label cancer cells in complex tumor microenvironment models.

Future Work

To improve the fluorescence enhancement in HeLa cells, background fluorescence will need to be reduced. A basal level of fluorescence was observed in samples without Gah, perhaps due to an undesired reaction between aldehyde-fluorescein and reactive lysines on cellular proteins.[21] Ketone dyes could potentially reduce the background fluorescence because they are less reactive towards amines[22] and should exhibit more selective reactivity toward

hydrazides. Having optimized dye-labeling in separate cultures of HeLa and NHDF, we will assess the selectivity of labeling in co-culture systems.

Materials and Methods

Cell culture. HeLa and NHDF cells (ATCC) were cultured at 37°C under a humidified atmosphere of 5% CO_2. Cells were maintained in Dulbecco's modified Eagle's medium (DMEM) supplemented with 10% (v/v) fetal bovine serum (Invitrogen), 50 U/mL penicillin, and 50 μg/mL streptomycin. Near-confluent cells were passaged with 0.05% trypsin in 0.52 mM EDTA (Invitrogen). The cells were continuously maintained in the culture medium and subcultured every 3-4 days.

MTT cell viability assay. Cells were seeded at a density of 10,000 cells/well in a 96-well plate and grown for 20 h. Prior to Gah exposure, the culture medium was removed and the cells were washed once with warm PBS. Fresh media containing Gah at concentrations ranging from 0 to 4 mM, was added to appropriate wells. Cells were subsequently incubated at 37 °C for 96 h. The Gah-supplemented medium was then removed and the cells were washed twice with warm PBS before being subjected to the MTT cell proliferation assay according to the manufacturer's instructions (ATCC). Cells were incubated with fresh medium containing MTT reagent for 3 h at 37 °C before detergent was added to solubilize purple formazan crystals formed by proliferating cells. Absorbance at 570 nm was then measured on a Safire II (Tecan) plate reader.

Preparation of cells for fluorescence microscopy. Near-confluent cells were washed twice with 5 mL warm PBS. Cells were detached with trypsin in EDTA and treated with 3 mL of complete DMEM. The cells were pelleted via centrifugation (200 g, 3 min), resuspended in 1 mL of serum-free medium (DMEM lacking glutamine and FBS), and counted. Cells were seeded at a density of 2.5×10^4 per well to prepared slides.

Eight-well Lab-Tek II chamber slides (Nalge Nunc International) were prepared by treatment with fibronectin solution (10 μg/mL) at 4°C overnight. The wells were rinsed three times with PBS, blocked with a 2 mg/mL solution of heat-inactivated BSA for 30 min at RT, and washed with PBS.

Cells were incubated for 30 min in SFM to deplete residual glutamine. After incubation, Gah was added to appropriate wells at final concentrations of 0, 1, 5, or 10 mM. After either 2 or 6 h, cells were rinsed three times with warm PBS, fixed with 3.7% paraformaldehyde solution for 15 min, and rinsed twice with PBS. Cells were permeabilized with 0.1% Triton X-100 for 3 min and treated with a blocking solution containing 10% (v/v) FBS, 50 mg/mL sucrose, and 20 mg/mL BSA for 30 min at RT. Cells were washed twice with PBS and treated with 10 μM **1** in PBS, pH 6.5 for 2 h at RT, in the dark. After reaction, cells were washed four times with 1% Tween 20 in PBS at 10 min intervals with agitation to remove excess dye. Cells were rinsed once with PBS. Chamber walls were removed and slides were mounted for visualization.

Fluorescence microscopy. Fixed cells were imaged on an inverted epifluorescence microscope (Olympus) in the laboratory of Professor Chin-Lin Guo at Caltech. Each set of

images was obtained with identical settings. All images were acquired with a 10X objective and analyzed with imageJ.

Acknowledgements

We thank Daniela Espinosa for contributing to this work during her undergraduate summer research program. We thank Dr. Cole DeForest for providing the fluorophore used in this study. We also thank Jiun-Yann Yu and Professor Chin-Lin Guo for graciously allowing us to use their fluorescence microscope.

References

1. Whiteside, T. L., The tumor microenvironment and its role in promoting tumor growth. *Oncogene* **2008,** *27* (45), 5904-12.

2. Albini, A.; Sporn, M. B., The tumour microenvironment as a target for chemoprevention. *Nat Rev Cancer* **2007,** *7* (2), 139-47.

3. Gerlinger, M.; Rowan, A. J.; Horswell, S.; Larkin, J.; Endesfelder, D.; Gronroos, E.; Martinez, P.; Matthews, N.; Stewart, A.; Tarpey, P.; Varela, I.; Phillimore, B.; Begum, S.; McDonald, N. Q.; Butler, A.; Jones, D.; Raine, K.; Latimer, C.; Santos, C. R.; Nohadani, M.; Eklund, A. C.; Spencer-Dene, B.; Clark, G.; Pickering, L.; Stamp, G.; Gore, M.; Szallasi, Z.; Downward, J.; Futreal, P. A.; Swanton, C., Intratumor heterogeneity and branched evolution revealed by multiregion sequencing. *N Engl J Med* **2012,** *366* (10), 883-92.

4. Centenera, M. M.; Raj, G. V.; Knudsen, K. E.; Tilley, W. D.; Butler, L. M., Ex vivo culture of human prostate tissue and drug development. *Nat Rev Urol* **2013**.

5. Warburg, O., On the origin of cancer cells. *Science* **1956,** *123* (3191), 309-14.

6. Furuta, E.; Okuda, H.; Kobayashi, A.; Watabe, K., Metabolic genes in cancer: their roles in tumor progression and clinical implications. *Biochim Biophys Acta* **2010,** *1805* (2), 141-52.

7. (a) Lum, J. J.; Bui, T.; Gruber, M.; Gordan, J. D.; DeBerardinis, R. J.; Covello, K. L.; Simon, M. C.; Thompson, C. B., The transcription factor HIF-1alpha plays a critical role in the growth factor-dependent regulation of both aerobic and anaerobic glycolysis. *Genes Dev* **2007,** *21* (9), 1037-49; (b) Bauer, D. E.; Hatzivassiliou, G.; Zhao, F.; Andreadis, C.; Thompson, C. B., ATP citrate lyase is an important component of cell growth and transformation. *Oncogene* **2005,** *24* (41), 6314-22; (c) Elstrom, R. L.; Bauer, D. E.; Buzzai, M.; Karnauskas, R.; Harris, M. H.; Plas, D. R.; Zhuang, H.; Cinalli, R. M.; Alavi, A.; Rudin, C. M.; Thompson, C. B., Akt stimulates aerobic glycolysis in cancer cells. *Cancer Res* **2004,** *64* (11), 3892-9.

8. Vander Heiden, M. G.; Cantley, L. C.; Thompson, C. B., Understanding the Warburg Effect: The Metabolic Requirements of Cell Proliferation. *Science* **2009,** *324* (5930), 1029-1033.

9. (a) Neu, J.; Shenoy, V.; Chakrabarti, R., Glutamine nutrition and metabolism: where do we go from here ? *FASEB J* **1996,** *10* (8), 829-37; (b) Eagle, H., Nutrition needs of mammalian cells in tissue culture. *Science* **1955,** *122* (3168), 501-14.

10. Brosnan, J. T., Interorgan amino acid transport and its regulation. *J Nutr* **2003,** *133* (6 Suppl 1), 2068S-2072S.

11. DeBerardinis, R. J.; Mancuso, A.; Daikhin, E.; Nissim, I.; Yudkoff, M.; Wehrli, S.; Thompson, C. B., Beyond aerobic glycolysis: transformed cells can engage in glutamine metabolism that exceeds the requirement for protein and nucleotide synthesis. *Proc Natl Acad Sci U S A* **2007,** *104* (49), 19345-50.

12. Baggetto, L. G., Deviant energetic metabolism of glycolytic cancer cells. *Biochimie* **1992,** *74* (11), 959-74.

13. Coles, N. W.; Johnstone, R. M., Glutamine metabolism in Ehrlich ascites-carcinoma cells. *Biochem J* **1962,** *83*, 284-91.

14. (a) Chen, M. K.; Espat, N. J.; Bland, K. I.; Copeland, E. M., 3rd; Souba, W. W., Influence of progressive tumor growth on glutamine metabolism in skeletal muscle and kidney. *Ann Surg* **1993,** *217* (6), 655-66; discussion 666-7; (b) Suzannec Klimberg, V.; McClellan, J. L., Glutamine, cancer, and its therapy. *The American Journal of Surgery* **1996,** *172* (5), 418-424.

15. Reitzer, L. J.; Wice, B. M.; Kennell, D., Evidence that glutamine, not sugar, is the major energy source for cultured HeLa cells. *J Biol Chem* **1979,** *254* (8), 2669-76.

16. Hartman, M. C.; Josephson, K.; Lin, C. W.; Szostak, J. W., An expanded set of amino acid analogs for the ribosomal translation of unnatural peptides. *PLoS One* **2007,** *2* (10), e972.

17. Delinassios, J. G., Fibroblasts against cancer cells in vitro. *Anticancer Res* **1987,** *7* (5B), 1005-10.

18. Mosmann, T., Rapid colorimetric assay for cellular growth and survival: application to proliferation and cytotoxicity assays. *J Immunol Methods* **1983,** *65* (1-2), 55-63.

19. Chang, P. V.; Prescher, J. A.; Hangauer, M. J.; Bertozzi, C. R., Imaging cell surface glycans with bioorthogonal chemical reporters. *J Am Chem Soc* **2007,** *129* (27), 8400-1.

20. (a) Thompson, C. B.; Bauer, D. E.; Lum, J. J.; Hatzivassiliou, G.; Zong, W. X.; Zhao, F.; Ditsworth, D.; Buzzai, M.; Lindsten, T., How do cancer cells acquire the fuel needed to support cell growth? *Cold Spring Harb Symp Quant Biol* **2005,** *70*, 357-62; (b) Shaw, R. J.; Cantley, L. C., Ras, PI(3)K and mTOR signalling controls tumour cell growth. *Nature* **2006,** *441* (7092), 424-30.

21. Robert, L.; Penaranda, F. S., Studies on aldehyde-protein interactions. I. Reaction of amino acids with lower aldehydes. *Journal of Polymer Science* **1954,** *12* (1), 337-350.

22. Lowry, T. H., Richardson, Kathleen Schueller, *mechanism and theory in organic chemsitry*. 3rd ed.; Harper Collins: 1987.

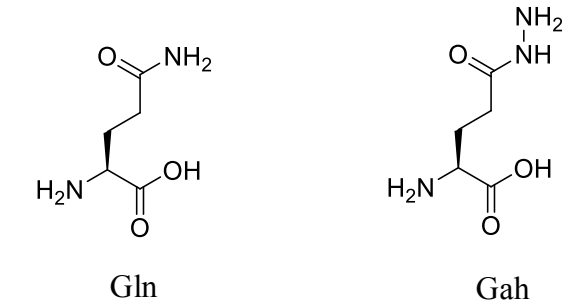

Gln Gah

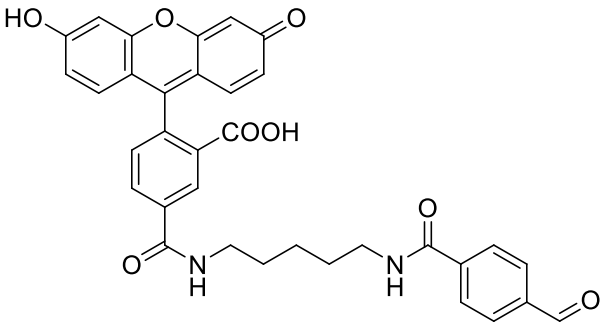

1

Scheme 5.1. Chemical structures of amino acids and fluorophore.

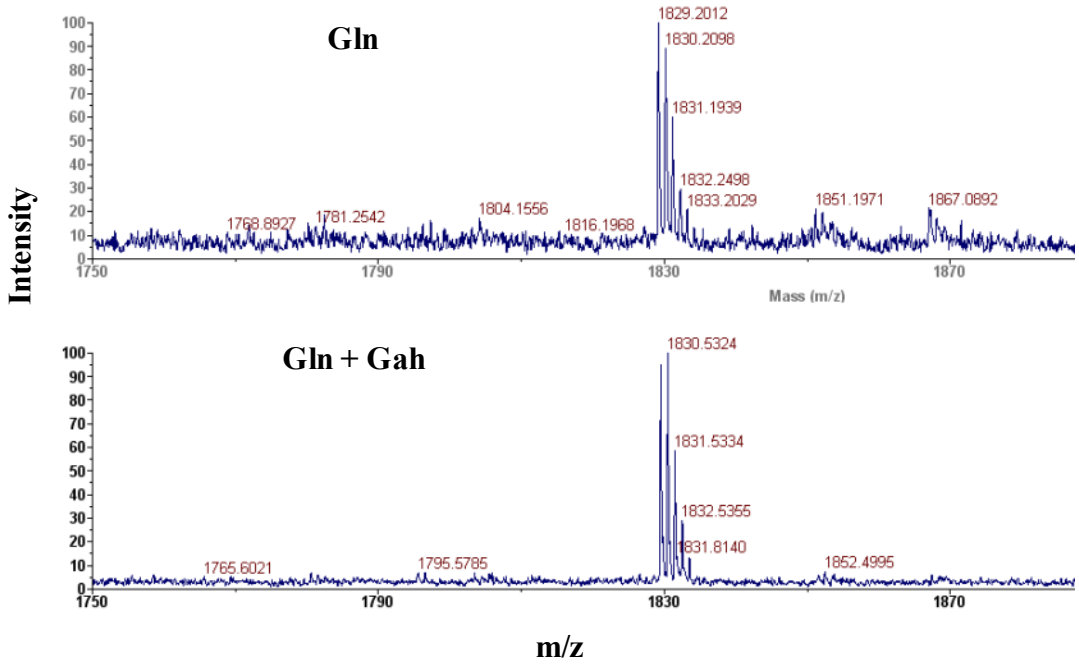

Figure 5.1. Gah cannot be incorporated into proteins in the presence of glutamine. Glutamine auxotrophic cells were grown in medium supplemented with 20 aa (0.27 mM Gln) for 5 h prior to DHFR induction in the presence of 4 mM Gah for 4 h. Tryptic digested mDHFR peptides were analyzed by MALDI-MS. A Gln-containing peptide with sequence LLPEYPGVLSEVQEEK (amino acids 173-188, expected mass 1830.79 Da) yields the spectra shown. Replacement of Gln by Gah should give rise to a new peptide peak that is 15 Da away. The absence of new peaks indicates no replacement of Gln by Gah

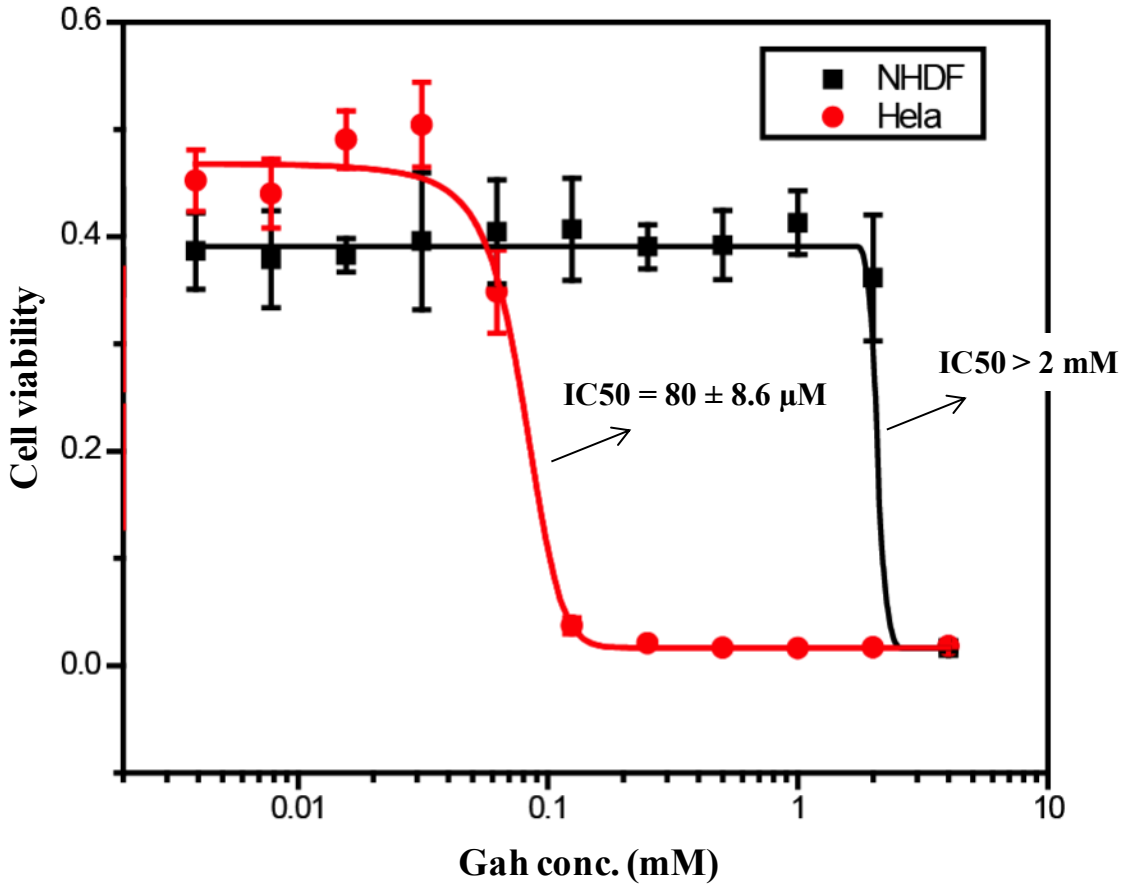

Figure 5.2. Gah is toxic to HeLa cells. HeLa and NHDF cells were grown in glutamine-free medium supplemented with Gah concentrations ranging from 0 to 4 mM. Cell viability was assessed 96 h later by measuring cellular metabolic activities using the MTT assay. Gah exhibits specific toxicity to HeLa cells with an IC50 of 80 µM, 25-fold lower than in NHDF cells.

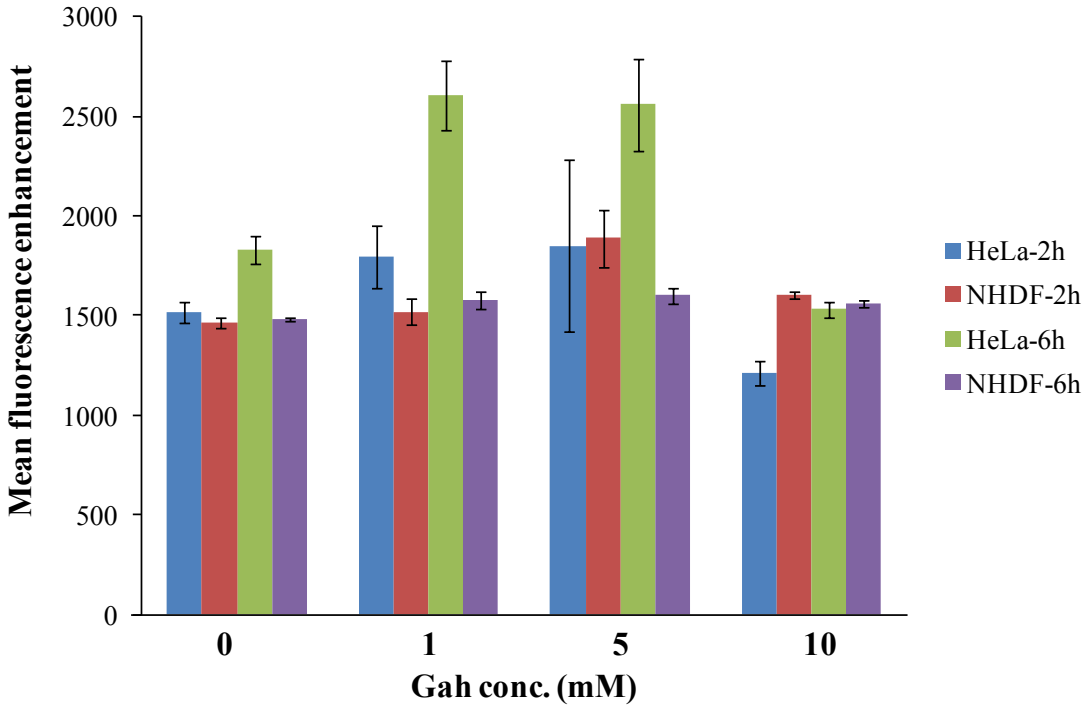

Figure 5.3. Mean fluorescence comparison of dye-labeled cells. Cells were grown in media containing Gah at concentrations ranging from 0 to 10 mM for either 2 or 6 h. Cells were fixed, permeabilized, and labeled with **1** for 2 h. Cells were then imaged and mean fluorescence was calculated using ImageJ software.

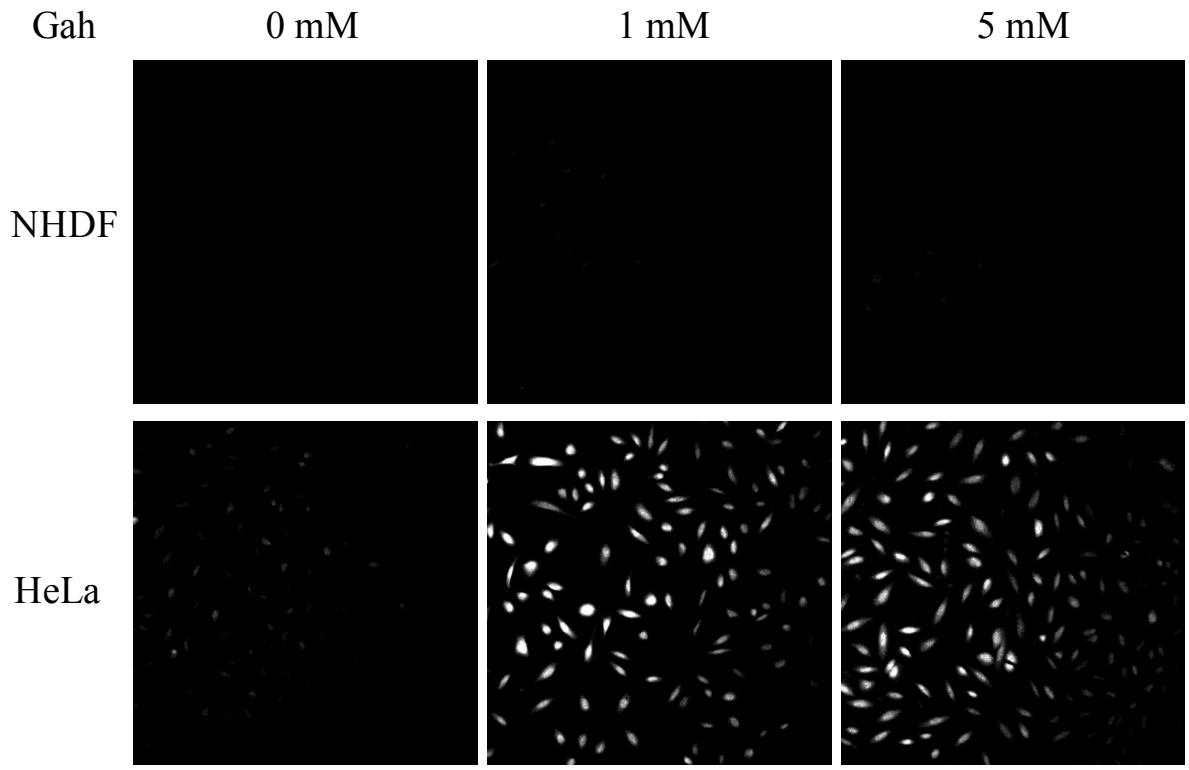

Figure 5.4. Gah enables selective visualization of tumor cells. Bright fluorescence was observed in HeLa cells treated with 1 mM and 5 mM Gah, while NHDF cells exhibited little fluorescence under any conditions.

Appendix I

Core-Clickable PEG-*Branch*-Azide Bivalent-Bottle-Brush Polymers by ROMP: Grafting-Through and Clicking-To

J|A|C|S ARTICLES

Published on Web 12/13/2010

Core-Clickable PEG-*Branch*-Azide Bivalent-Bottle-Brush Polymers by ROMP: Grafting-Through and Clicking-To

Jeremiah A. Johnson,[†] Ying Y. Lu,[†] Alan O. Burts,[†] Yeon-Hee Lim,[‡] M. G. Finn,[‡] Jeffrey T. Koberstein,[§] Nicholas J. Turro,[||] David A. Tirrell,*[,†] and Robert H. Grubbs*[,†]

Division of Chemistry and Chemical Engineering, California Institute of Technology, 1200 E. California Blvd., Pasadena, California 91125; Department of Chemistry and The Skaggs Institute for Chemical Biology, The Scripps Research Institute, 10550 North Torrey Pines Road, La Jolla, California 92037; Department of Chemical Engineering, Columbia University, 500 West 120th Street, New York, New York, 10027; and Department of Chemistry, Columbia University, 3000 Broadway, New York, New York 10027

Received September 18, 2010; E-mail: rhg@caltech.edu; tirrell@caltech.edu

Abstract: The combination of highly efficient polymerizations with modular "click" coupling reactions has enabled the synthesis of a wide variety of novel nanoscopic structures. Here we demonstrate the facile synthesis of a new class of clickable, branched nanostructures, polyethylene glycol (PEG)-*branch*-azide bivalent-brush polymers, facilitated by "graft-through" ring-opening metathesis polymerization of a branched norbornene-PEG-chloride macromonomer followed by halide-azide exchange. The resulting bivalent-brush polymers possess azide groups at the core near a polynorbornene backbone with PEG chains extended into solution; the structure resembles a unimolecular micelle. We demonstrate copper-catalyzed azide−alkyne cycloaddition (CuAAC) "click-to" coupling of a photocleavable doxorubicin (**DOX**)-alkyne derivative to the azide core. The CuAAC coupling was quantitative across a wide range of nanoscopic sizes (∼6−∼50 nm); UV photolysis of the resulting **DOX**-loaded materials yielded free **DOX** that was therapeutically effective against human cancer cells.

Introduction

The explosion of nanoscience is fuelled by problems that require nanoscale solutions and by the inherent challenges of nanoscale synthesis.[1−3] In drug delivery, for example, plasma clearance time of a polymer−drug conjugate is closely linked to its nanoscopic size; materials smaller than 10 nm are excreted rapidly whereas larger materials often display significantly longer retention times.[3−9] Nanoscopic architecture also plays an important role in determining in vivo retention time.[10−12] Branched polymeric structures such as dendrimers, star polymers, bottle-brush polymers, and hyperbranched polymers generally display longer in vivo retention times compared to their linear polymer analogues.[11,13] A wealth of research attention has focused on synthetic approaches to branched, stimuli-responsive, nanoscopic materials that possess orthogonal functionality for incorporation of therapeutic, imaging, and targeting molecules.[14−25]

[†] Division of Chemistry and Chemical Engineering, California Institute of Technology.
[‡] Department of Chemistry and The Skaggs Institute for Chemical Biology, The Scripps Research Institute.
[§] Department of Chemical Engineering, Columbia University.
[||] Department of Chemistry, Columbia University.

(1) Whitesides, G. M. *Small* **2005**, *1*, 172–179.
(2) Steigerwald, M. L.; Brus, L. E. *Acc. Chem. Res.* **1990**, *23*, 183–188.
(3) Peer, D.; Karp, J. M.; Hong, S.; Farokhzad, O. C.; Margalit, R.; Langer, R. *Nat. Nanotechnol.* **2007**, *2*, 751–760.
(4) Matsumura, Y.; Maeda, H. *Cancer Res.* **1986**, *46*, 6387–6392.
(5) Gref, R.; Minamitake, Y.; Peracchia, M. T.; Trubetskoy, V.; Torchilin, V.; Langer, R. *Science* **1994**, *263*, 1600–1603.
(6) Gref, R.; Domb, A.; Quellec, P.; Blunk, T.; Mueller, R. H.; Verbavatz, J. M.; Langer, R. *Adv. Drug Delivery Rev.* **1995**, *16*, 215–233.
(7) Edwards, D. A.; Hanes, J.; Caponetti, G.; Hrkach, J.; Ben-Jebria, A.; Eskew, M. L.; Mintzes, J.; Deaver, D.; Lotan, N.; Langer, R. *Science* **1997**, *276*, 1868–1871.
(8) Langer, R. *Nature (London)* **1998**, *392*, 5–10.
(9) Mammen, M.; Chio, S.-K.; Whitesides, G. M. *Angew. Chem., Int. Ed.* **1998**, *37*, 2755–2794.
(10) Qiu, L. Y.; Bae, Y. H. *Pharm. Res.* **2006**, *23*, 1–30.
(11) Fox, M. E.; Szoka, F. C.; Frechet, J. M. J. *Acc. Chem. Res.* **2009**, *42*, 1141–1151.
(12) Chen, B.; Jerger, K.; Frechet, J. M. J.; Szoka, F. C. *J. Controlled Release* **2009**, *140*, 203–209.
(13) Grayson, S. M.; Godbey, W. T. *J. Drug Targeting* **2008**, *16*, 329–356.
(14) Duncan, R. *Nat. Rev. Drug Discovery* **2003**, *2*, 347–360.
(15) Bartlett, D. W.; Su, H.; Hildebrandt, I. J.; Weber, W. A.; Davis, M. E. *Proc. Natl. Acad. Sci. U.S.A.* **2007**, *104*, 15549–15554.
(16) Wu, P.; Malkoch, M.; Hunt, J. N.; Vestberg, R.; Kaltgrad, E.; Finn, M. G.; Fokin, V. V.; Sharpless, K. B.; Hawker, C. J. *Chem. Commun.* **2005**, 5775–5777.
(17) Ihre, H. R.; Padilla De Jesus, O. L.; Szoka, F. C., Jr.; Frechet, J. M. J. *Bioconj. Chem.* **2002**, *13*, 443–452.
(18) Breitenkamp, K.; Emrick, T. *J. Am. Chem. Soc.* **2003**, *125*, 12070–12071.
(19) Becker, M. L.; Remsen, E. E.; Pan, D.; Wooley, K. L. *Bioconj. Chem.* **2004**, *15*, 699–709.
(20) Such, G. K.; Tjipto, E.; Postma, A.; Johnston, A. P. R.; Caruso, F. *Nano Lett.* **2007**, *7*, 1706–1710.
(21) Cengelli, F.; Grzyb, J. A.; Montoro, A.; Hofmann, H.; Hanessian, S.; Juillerat-Jeanneret, L. *ChemMedChem* **2009**, *4*, 988–997.
(22) Tong, G. J.; Hsiao, S. C.; Carrico, Z. M.; Francis, M. B. *J. Am. Chem. Soc.* **2009**, *131*, 11174–11178.
(23) Lee, S.-M.; Chen, H.; O'Halloran, T. V.; Nguyen, S. T. *J. Am. Chem. Soc.* **2009**, *131*, 9311–9320.

The most widely studied branched macromolecules for drug delivery are dendrimers; their nanoscale, monodisperse, multivalent structures provide functional handles for elaboration with bioactive groups of interest.[26−28] One factor that limits widespread application of dendrimers is synthetic difficulty. Though recent synthetic advances are impressive,[16,29−32] it remains a challenge to prepare functionally diverse dendrimers of variable sizes. To overcome this challenge, researchers have appended linear polymers to dendrimers[33−36] or prepared linear polymers with dendritic fragments attached to their side chains. The latter "dendronized linear polymers" have attracted attention as nanoscopic building blocks; their cylindrical shapes can provide important advantages in nanoscale fabrication when compared to spherical dendrimers.[37−43] Similar nanoscale structures can be formed from bottle-brush-polymers that carry long chains grafted at high density to linear polymer backbones.[44−63] Bottle-brush polymers are prepared by graft-to, graft-from, or graft-through methodologies. The graft-to strategy requires an efficient coupling reaction to attach a functional molecule to every monomer unit of a linear polymer; "click"[64] reactions such as the copper-catalyzed azide−alkyne cycloaddition[65,66] (CuAAC) and thiol−ene coupling have proven useful in this regard.[43,46,67−70] Graft-from and graft-through methodologies require highly efficient polymerization reactions capable of initiation and propagation in sterically demanding environments.[48,51−53,71] Recent developments in efficient, controlled polymerization coupled with new click reactions provide materials chemists with the tools to generate novel functional nanoscopic materials.[72−77]

Ring-opening metathesis polymerization (ROMP) of strained alkene- (e.g., norbornene)-terminated macromonomers (MM) initiated by ruthenium *N*-heterocyclic carbene complexes (e.g., **1**, Figure 1) has recently proven useful for graft-through synthesis of functional bottle-brush polymers;[50,78−83] fast initiation leads to low polydispersities (PDIs) while release of ring

(24) Lee, J.-S.; Green, J. J.; Love, K. T.; Sunshine, J.; Langer, R.; Anderson, D. G. *Nano Lett.* **2009**, *9*, 2402–2406.
(25) Shen, Y.; Jin, E.; Zhang, B.; Murphy, C. J.; Sui, M.; Zhao, J.; Wang, J.; Tang, J.; Fan, M.; Van Kirk, E.; Murdoch, W. J. *J. Am. Chem. Soc.* **2010**, *132*, 4259–4265.
(26) Helms, B.; Meijer, E. W. *Science* **2006**, *313*, 929–930.
(27) Tomalia, D. A.; Baker, H.; Dewald, J.; Hall, M.; Kallos, G.; Martin, S.; Roeck, J.; Ryder, J.; Smith, P. *Polym. J.* **1985**, *17*, 117–132.
(28) Bosman, A. W.; Janssen, H. M.; Meijer, E. W. *Chem. Rev.* **1999**, *99*, 1665–1688.
(29) Montanez, M. I.; Campos, L. M.; Antoni, P.; Hed, Y.; Walter, M. V.; Krull, B. T.; Khan, A.; Hult, A.; Hawker, C. J.; Malkoch, M. *Macromolecules* **2010**, *43*, 6004–6013.
(30) Antoni, P.; Robb, M. J.; Campos, L.; Montanez, M.; Hult, A.; Malmstrom, E.; Malkoch, M.; Hawker, C. J. *Macromolecules* **2010**, *43*, 6625–6631.
(31) Killops, K. L.; Campos, L. M.; Hawker, C. J. *J. Am. Chem. Soc.* **2008**, *130*, 5062–5064.
(32) Wu, P.; Feldman, A. K.; Nugent, A. K.; Hawker, C. J.; Scheel, A.; Voit, B.; Pyun, J.; Frechet, J. M. J.; Sharpless, K. B.; Fokin, V. V. *Angew. Chem., Int. Ed.* **2004**, *43*, 3928–3932.
(33) Lee, C. C.; Gillies, E. R.; Fox, M. E.; Guillaudeu, S. J.; Frechet, J. M. J.; Dy, E. E.; Szoka, F. C. *Proc. Natl. Acad. Sci. U.S.A.* **2006**, *103*, 16649–16654.
(34) Gillies, E. R.; Dy, E.; Frechet, J. M. J.; Szoka, F. C. *Mol. Pharm.* **2005**, *2*, 129–138.
(35) Gillies, E. R.; Frechet, J. M. J. *J. Org. Chem.* **2004**, *69*, 46–53.
(36) Gillies, E. R.; Frechet, J. M. J. *J. Am. Chem. Soc.* **2002**, *124*, 14137–14146.
(37) Grayson, S. M.; Frechet, J. M. J. *Macromolecules* **2001**, *34*, 6542–6544.
(38) Boydston, A. J.; Holcombe, T. W.; Unruh, D. A.; Frechet, J. M. J.; Grubbs, R. H. *J. Am. Chem. Soc.* **2009**, *131*, 5388–5389.
(39) Zhang, A.; Zhang, B.; Waechtersbach, E.; Schmidt, M.; Schlueter, A. D. *Chem.−Eur. J.* **2003**, *9*, 6083–6092.
(40) Lee, C. C.; Grayson, S. M.; Frechet, J. M. J. *J. Polym. Sci., Part A: Polym. Chem.* **2004**, *42*, 3563–3578.
(41) Yoshida, M.; Fresco, Z. M.; Ohnishi, S.; Frechet, J. M. J. *Macromolecules* **2005**, *38*, 334–344.
(42) Canilho, N.; Kaseemi, E.; Mezzenga, R.; Schlueter, A. D. *J. Am. Chem. Soc.* **2006**, *128*, 13998–13999.
(43) Helms, B.; Mynar, J. L.; Hawker, C. J.; Frechet, J. M. J. *J. Am. Chem. Soc.* **2004**, *126*, 15020–15021.
(44) Zhang, M.; Mueller, A. H. E. *J. Polym. Sci., Part A: Polym. Chem.* **2005**, *43*, 3461–3481.
(45) Jiang, X.; Lok, M. C.; Hennink, W. E. *Bioconj. Chem.* **2007**, *18*, 2077–2084.
(46) Tsarevsky, N. V.; Bencherif, S. A.; Matyjaszewski, K. *Macromolecules* **2007**, *40*, 4439–4445.
(47) Lutz, J.-F.; Boerner, H. G.; Weichenhan, K. *Macromolecules* **2006**, *39*, 6376–6383.
(48) Allen, M. J.; Wangkanont, K.; Raines, R. T.; Kiessling, L. L. *Macromolecules* **2009**, *42*, 4023–4027.
(49) Cheng, G.; Boeker, A.; Zhang, M.; Krausch, G.; Mueller, A. H. E. *Macromolecules* **2001**, *34*, 6883–6888.
(50) Lu, H.; Wang, J.; Lin, Y.; Cheng, J. *J. Am. Chem. Soc.* **2009**, *131*, 13582–13583.
(51) Morandi, G.; Pascual, S.; Montembault, V.; Legoupy, S.; Delorme, N.; Fontaine, L. *Macromolecules* **2009**, *42*, 6927–6931.
(52) Neugebauer, D.; Sumerlin, B. S.; Matyjaszewski, K.; Goodhart, B.; Sheiko, S. S. *Polymer* **2004**, *45*, 8173–8179.
(53) Sumerlin, B. S.; Neugebauer, D.; Matyjaszewski, K. *Macromolecules* **2005**, *38*, 702–708.
(54) Gao, H.; Matyjaszewski, K. *J. Am. Chem. Soc.* **2007**, *129*, 6633–6639.
(55) Hadjichristidis, N.; Pitsikalis, M.; Iatrou, H.; Pispas, S. *Macromol. Rapid Commun.* **2003**, *24*, 979–1013.
(56) Tsukahara, Y.; Mizuno, K.; Segawa, A.; Yamashita, Y. *Macromolecules* **1989**, *22*, 1546–1552.
(57) Tsukahara, Y.; Tsutsumi, K.; Yamashita, Y.; Shimada, S. *Macromolecules* **1990**, *23*, 5201–5208.
(58) Dziezok, P.; Sheiko, S. S.; Fischer, K.; Schmidt, M.; Moller, M. *Angew. Chem., Int. Ed.* **1998**, *36*, 2812–2815.
(59) Neiser, M. W.; Okuda, J.; Schmidt, M. *Macromolecules* **2003**, *36*, 5437–5439.
(60) Neiser, M. W.; Muth, S.; Kolb, U.; Harris, J. R.; Okuda, J.; Schmidt, M. *Angew. Chem., Int. Ed.* **2004**, *43*, 3192–3195.
(61) Yuan, Y.-Y.; Du, Q.; Wang, Y.-C.; Wang, J. *Macromolecules* **2010**, *43*, 1739–1746.
(62) Li, C.; Ge, Z.; Fang, J.; Liu, S. *Macromolecules* **2009**, *42*, 2916–2924.
(63) Li, A.; Lu, Z.; Zhou, Q.; Qiu, F.; Yang, Y. *J. Polym. Sci., Part A: Polym. Chem.* **2006**, *44*, 3942–3946.
(64) Kolb, H. C.; Finn, M. G.; Sharpless, K. B. *Angew. Chem., Int. Ed.* **2001**, *40*, 2004–2021.
(65) Tornoe, C. W.; Christensen, C.; Meldal, M. *J. Org. Chem.* **2002**, *67*, 3057–3064.
(66) Rostovtsev, V. V.; Green, L. G.; Fokin, V. V.; Sharpless, K. B. *Angew. Chem., Int. Ed.* **2002**, *41*, 2596–2599.
(67) Sumerlin, B. S.; Tsarevsky, N. V.; Louche, G.; Lee, R. Y.; Matyjaszewski, K. *Macromolecules* **2005**, *38*, 7540–7545.
(68) Gao, H.; Matyjaszewski, K. *J. Am. Chem. Soc.* **2007**, *129*, 6633–6639.
(69) Tsarevsky, N. V.; Bernaerts, K. V.; Dufour, B.; Du Prez, F. E.; Matyjaszewski, K. *Macromolecules* **2004**, *37*, 9308–9313.
(70) Campos, L. M.; Killops, K. L.; Sakai, R.; Paulusse, J. M. J.; Damiron, D.; Drockenmuller, E.; Messmore, B. W.; Hawker, C. J. *Macromolecules* **2008**, *41*, 7063–7070.
(71) Boerner, H. G.; Beers, K.; Matyjaszewski, K.; Sheiko, S. S.; Moeller, M. *Macromolecules* **2001**, *34*, 4375–4383.
(72) Golas, P. L.; Matyjaszewski, K. *Chem. Soc. Rev.* **2010**, *39*, 1338–1354.
(73) Iha, R. K.; Wooley, K. L.; Nystrom, A. M.; Burke, D. J.; Kade, M. J.; Hawker, C. J. *Chem. Rev.* **2009**, *109*, 5620–5686.
(74) Hawker, C. J.; Wooley, K. L. *Science* **2005**, *309*, 1200–1205.
(75) Johnson, J. A.; Finn, M. G.; Koberstein, J. T.; Turro, N. J. *Macromol. Rapid Commun.* **2008**, *29*, 1052–1072.
(76) Binder, W. H.; Sachsenhofer, R. *Macromol. Rapid Commun.* **2007**, *28*, 15–54.
(77) Hawker, C. J.; Fokin, V. V.; Finn, M. G.; Sharpless, K. B. *Aust. J. Chem.* **2007**, *60*, 381–383.
(78) Xia, Y.; Kornfield, J. A.; Grubbs, R. H. *Macromolecules* **2009**, *42*, 3761–3766.
(79) Xia, Y.; Olsen, B. D.; Kornfield, J. A.; Grubbs, R. H. *J. Am. Chem. Soc.* **2009**, *131*, 18525–18532.

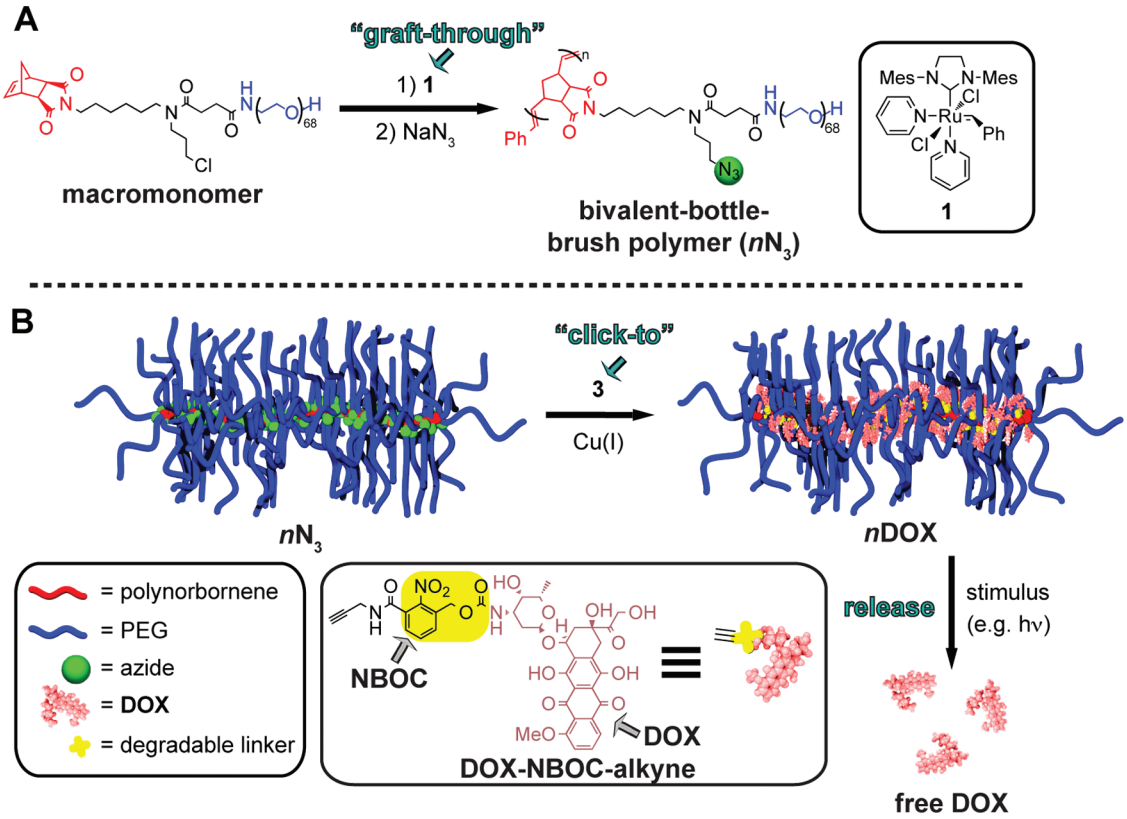

Figure 1. Schematic depiction of the "graft-through and click-to" approach described in this work. **A**: We start with a bivalent macromonomer (**2**) and perform "graft-through" ROMP with catalyst **1** followed by in situ chloride-azide exchange. **B**: The resulting azido-bivalent-brush polymer is then functionalized with an alkyne by click chemistry in a "click-to" step. If the alkyne partner is a drug molecule linked via a cleavable linker, then the resulting brush polymer can release the drug in response to an external stimulus. In this work, we demonstrate controlled release of the anticancer agent doxorubicin (**DOX**) in response to 365 nm UV light.

strain provides the driving force for high conversion in these systems. Although catalyst **1** is incompatible with azides and alkynes, its functional group tolerance enables use of monomers bearing azide and alkyne precursors that are easily converted to the requisite click groups after polymerization. Binder and co-workers used ROMP combined with CuAAC to append various small molecules to clickable linear polymers.[84,85] We have used ROMP in conjunction with CuAAC to generate cyclic polymers by end-to-end coupling.[86] To our knowledge, there are no examples of water-soluble brush polymers prepared by graft-through ROMP that are subsequently functionalized via click reactions. Such a strategy combines the benefits of ROMP for graft-through brush polymer synthesis with the modularity and efficiency of CuAAC for clicking-to; branched nanoscopic polymers with easily addressable functional groups can be rapidly prepared over a wide range of sizes simply by altering the ratio of catalyst to MM.

In this report, we demonstrate the sequential combination of graft-through- and click-to synthetic strategies to generate a clickable polyethylene glycol (PEG)-azide branched polymer material: a bivalent-bottle-brush polymer (Figure 1). Graft-through ROMP of a PEG-chloride macromonomer (Figure 1, Scheme 1, **6**) gave bivalent-brush polymers of varying nanoscopic sizes. These materials resemble first-generation dendronized polymers with branch points located near the linear polymer backbone (Figure 1); attached on one side of the branch point is a linear polymer and on the other side a small molecule (e.g., a drug). This design incorporates a water-soluble PEG domain that extends into solvent and a hydrophobic alkyl chloride near the core. We hypothesize that PEG attachment to one branch of these bivalent-brush polymers will confer the biocompatibility widely observed for PEGylated systems.[6,87] Core-functionalized nanomaterials have been elaborated with functional small molecules by click chemistry;[88−92] in this work, we convert the core alkyl chlorides to azides by treatment with sodium azide. Then, we utilize CuAAC to couple doxorubicin (**DOX**), to the core via a photocleavable nitrobenzyloxylcarbonyl (NBOC) linker. The latter enables controlled release of free **DOX** in response to long-wavelength (~365 nm) ultraviolet

(80) Li, Z.; Ma, J.; Cheng, C.; Zhang, K.; Wooley, K. L. *Macromolecules* **2010**, *43*, 1182–1184.
(81) Li, Z.; Zhang, K.; Ma, J.; Cheng, C.; Wooley, K. L. *J. Polym. Sci., Part A: Polym. Chem.* **2009**, *47*, 5557–5563.
(82) Conrad, R. M.; Grubbs, R. H. *Angew. Chem., Int. Ed.* **2009**, *48*, 8328–8330.
(83) Le, D.; Montembault, V.; Soutif, J. C.; Rutnakornpituk, M.; Fontaine, L. *Macromolecules* **2010**, *43*, 5611–5617.
(84) Binder, W. H.; Kluger, C. *Macromolecules* **2004**, *37*, 9321–9330.
(85) Binder, W. H.; Kluger, C.; Josipovic, M.; Straif, C. J.; Friedbacher, G. *Macromolecules* **2006**, *39*, 8092–8101.
(86) Clark, P. G.; Guidry, E. N.; Chan, W. Y.; Steinmetz, W. E.; Grubbs, R. H. *J. Am. Chem. Soc.* **2010**, *132*, 3405–3412.
(87) Otsuka, H.; Nagasaki, Y.; Kataoka, K. *Adv. Drug Delivery Rev.* **2003**, *55*, 403–419.
(88) O'Reilly, R. K.; Joralemon, M. J.; Hawker, C. J.; Wooley, K. L. *New J. Chem.* **2007**, *31*, 718–724.
(89) O'Reilly, R. K.; Joralemon, M. J.; Hawker, C. J.; Wooley, K. L. *Chem.—Eur. J.* **2006**, *12*, 6776–6786.
(90) O'Reilly, R. K.; Joralemon, M. J.; Wooley, K. L.; Hawker, C. J. *Chem. Mater.* **2005**, *17*, 5976–5988.
(91) Joralemon, M. J.; O'Reilly, R. K.; Hawker, C. J.; Wooley, K. L. *J. Am. Chem. Soc.* **2005**, *127*, 16892–16899.
(92) Prasuhn, D. E., Jr.; Singh, P.; Strable, E.; Brown, S.; Manchester, M.; Finn, M. G. *J. Am. Chem. Soc.* **2008**, *130*, 1328–1334.

Scheme 1. Synthesis of PEG-Norbornene-Chloride MM **6**

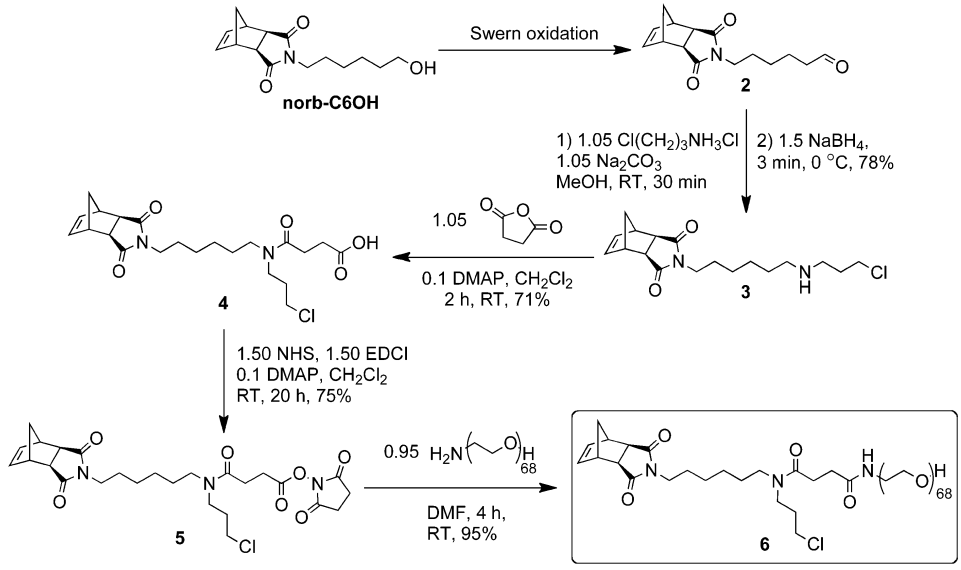

(UV) light; we demonstrate that released **DOX** is therapeutically active against human cancer cells in culture.

Results and Discussion

Synthesis of MM 6. Clickable bivalent PEG brush polymers can be generated from an MM containing a strained norbornene derivative for ROMP, a PEG chain, and a functional group suitable for CuAAC (Figure 1, Scheme 1). Since neither azides nor alkynes are compatible with catalyst **1**, we designed MM **6** to carry an alkyl chloride for facile conversion to an azide in a post-ROMP modification step. We incorporated a 6-carbon spacer between the strained norbornene moiety and the tertiary amide branch point to reduce steric hindrance between the growing polymer chain end and the branched side-chains. This spacer may also facilitate subsequent side chain modification reactions, such as chloride to azide conversion and CuAAC. MM **6** was obtained in five steps from *exo-N*-(6-hydroxyhexyl)-5-norbornene-2,3-dicarboximide (**norb-C6OH**, Scheme 1). The synthesis commenced with Swern oxidation of **norb-C6OH** to give aldehyde **2**. Reductive amination using **2** and 3-chloropropylamine hydrochloride gave secondary amine **3**, which was readily converted to acid **4** by treatment with succinic anhydride. Reaction of **4** with *N*-hydroxysuccinimide (NHS) in the presence of *N*-(3-dimethylaminopropyl)-*N*′-ethylcarbodiimide hydrochloride (EDC) and catalytic 4-(dimethylamino)pyridine (DMAP) gave NHS ester **5**. We have prepared **5** on a multigram scale and expect it to be useful for the preparation of a variety of multifunctional ROMP monomers. In this work, commercially available 3 kDa PEG-NH_2 was treated with a slight excess of **5** to give MM **6**. Excess **5** was used to ensure complete conversion of every PEG-amine to amide **6**; the only polymeric species in the final reaction mixture was **6** and it was easily purified via repeated precipitation in diethyl ether. The ^{1}H NMR, ^{13}C NMR, and MALDI spectra for MM **6** are provided in the Supporting Information.

Graft-Through ROMP of 6 and Halide-Azide Exchange to Generate nN_3 Bivalent-Brush Polymers. We pursued a one-pot synthetic strategy to rapidly generate a library of azide-functional brush polymers (***n*N$_3$**) with variable number-average degrees of polymerization (DP) and hydrodynamic radii. A strength of this approach is the ease of generating branched functional materials of variable sizes rapidly and efficiently; each of the polymers described here was prepared by adding an aliquot of catalyst **1** to a vial containing MM **6**, allowing 60 min for ROMP to proceed, quenching the polymerization by addition of ethyl vinyl ether, solvent exchange, and finally treatment with sodium azide (Scheme 2). The first several steps were performed within a few hours, whereas the final step, attaching azides to the polymer side chains, was left for 48 h to ensure high conversion.

Scheme 2. Synthesis of Azido-Bivalent-Brush Polymers (***n*N$_3$**) by ROMP and Chloride-Azide Exchange

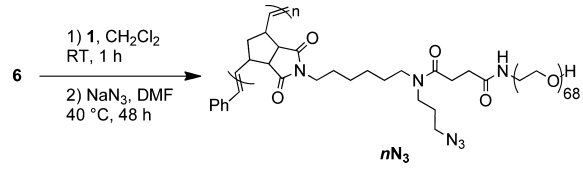

Table 1. Characterization of **nN_3** Bivalent Brush Polymers by GPC (room temp., 0.2 M LiBr in DMF, 1 mL/min) and DLS (aqueous)

n (theo.)[a]	DP[b]	M_n (GPC, kDa)	PDI	R_h[c]/nm
10	10	34.1	1.11	3.1 (0.3)
30	32	109	1.04	6.3 (0.8)
50	53	180	1.07	6.9 (0.9)
70	70	238	1.14	7.3 (0.3)
80	80	272	1.14	7.5 (0.8)
100	101	343	1.06	11 (1)
300	295	1,000	1.11	15 (1)
400	575	1,960	1.27	25 (2)

[a] Ratio of MM to catalyst (i.e., theoretical DP). This number is used to identify **nN_3** and **nDOX** samples throughout the text. [b] DP observed derived from M_n(GPC)/M_n(MM). [c] Hydrodynamic radii measured by dynamic light scattering (DLS). DLS correlation functions were fit using the CONTIN algorithm.

The polymer characterization data in Table 1 demonstrate that ROMP of **6** is well-controlled up to the highest DP tested; a small amount of catalyst deactivation and/or experimental error may explain the larger-than-expected DP for the **400N_3** samples. In general, polymers with low polydispersities and molecular weights defined by the ratio of **6**:**1** were obtained. The GPC traces for all samples (Figure 2A) show monomodal molecular weight distributions and very high (>95%) MM conversions. All of the polymers were highly soluble (>100 mg/mL) in water;

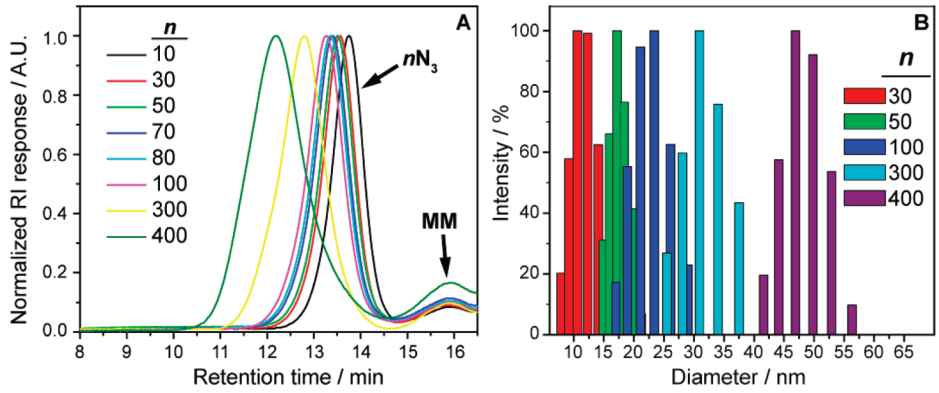

Figure 2. **A**: Representative GPC traces for $n\mathbf{N_3}$ bivalent-brush polymer samples show monomodal molecular weight distributions, low polydispersities, and high conversions. **B**: Hydrodynamic diameter histograms for selected $n\mathbf{N_3}$ polymers obtained from DLS measurements using the CONTIN fitting algorithm. The particle sizes increase with increasing DP and are varied over a wide range by adjusting the ratio of MM to catalyst (**6**:**1**) before graft-through ROMP.

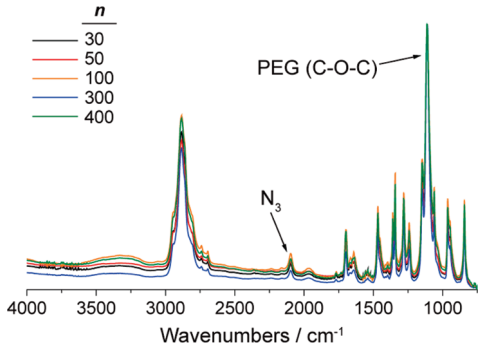

Figure 3. FTIR spectra of $n\mathbf{N_3}$ bivalent-brush polymers normalized to the strong PEG ether (C−O−C) antisymmetric stretch absorbance. The relative amount of azide is approximately the same for each ***n*** value which suggests that chloride-azide exchange is not sterically limited with increased DP.

aqueous DLS measurements (Table 1, Figure 2B) confirm that their nanoscopic dimensions increased with DP and were tunable over a broad range (radii from 3−25 nm) of relevant sizes for drug delivery applications. Furthermore, DLS (Figure 2B) shows that the particle size distributions are monomodal.

Graft-through ROMP ensures that every side chain unit possesses both a PEG chain and an alkyl chloride; the weight percentage of chloride is independent of DP. It follows that if every chloride is converted to an azide then the weight percentage of azide is also independent of DP. One may expect side chain modification reactions with bivalent-brush polymers to display DP-dependent conversion; perhaps increased DP would lead to lower reaction yields because of increased steric hindrance. We have found that for both chloride-azide exchange and CuAAC reactions there is no apparent difference in reaction yield across the DP values studied here. Figure 3 shows the FTIR spectra for a subset of $n\mathbf{N_3}$ polymers normalized to the PEG ether (C−O−C antisymmetric stretch) absorbance at ∼1100 cm^{-1}. The intensities of the characteristic azide antisymmetric stretch (∼2100 cm^{-1}) are the same for each DP, which suggests that the azide:PEG ratio is the same for each sample and that the chloride-azide exchange reaction occurred with equal efficiency for each DP value.

Click Chemistry Using DOX-NBOC-Alkyne 9. The ultimate application of these $n\mathbf{N_3}$ bivalent-brush polymers is defined by how they are decorated with functional groups. For drug delivery applications, one can imagine clicking a drug-alkyne derivative attached via a cleavable linker group (Figure 1). The resulting polymer would undergo controlled drug release in response to an external stimulus leaving the brush polymer scaffold intact. In this work, we designed **9** for controlled release of **DOX** in response to UV light after click coupling to the $n\mathbf{N_3}$ polymer scaffold (Scheme 3). Photoinitiated release from macromolecules provides a means for site-specific, controlled drug delivery and could potentially complement traditional phototherapeutic methods.[93−103] Though placement of azide groups near the core of these bivalent-brush polymers should allow PEG to extend into solution and increase the biocompatibility of these materials, a buried location may make them difficult to functionalize with subsequent reactions. Anticipating this challenge was one reason we chose two highly efficient reactions, halide-azide exchange and CuAAC, as the modification reactions; as described above, CuAAC has proven useful for quantitative attachment of small molecules to the side chains of ROMP polymers[84,85] and we expected that it would provide the best opportunity for high-yield coupling of sterically demanding alkyne reagents to bivalent-branch polymers. There are a variety of CuAAC conditions throughout the literature and the catalyst/ligand/solvent system depends on the application;[104−107] perhaps the most impressive applications of CuAAC are in the field of

(93) Dolmans, D. E. J. G. J.; Fukumura, D.; Jain, R. K. *Nat. Rev. Cancer* **2003**, *3*, 380–387.
(94) Bethea, D.; Fullmer, B.; Syed, S.; Seltzer, G.; Tiano, J.; Rischko, C.; Gillespie, L.; Brown, D.; Gasparro, F. P. *J. Dermatol. Sci.* **1999**, *19*, 78–88.
(95) Mal, N. K.; Fujiwara, M.; Tanaka, Y. *Nature* **2003**, *421*, 350–353.
(96) Skwarczynski, M.; Noguchi, M.; Hirota, S.; Sohma, Y.; Kimura, T.; Hayashi, Y.; Kiso, Y. *Bioorg. Med. Chem. Lett.* **2006**, *16*, 4492–4496.
(97) McCoy, C. P.; Rooney, C.; Edwards, C. R.; Jones, D. S.; Gorman, S. P. *J. Am. Chem. Soc.* **2007**, *129*, 9572–9573.
(98) Jiang, M. Y.; Dolphin, D. *J. Am. Chem. Soc.* **2008**, *130*, 4236–4237.
(99) Agasti, S. S.; Chompoosor, A.; You, C.-C.; Ghosh, P.; Kim, C. K.; Rotello, V. M. *J. Am. Chem. Soc.* **2009**, *131*, 5728–5729.
(100) Lee, H.-i.; Wu, W.; Oh, J. K.; Mueller, L.; Sherwood, G.; Peteanu, L.; Kowalewski, T.; Matyjaszewski, K. *Angew. Chem., Int. Ed.* **2007**, *46*, 2453–2457.
(101) Pastine, S. J.; Okawa, D.; Zettl, A.; Frechet, J. M. J. *J. Am. Chem. Soc.* **2009**, *131*, 13586–13587.
(102) Kim, H.-C.; Hartner, S.; Behe, M.; Behr Thomas, M.; Hampp Norbert, A. *J. Biomed. Opt.* **2006**, *11*, 34024.
(103) Haertner, S.; Kim, H.-C.; Hampp, N. *J. Polym. Sci., Part A: Polym. Chem.* **2007**, *45*, 2443–2452.
(104) Lewis, W. G.; Magallon, F. G.; Fokin, V. V.; Finn, M. G. *J. Am. Chem. Soc.* **2004**, *126*, 9152–9153.
(105) Rodionov, V. O.; Fokin, V. V.; Finn, M. G. *Angew. Chem., Int. Ed.* **2005**, *44*, 2210–2215.
(106) Rodionov, V. O.; Presolski, S. I.; Diaz, D. D.; Fokin, V. V.; Finn, M. G. *J. Am. Chem. Soc.* **2007**, *129*, 12705–12712.
(107) Rodionov, V. O.; Presolski, S. I.; Gardinier, S.; Lim, Y.-H.; Finn, M. G. *J. Am. Chem. Soc.* **2007**, *129*, 12696–12704.

Scheme 3. Synthesis of **DOX**-Nitrobenzyloxycarbonyl (NBOC)-Alkyne Derivative **9** for Click Chemistry and Photorelease of **DOX**

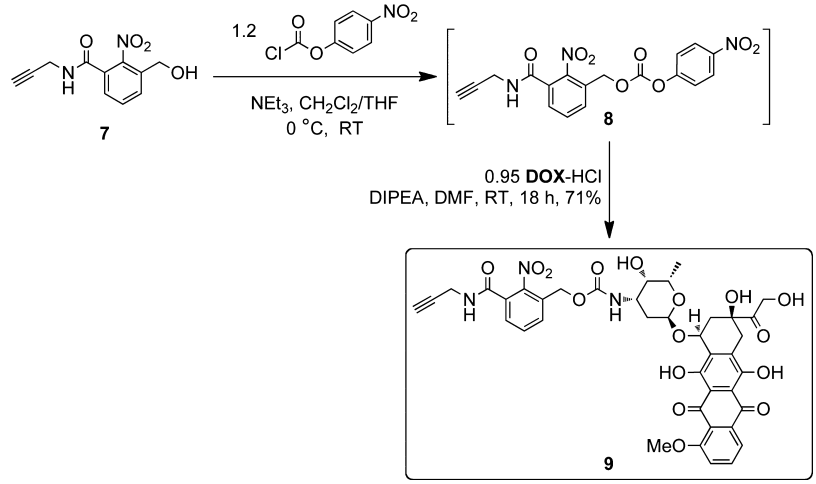

Scheme 4. CuAAC Coupling of **9** to ***n*N$_3$** Brush Using Tris(hydroxypropyltriazolylmethyl)amine (**THPTA**) Ligand, Copper(II) Sulfate, and Sodium Ascorbate As an in Situ Reductant

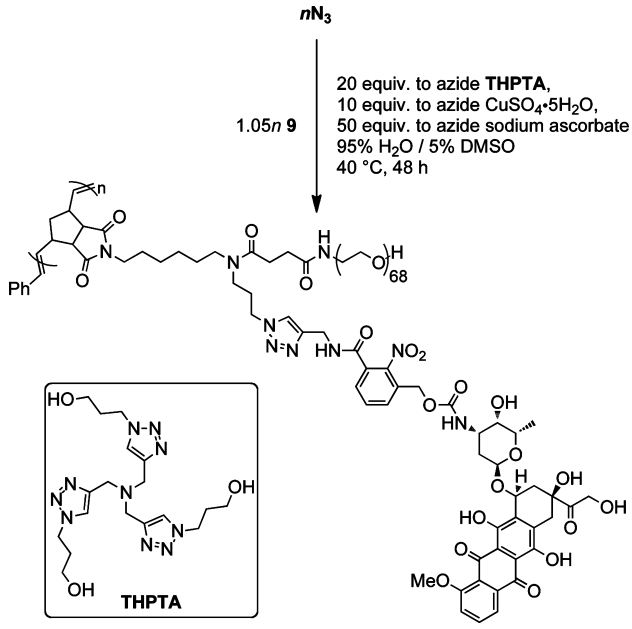

bioconjugation where the requisite azide and alkyne functional groups are present in very low concentration among a number of other reactive groups.[108−111] The Finn laboratory recently reported optimized CuAAC conditions for bioconjugation which utilize a new accelerating ligand THPTA (Scheme 4).[112] Aqueous CuAAC was found to proceed orders of magnitude faster with THPTA than in the absence of a ligand. Since these ***n*N$_3$** bivalent-brush polymers are nanoscopic, narrowly dispersed, water-soluble materials with buried functional groups, we envisioned CuAAC reactions to them as similar to bioconjugation reactions to proteins bearing multiple azide or alkyne groups. After initial attempts without accelerating ligand, which led to <20% conversion after several days, we were pleased to find that addition of THPTA to the reaction mixture gave quantitative conversions. In a typical reaction, the polymer, THPTA (20 equiv. to azide), and alkyne **9** (1.05 equiv. to azide) were dissolved in 95% H_2O/5% DMSO such that the concentration of alkyne **9** was 2 mM. Aqueous sodium ascorbate (1.0 M) was added followed by copper(II) sulfate (1.0 M); two more aliquots of aqueous copper sulfate and sodium ascorbate were added over 2 days such that their final amounts were 10 and 50 equiv., respectively, relative to azide. The reactions were performed at 40 °C to achieve the maximum rate possible without inducing potential azide-olefin cycloaddition side reactions.[84]

Figure 4A (inset) depicts the CuAAC coupling of **9** to **100N$_3$** as monitored by liquid-chromatography mass-spectrometry (LC-MS). Compound **9** eluted at ∼4.2 min while **DOX**-loaded polymer eluted from ∼3.5 - ∼4 min. The unique absorbance of **DOX** (∼500 nm) enables facile monitoring of the CuAAC reaction; the **100N$_3$** polymer does not absorb at 500 nm and therefore the growth of a new, broad polymer peak is attributed to CuAAC coupling of **9** to the polymer. The time-dependent LC-MS traces (Figure 4A, inset) show an increasing polymer absorbance at the expense of the alkyne **9** absorbance until a final, very high (>97%) conversion is reached. As for the case with chloride-azide exchange, one may expect the CuAAC reaction progress to depend on DP. Figure 4A shows preparatory high-performance liquid chromatography (prep-HPLC) 500 nm absorbance traces for several crude ***n*DOX** polymers; the total ratio of ***n*DOX**:**9** is the same for each DP which again suggests that DP has little effect on the efficiency of reactions to these structures. The retention times for the ***n*DOX** polymers increase slightly for each DP indicating that polymer-column interactions are dependent on DP. The pure polymer fractions were collected and either lyophilized to dryness or concentrated before use in subsequent experiments. Figure 4B shows the FTIR spectrum of purified **50DOX** compared to that of **50N$_3$**. The azide antisymmetric stretch at ∼2100 cm^{-1}, present in the spectrum of **50N$_3$**, is completely absent from the **50DOX** spectrum which suggests very high consumption of the azide group. Integration of the broad aromatic resonances in the ^{1}H NMR spectrum of **50DOX** compared to the PEG methylene groups is in close agreement to that expected for fully **DOX**-functionalized polymer (Figure S5). The final **DOX** weight percentage for the

(108) Ngo, J. T.; Champion, J. A.; Mahdavi, A.; Tanrikulu, I. C.; Beatty, K. E.; Connor, R. E.; Yoo, T. H.; Dieterich, D. C.; Schuman, E. M.; Tirrell, D. A. *Nat. Chem. Biol.* **2009**, *5*, 715–717.
(109) Dieterich, D. C.; Link, A. J.; Graumann, J.; Tirrell, D. A.; Schuman, E. M. *Proc. Natl. Acad. Sci. U.S.A.* **2006**, *103*, 9482–9487.
(110) Speers, A. E.; Cravatt, B. F. *Chem. Biol.* **2004**, *11*, 535–546.
(111) Prescher, J. A.; Bertozzi, C. R. *Nat. Chem. Biol.* **2005**, *1*, 13–21.
(112) Hong, V.; Presolski, S. I.; Ma, C.; Finn, M. G. *Angew. Chem., Int. Ed.* **2009**, *48*, 9879–9883.

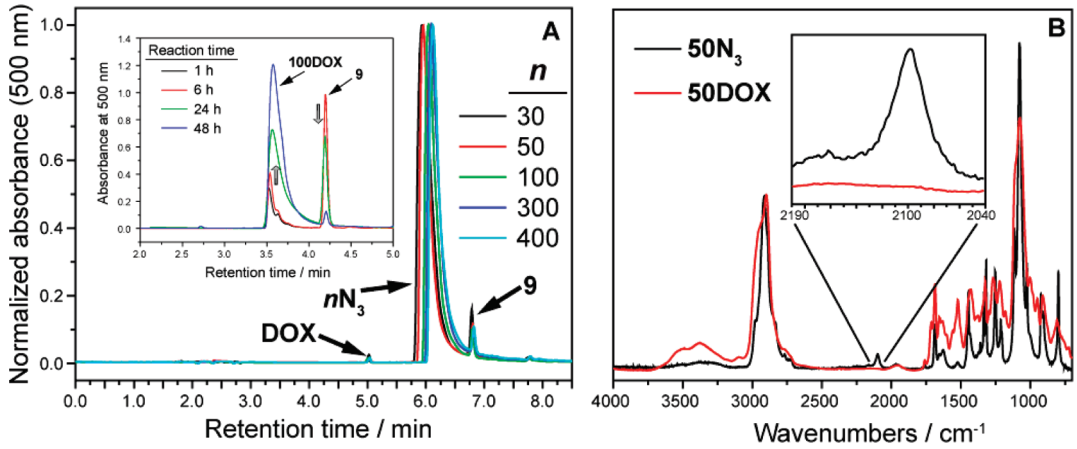

Figure 4. **A:** Prep-HPLC traces of crude CuAAC mixtures which depict similar conversion for each ***n*** value. **A (inset):** Progress of CuAAC coupling of **9** to **100N$_3$** monitored by LC-MS. **B:** FTIR spectra of **50N$_3$** and **50DOX** confirming complete loss of azide after CuAAC.

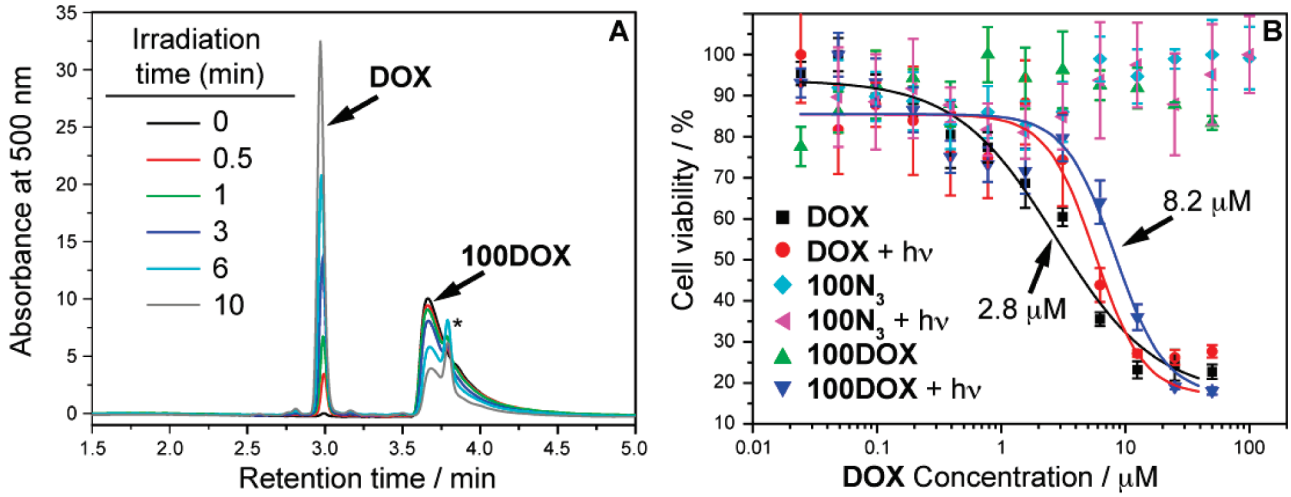

Figure 5. **A:** Time-dependent UV photolysis of **100DOX** monitored by LC−MS; after 10 min irradiation ∼70% of free **DOX** was released. A minor product (labeled "*", see Scheme 5) was also observed at longer irradiation times. **B:** Viability of MCF-7 human breast cancer cells treated with free **DOX**, **100N$_3$** bivalent-brush polymer, and drug-loaded **100DOX** polymer both with and without UV irradiation. Data points were fit to a sigmoidal function and the half-maximum inhibitory concentrations (IC_{50}) are shown for **DOX** and the photocleaved **100DOX**. The *x*-axis labels refer to the concentration of both free and polymer-conjugated drug.

functionalized polymers is 12.6%. As mentioned above, this value is independent of DP; it could be adjusted by varying the PEG length or the degree of branching in the MM precursor.

Photorelease of DOX and Cell Culture Studies. Having successfully coupled **9** to ***n*N$_3$** we next studied the release of free **DOX** from the brush polymer in response to UV light (∼365 nm). An aqueous solution of purified ***n*DOX** polymer was irradiated at 365 nm for a given time and subjected to LC−MS analysis. The progress of photorelease was monitored over 10 min by repeated irradiation and LC−MS; the data for **100DOX** are shown in Figure 5A. As irradiation time increased, we observed a new peak at ∼3 min that increased in intensity at the expense of the **100DOX** polymer peak. The new peak corresponds to the retention time and mass of free **DOX**. We also observed a small side product at ∼3.8 min with a mass of 569 Da (labeled "*" in Figure 5A), which is likely the result of intramolecular trapping of carbamic acid **10** to give cyclic carbamate **11** (Scheme 5). Nevertheless, the major product of UV photolysis was free **DOX**; the photolysis yield after 10 min irradiation was ∼70% for all ***n*DOX** polymers which led us to examine the effectiveness of these materials against human cancer cells in cell culture.

We performed cell viability experiments using MCF-7 human breast cancer cells. Cells were treated with aqueous solutions of either free **DOX** or the corresponding ***n*DOX** polymer at various concentrations and irradiated for 10 min using 365 nm light or kept in the dark. The cells were then incubated in the dark for 24 h, washed twice, and incubated for another 24 h in fresh, drug-free growth medium. Cell viability was assessed using the MTT assay (see Methods and Materials for details). Data for $n = 100$ polymers (**100N$_3$** and **100DOX**) are shown in Figure 5B (cell viability data for other ***n*** values is given in the Supporting Information). Free **DOX**, with and without UV irradiation, effectively killed the cells at 3−5 μM while azide polymer **100N$_3$** was nontoxic with and without light up to 100 μM; these data taken together suggest that under our conditions 10 min of 365 nm UV irradiation has no adverse affect on cell viability nor does it interrupt the cellular toxicity of **DOX**. None of the ***n*DOX** bivalent-brush polymers studied were toxic up to 50 μM in the absence of UV irradiation; irradiation for 10 min yielded IC_{50} values ∼7−10 μM which confirms that free **DOX** generated by photorelease is therapeutically active. The IC_{50} values were not DP-dependent. This observation suggests that the ***n*DOX** polymers remain in the extracellular environment

Scheme 5. Photolysis of ***n*DOX** Polymers Gives Carbamic Acid **10**[a]

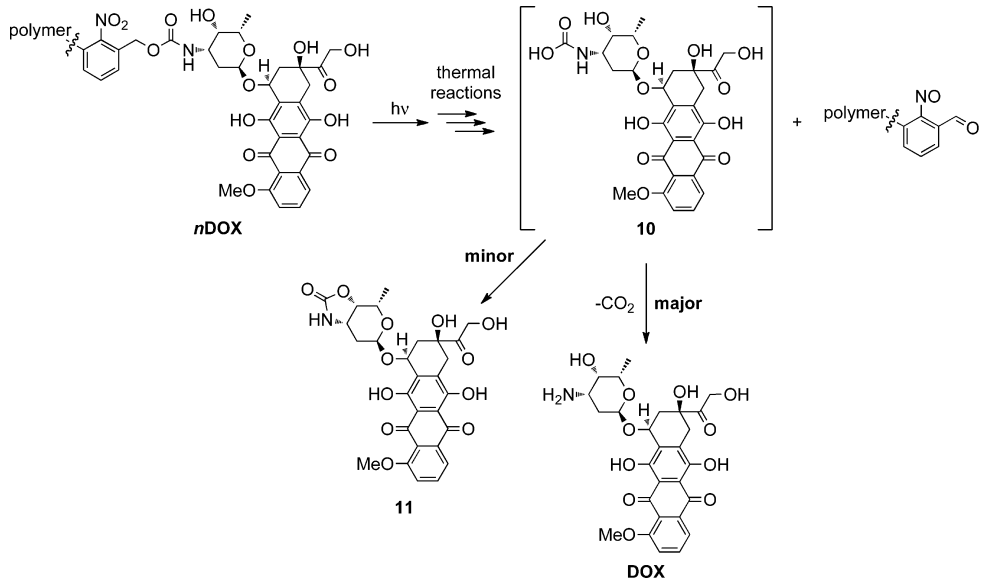

[a] Decarboxylation of **10** yields free **DOX** as the major product while intramolecular trapping provides **DOX**-carbamate derivative **11** as a minor product. Reactive nitrosobenzaldehyde photoproducts remain bound to the polymer core after photolysis.

and upon photolysis free **DOX** is released and diffuses into the cell nucleus where it induces apopotosis. Although in vitro experiments do not show DP-dependent cytotoxicity, we expect that DP will affect in vivo trafficking and thus the overall utility of these materials in drug delivery. Targeting groups could be appended to the periphery of these materials to promote trafficking into the cell.[113]

Conclusions

Here we have demonstrated the utility of a combined graft-through/click-to strategy for the synthesis of a new class of clickable, branched nanostructures: PEG-*branch*-azide bivalent-brush polymers. This approach makes use of the remarkable efficiency of ROMP for graft-through polymerization and the modular coupling power of click chemistry for polymer functionalization. A wide range of nanoscale sizes is accessible which will enable detailed structure/function correlation in biological settings. We are currently exploring applications for these materials in drug delivery. Design and synthesis of novel clickable linkers (e.g., longer wavelength-, pH-, and redox-cleavable), attachment of targeting moieties at the PEG periphery, incorporation of degradable units within the polymer backbone, and use of chain-transfer agents to append orthogonal groups selectively to the ends of these polymers are being studied. Furthermore, copolymerization of MMs like **6** with other monomers (such as a norbornene-alkyl halide small molecule) will provide access to new multiblock polymer structures with the potential for higher drug loadings.

Acknowledgment. We thank Dr. S. Virgil and Mr. S. Presolski for helpful advice. This work was supported by the National Institutes of Health (NIH, R01-GM31332), the Beckman Institute at Caltech (postdoctoral fellowship for J.A.J.), and the MRSEC program of the National Science Foundation (NSF) under Award No. DMR-0520565.

Supporting Information Available: Synthetic procedures, spectral data, liquid chromatography methods, and details of cell viability studies. This material is available free of charge via the Internet at http://pubs.acs.org.

JA108441D

(113) Kolonko, E. M.; Kiessling, L. L. *J. Am. Chem. Soc.* **2008**, *130*, 5626–5627.

Appendix II

Drug-Loaded, Bivalent-Bottle-Brush Polymers by Graft-through ROMP

10326 *Macromolecules* **2010**, *43*, 10326–10335
DOI: 10.1021/ma1021506

Macromolecules
ARTICLE

Drug-Loaded, Bivalent-Bottle-Brush Polymers by Graft-through ROMP

Jeremiah A. Johnson, Ying Y. Lu, Alan O. Burts, Yan Xia, Alec C. Durrell, David A. Tirrell,* and Robert H. Grubbs*

Division of Chemistry and Chemical Engineering, California Institute of Technology, 1200 E. California Boulevard, Pasadena, California 91125, United States

Received September 15, 2010; Revised Manuscript Received November 8, 2010

ABSTRACT: Graft-through ring-opening metathesis polymerization (ROMP) using ruthenium *N*-heterocyclic carbene catalysts has enabled the synthesis of bottle-brush polymers with unprecedented ease and control. Here we report the first bivalent-brush polymers; these materials were prepared by graft-through ROMP of drug-loaded poly(ethylene glycol) (PEG) based macromonomers (MMs). Anticancer drugs doxorubicin (**DOX**) and camptothecin (**CT**) were attached to a norbornene-alkyne-PEG MM via a photocleavable linker. ROMP of either or both drug-loaded MMs generated brush homo- and copolymers with low polydispersities and defined molecular weights. Release of free **DOX** and **CT** from these materials was initiated by exposure to 365 nm light. All of the **CT** and **DOX** polymers were at least 10-fold more toxic to human cancer cells after photoinitiated drug release while a copolymer carrying both **CT** and **DOX** displayed 30-fold increased toxicity upon irradiation. Graft-through ROMP of drug-loaded macromonomers provides a general method for the systematic study of structure−function relationships for stimuli-responsive polymers in biological systems.

Introduction

Recent advances in catalysis and polymer synthesis have allowed the preparation of new materials with unprecedented functional and structural diversity and blurred the line between small-molecule and polymer synthesis.[1,2] Ring-opening metathesis polymerization (ROMP) using fast-initiating ruthenium catalysts (e.g., **1**, Figure 1) is particularly suited for the synthesis of diverse side-chain functional polymers with controllable molecular weights (M_n) and low polydispersities (PDI).[3−6]

Discrete bottle-brush polymers (brush polymers) are typically comprised of a linear polymer backbone connected at each monomer unit to a polymeric side chain. Brush polymers with two polymer side-chains attached to each monomer unit of a polymer backbone (centipede-brushes) have been reported; these materials can possess disparate polymer domains within the same polymer structure.[7−9] Synthetic approaches to all types of brush polymers fall into "graft-to," "graft-from," or "graft-through" categories; each approach has advantages and disadvantages.[10] For example, graft-to and graft-from strategies, whereby linear polymers are coupled to the backbone of a linear polymer or are grown from the backbone of a linear macroinitiator respectively, are suited to most polymerization methods but suffer from sterically limited grafting densities for even the most efficient coupling and polymerization reactions.[11−20] The alternative graft-through approach, which involves polymerization of well-defined monofunctional macromonomers (MMs), ensures quantitative grafting density but requires a polymerization method capable of propagation under conditions of very low monomer concentration and high steric hindrance.[21−26] Thus, most brush polymers made by graft-through approaches have significant amounts of MM impurities due to incomplete conversion; few examples of functional systems of high degree of polymerization (DP_n) have been reported.[27,28]

Recently, our group and others have shown the utility of ROMP using catalyst **1** for the graft-through polymerization of a variety of norbornene-terminated MMs to yield brush homo- and copolymers that have high DP_ns and low PDIs.[27−31] These studies have set a benchmark for efficiency in brush polymer synthesis and led us to explore the application of graft-through ROMP to the synthesis of novel bivalent-brush polymers (Figure 1) with one branch comprised of a hydrophilic solubilizing polymer and the other a drug molecule covalently attached through a degradable linker. Brush polymers and other branched polymeric architectures (dendrimers, hyperbranched polymers, dendronized polymers, etc.) possess features, such as multivalency and nanoscopic size, which make them attractive for *in vivo* drug delivery applications.[32−34] Branched structures of sufficient size display extended *in vivo* circulation times in comparison to their linear analogues−an advantageous feature for passive tumor targeting via the enhanced permeation and retention effect (EPR effect).[35,36] Dendrimers are the most extensively studied branched polymers in this regard; their monodisperse, globular structures resemble those of proteins and render them attractive for biological applications.[37,38] Despite the promise of dendrimers, synthetic challenges limit their utility in therapeutic applications. It is difficult to prepare dendrimers larger than ∼10 nm due to the steric hindrance which must be overcome when functionalizing the periphery of a high-generation dendritic structure. To overcome this limitation, the Fréchet group has appended linear poly(ethylene glycol) (PEG) chains to dendrimers to increase their size, water solubility, and biocompatibility while retaining their inherent multivalency.[39−41] These "PEGylated" dendrimers have proven remarkably effective for treatment of cancer in mice via controlled delivery of doxorubicin (**DOX**)[39] and camptothecin (**CT**).[41] Though large polymers may be preferable in certain applications, several reports suggest that non-degradable polymers for drug delivery applications must be no larger than ∼10 nm to ensure complete renal clearance.[35,42] A synthetic approach capable of rapidly generating branched polymeric structures of easily variable sizes is highly desirable.

Here we introduce a new bivalent-brush polymer structure for use in chemotherapy delivery. Figure 1 depicts a schematic of our

*Corresponding authors.

 Published on Web 12/02/2010

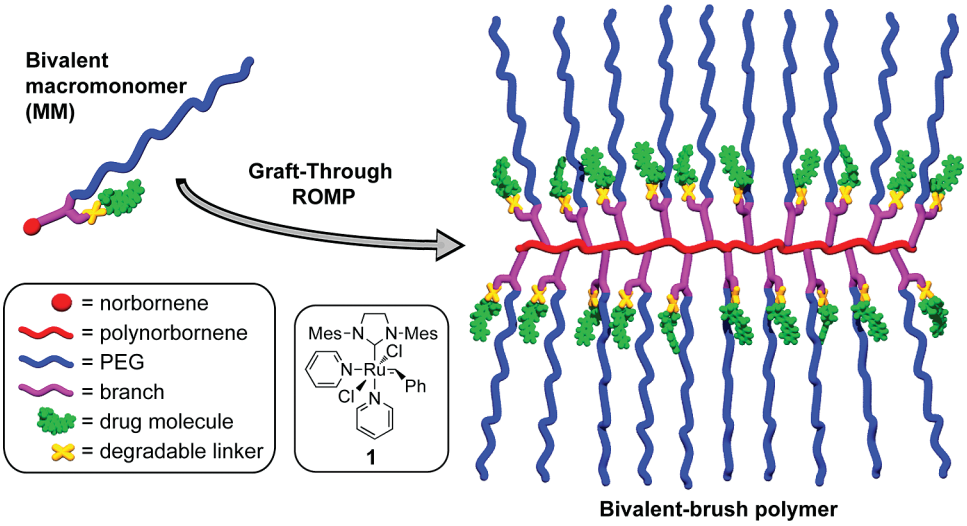

Figure 1. Schematic depiction of bivalent macromonomer (MM) and bivalent-brush polymer described in this work. Mes = mesityl.

design; a water-soluble PEG side chain and a drug molecule are attached to a polynorbornene backbone via a branch point. The drug is attached via a degradable linker that allows controlled release in response to an appropriate stimulus. We expect the PEG chains to extend into solution effectively shielding the hydrophobic drug + polynorbornene core; the structure resembles that of a unimolecular micelle. We reasoned that these bivalent-brush polymers might exhibit similar drug-delivery attributes when compared to PEGylated dendrimers but may be easier to synthesize, especially over a wide range of nanoscale sizes and with greater functional diversity, using graft-through ROMP of a PEGylated-norbornene MM. Here we demonstrate the power of this approach for the preparation of water-soluble polynorbornene-*g*-PEG brush polymers and copolymers that have **DOX** and **CT** covalently bound near the core through a photocleavable linker. Brief ultraviolet (UV, 365 nm) irradiation of these brush polymers releases the respective drug molecules in unmodified form; we demonstrate the utility of these systems for photoregulated chemotherapy delivery in human cancer cell culture.

Materials and Methods

All reagents and solvents were purchased from Aldrich or VWR chemical companies and were used as supplied unless otherwise noted. Ruthenium catalyst **1**,[43] 3-azidopropyl-1-amine (note: care must be taken when working with small-molecule, < 6 carbons per azide, azides. In this work, 3-azidopropyl-1-amine is used as a ~1 M solution in toluene and never isolated),[44] and 3-(*tert*-butyldimethylsilyloxymethyl)-2-nitrobenzoic acid **8**[45] were prepared according to literature procedures. Degassed dichloromethane (DCM), tetrahydrofuran (THF), and dimethyl sulfoxide (DMSO) solvents were passed through solvent purification columns prior to use.[46] Doxorubicin hydrochloride (**DOX**-HCl) was purchased from Axxora LLC.

Gel permeation chromatography (GPC) was performed using two I-series Mixed Bed Low MW ViscoGel columns (Viscotek) connected in series with a DAWN EOS multiangle laser light scattering (MALLS) detector (Wyatt Technology) and an Optilab DSP differential refractometer (Wyatt Technology). Experiments were performed at room temperature using 0.2 M LiBr in *N*,*N*-dimethylformamide (DMF) eluant at a flow rate of 1 mL/min. Molecular weights were calculated from *dn*/*dc* values that were obtained assuming 100% mass elution from the columns. Dynamic light scattering (DLS) measurements were made at room temperature using a Brookhaven ZetaPALS DLS instrument. Samples were dissolved in nanopure water at a concentration of ~1 mg/mL. A fresh, clean, polystyrene cuvette was washed with compressed air to remove dust. The sample solution was passed through a 0.4 μm Teflon syringe filter directly into the cuvette; the cuvette was capped and placed in the DLS for particle sizing. At least three measurements were made per sample and average hydrodynamic diameters were calculated by fitting the DLS correlation function using the CONTIN routine (ISDA software package from Brookhaven instruments). Nuclear magnetic resonance (NMR) experiments were performed on either a Mercury 300 MHz spectrometer, an INOVA 500 MHz spectrometer, or an INOVA 600 MHz spectrometer. Varian VNMRJ and MestReNove NMR 5.3.2 software were used to obtain and analyze the NMR spectra, respectively. Analytical high-performance liquid chromatography mass spectrometry (HPLC−MS or LC−MS) data was obtained using an Agilent 1100 series HPLC system equipped with a variable wavelength ultraviolet−visible (UV−vis) detector and an Agilent 1100 VL LC/MSD mass spectrometer. Separation was achieved using a 9.4 × 50 mm Agilent Zorbax XDB-C18 column with mobile phase gradients of 0.1% acetic acid in water and acetonitrile. Experiments were performed at room temperature with a flow rate of 1.0 mL/min. Preparatory HPLC was performed on an Agilent 1100 series HPLC system with an Agilent 1200 series automated fraction collector and an 1100 series variable wavelength detector. Separation was achieved using a 9.4 × 250 mm Agilent Eclipse XDB-C18 column with 0.1% acetic acid in water and acetonitrile mobile phase. Experiments were performed at room temperature with a flow rate of 5 mL/min. High-resolution mass spectrometry data was obtained on an Agilent 6200 series accurate-mass time-of-flight (TOF) LC/MS. Matrix assisted laser desorption ionization mass spectrometry (MALDI) measurements were performed by the California Institute of Technology mass spectrometry facility using a Voyager De_Pro TOF mass spectrometer (Applied Biosystems) fitted with a 355 nm YAG laser from Blue Ion Technologies. In a typical experiment, 1.0 mg of polymer sample was dissolved in 100 μL of THF and diluted 10-fold with the MALDI matrix, dithranol (10 mg/mL in THF). To each sample was added 0.1 μL of saturated NaI in ethanol and 0.35 μL of the sample-matrix mixture was spotted on a MALDI plate for analysis. The Voyager De_Pro was operated in linear mode with an accelerating voltage of 20 000 V, grid voltage of 95.2%, guide wire 0.03%, extraction delay time 250 ns, acquisition mass range 800−5000 Da, and laser rep rate 20 Hz. The instrument was calibrated externally using a Sequazyme Mass Standard Kit supplied by Applied Biosystems. Brush polymer purification was performed by centrifugal filtration through 30 kDa molecular-weight cut off (MWCO) Amicon Ultra-15 centrifugal filter units (Millipore Inc.). Photolysis experiments were performed using a Multiple Ray Lamp (UVP) fitted with an 8 W, longwave, filtered blacklight bulb (365 nm). Sample

vials were placed as close as possible to the light source and irradiated for the desired time before analysis by LC−MS.

Norbornene−Hexanol (2). A solution of 6-amino-1-hexanol (3.0 g, 25.6 mmol) and *cis*-5-norbornene-*exo*-2,3,-dicarboxylic anhydride (4.0 g, 24.4 mmol) in toluene (50 mL) was added to a dried, 150 mL round-bottom flask fitted with a Dean−Stark trap and placed in an oil bath preset to 140 °C for 24 h while stirring. The reaction mixture was transferred to a silica gel column primed using 10% ethyl acetate in hexanes (10% EtOAc/hexane). A 300 mL portion of 10% EtOAc/hexanes was flushed through the column before elution of the product using 50% EtOAc/hexanes (TLC R_f = 0.3, 50% EtOAc/hexanes, $KMnO_4$ stain). Removal of solvent by rotary evaporation yielded 6.0 g of **2** as a colorless oil (94%). ^{1}H NMR (300 MHz, $CDCl_3$): δ 6.00 (s, 2H), 3.26 (t, J = 6.4 Hz, 2H), 3.13 (t, J = 7.3, 2H), 2.93 (s, 2 H), 2.38 (s, 2H), 1.31−1.15 (m, 5H), 1.14−0.95 (m, 4H), 0.92 (t, J = 7.4 Hz, 1H). ^{13}C NMR (300 MHz, $CDCl_3$): δ 177.9, 137.5, 61.8, 47.5, 44.8, 42.4, 38.3, 32.2, 27.4, 26.4, 25.0. TOF HRMS: calcd for $C_{15}H_{22}NO_3$ $[M + H]^+$, 264.1600; found, 264.1612.

Norbornene-aldehyde (3). A three-neck round-bottom flask containing a stir bar was equipped with a vacuum adaptor and two 150 mL addition funnels each capped with a rubber septum. The flask was flame-dried under vacuum, cooled to room temperature, and backfilled with argon. A positive argon pressure (using a mercury bubbler) was maintained through the course of the reaction. DCM (58 mL) was added to the flask via cannula followed by oxalyl chloride (3.21 mL, 37.36 mmol). The solution was cooled to −76 °C using an acetone/dry ice bath. One of the addition funnels was charged with DCM (7.3 mL) and DMSO (5.31 mL, 74.72 mmol) while alcohol **2** (6.60 g, 24.90 mmol) dissolved in DCM (43 mL) was added to the other. The DMSO/DCM solution was added dropwise to the flask containing oxalyl chloride over 15 min while stirring. After the addition, the solution was stirred for 15 min at −76 °C. The solution of **2** in DCM was then added dropwise over 20 min while stirring. The addition funnel was washed twice with 5 mL of DCM and the reaction mixture was stirred for 30 min at −76 °C. Triethylamine (20.83 mL, 149.4 mmol) and DCM (3.7 mL) were combined in the washed addition funnel that previously held **2** and this solution was added dropwise over 15 min to the flask during which time a thick white precipitate formed. After the addition the mixture was stirred for 10 min before warming to room temperature and transferring to a separatory funnel. The mixture was washed twice with 50 mL of 1 M HCl and once with brine, dried over Na_2SO_4 and concentrated on a rotary evaporator. The crude product was purified by silica gel column chromatography (30% EtOAc/hexanes, TLC R_f = 0.25, stain with anisaldehyde solution) to yield **3** (5.83 g, 89%) as a colorless oil. ^{1}H NMR (300 MHz, $CDCl_3$): δ 9.52 (s, 1H), 6.08 (s, 2H) 3.23 (t, J = 7.3 Hz, 2H), 3.02 (s, 2H), 2.46 (s, 2H), 2.22 (td, J = 7.2, 1.4 Hz, 2H), 1.52−1.22 (m, 5H), 1.21−1.05 (m, 2H), 0.99 (d, J = 9.8 Hz, 1H). ^{13}C NMR (300 MHz, $CDCl_3$): δ 202.0, 177.7, 137.6, 47.6, 44.9, 43.3, 42.5, 38.1, 27.3, 26.2, 21.3. TOF HRMS: calcd for $C_{15}H_{19}NO_3$ $[M + H]^+$, 262.1443; found, 262.1438.

Norbornene−Alkyne−Amine (4). Aldehyde **3** (1.0 g, 3.83 mmol) and propargyl amine (258 μL, 4.0 mmol) were dissolved in methanol (10 mL) in a round-bottom flask. The mixture was stirred at room temperature under argon atmosphere for 30 min to form an imine intermediate (reaction monitored by TOF−LC/MS: calcd for imine $C_{18}H_{22}N_2O_2$ $[M + H]^+$, 299.1754; found, 299.1856). The reaction mixture was cooled to 0 °C using an ice bath; $NaBH_4$ (232 mg, 6.13 mmol) was carefully added. The ice bath was removed and the mixture was stirred for 3 min before quenching with 100 mL of saturated $NaHCO_{3(aq.)}$. The mixture was transferred to a separatory funnel and washed five times with DCM (100 mL). The organic fractions were combined and dried over Na_2SO_4, filtered, and concentrated on a rotary evaporator. The resulting oil was purified by silica gel chromatography (2% MeOH/CH_2Cl_2, TLC R_f = 0.2, stain with ninhydrin solution) to yield **4** as a colorless oil (836 mg, 73%). ^{1}H NMR (300 MHz, $CDCl_3$): δ 6.18 (s, 2H), 3.33 (t, J = 7.3 Hz, 2H), 3.29 (d, J = 2.4 Hz, 2H), 3.14 (s, 2H), 2.62−2.46 (m, 4H), 2.12 (t, J = 2.4 Hz, 1H), 1.53−1.30 (m, 5H), 1.30−1.14 (m, 5H), 1.10 (d, J = 9.8 Hz, 1H). ^{13}C NMR (300 MHz, $CDCl_3$): δ 177.9, 137.7, 82.2, 71.2, 48.3, 47.7, 45.0, 42.6, 38.5, 38.0, 29.5, 27.6, 26.7, 26.6. TOF HRMS: calcd for $C_{18}H_{24}N_2O_2$ $[M + H]^+$, 301.1911; found, 301.1951.

Norbornene−Acid−Alkyne (5). Succinic anhydride (134 mg, 1.34 mmol) was combined with amine **4** (382 mg, 1.28 mmol) in DCM (13 mL) and the resulting solution was stirred for 1 h at room temperature before transferring to a silica gel column. Elution with 60% EtOAc/hexanes (TLC R_f = 0.2, stain with bromocresol green solution) gave the purified acid **5** (364 mg, 71%) as a mixture of amide rotamers after concentration on a rotary evaporator. ^{1}H NMR (300 MHz, $CDCl_3$): δ 9.25 (b, 1H), 6.24 (s, 2H), 4.15 (d, J = 2.4 Hz, 1.2H), 4.01 (d, J = 2.3 Hz, 0.8H), 3.50−3.31 (m, 4H), 3.22 (s, 2H), 2.82−2.50 (m, 6H), 2.29 (t, J = 2.3 Hz, 0.3H), 2.17 (t, J = 2.5 Hz, 0.7H), 1.68−1.40 (m, 5H), 1.39−1.21 (m, 5H), 1.16 (d, J = 9.8 Hz, 1H). ^{13}C NMR (300 MHz, $CDCl_3$): δ 178.2, 177.0, 171.6, 171.1, 137.8, 78.9, 78.4, 72.8, 71.8, 47.8, 47.1, 46.6, 45.1, 42.7, 38.5, 38.4, 37.5, 34.6, 29.4, 29.3, 28.1, 28.0, 27.9, 27.5, 27.2, 26.5, 26.2. TOF HRMS: calcd for $C_{22}H_{27}N_2O_5$ $[M - H]^-$, 399.1920; found, 399.1941.

Norbornene−Alkyne−*N*-Hydroxysuccinimidyl (NHS)−Ester (6). DCM (10 mL) was added to a flask containing *N*-(3-(dimethylamino)propyl)-*N*′-ethylcarbodiimide hydrochloride (EDCI, 262 mg, 1.36 mmol), *N*-hydroxysuccinimide (157 mg, 1.36 mmol), 4-(dimethylamino)pyridine (DMAP, 11.1 mg, 0.091 mmol), and **5** (364 mg, 0.91 mmol). The resulting solution was stirred under argon at room temperature for 20 h. The mixture was transferred to a silica gel column. Elution with 70% EtOAc/hexanes (TLC R_f = 0.2, stain with anisaldehyde solution and/or visualize under UV light) gave norbornene **6** (339 mg, 75%) after concentration on a rotary evaporator. ^{1}H NMR (300 MHz, $CDCl_3$): δ 6.23 (s, 2H), 4.16 (d, J = 2.4 Hz, 1.2 H), 3.98 (d, J = 2.2 Hz, 0.8 H), 3.49−3.26 (m, 4H), 6.23 (s, 2H), 2.95 (t, J = 6.9 Hz, 2H), 2.79 (s, 4H), 2.70 (t, J = 6.9 Hz, 2H), 2.62 (s, 2H), 2.29 (t, J = 2.4 Hz, 0.3H), 2.17 (t, J = 2.5 Hz, 0.7H), 1.68−1.40 (m, 5H), 1.39−1.20 (m, 5H). ^{13}C NMR (300 MHz, $CDCl_3$): δ 178.0, 169.6, 169.3, 169.0, 168.4, 137.8, 78.9, 78.4, 77.5, 76.7, 72.9, 71.8, 47.7, 46.9, 46.6, 45.1, 42.7, 38.5, 38.3, 37.4, 34.4, 28.1, 28.0, 27.8, 27.6, 27.5, 27.3, 26.5, 26.2, 25.6. TOF HRMS: calcd for $C_{26}H_{32}N_3O_7$ $[M + H]^+$, 498.2241; found, 498.2203.

Norbornene−Alkyne−PEG(3000) Macromonomer (7). *O*-(2-Aminoethyl)poly(ethylene glycol) (100 mg, 33.3 μmol) and **6** (17.4 mg, 35 μmol) were dissolved in anhydrous DMF (1 mL) and the resulting solution was stirred at room temperature for 4 h. The reaction mixture was added dropwise to diethyl ether (20 mL) to precipitate **7** as a white solid which was collected by centrifugation and decanting of the ether before redissolving in DCM (1 mL). This process of precipitation, centrifugation, and redissolving was repeated five times. On the fifth iteration, the precipitate was dried under vacuum to afford macromonomer **7** as a white powder (78.1 mg, 69%). GPC (0.2 M LiBr in DMF) 3300 Da, PDI 1.10. MALDI mass spectrum and NMR are shown in the Supporting Information (Figures S1−S3).

***N*-(3-Azidopropyl)-3-(*tert*-butyldimethylsilyloxymethyl)-2-nitrobenzamide (9).** EDC (92.4 mg, 0.48 mmol) was added to a suspension of acid **8** (100 mg, 0.32 mmol) and DMAP (3.9 mg, 0.032 mmol) in DCM (4.0 mL). The suspension became a clear solution within 2 min indicating formation of a soluble acylisourea intermediate. At this time, 3-azidopropyl-1-amine (1.0 M in toluene, 482 μL, 0.48 mmol) was added dropwise to the reaction mixture. The resulting solution was stirred overnight at room temperature under an argon atmosphere. The reaction mixture was diluted with 100 mL EtOAc and washed three times with 1.0 M HCl (50 mL), three times with sat. $NaHCO_3$ (50 mL), and once with brine (50 mL). The organic layer was then dried over $MgSO_4$, filtered, and concentrated on a rotary evaporator. The resulting white solid was passed through a silica plug using

Scheme 1. Synthesis of PEG−Norbornene−Alkyne Macromoner 7

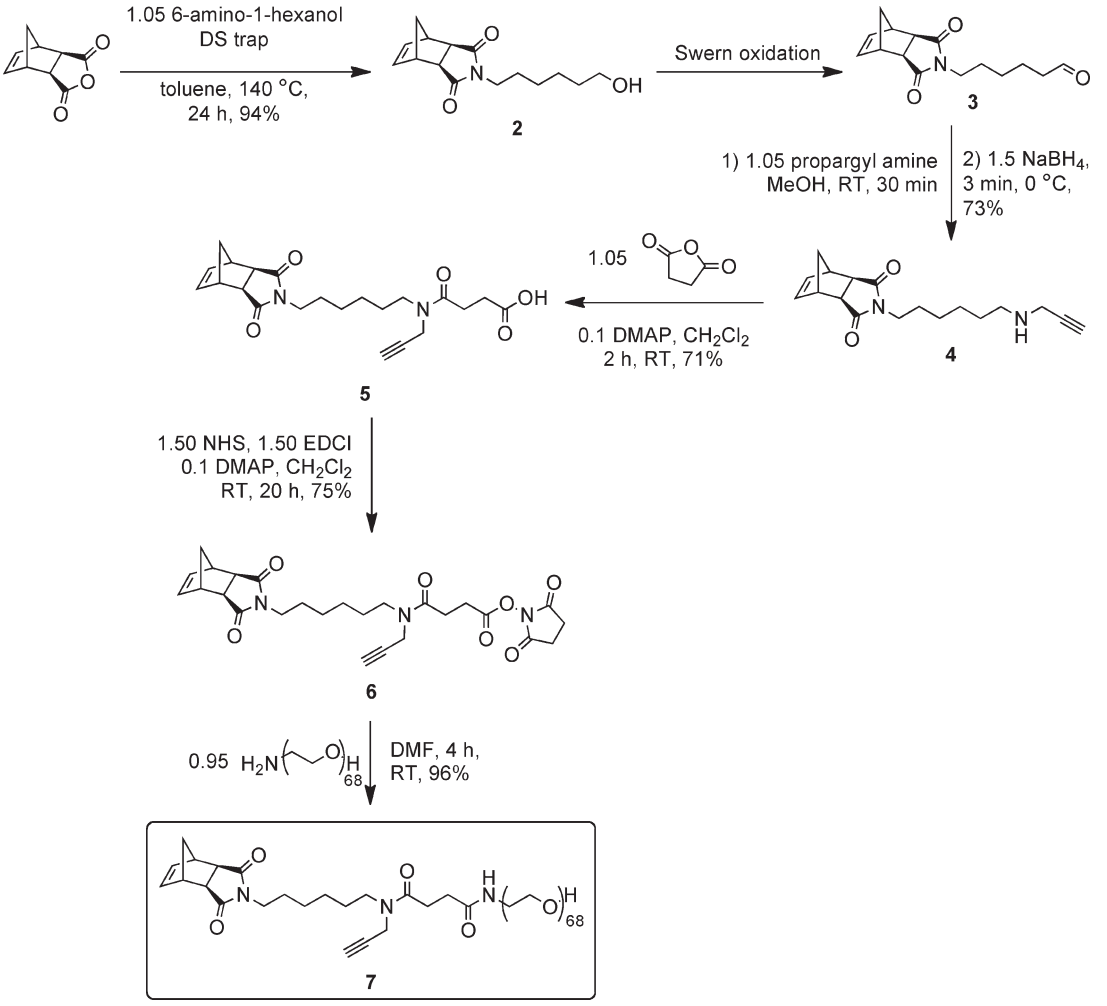

50% EtOAc/hexanes and evaporated to dryness to give **9** (101 mg, 80%) as a white crystalline solid (128 mg, 80%). ^{1}H NMR (300 MHz, $CDCl_3$): δ 7.75 (d, J = 6.4 Hz, 1H), 7.52 (t, J = 7.7 Hz, 1H), 7.41 (d, J = 6.2 Hz, 1H), 6.46 (b, 1H), 4.78 (s, 2H), 3.65−3.15 (m, 4H), 1.84 (p, J = 6.6 Hz, 2H), 0.92 (s, 9H), 0.09 (s, 6H). ^{13}C NMR (300 MHz, $CDCl_3$): δ 165.8, 146.4, 135.4, 131.2, 130.7, 129.9, 126.5, 60.8, 49.3, 37.8, 28.4, 25.0, 18.3, 5.6. TOF HRMS: calcd for $C_{17}H_{28}N_5O_4Si$ $[M + H]^+$, 394.1911; found, 394.1900.

***N*-(3-Azidopropyl)-3-(hydroxymethyl)-2-nitrobenzamide (10).** Compound **9** (101 mg, 0.26 mmol) was dissolved in tetrahydrofuran (3 mL) in a round-bottom flask which was subsequently cooled to 0 °C. Tetrabutylammonium fluoride (1.0 M in THF, 0.385 mL, 0.39 mmol) was added dropwise and the mixture was stirred for 15 min. The solution was diluted with EtOAc (50 mL) and washed three times with 1.0 M HCl (25 mL) and once with brine (50 mL). The organic layer was dried over $MgSO_4$, filtered, and passed through a silica plug to give pure **10** (56 mg, 78%) as a white solid. ^{1}H NMR (300 MHz, acetone): δ 7.98 (b, 1H), 7.82 (d, J = 4.6 Hz, 1H), 7.69−7.56 (m, 2H), 4.71 (s, 2H), 3.63−3.28 (m, 4H), 1.88 (p, J = 6.8 Hz, 2H). ^{13}C NMR (300 MHz, acetone): δ 205.4, 165.2, 135.3, 130.8, 130.1, 126.9, 59.4, 48.8, 36.9. TOF HRMS: calcd for $C_{11}H_{13}N_5O_4$ $[M + H]^+$, 280.1046; found, 280.1067.

CT-NBOC-N3. The following reaction (see Scheme 2) was a modified literature procedure for the preparation of 20-*O*-acylcamptothecins.[47] (*S*)-(+)-Camptothecin (**CT**, 62.7 mg, 0.18 mmol) and DMAP (70.1 mg, 0.57 mmol) were suspended in DCM (5 mL) under argon atmosphere. Triphosgene (19.6 mg, 0.066 mmol) was added and the mixture was stirred for 30 min at room temperature. Alcohol **10** (55.2 mg, 0.2 mmol, in 2 mL THF) was added dropwise via a rubber septum using a gastight syringe. The reaction was stirred overnight during which time a white precipitate formed. The reaction mixture was diluted with EtOAc (100 mL) and washed once with water (50 mL), twice with 1.0 M HCl (25 mL), and once with brine (50 mL). The organic layer was dried over $MgSO_4$, filtered, and concentrated on a rotary evaporator. The solid residue was purified by column chromatography (100% EtOAc, TLC R_f = 0.2, visualize under UV light) to give **CT-NBOC-N$_3$** as a white solid (106 mg, 90%). ^{1}H NMR (600 MHz, $CDCl_3$): δ 8.41 (s, 1H), 8.26 (d, J = 8.6 Hz, 1H), 7.95 (d, J = 7.8 Hz, 1H), 7.86 (ddd, J = 8.4, 6.9, 1.4 Hz, 1H), 7.72−7.68 (m, 2H), 7.56 (t, J = 7.7 Hz, 1H), 7.43 (dd, J = 7.6, 1.3 Hz, 1H), 7.34 (s, 1H), 6.33 (t, J = 5.8 Hz, 1H), 5.59 (d, J = 17.1 Hz, 1H), 5.34 (d, J = 17.1 Hz, 1H), 5.32−5.19 (m, 4H), 3.46 (q, J = 6.5 Hz, 2H), 3.42 (t, J = 6.5 Hz, 2H), 2.27 (dt, J = 14.9, 7.5 Hz, 1H), 2.21−2.11 (m, 1H), 1.85 (p, J = 6.5 Hz, 2H), 1.01 (t, J = 7.5 Hz, 3H). ^{13}C NMR (300 MHz, $CDCl_3$): δ 167.1, 165.5, 157.2, 153.0, 151.9, 148.5, 146.9, 146.3, 145.4, 131.9, 131.8, 131.5, 131.0, 130.4, 129.5, 129.3, 128.5, 128.3, 128.2,128.1, 120.3, 96.1, 78.5, 67.0, 65.3, 50.0, 49.2, 45.0, 37.8, 31.8, 28.4, 7.6; TOF HRMS: calcd for $C_{32}H_{28}N_7O_9$ $[M + H]^+$, 654.1949; found, 654.2010.

DOX-NBOC-N3. A suspension of **10** (45 mg, 0.16 mmol) in THF (2 mL) and triethylamine (25 μL, 0.18 mmol) was treated with 4-nitrophenyl chloroformate (35 mg, 0.18 mmol). TLC and ^{1}H NMR confirmed complete conversion to carbonate **11** within 15 min. The reaction mixture was transferred to a short silica gel column and eluted with 70% EtOAc. UV active fractions with R_f = 0.4 were combined and dried on a rotary evaporator. The resulting white solid, **11** (40 mg, 90 μmol), was immediately

Scheme 2. Synthesis of Clickable, Photocleavable Drugs CT-NBOC-N_3 and DOX-NBOC-N_3

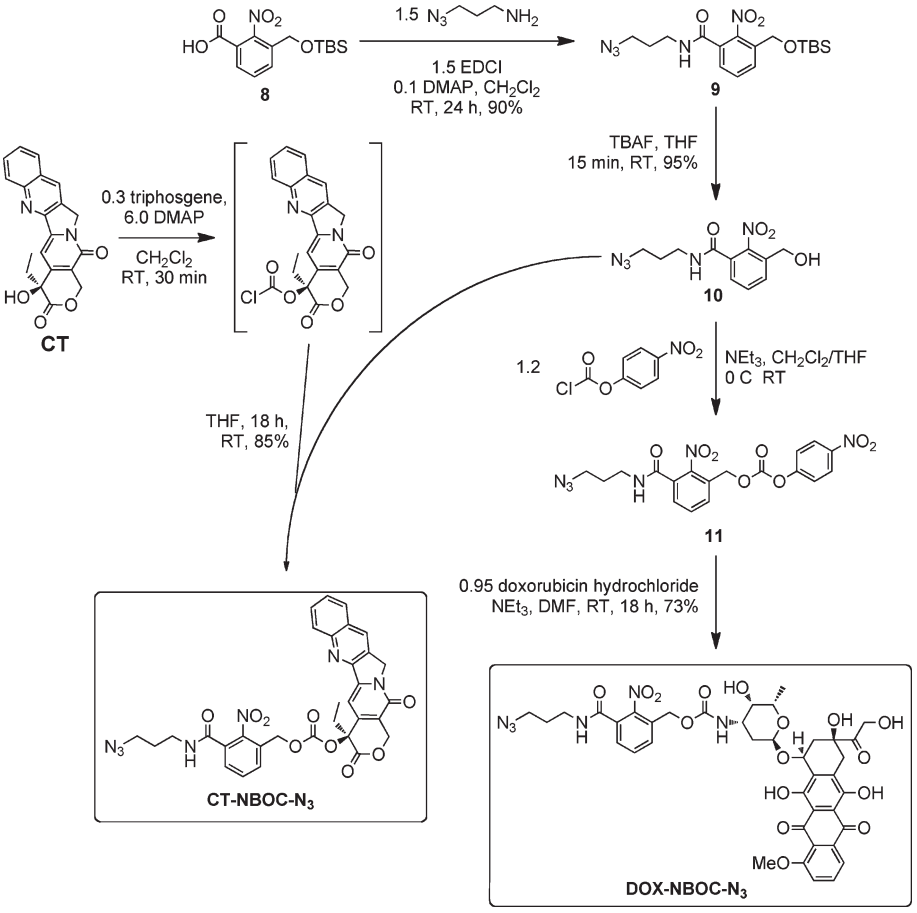

Scheme 3. Click Coupling of 7 to Photocleavable Drug Derivatives

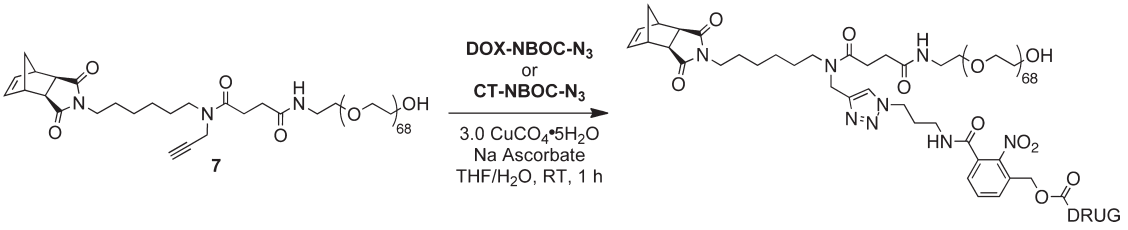

dissolved in anhydrous DMF (1 mL). **DOX**-HCl (53 mg, 91 μmol) and anhydrous *N*,*N*-diisopropylethylamine (DIPEA, 17 μL, 99 μmol) were added and the resulting solution was stirred overnight at room temperature. The reaction mixture was diluted with 50 mL EtOAc and washed twice with 0.1 M HCl (20 mL), once with H_2O (20 mL), and once with brine (20 mL) before drying over magnesium sulfate, filtration, and concentration on a rotary evaporator. The resulting red solid was purified by column chromatography. The column was eluted first with 3% MeOH/CH_2Cl_2 and then with 5% MeOH/CH_2Cl_2 to give **DOX-NBOC-N3** as a red solid (73 mg, 95%). ^{1}H NMR (600 MHz, DMSO-d_6): δ 8.77 (t, J = 5.6 Hz, 1H), 7.96−7.87 (m, 2H), 7.67−7.61 (m, 3H), 7.57 (dd, J = 6.9, 2.1 Hz, 1H), 7.00 (d, J = 8.0 Hz, 1H), 5.42 (s, 1H), 5.20 (s, 1H), 5.01 (dd, J = 37.8, 13.7 Hz, 2H), 4.92 (m, 1H), 4.81 (t, J = 6.0 Hz, 1H), 4.69 (d, J = 5.7 Hz, 1H), 4.54 (d, J = 6.0 Hz, 2H), 4.14−4.09 (m, 1H), 3.98 (s, 3H), 3.71−3.60 (m, 1H), 3.42−3.39 (m, 1H), 3.38−3.35 (m, 2H), 3.24−3.19 (m, 2H), 2.96 (q, J = 18.3 Hz, 2H), 2.12 (dt, J = 14.5, 9.0 Hz, 2H), 1.83 (dd, J = 12.8, 9.2 Hz, 1H), 1.69 (p, J = 6.7 Hz, 2H), 1.09 (d, J = 6.5 Hz, 4H). ^{13}C NMR (500 MHz, CD_2Cl_2): δ 213.1, 186.1, 164.5, 160.4, 155.3, 154.7, 154.0, 146.7, 135.0, 134.6, 132.8, 132.7, 130.6, 130.5, 130.4, 130.1, 126.7, 120.0, 118.7, 117.9, 110.8, 110.7, 99.8, 75.9, 68.7, 68.6, 66.6, 64.7, 61.2, 55.8, 48.6, 46.4, 37.0, 34.8, 33.2, 28.9, 27.7, 15.8. TOF HRMS: calcd for $C_{39}H_{40}N_6O_{16}$ [M − H]$^-$, 847.2423; found, 847.2418.

General Macromonomer Synthesis by Copper-Catalyzed Azide−Alkyne Cycloaddition (CuAAC) Click Chemistry. Drug azide, **CT-NBOC-N_3** or **DOX-NBOC-N_3**, (1.01 equiv to alkyne) was combined with norbornene−PEG−alkyne **7** (100 mg, 29.4 μmol) in a 2 mL HPLC vial and THF (0.5 mL) was added. A spatula tip of sodium ascorbate was added followed by a 1.0 M solution of $CuSO_4$ in H_2O (88 μL, 3 equiv to alkyne). The mixture was flushed with argon, sealed with a septum, and stirred until completion (as monitored by LC−MS) which was typically ~1 h. After the required time, the drug-loaded macromonomer was purified by preparative HPLC (linear gradient of 95:5 water−0.1% AcOH:MeCN to 5:95 water−0.1% AcOH−MeCN over 12 min). The fractions containing pure MM were combined and concentrated on a rotary evaporator. The resulting residue was dissolved in DCM, dried over Na_2SO_4, filtered, and dried under vacuum to give pure macromonomer **CT-MM** or **DOX-MM** (typical yield ~75 mg, ~70%). MALDI and ^{1}H NMR spectra are shown

Scheme 4. Synthesis and Structure of Poly(norbornene)−PEG Brush Polymers with DOX or CT Attached via a Photocleavable NBOC Linker. Pyr = pyridine.

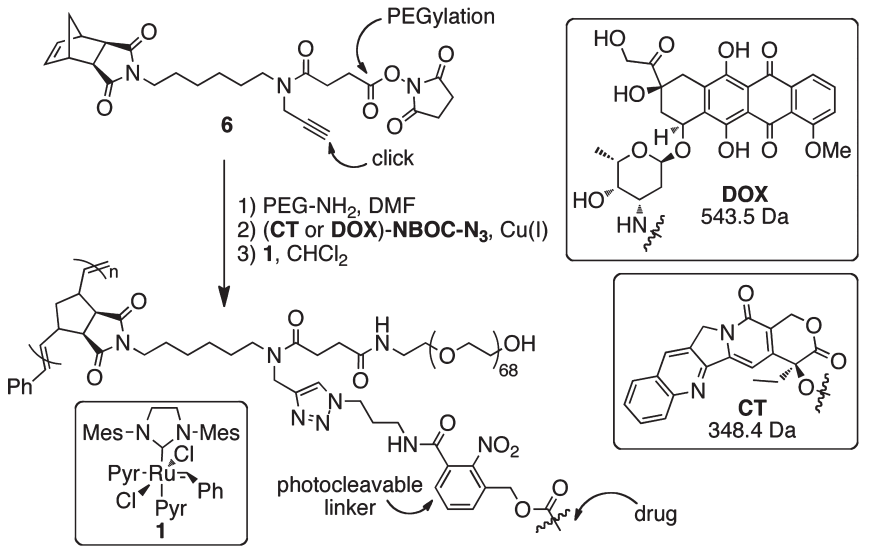

in the Supporting Information (Figures S4−S7). The synthesis is depiced in Scheme 3.

General ROMP Polymerization. Macromonomer **DOX-MM** or **CT-MM** (20 mg, ~5 μmol), or a combination of the two, was added to a 2 mL vial containing a stir bar. The vial was capped with a septum and placed under vacuum for 5 min and then purged with argon. DCM was added followed by a freshly prepared solution of catalyst **1** in DCM (1 mg **1**/mL DCM, amount added to give the desired MM:**1**) such that the total concentration of MM was 0.05 M. The mixture was stirred at room temperature under argon for 90 min after which time the reaction became noticeably viscous. One drop of ethyl vinyl ether was added to quench the polymerization and the vial was placed under vacuum to remove volatiles. The resulting polymer film was dissolved in deionized water (15 mL) and transferred to a centrifugal filter tube (30 kDa MWCO). The tube was spun at 4000 rpm until all of the solvent had passed through the filter except for ~1 mL (typically ~45 min). More water was added (14 mL) and this process was repeated at least 5 times to remove any remaining MM. After the last centrifugation, the 1 mL solution of brush polymer in water was transferred to a weighed glass vial and lyophilized to dryness. Typical yields after purification were ~15 mg (75%). Representative ^{1}H NMR spectra are shown in the Supporting Information (Figures S8 and S9).

LC−MS Methods. Two methods were used for analytical LC−MS experiments; acetonitrile (MeCN) percentage was varied. Method A was a linear gradient of 5% MeCN to 95% MeCN over 5 min followed by a 2 min hold at 95% MeCN to flush the column. Method B began at 5% MeCN and ran to 70% MeCN linearly over 5 min followed by a 2 min flush at 95% MeCN. Method A was used for the **DOX** loaded polymers (**pDOX02** and the copolymer) and method B for **pCT03**. The concentration of **CT** and/or **DOX** in photolyzed samples was estimated from free **CT** and **DOX** calibration curves, respectively. The calibration curves were generated as follows. A 1 mM solution of **CT** in DMSO was serially diluted with DMSO to generate 100 μM, 10 μM, and 1 μM solutions. In a similar fashion, a 1 mM solution of **DOX**-HCl in water was serially diluted with water to generate solutions of known concentration. Each of these samples was analyzed by LC−MS with wavelength detection set at 368 and 500 nm for **CT** and **DOX** respectively. Method A was used in both cases. The area under the absorbance curve for each run was calculated and plotted against the concentration of drug (Supporting Information, Figure S10). Linear fitting of the resulting calibration curve gave an extinction coefficient that was used to estimate the concentration of drug released in photolysis experiments.

Cell Culture. Human breast cancer cell line MCF-7 (ATCC, HTB-22) was cultured at 37 °C under a humidified atmosphere of 5% CO_2. The cells were grown in Eagle's minimum essential medium (EMEM, ATCC, 30−2003) supplemented with 10% fetal bovine serum (Gibco, 10437028), 1% antibiotics (100 U/mL penicillin and 100 μg/mL streptomycin, Gibco, 105140122), and 10 μg/mL bovine insulin (Sigma, I0516). The cells were continuously maintained in the culture medium and subcultured every 3−4 days.

Drug Treatment and Cell Viability Assay. MCF-7 cells were seeded at 10,000 cells/well in a 96-well plate and allowed to attach for 20 h before drug treatment. Prior to drug exposure, the culture medium was removed and the cells were washed once with warm phosphate-buffered saline (PBS). Then, fresh media with drug concentrations ranging from 0 to 100 μM (based on dry weight of polymer dissolved in H_2O) were added to the appropriate wells. After recovering for 10 min at 37 °C, one plate of cells was submitted to UV light (Multiple Ray Lamp with filtered blacklight bulb, 365 nm) for 10 min while the control plate was kept in the dark. The cells were subsequently incubated in a cell culture incubator for 24 h. The medium was removed and the cells were washed twice with warm PBS before fresh drug-free medium was added to each well. The cells were incubated for another 24 h before analysis by the MTT cell proliferation assay (ATCC, 30−1010K). Cells were washed once with warm PBS and incubated with fresh medium containing MTT reagent for 3 h at 37 °C. Detergent was added to solubilize the purple formazan crystals formed by proliferating cells. Absorbance at 570 nm was measured on a Safire II (Tecan) plate reader. Data were fit to a sigmoidal function to determine the half-maximum inhibitory concentration (IC_{50}).

Results and Discussion

Synthesis of Norbornene−PEG−Alkyne MM. Graft-through ROMP reduces the problem of brush polymer synthesis to design of an appropriate, strained alkene MM; a bivalent-brush is derived from a bivalent norbornene MM (Figure 1). Using a branched MM avoids the need for copolymerization of two different monomers, one PEG-MM and one drug-loaded monomer; a high drug loading is maintained and issues arising from different propagation rates between MM and small-molecule monomers are negated. Toward this end, we prepared norbornene-imide derivative **6** (Schemes 1 and 4) which carries two orthogonally addressable functional groups, an *N*-hydroxysuccinimidyl (NHS) ester and an alkyne.

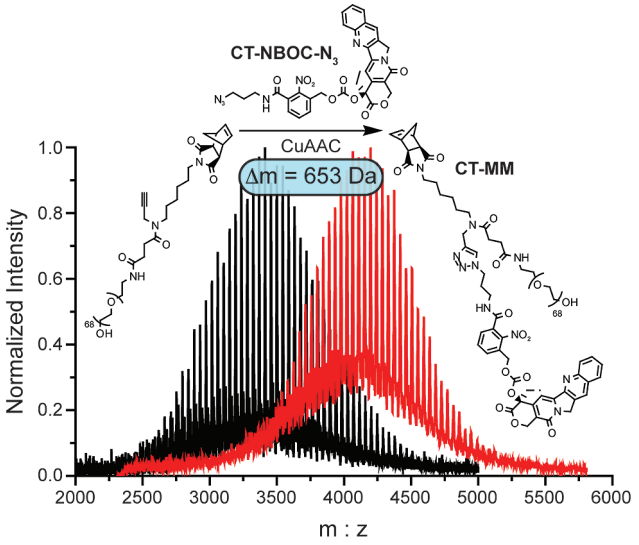

Figure 2. MALDI spectra for PEG−norbornene **7** before (black trace) and after (red trace) CuAAC click coupling of **CT-NBOC-N_3** to give **CT-MM**. The observed mass shift of 653 Da agrees with the calculated mass of **CT-NBOC-N_3** and confirms successful attachment of the photocleavable drug moiety.

The NHS-ester of **6** was efficiently coupled to water-soluble PEG-NH_2 (M_n = 3 kDa) to give PEG-MM **7** (Figure 2). We independently prepared **DOX**- and **CT**- nitrobenzyloxycarbonyl-azide analogues (**DOX-NBOC-N_3** and **CT-NBOC-N_3**, Scheme 2 and Figure 2) that allow for drug attachment via copper-catalyzed azide−alkyne cycloaddition (CuAAC) click chemistry[48−50] and controlled drug release in response to long wavelength UV irradiation (~365 nm). CuAAC coupling of **7** to either drug-azide proceeded in high yield to give the desired drug-loaded PEG-MMs (**DOX-MM** and **CT-MM**). The MALDI spectra of **CT-MM** and its alkyne precursor **7** confirmed the expected mass increase after CuAAC coupling (Figure 2).

ROMP of Drug-Loaded, PEGylated MMs. Treatment of either MM with **1** in methylene chloride (DCM) for 90 min under N_2 yielded polymers (**pDOX** and **pCT**) with low PDIs and M_n dependent on the ratio of MM to **1** (Table 1). The **pDOX** brushes were characterized by PDIs on the order of 1.1 as previously reported for graft-through ROMP polymerizations using catalyst **1**.[27,28] The PDI values for **pCT** samples were low for DP_n below ~30 but higher at high DP_n and the overall attainable DP_n was limited to ~150. For *in vivo* delivery of nondegradable polymers, hydrodynamic radii of < 5−10 nm are often desirable;[35,42] graft-through ROMP of either MM is highly controlled within this size domain (Table 1). For the higher DP_n **CT-MM** polymerizations, we hypothesize that the presence of potential chelating moieties (quinoline and pyrrole) in **CT** may interfere with catalyst initiation and propagation especially at high DP_n. Nevertheless, the success of the graft-through ROMP polymerizations for both MMs attests to the remarkable functional-group tolerance of catalyst **1**. Figure 2 shows gel-permeation chromatography (GPC) traces of brush polymer samples **pCT03** and **pDOX02** without purification, confirming a monomodal MW distribution and a very high conversion (>95%). All of the polymer samples were highly soluble in water (>100 mg/mL); trace MM was removed by passage of an aqueous solution of polymer through a 30 kDa cutoff centrifuge filter to give pure brush polymer (Figure 3, red trace). The purified samples were lyophilized to dryness and redissolved in water prior to subsequent experiments.

Table 1. GPC Characterization of pDOX and pCT Brush Polymer Samples and Random Copolymer $pDOX_{50}$-pCT_{50}

sample	MM:1[a]	DP_n[b]	M_n (GPC, kDa)	PDI	D_h[c]
pDOX01	10	9	33.7	1.07	6.2 (0.5)
pDOX02	50	58	227	1.05	12 (2)
pDOX03	100	96	352	1.04	15 (2)
pCT01	15	15	55.4	1.09	7.1 (0.5)
pCT02	25	30	111	1.17	8.7 (0.9)
pCT03	100	75	276	1.38	n.d.[e]
pCT04	150	107	394	1.61	n.d.
pCT05	200	135	499	1.70	n.d.
$pDOX_{50}$-pCT_{50}[d]	100	101	393	1.13	15 (1)

[a] Ratio of MM to catalyst (i.e., theoretical DP_n). [b] DP_n observed derived from M_n(GPC)/M_n(MM). [c] Hydrodynamic diameter measured by dynamic light scattering (DLS) using the CONTIN fitting algorithm. Reported values are the average of three experiments with error shown in parentheses. [d] **$pDOX_{50}$-pCT_{50}** carries approximately 50 **DOX** and 50 **CT** based on MM stoichiometry prior to ROMP. [e] D_h values not determined for these samples due to high polydispersity.

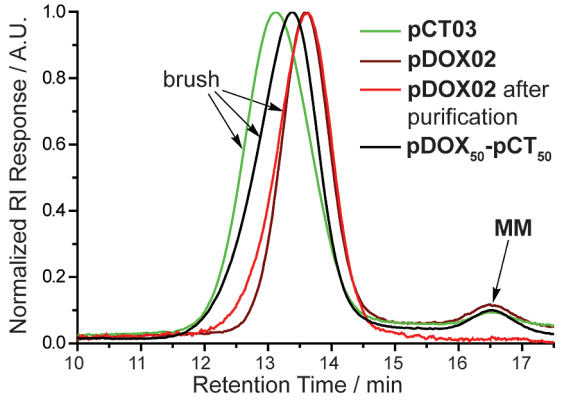

Figure 3. Representative GPC traces for brush polymer samples. Black and red chromatograms correspond to crude ROMP reaction mixtures. The brush polymers display narrowly dispersed, monomodal molecular weight distributions. The GPC trace for purified **pDOX02** is shown in orange, indicating that it is possible to remove trace MM impurity.

As demonstrated above, graft-through ROMP allows for rapid access to brush polymers of controlled, variable molecular weights. We envisioned this methodology also being useful for preparing multiple-drug-loaded brush polymers via copolymerization of appropriate MMs. For example, treatment of equimolar mixtures of **DOX-MM** and **CT-MM** with catalyst **1** in DCM yielded copolymer **$pDOX_{50}$-pCT_{50}** which exhibited a narrow, monomodal MW distribution (Table 1, Figure 3). Combination of a variety of therapeutic moieties within the same polymer system and controlled release using external, and perhaps different, stimuli will enable study and discovery of synergistic drug effects and design of synchronized drug releasing systems.

UV Photolysis Experiments. To demonstrate controlled release of **DOX** and **CT** from these brush polymer scaffolds in response to 365 nm UV light we irradiated aqueous solutions of the polymers for various times from 30 s to 10 min and monitored the progress of photorelease by high-performance liquid chromatography connected in series to a single wavelength UV detector and an electrospray mass spectrometer (LC−MS). The resulting chromatograms for brush polymer **pDOX02** (~1.1 μM of bound **DOX** in H_2O) before and after irradiation are shown in Figure 4a. With increasing irradiation time, the polymer absorbance at 500 nm is diminished and a new peak is observed at ~3.1 min; the mass of the species giving rise to this new peak is 542.30 Da which corresponds to that of free **DOX**-H^+. The yield for photocleavage in this time was ~50% based on integration of the polymer and free **DOX** peaks.

Similar data for **pCT03** (~2.6 μM bound **CT** in H_2O) are shown in Figure 4b. After 10 min irradiation we observed ~64% release of free **CT** along with two minor peaks labeled "*" in Figure 4b. **CT** is a common target for drug delivery because it is highly active against cancer cells but insoluble and unstable in neutral, aqueous solution.[47] We believe that these two peaks may represent degradation products of **CT** that result from hydrolysis (open lactone form) or photochemical degradation; however we have been unable to generate the same chromatogram by simply photolyzing free **CT** in solution due to its insolubility and we did not observe a molecular ion in the LC−MS that corresponds to the mass of the open lactone form (the major peak at ~4.1 min corresponds to the therapeutically active lactone form of **CT**). These experiments show that the **pCT** brush polymers effectively solubilize their **CT** payload and allow for drug release even in aqueous solution where the **CT** cargo is insoluble.

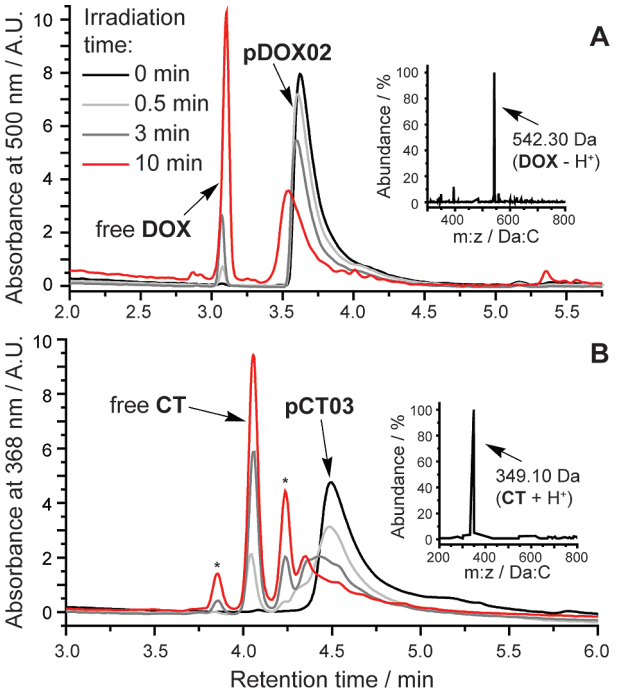

Figure 4. HPLC−MS traces of aqueous brush polymer solutions before and after 365 nm UV irradiation for various times. **pDOX02** and **pCT03** yield free **DOX** and **CT**, respectively. LC−MS method A (see Methods and Materials) was used for **pDOX02** while method B was used for **pCT03**. Inset mass spectra, obtained from the free **DOX** and **CT** peaks, show strong signals at m:z ratios that correspond to the molecular ions of **DOX** and **CT**.

We recorded the UV−vis absorption spectra for **pDOX01**, **pCT01**, and **pDOX$_{50}$-pCT$_{50}$** in water to verify that **CT** and **DOX** were present (Figure 5a). The spectra of **pCT01** and **pDOX01** display broad absorption bands at wavelengths above 300 nm that result from bound **CT** or **DOX**, respectively. The spectrum of the copolymer shows both bands. This information, along with the monomodal GPC trace (Figure 3) and photolysis data (Figure 5b) suggests that copolymer **pDOX$_{50}$-pCT$_{50}$** does indeed carry both drug molecules bound to the same polymer chain (rather than a mixture of two homopolymers which would likely result in broadening of the GPC trace). LC-MS traces for the copolymer (~1.5 μM in H_2O) both before and after irradiation are shown in Figure 5b. Absorption was monitored at two wavelengths, 368 and 500 nm, to detect **CT** and **DOX** respectively. As expected, UV irradiation induced release of both drugs from the copolymer; to our knowledge, this is the first example of a polymer system capable of releasing two covalently bound anticancer drugs (**DOX** and **CT**) in response to a controlled external stimulus. A recent report by Shen and co-workers suggests that materials capable of releasing both **DOX** and **CT** will display synergistic cytotoxicity when compared to either drug alone.[51]

Cell Culture Studies. To confirm that these drug-bound, PEG-based brush polymers were inherently nontoxic, and that photoinitiated drug release did indeed yield sufficient amounts of chemotherapeutic agent to kill cancer cells, we performed cell viability experiments using MCF-7 human breast cancer cells. Cells were treated with aqueous solutions of either free drug or the corresponding drug-loaded brush polymer at various concentrations and irradiated for 10 min using 365 nm light or kept in the dark. The cells were then incubated in the dark for 24 h, washed twice, and incubated for another 24 h in fresh, drug-free growth medium. After this time, cell viability was assessed using the MTT assay (see Methods and Materials for details). Representative data are shown in Figure 6a−c. In parts a and b of Figure 6, both free **CT** and **DOX** controls, with and without UV irradiation, gave similar dose−response curves with IC_{50} values of ~1.2 μM and ~4.9 μM, respectively. These data suggest that UV irradiation at 365 nm for 10 min is not by itself toxic to the cells nor is it detrimental to the drug toxicity. On the other hand, polymer samples **pCT01** and **pDOX02** without UV irradiation were nontoxic to cells at concentrations greater than 10 times those of the free drugs (39 μM and 105 μM, respectively) indicating that the PEG brush polymers effectively shield the toxic effects of **CT** and **DOX** prior to drug release. We were pleased to find that irradiation of the drug-bound polymers led to greatly increased cytotoxicity (IC_{50} = 2.2 μM and 8.7 μM for **pCT01** and **pDOX02**, respectively) compared to the nonirradiated samples suggesting that photoreleased

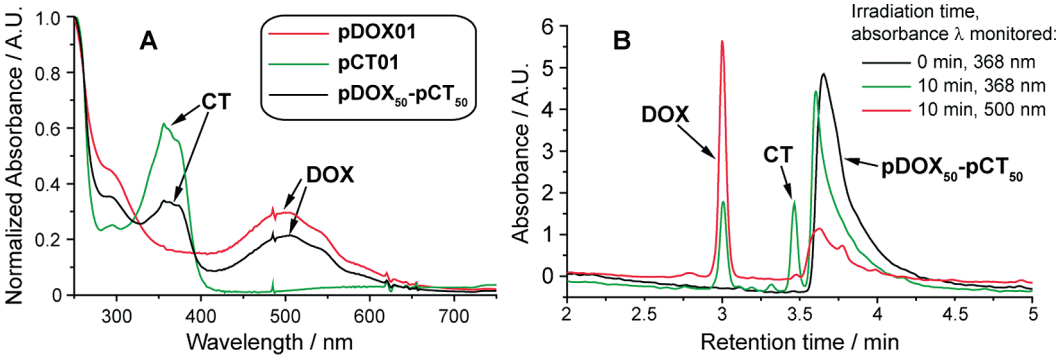

Figure 5. (A) UV−vis absorption of **pDOX01**, **pCT01**, and copolymer **pDOX$_{50}$-pCT$_{50}$**. (B) HPLC traces of an aqueous solution of **pDOX$_{50}$-pCT$_{50}$** before and after 365 nm UV irradiation for 10 min.

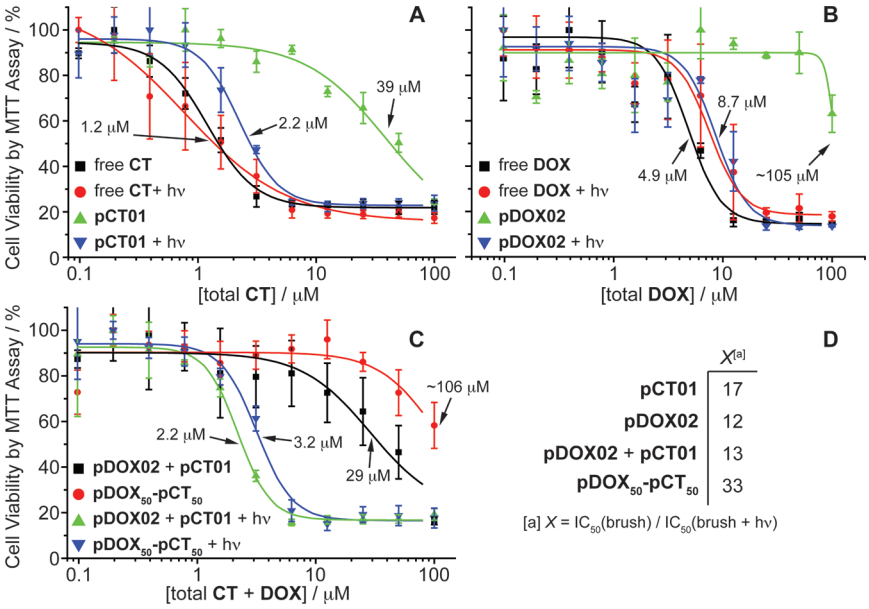

Figure 6. (A−C) Viability of MCF-7 human breast cancer cells treated with free **DOX** and **CT** and drug-loaded brush polymers both with and without UV irradiation. Data points were fit to a sigmoidal function and the half-maximum inhibitory concentrations (IC_{50}) are shown. The *x*-axis labels refer to the concentration of both free and polymer-conjugated drug. (D) Table of therapeutic factors for each brush polymer formulation. These values represent the fold-increase in toxicity after irradiation and drug release.

CT and **DOX** were therapeutically effective. Figure 6c compares the toxicity of copolymer **pDOX$_{50}$-pCT$_{50}$** with a 1:1 mixture of **pDOX02** and **pCT01** before and after irradiation. The copolymer was nontoxic prior to irradiation at concentrations less than 100 μM whereas the mixture of both polymers appeared to be toxic at lower concentration (29 μM). UV induced drug release, however, led to a similar IC_{50} for both systems (3.2 μM for **pDOX$_{50}$-pCT$_{50}$** and 2.2 μM for the mixture). Figure 6d shows the therapeutic factors (X) for these materials: a measure of the increase in cytotoxicity after photoinduced drug release. All of the polymers studied showed at least a 12X increase in toxicity upon drug release; these results are encouraging and suggest the utility of these brush polymer systems for *in vivo* drug delivery applications.

Conclusions

To our knowledge, this report is the first example of simultaneous photoregulated release of **DOX** and **CT** and the first example of bivalent-brush polymers capable of controlled release of anticancer drugs (for other examples of photorelease of anticancer drugs see refs 52−54). The graft-through approach ensures that the weight percentage of drug loaded onto the brush polymers is the same as the weight percentage of drug on the MM (because of 100% grafting density) and is independent of DP_n and conversion. Thus, **pCT** and **pDOX** polymers carry 8.5% **CT** and 12.6% **DOX** by weight, respectively. These values could be increased by shortening the length of the PEG side chain prior to ROMP or designing an MM linked to more than one drug molecule. The synthesis of these materials was facilitated by the graft-through ROMP paradigm and we expect this approach to prove useful for the synthesis of a range of other functional multivalent-brush polymer systems. We are also developing clickable linkers with alternate drug release mechanisms; one limitation of this system is the requirement for UV light to initiate drug release. Though long-wavelength UV (UVA) is used for photochemotherapeutic treatment of various cancers and skin disorders,[55−61] there is need for new photocleavable groups with longer absorption wavelengths and high two-photon cross sections to increase tissue penetration.[62,63] The modularity of this system combined with the versatility of graft-through ROMP will enable incorporation of new cleavable linkers into bivalent-brush polymers.

Acknowledgment. We thank Dr. S. Virgil for helpful discussion and advice. We also thank the Beckman Institute for a postdoctoral fellowship for JAJ. UV-vis experiments were performed in the Beckman Institute Laser Center. This work was supported by the National Institutes of Health (NIH, R01-GM31332), the MRSEC program of the National Science Foundation (NSF) under award number DMR-0520565, and the NSF Center for Chemical Innovation (Powering the Planet, CHE-0802907 and CHE-0947829).

Supporting Information Available: Figures showing MALDI and ^{1}H NMR spectral data for polymer samples and liquid chromatography calibration curves. This material is available free of charge via the Internet at http://pubs.acs.org.

References and Notes

(1) Hawker, C. J.; Wooley, K. L. *Science* (*Washington, DC*) **2005**, *309*, 1200–1205.
(2) Hawker, C. J.; Fokin, V. V.; Finn, M. G.; Sharpless, K. B. *Aust. J. Chem.* **2007**, *60*, 381–383.
(3) Kolonko, E. M.; Pontrello, J. K.; Mangold, S. L.; Kiessling, L. L. *J. Am. Chem. Soc.* **2009**, *131*, 7327–7333.
(4) Conrad, R. M.; Grubbs, R. H. *Angew. Chem., Int. Ed.* **2009**, *48*, 8328–8330.
(5) Clark, P. M.; Dweck, J. F.; Mason, D. E.; Hart, C. R.; Buck, S. B.; Peters, E. C.; Agnew, B. J.; Hsieh-Wilson, L. C. *J. Am. Chem. Soc.* **2008**, *130*, 11576–11577.
(6) Rawat, M.; Gama, C. I.; Matson, J. B.; Hsieh-Wilson, L. C. *J. Am. Chem. Soc.* **2008**, *130*, 2959–2961.
(7) Yuan, Y.-Y.; Du, Q.; Wang, Y.-C.; Wang, J. *Macromolecules* **2010**, *43*, 1739–1746.
(8) Li, C.; Ge, Z.; Fang, J.; Liu, S. *Macromolecules* **2009**, *42*, 2916–2924.
(9) Li, A.; Lu, Z.; Zhou, Q.; Qiu, F.; Yang, Y. *J. Polym. Sci., Part A: Polym. Chem.* **2006**, *44*, 3942–3946.
(10) Zhang, M.; Mueller, A. H. E. *J. Polym. Sci., Part A: Polym. Chem.* **2005**, *43*, 3461–3481.
(11) Jiang, X.; Lok, M. C.; Hennink, W. E. *Bioconjugate Chem.* **2007**, *18*, 2077–2084.

(12) Tsarevsky, N. V.; Bencherif, S. A.; Matyjaszewski, K. *Macromolecules* **2007**, *40*, 4439–4445.
(13) Lutz, J.-F.; Boerner, H. G.; Weichenhan, K. *Macromolecules* **2006**, *39*, 6376–6383.
(14) Allen, M. J.; Wangkanont, K.; Raines, R. T.; Kiessling, L. L. *Macromolecules* **2009**, *42*, 4023–4027.
(15) Cheng, G.; Boeker, A.; Zhang, M.; Krausch, G.; Mueller, A. H. E. *Macromolecules* **2001**, *34*, 6883–6888.
(16) Lu, H.; Wang, J.; Lin, Y.; Cheng, J. *J. Am. Chem. Soc.* **2009**, *131*, 13582–13583.
(17) Morandi, G.; Pascual, S.; Montembault, V.; Legoupy, S.; Delorme, N.; Fontaine, L. *Macromolecules* **2009**, *42*, 6927–6931.
(18) Neugebauer, D.; Sumerlin, B. S.; Matyjaszewski, K.; Goodhart, B.; Sheiko, S. S. *Polymer* **2004**, *45*, 8173–8179.
(19) Sumerlin, B. S.; Neugebauer, D.; Matyjaszewski, K. *Macromolecules* **2005**, *38*, 702–708.
(20) Gao, H.; Matyjaszewski, K. *J. Am. Chem. Soc.* **2007**, *129*, 6633–6639.
(21) Hadjichristidis, N.; Pitsikalis, M.; Iatrou, H.; Pispas, S. *Macromol. Rapid Commun.* **2003**, *24*, 979–1013.
(22) Tsukahara, Y.; Mizuno, K.; Segawa, A.; Yamashita, Y. *Macromolecules* **1989**, *22*, 1546–1552.
(23) Tsukahara, Y.; Tsutsumi, K.; Yamashita, Y.; Shimada, S. *Macromolecules* **1990**, *23*, 5201–5208.
(24) Dziezok, P.; Sheiko, S. S.; Fischer, K.; Schmidt, M.; Moller, M. *Angew. Chem., Int. Ed.* **1998**, *36*, 2812–2815.
(25) Neiser, M. W.; Okuda, J.; Schmidt, M. *Macromolecules* **2003**, *36*, 5437–5439.
(26) Neiser, M. W.; Muth, S.; Kolb, U.; Harris, J. R.; Okuda, J.; Schmidt, M. *Angew. Chem., Int. Ed.* **2004**, *43*, 3192–3195.
(27) Xia, Y.; Kornfield, J. A.; Grubbs, R. H. *Macromolecules* **2009**, *42*, 3761–3766.
(28) Xia, Y.; Olsen, B. D.; Kornfield, J. A.; Grubbs, R. H. *J. Am. Chem. Soc.* **2009**, *131*, 18525–18532.
(29) Li, Z.; Zhang, K.; Ma, J.; Cheng, C.; Wooley, K. L. *J. Polym. Sci., Part A: Polym. Chem.* **2009**, *47*, 5557–5563.
(30) Li, Z.; Ma, J.; Cheng, C.; Zhang, K.; Wooley, K. L. *Macromolecules* **2010**, *43*, 1182–1184.
(31) Le, D.; Montembault, V.; Soutif, J. C.; Rutnakornpituk, M.; Fontaine, L. *Macromolecules* **2010**, *43*, 5611–5617.
(32) Duncan, R. *Nat. Rev. Drug Discovery* **2003**, *2*, 347–360.
(33) Peer, D.; Karp, J. M.; Hong, S.; Farokhzad, O. C.; Margalit, R.; Langer, R. *Nat. Nanotechnol.* **2007**, *2*, 751–760.
(34) Mammen, M.; Chio, S.-K.; Whitesides, G. M. *Angew. Chem., Int. Ed.* **1998**, *37*, 2755–2794.
(35) Fox, M. E.; Szoka, F. C.; Frechet, J. M. J. *Acc. Chem. Res.* **2009**, *42*, 1141–1151.
(36) Matsumura, Y.; Maeda, H. *Cancer Res.* **1986**, *46*, 6387–6392.
(37) Tomalia, D. A.; Baker, H.; Dewald, J.; Hall, M.; Kallos, G.; Martin, S.; Roeck, J.; Ryder, J.; Smith, P. *Polym. J.* (*Tokyo, Jpn.*) **1985**, *17*, 117–132.
(38) Bosman, A. W.; Janssen, H. M.; Meijer, E. W. *Chem. Rev.* (*Washington, DC*) **1999**, *99*, 1665–1688.
(39) Lee, C. C.; Gillies, E. R.; Fox, M. E.; Guillaudeu, S. J.; Frechet, J. M. J.; Dy, E. E.; Szoka, F. C. *Proc. Natl. Acad. Sci. U.S.A.* **2006**, *103*, 16649–16654.
(40) Guillaudeu, S. J.; Fox, M. E.; Haidar, Y. M.; Dy, E. E.; Szoka, F. C.; Frechet, J. M. J. *Bioconjugate Chem.* **2008**, *19*, 461–469.
(41) Fox, M. E.; Guillaudeu, S.; Frechet, J. M. J.; Jerger, K.; Macaraeg, N.; Szoka, F. C. *Mol. Pharm.* **2009**, *6*, 1562–1572.
(42) Grayson, S. M.; Godbey, W. T. *J. Drug Targeting* **2008**, *16*, 329–356.
(43) Love, J. A.; Morgan, J. P.; Trnka, T. M.; Grubbs, R. H. *Angew. Chem., Int. Ed.* **2002**, *41*, 4035–4037.
(44) Vercillo, O. E.; Andrade, C. K. Z.; Wessjohann, L. A. *Org. Lett.* **2008**, *10*, 205–208.
(45) Johnson, J. A.; Finn, M. G.; Koberstein, J. T.; Turro, N. J. *Macromolecules* **2007**, *40*, 3589–3598.
(46) Pangborn, A. B.; Giardello, M. A.; Grubbs, R. H.; Rosen, R. K.; Timmers, F. J. *Organometallics* **1996**, *15*, 1518–1520.
(47) Zhao, H.; Lee, C.; Sai, P.; Choe, Y. H.; Boro, M.; Pendri, A.; Guan, S.; Greenwald, R. B. *J. Org. Chem.* **2000**, *65*, 4601–4606.
(48) Kolb, H. C.; Finn, M. G.; Sharpless, K. B. *Angew. Chem., Int. Ed.* **2001**, *40*, 2004–2021.
(49) Rostovtsev, V. V.; Green, L. G.; Fokin, V. V.; Sharpless, K. B. *Angew. Chem., Int. Ed.* **2002**, *41*, 2596–2599.
(50) Tornoe, C. W.; Christensen, C.; Meldal, M. *J. Org. Chem.* **2002**, *67*, 3057–3064.
(51) Shen, Y.; Jin, E.; Zhang, B.; Murphy, C. J.; Sui, M.; Zhao, J.; Wang, J.; Tang, J.; Fan, M.; Van Kirk, E.; Murdoch, W. J. *J. Am. Chem. Soc.* **2010**, *132*, 4259–4265.
(52) Agasti, S. S.; Chompoosor, A.; You, C.-C.; Ghosh, P.; Kim, C. K.; Rotello, V. M. *J. Am. Chem. Soc.* **2009**, *131*, 5728–5729.
(53) Kim, H.-C.; Hartner, S.; Behe, M.; Behr Thomas, M.; Hampp Norbert, A. *J. Biomed. Opt.* **2006**, *11*, 34024.
(54) Choi, S. K.; Thomas, T.; Li, M.-H.; Kotlyar, A.; Desai, A.; Baker, J. R., Jr. *Chem. Commun.* (*Cambridge, U.K.*) **2010**, *46*, 2632–2634.
(55) Krutmann, J. *J. Photochem. Photobiol., B* **1998**, *44*, 159–164.
(56) Bethea, D.; Fullmer, B.; Syed, S.; Seltzer, G.; Tiano, J.; Rischko, C.; Gillespie, L.; Brown, D.; Gasparro, F. P. *J. Dermatol. Sci.* **1999**, *19*, 78–88.
(57) Breuckmann, F.; Gambichler, T.; Altmeyer, P.; Kreuter, A. *BMC Dermatol.* **2004**, *4*.
(58) Diffey, B. *Phys. Med. Biol.* **2006**, *51*, R229–R244.
(59) Dolmans, D. E. J. G. J.; Fukumura, D.; Jain, R. K. *Nat. Rev. Cancer* **2003**, *3*, 380–387.
(60) Dolmans, D. E. J. G. J.; Kadambi, A.; Hill, J. S.; Flores, K. R.; Gerber, J. N.; Walker, J. P.; Borel Rinkes, I. H. M.; Jain, R. K.; Fukumura, D. *Cancer Res.* **2002**, *62*, 4289–4294.
(61) Wozniak, M. B.; Tracey, L.; Ortiz-Romero, P. L.; Montes, S.; Alvarez, M.; Fraga, J.; Herrera, J. F.; Vidal, S.; Rodriguez-Peralto, J. L.; Piris, M. A.; Villuendas, R. *Br. J. Dermatol.* **2009**, *160*, 92–102.
(62) Buckup, T.; Southan, A.; Kim, H. C.; Hampp, N.; Motzkus, M. *J. Photochem. Photobiol., A* **2010**, *210*, 188–192.
(63) Haertner, S.; Kim, H.-C.; Hampp, N. *J. Polym. Sci., Part A: Polym. Chem.* **2007**, *45*, 2443–2452.

Appendix III

Synthesis and Cell Adhesive Properties of Linear and Cyclic RGD Functionalized Polynorbornene Thin Films

Article

pubs.acs.org/Biomac

Synthesis and Cell Adhesive Properties of Linear and Cyclic RGD Functionalized Polynorbornene Thin Films

Paresma R. Patel, Rosemary Conrad Kiser,[‡] Ying Y. Lu, Eileen Fong,[§] Wilson C. Ho, David A. Tirrell, and Robert H. Grubbs*

Division of Chemistry and Chemical Engineering, California Institute of Technology, Pasadena, California 91125, United States

Supporting Information

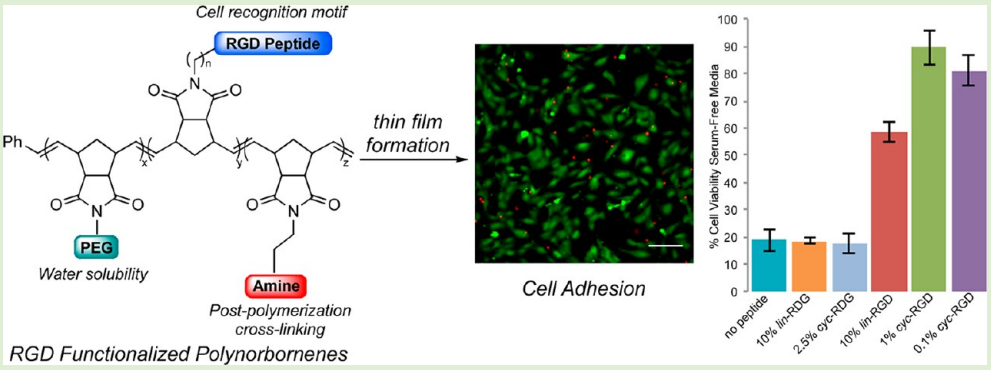

ABSTRACT: Described herein is the efficient synthesis and evaluation of bioactive arginine-glycine-aspartic acid (RGD) functionalized polynorbornene-based materials for cell adhesion and spreading. Polynorbornenes containing either linear or cyclic RGD peptides were synthesized by ring-opening metathesis polymerization (ROMP) using the well-defined ruthenium initiator [$(H_2IMes)(pyr)_2(Cl)_2Ru{=}CHPh$]. The random copolymerization of three separate norbornene monomers allowed for the incorporation of water-soluble polyethylene glycol (PEG) moieties, RGD cell recognition motifs, and primary amines for postpolymerization cross-linking. Following polymer synthesis, thin-film hydrogels were formed by cross-linking with bis(sulfosuccinimidyl) suberate (BS^3), and the ability of these materials to support human umbilical vein endothelial cell (HUVEC) adhesion and spreading was evaluated and quantified. When compared to control polymers containing either no peptide or a scrambled RDG peptide, polymers with linear or cyclic RGD at varying concentrations displayed excellent cell adhesive properties in both serum-supplemented and serum-free media. Polymers with cyclic RGD side chains maintained cell adhesion and exhibited comparable integrin binding at a 100-fold lower concentration than those carrying linear RGD peptides. The precise control of monomer incorporation enabled by ROMP allows for quantification of the impact of RGD structure and concentration on cell adhesion and spreading. The results presented here will serve to guide future efforts for the design of RGD functionalized materials with applications in surgery, tissue engineering, and regenerative medicine.

INTRODUCTION

Synthetic polymers are important as materials for biomedical applications including uses in implants, tissue engineering, and regenerative medicine.[1−3] Many of these materials have the desired mechanical properties, stability, and elasticity, while remaining nontoxic. Nevertheless, inadequate in vivo interaction remains a problem, often leading to foreign body responses that prevent the clinical use of these materials.[1] Cell adhesion, migration, and intracellular signaling in vivo are mediated by integrins, a class of heterodimeric transmembrane receptors that bind extracellular matrix proteins such as fibronectin.[4] One approach to promote biological recognition of synthetic materials is the incorporation of cell adhesive proteins or peptides, thereby promoting cell recognition via interactions with integrins.[1−4]

The use of small peptides has significant benefits relative to coating synthetic surfaces with matrix proteins such as fibronectin, which suffer from susceptibility to enzymatic degradation, immunogenicity, and high cost.[1−3] The arginine-glycine-aspartic (RGD) sequence is the minimal binding domain of fibronectin necessary to recognize cell surface integrins,[5−7] and materials modified with RGD peptides have been shown to facilitate cell adhesion, spreading, and wound healing via enhanced rates of migration of individual cells.[8−10] In a similar fashion, materials formed from cross-linked artificial extracellular matrix proteins presenting the RGD sequence promote cell spreading and adhesion in a manner that can be modulated by varying the density of the RGD ligand.[11−14]

Significant work has been reported regarding the interaction of structurally varied RGD peptides with $\alpha_v\beta_3$ and $\alpha_5\beta_1$ integrin

Received: May 21, 2012
Revised: July 5, 2012
Published: July 11, 2012

receptors due to their central roles in homeostasis and disease.[15−17] In particular, cyclic RGD peptides have been shown to exhibit improved affinity, receptor selectivity, and enzymatic stability relative to linear peptides.[18−21] Kessler and co-workers have developed a class of cyclic RGD peptides that have been reported to demonstrate subnanomolar affinity for the $\alpha_v\beta_3$ receptor and low nanomolar affinity for the $\alpha_5\beta_1$ receptor.[16,22,23] The functionalization of surfaces with *cyclo*(RGDfK) peptides was found to stimulate osteoblast adhesion and proliferation, while the soluble peptide *cyclo*(RGDf(NMe)V) is currently in phase III trials for treatment of glioblastoma.[22,23] Few efficient methods for the incorporation of cyclic RGD peptides in synthetic materials have been described with applications for promoting cell adhesion and spreading.[1,23]

Synthetic polymers covalently modified with RGD peptides can be formed by blending, copolymerization, or postpolymerization modification, methods that do not ensure maximal incorporation of the bioactive peptide and often provide little control over polymer molecular weights.[1,24] Ring-opening metathesis polymerization (ROMP) is an ideal method for polymer synthesis because of its high functional group tolerance, excellent control of molecular weight, and ability to provide narrow PDIs.[25−27] Notably, ROMP polymers containing polynorbornene backbones have been demonstrated to be nontoxic in a variety of systems including mammalian cell lines.[25,28−30] Methods for the postpolymerization modification of ROMP polymers with *cyclo*(RGDfK) have recently been described with applications for tumor imaging.[31,32] Seminal studies reported ROMP of norbornene monomers covalently modified with bioactive peptides, including the RGD motif, for the synthesis of oligomers as multivalent ligands for inhibition of cell adhesion.[33−35] These early studies examined only soluble materials and employed a linear variant of the RGD peptide. Since these initial reports, significant improvements in ruthenium-based catalysts for ROMP have been reported allowing for rapid initiation at room temperature and greater catalyst lifetimes. These improved catalysts provide increased stability to the polar functional groups found in peptides, and therefore, they give longer polymer chains, uniform incorporation of peptides, and low polydispersity indices (PDIs) with monomodal distributions.[36,37]

We sought to efficiently access a new class of RGD-functionalized materials that are amenable to postpolymerization cross-linking and that exhibit cell adhesive properties. To this end, we synthesized linear and cyclic RGD conjugated norbornenes that were copolymerized using ROMP. This work constitutes the first application of a recently reported bis-pyridine ruthenium catalyst for ROMP of complex RGD-conjugated norbornenes, providing copolymers with precise control of monomer incorporation and excellent control of molecular weights and PDIs. The synthesis of RGD-containing polymers described here is a vast improvement from previous reports using ROMP. Following polymer cross-linking, the resulting thin-film hydrogels were quantitatively evaluated to study the impact of RGD structure and content on HUVEC adhesion and spreading. Strikingly, cross-linked polynorbornene thin films containing cyclic RGD were observed to be effective at a 100-fold lower concentration than those containing the linear peptide at supporting cell adhesion and spreading under serum-free conditions.

EXPERIMENTAL SECTION

Polymer Synthesis General Procedure. The random copolymers were synthesized via ROMP with catalyst [$(H_2IMes)(pyr)_2(Cl)_2Ru{=}CHPh$] (**7**) at $[M]_0/[C]_0 = 99$ (Scheme 2). For all polymerizations, the protected amine monomer **2** (Nor-Amine) was held constant at 20 mol %, and the percentage of RGD (**3** or **4**) or control RDG peptides (**5** or **6**) was varied from 0 to 10 mol %. The norbornene-polyethylene glycol (PEG) monomer **1** (Nor-PEG) was added as needed to keep the ratio of monomers to catalyst constant. The polymerization reactions were run for 35 min, and complete incorporation of monomers was confirmed by ^{1}H NMR. Reactions were terminated upon addition of ethyl vinyl ether[38] followed by treatment with tris(hydroxymethyl)phosphine (THMP) for removal of ruthenium.[39] The polymers were precipitated into diethyl ether (Et_2O), and the side chains were deprotected with a mixture of trifluoroacetic acid (TFA), triisopropylsilane (TIPS), and water (95:2.5:2.5). Precipitation into Et_2O, followed by purification via dialysis (molecular weight cut-off (MWCO) = 25 000), and lyophilization of the aqueous solutions provided the pure polymers for biological evaluation. Polymers were stored as 10 wt % solutions in Nanopure water at −20 °C. Polymers with a range of molecular weights were synthesized by varying catalyst loadings from 0.5 to 4% while keeping the Nor-*cyc*RGD monomer **4** constant at 1%. The PDIs and average molecular weights (M_n) were calculated by gel permeation chromatography (GPC) following polymerization reactions. Complete side-chain deprotection of all polymers was confirmed by ^{1}H NMR. The synthetic details and characterization of monomers and copolymers, including a representative polymerization procedure, are provided in the Supporting Information.

Kinetic Analysis. A stock solution (1 mL) of the specified monomer at 0.02 M in CD_2Cl_2/CD_3OD (4:1) was added to an oven-dried septum screw cap NMR tube under an inert atmosphere. The ruthenium initiator **7** (10 μL of a 0.02 M solution in CD_2Cl_2) was then added to the NMR tube through the septum cap and inverted quickly to mix the solution. The tube was quickly placed in the NMR spectrometer (Varian Mercury 500 MHz) making note of the time before the first acquisition. Spectra were acquired at 26 s intervals (eight scans) using a 0.5 s interval between scans for proton relaxation. The polymerization was monitored until complete consumption of starting monomers. The percent conversion was calculated from integrations of [polymer]/[polymer + monomer] over time (see Supporting Information).

Preparation of Thin-Film Hydrogels. Samples for biological evaluation were prepared on 12 mm (Deckglaser) cover glasses that were functionalized with (3-aminopropyl)triethoxysilane.[40,41] Amine functionalization was performed by soaking coverslips in saturated KOH in EtOH for 5 min. The coverslips were then rinsed with Nanopure water, treated with 6N aq. NaOH for 5 min, rinsed again with water, and allowed to dry under a stream of air. The coverslips were added to a 95% EtOH/H_2O solution containing 2% (3-aminopropyl)triethoxysilane and allowed to soak for 2 min. The coverslips were then transferred to a MeOH bath, removed, and allowed to dry in air.

A 2.5 wt % solution of desired polymer in Nanopure water was added to 1 equiv of bis(sulfosuccinimidyl) suberate (BS^3) relative to the primary amine in the polymer. An amine functionalized coverslip was placed on the spin coater (Specialty Coating Systems, 6800 Spin Coater Series). Approximately 70 μL of the 2.5 wt % polymer/BS^3 solution was carefully added covering the entire glass surface. The sample was then allowed to coat the surface at 2500 rpm for 30 s. All coated samples were allowed to dry overnight to provide thin-film hydrogels for subsequent cell adhesion, viability, and spreading studies. Atomic force microscopy (AFM) analyses of representative thin films are included in the Supporting Information.

Cell Culture. Human umbilical vein endothelial cells (HUVECs) (Lonza, CC-2519) were cultured at 37 °C under a humidified atmosphere of 5% CO_2. The cells were grown in endothelial cell growth medium (Cell Applications, 211-500) supplemented with 1% penicillin/streptomycin (Gibco, 105140122). The cells were con-

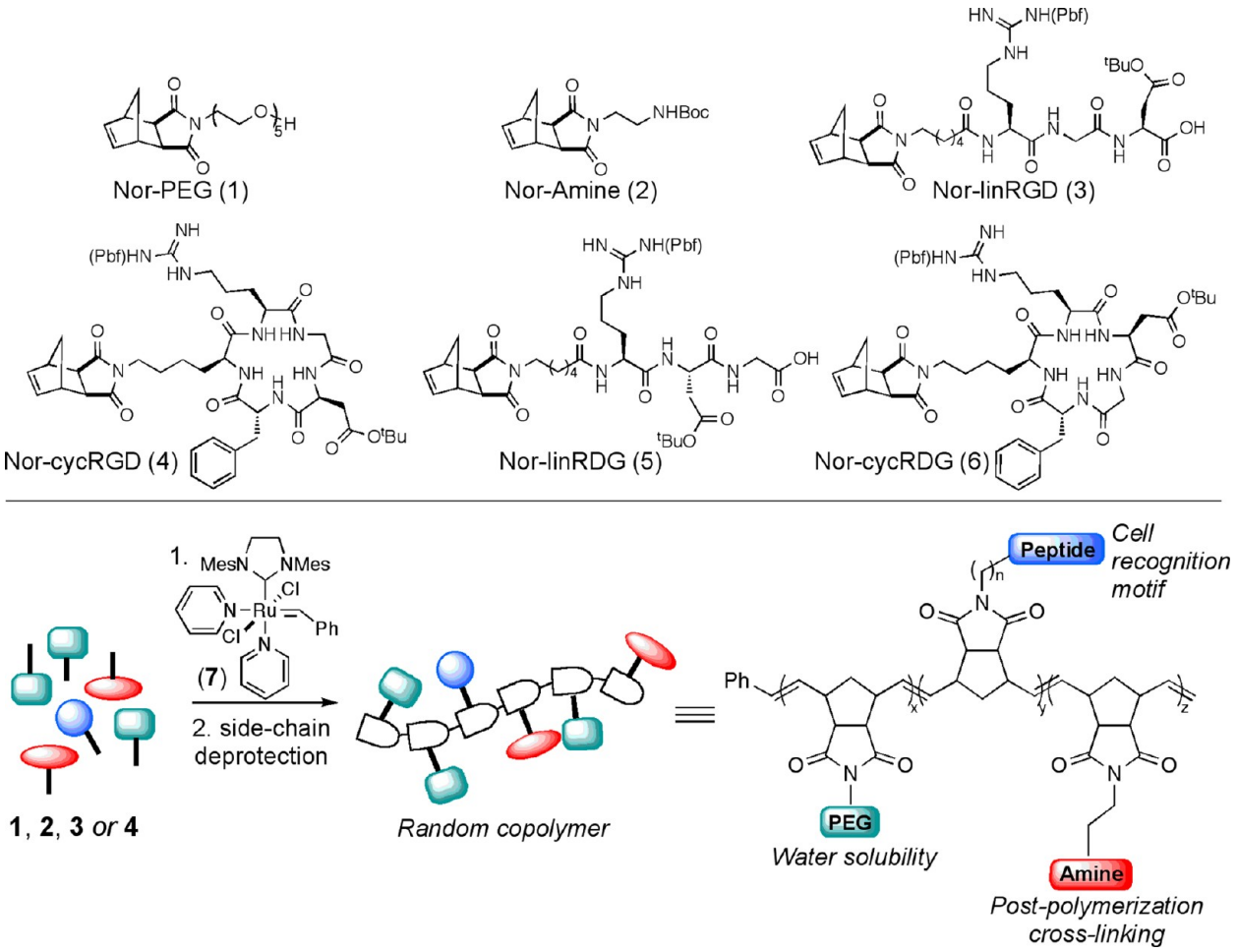

Figure 1. Ruthenium-catalyzed ROMP of norbornene monomers (top) for the synthesis of random copolymers incorporating water-soluble PEGs, RGD peptides, and amines for postpolymerization cross-linking (bottom).

tinuously maintained in the culture medium and subcultured every 3–4 days up to 10 passages. Cells from passages 6–10 were used in studies of adhesion, viability, and spreading.

Cell Adhesion Studies. Cells at 70–80% confluence were washed with warm PBS, detached, and resuspended in either regular growth medium or serum-free medium (Cell Applications, 113–500). An aliquot of 5×10^4 cells was seeded per well in a 24-well plate containing polymer-coated coverslips. Cells were allowed to attach for 24 h in the incubator before examination by phase contrast microscopy.

Cell Viability. Cell viability on thin-film hydrogels was assessed using a Live/Dead Viability kit (Invitrogen, L3224). HUVECs were seeded at a density of 5×10^4 cells per well in a 24-well plate containing coated coverslips. Cells were allowed to grow for 24 h in serum-supplemented or serum-free media in an incubator prior to staining according to the manufacturer's protocol. Cells were then imaged on an inverted epifluorescence microscope (IX71, Olympus) with a humidified chamber and temperature control at 37 °C. Images were taken with identical acquisition settings and processed using ImageJ 1.45s (National Institutes of Health, USA). Cell viability experiments were run in triplicate.

Cell Spreading. HUVECs were seeded at a concentration of 5×10^4 cells per well in a 24-well plate in serum-free medium. Cells were imaged on thin-film hydrogels at 15, 30, 45, 60, 90, 120, 180, 240, and 300 min. Images were taken using a 10× phase contrast objective on a Nikon Eclipse TE300 inverted microscope. Images were manually scored for the number of spread versus nonspread (rounded) cells. Spreading experiments were run in triplicate.

RESULTS AND DISCUSSION

Monomer and Polymer Design and Synthesis. The random copolymers were designed to incorporate three separate monomers: a water-soluble PEG unit (**1**), the RGD cell recognition motif (**3** or **4**), and a reactive amine functional group (**2**) for postpolymerization cross-linking (Figure 1). Monomers **1** and **2** were synthesized readily using previously reported condensation reactions of *cis*-5-norbornene-*exo*-2,3-dicarboxylic anhydride with the corresponding amines.[37,42] Peptide substituted norbornene monomers (**3**–**6**) were synthesized via Fmoc solid phase peptide synthesis (SPPS) on 2-chlorotrityl chloride resin. Notably, monomers **3**–**6** were designed to incorporate a linker between the highly functionalized peptide and the ROMP reactive norbornene unit, thereby ensuring good reactivity in polymerizations. For monomers Nor-*lin*RGD (**3**) or Nor-*lin*RDG (**5**), *N*-(hexanoic acid)-*cis*-5-norbornene-*exo*-dicarboximide was coupled to the amino terminus of the peptides on resin. The monomers were then cleaved from the resin using mild acidic conditions providing side-chain protected, norbornene-conjugated peptides **3** and **5**, which were used in polymerization reactions without further purification.

The structure of monomer Nor-*cyc*RGD (**4**) was designed based on the tumor targeting $\alpha_v\beta_3$ antagonist *cyclo*(RGDfK) and its more potent dimer.[43,44] Therefore, the synthesis of monomer Nor-*cyc*RGD (**4**) was initiated by SPPS of the side-

dx.doi.org/10.1021/bm300795y | *Biomacromolecules* 2012, 13, 2546–2553

chain protected linear sequence NH_2−Asp(O^tBu)-DPhe-Lys-(Nor)-Arg(Pbf)-Gly-CO_2H (**8**), where the lysine side chain incorporates the norbornene functionality (Scheme 1).

Scheme 1. Synthesis of Nor-*cyc*RGD (4)

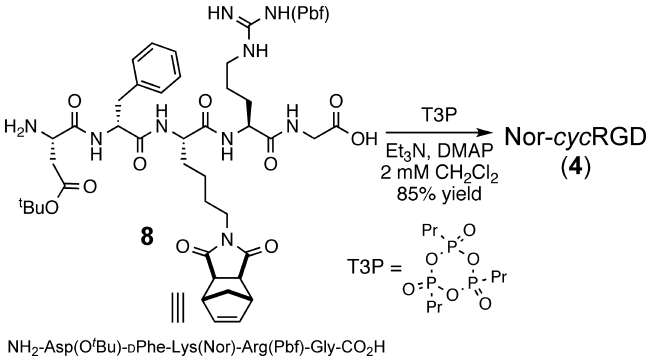

Cyclization of **8** with propylphosphonic anhydride (T3P), following the procedure of Liu et al.,[45] provided Nor-*cyc*RGD (**4**) in excellent yields (85%). The control monomer Nor-*cyc*RDG (**6**) was synthesized by a similar method with simple transposition of the Asp(O^tBu) and Gly residues during SPPS of the linear peptide prior to cyclization.

Polymers were synthesized readily from norbornene monomers **1**−**6** by initiation with ruthenium catalyst **7** (Scheme 2). Ruthenium catalysts containing bis-pyridine ligands have been demonstrated to initiate rapidly at room temperature, and therefore, provide good molecular weight control of the resulting polymers.[36,46] All copolymerizations were run for 35 min assuring complete reaction of all monomers, and terminated with the addition of ethyl vinyl ether.[38] The RGD content in the polymers was controlled by varying the percentage of the desired RGD monomer (**3** or **4**) in the monomer feed prior to initiation with **7**. For all polymerizations, 20% of the Nor-Amine (**2**) was incorporated with variable amounts of Nor-PEG (**1**) in order to keep the monomer to catalyst ratio constant. Polymers containing linear RGD peptides were synthesized with a range of 0−10% Nor-*lin*RGD (**3**) in the monomer feed. Polymers with no peptide or 10% of the scrambled sequence *lin*-RDG were also made as negative controls for biological evaluation. Polymers with cyclic peptide were synthesized with a range of 0−2.5% Nor-*cyc*RGD (**4**) in the polymerization reactions. A negative control polymer containing 2.5% scrambled *cyc*-RDG was prepared for biological studies. Polymers containing cyclic RGD were prepared with lower peptide concentrations due to the enhanced binding affinity of the cyclic peptide for cell surface integrins.[15−21]

Scheme 2. Random Copolymerizations of Norbornene Monomers via ROMP

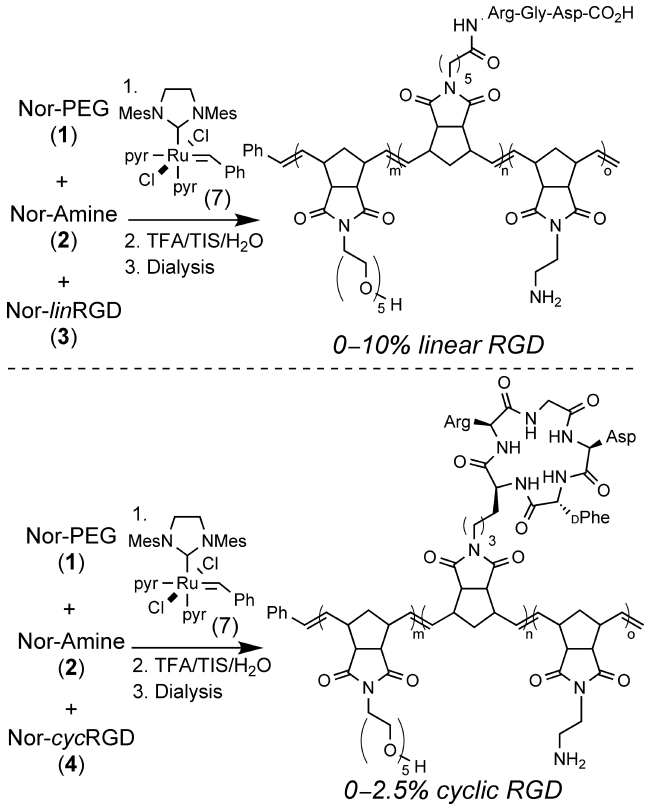

Because of the complexity of peptide substituted norbornene monomers (**3**−**6**), we examined whether polymerization reactions were characterized by a linear dependence of average molecular weight (M_n) on monomer-to-catalyst ratio ($[M]_0/[C]_0$) thereby indicating a living polymerization.[25−27,47] Polymers with 1% *cyc*-RGD were synthesized at varying monomer-to-catalyst ratios ($[M]_0/[C]_0$ = 199, 99, 49, and 24, Table 1 entries 7, 3, 8, and 9, respectively), and the molecular weights (M_n) of these polymers were found to increase linearly with increased $[M]_0/[C]_0$ (see Supporting Information). Consistent with the living nature of these polymerizations, all protected polymers were isolated in excellent yields (95−100%) and gave narrow PDIs (1.04−1.11). GPC analysis for all polymers showed good control of molecular weight as well as monomodal distributions for all polymers (see Table 1 for representative GPC data). Precise control of molecular weight and low PDI values are important factors for the use of ROMP as a general method for the synthesis of polymers. Additionally, since soluble polymers would inhibit cell adhesion,[33,34] narrow PDIs ensure consistent cross-linking of polymers. Following polymerization, the side-chain protecting groups were cleaved with TFA and purified by dialysis. The aqueous solutions were lyophilized to provide white foams in good yields (60−78%) and were characterized

Table 1. GPC Data for Random Copolymers Incorporating Linear or Cyclic RGD Peptides

entry	protected polymer[a]	$[M]_0/[C]_0$	M_n GPC (kDa)	M_n theo (kDa)	PDI
1	10% *lin*-RGD	99	52	42	1.05
2	10% *lin*-RDG	99	49	42	1.06
3	1% *cyc*-RGD	99	45	37	1.05
4	0.1% *cyc*-RGD	99	47	36	1.07
5	2.5% *cyc*-RDG	99	48	38	1.04
6	no peptide	99	45	36	1.04
7	1% *cyc*-RGD	199	74	74	1.11
8	1% *cyc*-RGD	49	25	18	1.05
9	1% *cyc*-RGD	24	15	8.9	1.10

[a]Determined by GPC with 0.2 M LiBr/DMF solution. GPC data collected postpolymerization with side chains protected. GPC traces and data for all other polymers can be found in the Supporting Information.

dx.doi.org/10.1021/bm300795y | *Biomacromolecules* 2012, 13, 2546−2553

by ^{1}H NMR to ensure complete deprotection of the polymer side chains.

In order to determine whether the copolymers described here were true random copolymers or contained gradients in composition, we examined the relative rates of incorporation for norbornene monomers **1**−**4** in homopolymerization reactions. Previously reported polymerizations with other peptide-conjugated norbornenes have demonstrated kinetic evidence for random copolymer formation.[37] Kinetic studies were conducted by observing the disappearance of monomer and appearance of polymer by ^{1}H NMR at monomer-to-catalyst ratios of 100:1. First-order kinetics was observed for all monomers examined with similar rates of incorporation for homopolymer formation (Figure 2). Monomer Nor-*cyc*RGD

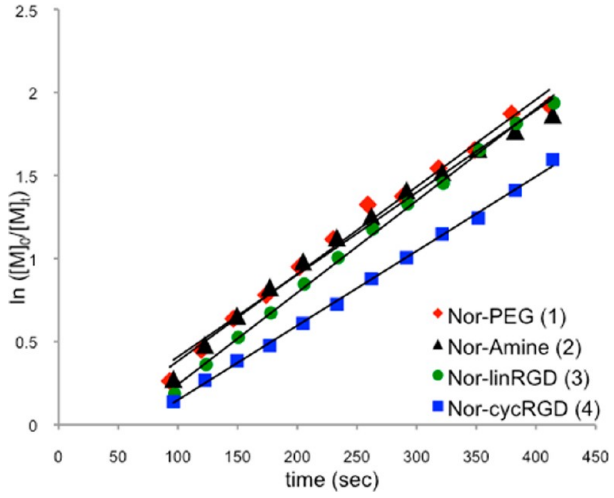

Figure 2. Log plot of the homopolymerization of monomers **1**−**4** with $[M]_0$:$[C]_0$ = 100:1 in 4:1 CD_2Cl_2/CD_3OD. Linear least-squares fitting provided the following slopes [k_{obs} (sec^{-1})]: monomer **1**: 0.0052, monomer **2**: 0.0049, monomer **3**: 0.0054, monomer **4**: 0.0045.

(**4**) reacts at a slightly lower rate than monomers **1**−**3**, possibly due to its larger size and increased steric hindrance closer to the reactive norbornene moiety. Nevertheless, all homopolymerization reactions reached full conversion within 12 min, indicating that RGD content in the final polymers can be controlled by the initial monomer feed ratios.

Following synthesis and characterization of RGD functionalized polymers and controls, samples for cell adhesion were prepared. A 2.5 wt % aqueous solution of polymer in the presence of BS^3 was spin-coated on amine functionalized coverslips. The coverslips were allowed to dry overnight prior to biological evaluation. Representative thin films were examined by AFM and ranged in thickness from 54 to 65 nm as dry films; upon absorption of water, the films swelled to 79−87 nm. The films were homogeneous and smooth.

Cell Adhesion and Viability. Cell adhesion was initially evaluated qualitatively via phase contrast microscopy 24 h post seeding of HUVECs on cross-linked polynorbornene thin films. A range of 1−10% linear RGD containing polymers (Table 2, **11**−**14**) were examined and compared to controls that contained either no peptide (**9**) or the scrambled polymer with 10% *lin*-RDG (**10**). Polymers containing linear RGD required peptide concentrations above 1% in order to promote cell attachment after 24 h. As expected, control polymers **9** and **10** did not promote cell adhesion. Polymer **14**, carrying 10% *lin*-RGD, was used as a comparison with cyclic RGD polymers since thin films of **14** demonstrated good cell attachment.

Table 2. Cell Adhesion on Polymer Thin Films Containing Linear RGD Peptides

polymer	% linear RGD	% linear RDG (control)	cell adhesion (±)
9	0	0	−
10	0	10	−
11	1	0	−
12	2.5	0	+
13	5	0	+
14	10	0	+

Polymers incorporating cyclic RGD at concentrations between 0.01 and 2.5% (Table 3, **16**−**22**) were subsequently examined for their ability to support cell adhesion and survival 24 h post seeding. Consistent with enhanced binding, these cyclic RGD containing thin films supported cell adhesion at concentrations as low as 0.05% (**17**), a 50-fold lower concentration than the minimum RGD concentration for linear RGD films. Positive cell adhesion of these synthetic polynorbornene thin films corresponds to integrin recognition of RGD concentrations in the low nanomolar range. Cell adhesion with 2.5% *cyc*-RGD (**22**) was observed to be comparable to that observed on thin films bearing 1% *cyc*-RGD (**21**). From the results of these cell adhesion assays, thin films containing 1% *cyc*-RGD (**21**) and 0.1% *cyc*-RGD (**18**) were examined quantitatively in cell viability and spreading assays.

Table 3. Cell Adhesion on Polymer Thin Films Containing Cyclic RGD Peptides

polymer	% cyclic RGD	% cyclic RDG (control)	cell adhesion (±)
9	0	0	−
15	0	2.5	−
16	0.01	0	−
17	0.05	0	+
18	0.1	0	+
19	0.25	0	+
20	0.5	0	+
21	1	0	+
22	2.5	0	+

Cell viability was assessed using a Live/Dead Viability assay (fluorescent dyes calcein-AM and ethidium homodimer-1), 24 h after seeding on polymer thin-film samples carrying either linear or cyclic RGD. Fluorescence images were acquired, and the number of live cells (green) versus dead cells (red) was quantified for thin films containing 10% *lin*-RGD (**14**), 1% *cyc*-RGD (**21**), and 0.1% *cyc*-RGD (**18**) (Figure 3). Negative control samples included scrambled sequences 10% *lin*-RDG (**10**), 2.5% *cyc*-RDG (**15**), and a polymer film with no peptide (**9**). Under serum-supplemented conditions (Figure 3, A), 87% of cells were alive in samples with 10% *lin*-RGD, while both *cyc*-RGD samples provided 95% cell viability. Examination of the fluorescence images illustrates that the negative controls have no attached cells (Figure 3, C−E). While cells exhibit similar characteristics on films with 10% *lin*-RGD (Figure 3, F) and 0.1% *cyc*-RGD (Figure 3, H), samples with 1% *cyc*-RGD (Figure 3, G) show an enhanced ability to support cell attachment. Under more stringent serum-free conditions (Figure 3, B), a significant decrease in cell viability was

dx.doi.org/10.1021/bm300795y | *Biomacromolecules* 2012, 13, 2546−2553

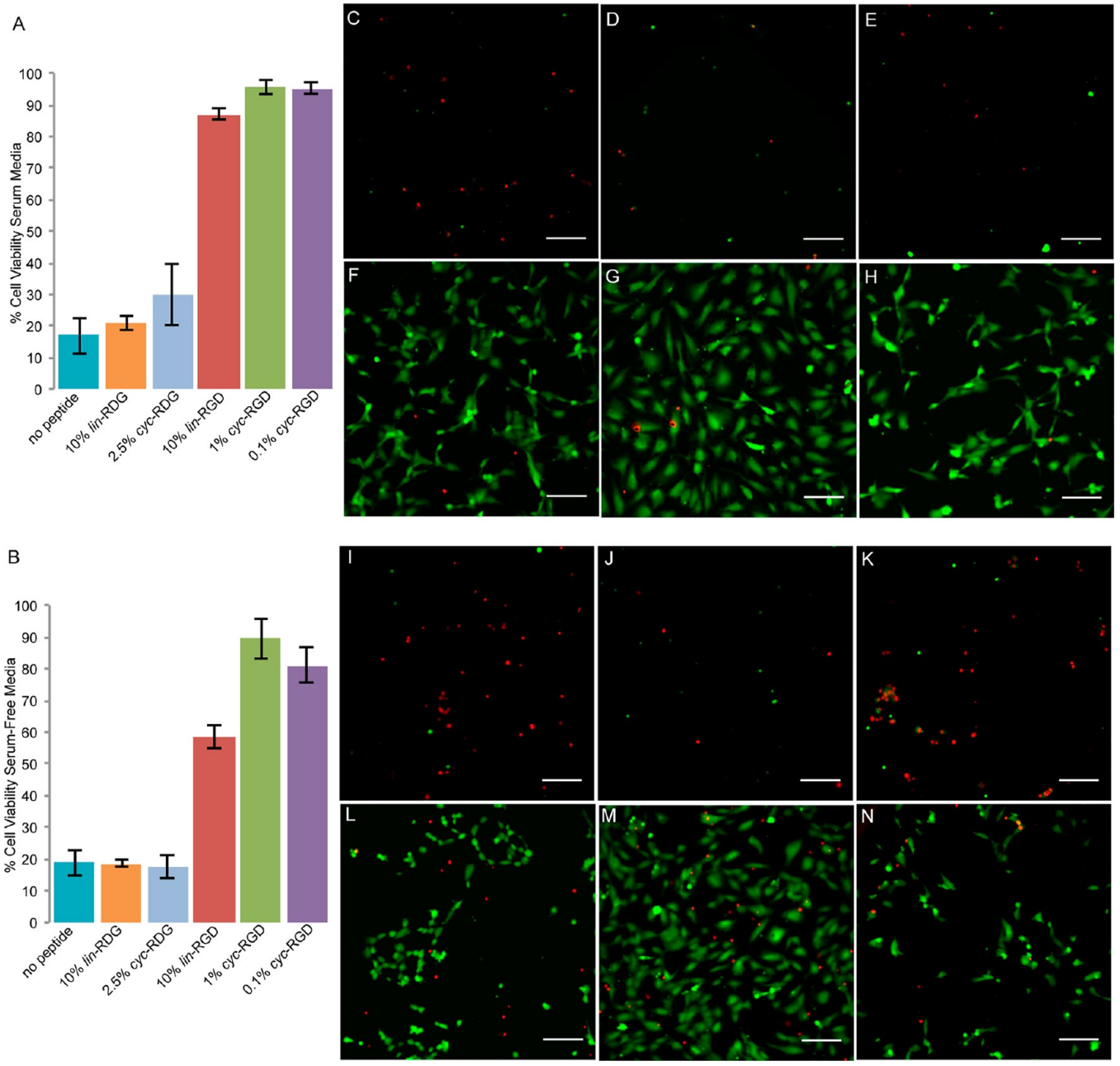

Figure 3. Quantitative and qualitative assessment of HUVEC cell viability on cross-linked polynorbornenes using a fluorescent Live/Dead Viability assay. Green fluorescence (calcein-AM) indicates live cells, and red fluorescence (ethidium homodimer-1) indicates dead cells. Cell viability in serum-supplemented media (A) and serum-free media (B) 24 h post seeding. Fluorescence images of HUVEC adhesion after 24 h in serum media (C–H) of polynorbornene thin films incorporating no peptide (C), 10% *lin*-RDG peptide (D), 2.5% *cyc*-RDG (E), 10% *lin*-RGD (F), 1% *cyc*-RGD (G), and 0.1% *cyc*-RGD (H). Fluorescence images of similar samples in serum-free media are shown in I–N. Scale bars =100 μm.

observed for 10% *lin*-RGD (59%), and modest decreases were found for samples with 0.1% *cyc*-RGD (81%) and 1% *cyc*-RGD (89%). As shown in Figure 3 (B, L, and N), both 10% *lin*-RGD (Figure 3, L) and 0.1% *cyc*-RGD (Figure 3, N), which differ 100-fold in peptide concentration, demonstrate similar levels of cell survival. Impressively, samples with 1% *cyc*-RGD (Figure 3, M) show similar adhesion and spreading in serum-free and serum-supplemented conditions. The superior cell viability of thin-film samples containing cyclic RGD peptides is consistent with the enhanced binding affinity of cyclic peptides for integrins, leading to increased cell adhesion and survival on *cyc*-RGD polynorbornene thin films. Specifically, the binding of cyclic RGD peptides to the $\alpha_v\beta_3$ integrins, which are overexpressed in HUVECs, has been reported to be subnanomolar in affinity.[22,23]

Cell Spreading. The time frame for cell attachment and spreading of HUVECs on cross-linked polynorbornene thin films was also investigated. HUVECs plated on thin films were examined at intervals of 15, 30, 45, 60, 90, 120, 180, 240, and 300 min using phase contrast microscopy. The more stringent, serum-free conditions were utilized for the comparison of cell spreading on 1% *cyc*-RGD versus 10% *lin*-RGD thin films alongside negative controls (no peptide and scrambled sequences; Figure 4). HUVECs on polymers containing both 1% *cyc*-RGD and 10% *lin*-RGD showed excellent adhesion and spreading within 300 min. With 1% *cyc*-RGD, half of the cells

dx.doi.org/10.1021/bm300795y | *Biomacromolecules* 2012, 13, 2546–2553

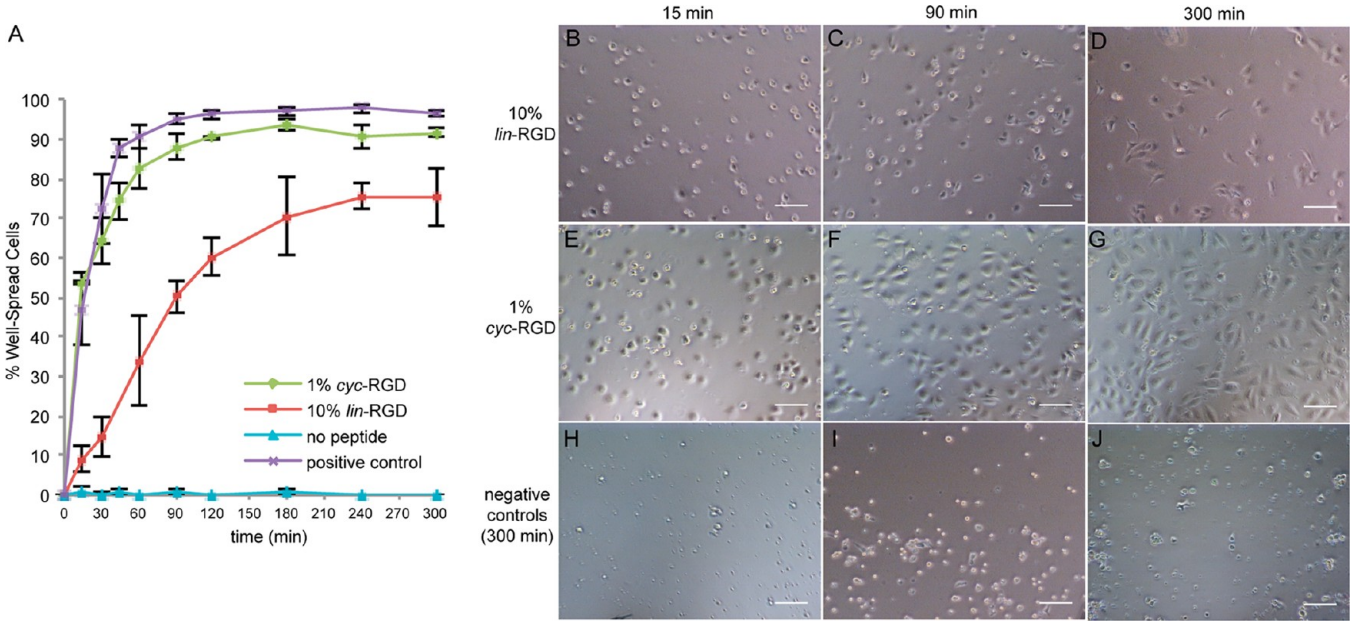

Figure 4. HUVEC spreading on cross-linked polynorbornene thin films (A). Positive control samples of HUVECs seeded directly in wells of tissue culture-treated plates were examined alongside polynorbornene thin films. Phase contrast images show cells cultured on 10% *lin*-RGD (B, C, D) and 1% *cyc*-RGD (E, F, G) spreading at 15, 90, and 300 min, respectively. These images can be compared to those on negative controls (no peptide (H), 10% *lin*-RDG (I), and 2.5% *cyc*-RDG (J)) each at 300 min. Data represents three separate experiments. Scale bars = 100 μm.

were spread as early as 15 min (Figure 4, E), while 10% *lin*-RGD provided similar results at 90 min (Figure 4, C). This significantly faster rate of adhesion is consistent with the increased affinity of cyclic RGD peptides for cell surface integrins.[23] As illustrated in Figure 4 (A), cell spreading and overall adhesion are significantly enhanced for the 1% *cyc*-RGD polymer compared to 10% *lin*-RGD. Additionally, cells cultured on the polymer thin films exhibit morphology and spreading similar to positive control samples of HUVECs seeded directly in wells of tissue culture treated plates.

CONCLUSIONS

The results reported here provide an efficient method for the preparation of linear and cyclic RGD-conjugated norbornene monomers **3** and **4**. Monomers containing the RGD cell recognition motifs were copolymerized with Nor-PEG (**1**) and Nor-Amine (**2**) to provide excellent yields of polynorbornenes with varying concentrations of linear or cyclic RGD peptide side chains. Cross-linked thin films of polymers carrying cyclic RGD were active at a 100-fold lower peptide concentration than linear RGD-containing polymers for cell viability of HUVECs. Polymer samples with 1% *cyc*-RGD were observed to be superior for cell attachment, viability, and spreading under stringent, serum-free conditions. The disclosed copolymer formation with RGD based monomers provides evidence for the broad utility of ROMP as a controlled method for incorporating a range of peptides into polymers. These results have important implications for the synthesis of biomaterials that support cell adhesion, and studies investigating the impact of incorporating multiple cell-recognition motifs and increasing the linker length between the polymer backbone and the RGD moiety are currently ongoing. The evaluation of these materials for supporting stem cell attachment and growth for biomedical applications is also underway.

ASSOCIATED CONTENT

Supporting Information

Additional details for the synthetic preparation of monomers **1**–**6**, preparation and characterization data for all polymers, AFM images of thin films, fluorescence images, and ^{1}H and ^{13}C NMR spectra. This material is available free of charge via the Internet at http://pubs.acs.org.

AUTHOR INFORMATION

Corresponding Author

*E-mail: rhg@caltech.edu.

Present Addresses

[‡]Materia, Inc., 60 North San Gabriel Boulevard, Pasadena, CA 91107.

[§]School of Materials Science and Engineering, Nanyang Technological University, 50 Nanyang Avenue, Singapore 639798.

Notes

The authors declare no competing financial interest.

ACKNOWLEDGMENTS

We thank Professor Chin-Lin Guo for use of his inverted epifluorescence microscope, and Mr. Jiun-Yann Yu for assistance with the microscope. Ms. Chithra Krishnamurthy is thanked for helpful discussions. This research was supported by the National Institutes of Health (5R01-GM31332, F32 HL091440), the NSF Materials Research Science and Engineering Center at Caltech (DMR 0520565), the Beckman Institute at Caltech (postdoctoral fellowship to R.C.K.), and grants from the California Institute for Regenerative Medicine. Materia, Inc. is thanked for its donation of metathesis catalysts.

REFERENCES

(1) Hersel, U.; Dahmen, C.; Kessler, H. *Biomaterials* **2003**, *24*, 4385–4415.

(2) Sakiyama-Elbert, S. E.; Hubbell, J. A. *Annu. Rev. Mater. Res.* **2001**, *31*, 183−201.
(3) Langer, R. *Acc. Chem. Res.* **2000**, *33*, 94−101.
(4) Akiyama, S. K.; Olden, K.; Yamada, K. M. *Cancer Metastasis Rev.* **1995**, *14*, 173−189.
(5) Pierschbacher, M. D.; Ruoslahti, E. *Nature* **1984**, *309*, 30−33.
(6) Massia, S. P.; Hubbell, J. A. *J. Cell. Biol.* **1991**, *114*, 1089−1100.
(7) Xiong, J.; Stehle, T.; Zhang, R.; Joachimiak, A.; Frech, M.; Goodman, S. L.; Arnaout, M. A. *Science* **2002**, *296*, 151−155.
(8) Pettit, D. K.; Hoffman, A. S.; Horbett, T. A. *J. Biomed. Mater. Res.* **1994**, *28*, 685−691.
(9) Aucoin, L.; Griffith, C. M.; Pleizier, G.; Deslandes, Y.; Sheardown, H. *J. Biomater. Sci., Polym. Ed.* **2002**, *13*, 447−462.
(10) Verrier, S.; Pallu, S.; Bareille, R.; Jonczyk, A.; Meyer, J.; Dard, M.; Amedee, J. *Biomaterials* **2002**, *23*, 585−596.
(11) Heilshorn, S. C.; Di Zio, K. A.; Welsh, E. R.; Tirrell, D. A. *Biomaterials* **2003**, *24*, 4245−4252.
(12) Liu, J. C.; Heilshorn, S. C.; Tirrell, D. A. *Biomacromolecules* **2004**, *5*, 497−504.
(13) Liu, J. C.; Tirrell, D. A. *Biomacromolecules* **2008**, *9*, 2984−2988.
(14) Fong, E.; Tzlil, S.; Tirrell, D. A. *Proc. Natl. Acad. Sci. U.S.A.* **2010**, *107*, 19302−19307.
(15) Risau, W. *Nature* **1997**, *386*, 671−674.
(16) Schottelius, M.; Laufer, B.; Kessler, H.; Wester, H. *Acc. Chem. Res.* **2009**, *42*, 969−980.
(17) Stepp, M. A. *Exp. Eye Res.* **2006**, *83*, 3−15.
(18) Koivunen, E.; Wang, B.; Ruoslahti, E. *Nat. Biotechnol.* **1995**, *13*, 265−270.
(19) Assa-Munt, N.; Jia, X.; Laakkonen, P.; Ruoslahti, E. *Biochemistry* **2001**, *40*, 2373−2378.
(20) Burkhart, D. J.; Kalet, B. T.; Coleman, M. P.; Post, G. C.; Koch, T. H. *Mol. Cancer. Ther.* **2004**, *3*, 1593−1604.
(21) Kolhar, P.; Kotamraju, V. R.; Hikita, S. T.; Clegg, D. O.; Ruoslahti, E. *J. Biotechnol.* **2010**, *146*, 143−146.
(22) Haubner, R.; Gratias, R.; Diefenbach, B.; Goodman, S. L.; Jonczyk, A.; Kessler, H. *J. Am. Chem. Soc.* **1996**, *118*, 7461−7472.
(23) Kantlehner, M.; Schaffner, P.; Finsinger, D.; Meyer, J.; Jonczyk, A.; Diefenbach, B.; Nies, B.; Holzemann, G.; Goodman, S. L.; Kessler, H. *ChemBioChem* **2000**, *1*, 107−114.
(24) Komazawa, H.; Saiki, I.; Igarashi, Y.; Azuma, I; Kojima, M.; Orikasa, A.; Ono, M.; Itoh, I. *J. Bioact. Compat. Polym.* **1993**, *8*, 258−274.
(25) Grubbs, R. H., Ed. *Handbook of Metathesis*; Wiley-VCH: Weinheim, Germany, 2003, Vol. 3.
(26) Trnka, T. M.; Grubbs, R. H. *Acc. Chem. Res.* **2001**, *34*, 18−29.
(27) Leitgeb, A.; Wappel, J.; Slugovc, C. *Polymer* **2010**, *51*, 2927−2946.
(28) Gestwicki, J. E.; Strong, L. E.; Cairo, C. W.; Boehm, F. J.; Kiessling, L. L. *Chem. Biol.* **2002**, *9*, 163−169.
(29) Kolonko, E. M.; Pontrello, J. K.; Mangold, S. L.; Kiessling, L. L. *J. Am. Chem. Soc.* **2009**, *131*, 7327−7333.
(30) Lienkamp, K.; Madkour, A. E.; Musante, A.; Nelson, C. F.; Nusslein, K.; Tew, G. N. *J. Am. Chem. Soc.* **2008**, *130*, 9836−9843.
(31) Biswas, S.; Wang, X.; Morales, A. R.; Ahn, H.; Belfield, K. D. *Biomacromolecules* **2011**, *12*, 441−449.
(32) Miki, K.; Kimura, A.; Oride, K.; Kuramochi, Y.; Matsuoka, H.; Harada, H.; Hiraoka, M.; Ohe, K. *Angew. Chem., Int. Ed.* **2011**, *50*, 6567−6570.
(33) Maynard, H. D.; Okada, S. Y.; Grubbs, R. H. *Macromolecules* **2000**, *33*, 6239−6248.
(34) Maynard, H. D.; Okada, S. Y.; Grubbs, R. H. *J. Am. Chem. Soc.* **2001**, *123*, 1275−1279.
(35) Nguyen, M. N.; Lebarbe, T.; Zouani, O. F.; Pichavant, L.; Durrieu, M. C. *Biomacromolecules* **2012**, *13*, 896−904.
(36) Love, J. A.; Morgan, J. P.; Trnka, T. M.; Grubbs, R. H. *Angew. Chem., Int. Ed.* **2002**, *41*, 4035−4037.
(37) Conrad, R. M.; Grubbs, R. H. *Angew. Chem., Int. Ed.* **2009**, *48*, 8328−8330.
(38) Schwab, P.; France, M. B.; Ziller, J. W.; Grubbs, R. H. *Angew. Chem., Int. Ed.* **1995**, *34*, 2039−2041.
(39) Maynard, H. D.; Grubbs, R. H. *Tetrahedron Lett.* **1999**, *40*, 4137−4140.
(40) Saneinejad, S.; Shoichet, M. S. *J. Biomed. Mater. Res.* **1998**, *42*, 13−19.
(41) Kleinfeld, D.; Kahler, K. H.; Hockberger, P. E. *J. Neurosci.* **1988**, *8*, 4098−4120.
(42) Matson, J. B.; Grubbs, R. H. *J. Am. Chem. Soc.* **2008**, *130*, 6731−6733.
(43) Janssen, M.; Oyen, W. J.; Massuger, L. F.; Frielink, C.; Dijkgraaf, I.; Edwards, D. S.; Radjopadhye, M.; Corstens, F. H.; Boerman, O. C. *Cancer Biother. Radiopharm.* **2002**, *17*, 641−646.
(44) Janssen, M. L.; Oyen, W. J.; Dijkgraaf, I.; Massuger, L. F.; Frielink, C.; Edwards, D. S.; Radjopadhye, M.; Boonstra, H.; Corstens, F. H.; Boerman, O. C. *Cancer Res.* **2002**, *62*, 6146−6151.
(45) Dai, X.; Su, Z.; Liu, J. O. *Tetrahedron Lett.* **2000**, *41*, 6295−6298.
(46) Choi, T. L.; Grubbs, R. H. *Angew. Chem., Int. Ed.* **2003**, *42*, 1743−1746.
(47) Gilliom, L. R.; Grubbs, R. H. *J. Am. Chem. Soc.* **1986**, *108*, 733−742.